Mechanisms of Inter-annual Rainfall Variability over Tropical Highlands of Africa and its Predictability Potential

Emmanuel Jonathan Mpeta

Department of Geography and Environmental Studies
University of Zululand

Thesis submitted to the Faculty of Science
for the Degree of Doctor Of Philosophy

November, 2002

Abstract

Modes of climate variability over tropical Africa and adjacent Atlantic and Indian Oceans are investigated using continental monthly averages of gridded rainfall and temperature and marine environmental data, which consists of monthly averages of sea surface temperature, sea level pressure and zonal and meridional wind components. Rainfall and temperature data are gridded at a resolution of 2° x 2° latitude, longitude and based on conventional station data reports (University of East Anglia CRU data set) in the domain 10°N-35°S over Africa except Madagascar. The environmental data is at a resolution of 10° x 10° latitude, longitude and based on ship reports (COADS) in the domain 30°N - 40°S, 70°W - 100°E. The data sets are subjected to Principal Component Analysis (PCA) using the correlation matrix technique, resulting in the gridded data being standardized. The data are analyzed for annual cycle and the departure therefrom (i.e. Inter-annual fluctuations). The time-varying spectral energy nature of time series is investigated using wavelet analysis technique.

PCA (with annual cycle) yielded 12 and 7 homogeneous rainfall and temperature regions, over the African continent south of 10°N, which explained a total of 81 and 91 variance respectively. PCA on marine environmental parameters over the Atlantic and Indian Oceans revealed a number of homogeneous regions, some of which could be associated with synoptic systems. Similarly, PCA was performed on the same data after removing the annual cycle. The time evolution of these PC modes or time scores were shown to oscillate with periods of 2-4, 4-6, 8-12 and 14 -16 years. Long period oscillating modes were revealed over tropics, particularly the Atlantic Ocean.

Possible causes of rainfall and temperature variability over the tropical highlands of Africa were investigated by correlation analysis between rainfall and temperature, and environmental parameters and other indices at lag 0, using monthly data. Some modes of marine environmental parameters over the Atlantic and Indian Oceans have shown good association with the climate over the tropical highlands of Africa up to three months. Results also show that modes over tropical equatorial belt of the Atlantic and Indian Oceans explain rainfall variability up to about 25% for some areas over Africa. Temperature variability over the continent is associated with SST modes over the equatorial tropical oceans and some of these explain more than 64% of temperature variability. ENSO has also shown good association with temperatures over the continent while QBO is poorly associated with temperatures over the continent. Analysis results have shown further that rainfall variability over east and southern Africa regions is associated with the variability of SST, SLP and U wind component in the box 60°E-90°E,5°N-10°S, over the Indian ocean. Time delay analyses have shown that generally environmental parameter indices lead rainfall for between 2 to 20 months. Results indicate that there is no clear picture as to which parameter leads the other, as oscillations are not always in phase or exhibiting constant lag. The un-harmonious nature of these features could sometimes undermine predictability in

statistical modelling. So the idea of reviewing predictor-predictant relationships in a time varying manner is well justified.

Some parameters extracted from key areas show persistency and stability up to three months while the Nino3 index has shown persistency and stability of up to 6 months. Results have also revealed good associations between some environmental parameters over some key areas of the Atlantic and Indian Oceans and rainfall over some areas of tropical Africa, at 0 to 3 month lags. Analyses results have shown that the potential of forecasting rainfall over some areas of tropical highlands of Africa exists.

PREFACE

Year-to-year fluctuations of rainfall in the highlands of tropical Africa are common because of atmospheric-ocean interaction. Variability of rainfall in tropical Africa has a major influence on vegetation, animals and human activities. This is particularly true in semiarid climates, where a departure from the average may be the critical factor in crop failure. In Africa the mainstay of the population is subsistence farming of rain-fed crops, which renders its society vulnerable to rainfall fluctuations. Inter-annual fluctuations of seasonal rainfall impact on hydro-power electricity and the planning of agricultural activities (e.g., selection of the right variety of crops). Reliable predictions can inform policy makers and water authorities.

The availability of accurate, reliable and timely seasonal forecasts rest on an understanding of inter-annual climate variability components and their relation to regional and global meteorological parameters. The knowledge of inter-annual rainfall variability can be used to develop seasonal rainfall prediction, which can form a tool for sustainable development, employing scientific information to improve the quality of life.

Many researchers have undertaken studies on annual, inter-annual, intra-seasonal rainfall variation, and their relations with regional/global parameters for different areas of tropical Africa, using different data sets such as SSTs (Sea Surface Temperatures), SO (Southern Oscillation), QBO (Quasi-Biennial Oscillation), SLP (Sea Level Pressure), Wind etc. Despite the research progress in the last decade that has begun to reveal the extent of regional and global influence on tropical African rainfall, much remains to be understood about the interaction between the climate system and the surrounding ocean-atmosphere system. One question, for example, which is yet to be fully answered, is: Why do extreme ENSO events bring different patterns over tropical Africa? Could there be regional processes which modulate ENSO events over tropical Africa? A good example is the 1997/98 ENSO episode. Expectations were that this extreme event would have caused extensive drought over southern Africa. Fortunately, this never happened.

The objective of this research is to study the inter-annual variability of seasonal rainfall over the tropical highlands of Africa for the period 1965-1995. Specifically to look at how the anti-phase relationship between the East Atlantic and West Indian SST and associated upper zonal winds affect convection over the tropical highlands of Africa.

Fluctuations of seasonal rainfall over the tropics pose a problem to farmers and water resource managers and related industries. Farmers, water resource managers, economic planners and others would be well armed if they were able to know what is going to happen in the coming season. In order to be able to predict seasonal climates therefore, there is a strong need to identify major patterns of climate variability on inter-annual time scale over tropical Africa and

its relation to regional/global meteorological parameters together with forcing mechanisms

The study is aimed at identifying regional/global ocean-atmosphere parameters which, influence inter-annual rainfall variability over the highlands of tropical Africa. This will give an insight on the relationship between inter-annual variability of rainfall/convection over the tropical highlands of Africa and ocean-atmosphere coupling; from which we can develop operational statistical models capable of predicting seasonal rainfall.

The specific objectives of the research:

- To identify major patterns of rainfall and temperature variability at the inter-annual time scales over the study area e.g. Africa south of 10°N, and identify the nature of the variability. This will be achieved by analyzing available observation/model derived data.

- To identify major patterns of SST, SLP, Zonal and Meridional wind components variability over the Indian and Atlantic Oceans between 70°W-100°E, 20°N-40°S at the inter-annual time scale and identify the nature of variability. This will be achieved by analyzing available observation/model derived data.

- To identify the role of remote SSTs and associated teleconnections in modulating inter-annual rainfall over the tropical highlands of southern Africa.

- To investigate the influence of Congo convection on the eastern highlands of Africa.

- To investigate whether the zonal circulations of the Atlantic Ocean interacts with thermodynamic energy released over the Indian Ocean.

- To synthesize this knowledge into predictive models

This thesis is comprised of seven chapters. Chapter one provides a short account on the background to the study problem, aims and objectives of the study, relevant literature review and hypothesis. The literature review briefly describes the observational studies on inter-annual rainfall variability over Africa and associated causing mechanism. The second chapter details data and its sources. Principal Component Analysis and Continuous Wavelet Transform are briefly described in this chapter. Continuous Wavelet Transform is a relatively new method in the meteorological field. Chapter three describes the climatology of tropical highlands of Africa and also discusses the characteristics of annual cycle of the first two PC modes for different parameter fields. Chapter four deals with the temporal and spatial characteristics of the inter-annual variability of different parameters extracted from different key areas, with the PCA guidance. Correlation analysis is covered in chapter five. Simultaneous correlations, at lag zero, between rainfall and temperature key areas and other parameter is detailed in this chapter. Spatial

correlations are also performed in this chapter. In this chapter, relationships between rainfall over east and southern Africa in the various period bands are studied using cross wavelet spectrum. Time delay between a predictor and a predictant is also discussed. Chapter six deal with the forecasting potential of rainfall over the tropical highlands of Africa. In this chapter correlation between rainfall key areas and other parameter over selected key areas, at lag 3 and 6 are calculated. Correlations between DJF and MAM rainfall and other parameters at season lags 0, 1 and 2 are calculated. Chapter seven summarises major findings of the study and conclusions.

Acknowledgment

I would like to thank the Director General, Tanzania Meteorological Agency, for giving me this opportunity, encouragement and support to do this study. The data used in this thesis were made available from the Tanzania Meteorological Agency, Tanzania- station rainfall data over the Tanzania; CRU gridded temperature and rainfall over the African continent; NCEP kinematic and thermodynamic data; and COADS ocean and atmospheric circulation data. A special mention is made here of Dr. Jean-Luc Melice who introduced me to the Continuous Wavelet Transform analysis technique and provided me with some WT programs. Also I would like to thank Mr. S. E. Nkosi who helped me in the analysis of CRU data. Anna has been very helpful in making sure that I get the right type of computer software as well as hardware. This research project was funded by the University of Zululand, the Tanzania Meteorological Agency, WRC, NRF, and DACST projects on statistical modeling of climate. Discussions with Drs. Henry M. Mulenga and N. Pyuzza have been most helpful. I also want to thank the following for giving me moral support during the time I was doing this work. Finally, with most gratitude I acknowledge the help I have received from my supervisor Professor M. R. Jury. The management, staff of the Tanzania Meteorological Agency and the community at the University of Zululand for giving me all the help I needed during the whole period of this research.

CONTENTS

CHAPTER 1

CHAPTER 2

CHAPTER 3

CHAPTER 4

CHAPTER 1

1.0 Introduction

Year-to-year fluctuations of rainfall in tropical Africa are common as a consequence of atmospheric-ocean interaction and other processes. Variability of precipitation in tropical Africa has influence on vegetation, animals and human activities. This is particularly true in semiarid climates, where a departure from the average may be the critical factor in crop failure. In Africa the mainstay of the population is subsistence farming of rain-fed crops, which renders its society vulnerable to seasonal rainfall fluctuations. Inter-annual fluctuations of seasonal rainfall impact on hydro-power electricity and the planning of agricultural activities (e.g., selection of the right variety of crops). Reliable prediction of climatic anomalies can be of importance to policy makers and water authorities.

The availability of accurate, reliable and timely seasonal forecasts rest on an understanding of the components of inter-annual climate variability and its relation to regional and global environmental conditions. Applications of seasonal rainfall prediction can form a tool for sustainable development, employing scientific information to improve the current standard of life.

Many researchers have undertaken studies on annual, inter-annual, and intra-seasonal rainfall variation, and their relation to regional/global parameters for different areas of tropical Africa, using diverse information such as SSTs (Sea Surface Temperatures), SO (Southern Oscillation), QBO (Quasi-Biennial Oscillation), SLP (Sea Level Pressure), wind etc. Despite the research progress in the last decade that has begun to reveal the extent of regional and global influence on tropical African precipitation, much remains to be understood about the interaction between the climate system and the surrounding ocean-atmosphere system. One question, for example, which is yet to be fully answered is: "Why do extreme ENSO events bring different patterns of rainfall over tropical Africa?" Could there be regional processes which modulate ENSO events over tropical Africa? A good example, is the 1997/98 ENSO episode. Expectations were that this extreme event would cause extensive drought over southern Africa. Fortunately this never happened. The objective of this research is to study the inter-annual variability of seasonal

rainfall over tropical Africa for the period 1965-1995. Specifically to look at SST and circulation patterns over the East Atlantic and West Indian and associated convection over the highlands of tropical Africa.

1.2 Motivation

The year-to-year fluctuations of seasonal rainfall over the tropics pose a problem to farmers and water resource managers and related industries. This becomes an even more serious problem when extreme cases of dry or wet seasons occur 2-3 years consecutively. Farmers, water resource managers, economic planners and others would be well prepared if they were able to adjust to what is going to happen in the coming season. In order to be able to predict seasonal climates therefore, there is a need to identify patterns of climate variability on the inter-annual time scale over tropical Africa and its relation to regional/global forcing mechanisms. This type of study can lead us to identifying indices which can be used in predicting seasonal rainfall over the continent.

1.3.0 Study Objectives

The inter-annual variability of seasonal rainfall over tropical highlands of Africa is believed to be related to the relative strength of subtropical highs and the ITCZ, and associated monsoon inflow. These factors affect the southeastward shift of the meridional arm of the ITCZ (the Congo airmass) and seasonal rains in east Africa. The east-west overturning circulation of the Atlantic is thought to interact with ENSO to modulate convection over the Congo Basin and surrounds. Sea surface temperature variability over the Atlantic and Indian oceans controls a portion of the climate of the region at the inter-annual time scale and affects the local uptake of global climatic signals.

The study is aimed at identifying regional ocean-atmosphere parameters which influence inter-annual rainfall variability over the highlands of tropical Africa. This will give insight to possible coupling mechanisms, from which we can develop operational statistical methods capable of predicting seasonal rainfall.

1.3.1 Specific study objectives

- To identify major patterns of rainfall and temperature variability at annual and inter-annual

time scales over the study area, e.g., Africa south of 10°N, and identify the nature of the variability. This will be achieved by analyzing model-interpolated observational data.

- To identify major patterns of SST, SLP, Zonal and Meridional wind variability over the Atlantic and Indian Oceans between 70°W-100°E, 20°N-40°S at the inter-annual time scale and identify the nature of variability. This will be achieved by analyzing Model-interpolated observational data.

- To identify the role of regional/global SSTs and associated teleconnections in modulating inter-annual rainfall over the tropical southern Africa.

-To investigate the relationship between African rainfall, the Indian monsoon and Congo convection.

- To investigate whether the zonal circulation of the Atlantic interacts with thermodynamic energy released over the Indian Ocean.

- To synthesize this knowledge into predictability potential

1.4.0 Study area and its climate

1.4.1 Study area

The study area lies between 10°N and 34°S and between 20°E and 40°E with elevation above 1000m

1.4.2 Climates of the study area

The mean state of atmospheric motion is mainly due to latitudinal temperature differences, the distribution of continents, oceans and major surface topography. The heating of the equatorial belt through the absorption of incoming solar radiation and cooling of polar regions through outgoing terrestrial radiation, provide energy to move the atmosphere and oceans. The mean circulation produces a seasonal cycle in precipitation and temperature. Through observations extreme cases may be identified and the space and time distribution of atmospheric and oceanographic parameters which govern such conditions may be studied. Characteristics of the study area include: (1) above 1000m elevation in Africa (2) Zones of inter-tropical Convergence

monsoon and trade wind flows where tropical wave motion, e.g., MJO (madden Julian Oscillation) is present. In the following sections the climate of the study area is described, which for convenience is subdivided into three parts, i.e., east, central and southern Africa.

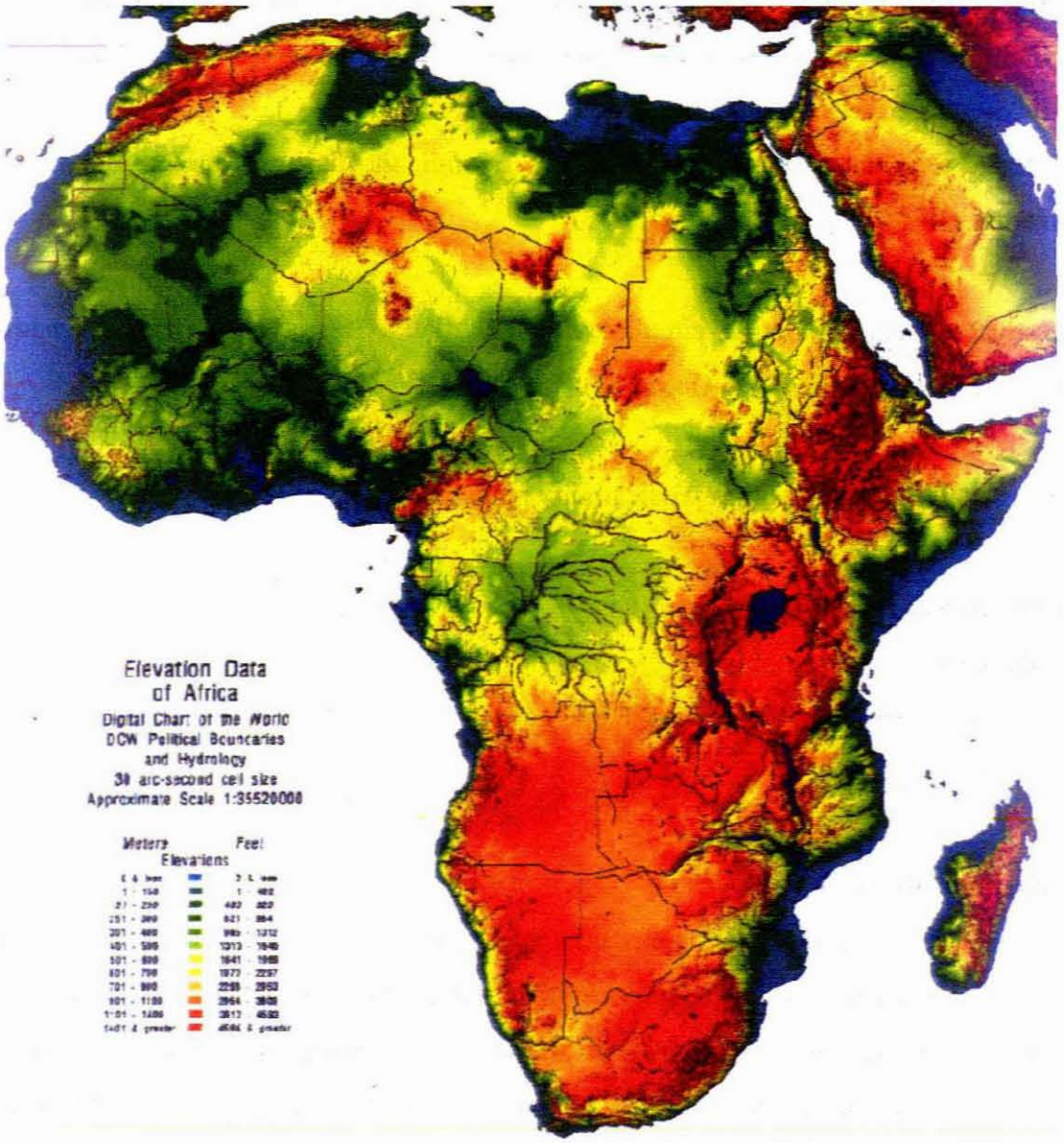

Fig 1.1 Relief map of Africa showing rivers. Topographic heights given in the scale

1.4.2.1.0 Annual cycles

1.4.2.1.1 East and central Africa

East Africa has two major rainfall divisions, the bimodal area and the unimodal area. The bimodal area has two rainy seasons, (October-December) and the (March to May). The unimodal division has one rainy season (November- March). The climate of this area can best be described as that of dry and wet tropics with a distinct dry season. The dry season normally coincides with the austral winter (June-August). The outstanding feature of tropical African precipitation is the marked annual cycle. Many stations have several months with no precipitation, whereas the wettest months have an average of 200 mm or more. The coefficient of variability of precipitation is greater than in the equatorial lowlands (Critchfield, 1975). The lowlands (i.e., the Congo Basin) and tropical coasts exposed to monsoon winds (e.g., Madagascar) experience a tropical rainy type of climate. Rains over the tropical highlands of Africa, South of Lake Victoria, generally begin in November and continue until April (EAMD, 1963; Alusa and Mushi, 1973), with the highest totals in January and February. Synoptic features and wind flow patterns which produce rains in this part of Africa are complex. Studies done by Griffiths, (1959); Nyenzi, 1988 and Ogallo, 1989 suggest that the inter-Tropical convergence zone (ITCZ) is the major source of rainfall in the region as it moves North and South of the Equator lagging behind the solar angle. Monsoon winds and subtropical high pressure systems also influence the rainfall pattern of the region.

1.4.2.1.2 Southern Africa

The annual rainfall distribution over southern Africa has been documented by many researchers (Keen and Tyson, 1977; Mason, 1992; Mulenga, 1998; Mason, 1992;). Apart from the area near Cape Town, southern Africa receives its rainfall from November to March, the Austral summer. Summer rainfall over southern Africa is mainly convective and is associated with the introduction of moist air from the tropics, via meridional cloud bands (Harrison, 1986). Summer rainfall can also be associated with easterly waves from the Indian ocean and the interaction of westerly wave disturbances in the south.

Observational records have revealed that seasonal rainfall over the study area varies from year to year. It is this variability which is a concern to people, especially when extreme cases occur. Are we able to foresee these extreme events? In the next section efforts to identify spatial and

temporal atmospheric and oceanographic patterns associated with precipitation variability at the inter-annual time scale are discussed. Forecasting of seasonal rainfall using statistical models will also be discussed.

1.4.2.2.0 Inter-annual rainfall variability over the study area.

Studies on temporal and spatial aspects of climates have recently revealed remote influences from the Pacific Ocean, El Nino Southern Oscillation. Potential regional/remote forcing of precipitation variability over Africa is discussed.

1.4.2.2.1 *Temporal and spatial variability*

A number of studies on rainfall variability at inter-annual time scale have been done over southern Africa. Over East and central Africa fewer studies have been done mainly focusing on the bimodal rainfall areas and ignoring the unimodal rainfall areas. The importance of these unimodal rainfall areas for Tanzania lies in the fact that the major cereal producing region and catchment areas for the rivers which have been tapped for hydroelectricity power generation are located in this area.

The spatial and temporal variability of rainfall over the continent of Africa with its relation to regional and remote atmospheric and oceanographic parameters have been studied by many researchers among them are Nicholson, 1986; Nyenzi, 1988; Mason, 1992; Janowiak, 1998; Mulenga, 1998. Monthly precipitation over different parts of Africa oscillates at different periods from 2-10 years (Tyson, 1980; Nicholson,1986; Nyenzi, 1988, Jury and McQueen, 1993).

Over East Africa precipitation oscillates with dominant periodicity of between 2.3 and 5 years, which appear to be related to Quasi-biennial oscillations and ENSO events respectively. Using rainfall data from Tanzanian stations similar, results were revealed by Jury and McQueen, (1993).

Over southern Africa a number of dominant periods of oscillation in precipitation have also been revealed. Among the dominant periods of oscillation are the Quasi-biennial oscillations (2-3 year), the Southern Oscillation with a period of 3-5years, the 11-year solar cycle and the 18-year

cycle (a Luni-solar tide). Using station data from 1910 to 1977, Tyson (1980) analysed rainfall anomalies over southern Africa, south of 22°S and revealed the existence of 18-20 year periods in the data.

Mulenga 1998 who performed principal component analysis on DJF rainfall anomalies over southern Africa, identified four regional scale spatial coherent rainfall patterns whose loadings centred over Angola, northern Malawi, eastern Botswana and eastern South Africa. The Quasi-biennial oscillation (2-3 years) was found to be strong in all modes while the Angola mode had ENSO temporal characteristics. The Botswana and Eastern South Africa modes exhibited more spectral energy around the 18 year periods.

Using precipitation data from 1901 to 1973 Nicholson (1986) found six spatial modes of precipitation variability over Africa. Dominant patterns were those with the same sign over the whole continent and another with out-of- phase relationships between precipitation over tropical and subtropical areas of the African continent. Spectral energy of the 5-6 year oscillation was dominant over tropical Africa, whilst periods of 3.3-3.8-years were over eastern Africa. Principal component analysis has been used widely in studying the spatial and temporal pattern of precipitation over Africa. Dyer (1981) described the first four of South African station's annual rainfall from 1921 to 1975. The first mode, with an explained variance of 32%, was loaded over Central South Africa. Spectral peaks for the first PC had (2 - 3-year) Quasi-biennial oscillation and 10-13 year period (solar cycle).

1.5.0 Causes of climate variability

Precipitation over the tropical highlands of east Africa is influenced by the convergence of the moist southeast and northeast trade winds which forms part of the monsoon system of the western Indian Ocean. Westerlies from the Atlantic ocean also influence the precipitation over these areas. Precipitation over the tropical highlands of Africa is associated with the passage of easterly waves and MJO. Further south the passage of temperate westerly wave disturbances and the interaction of these disturbances and easterly wave disturbances from the tropics are associated with precipitation over southern Africa. Winds and rainfall over Africa depend on the relative strength of the subtropical marine high pressure systems while the thermodynamic state of the adjacent Indian and Atlantic Oceans determine the moisture flux.

A number of studies have been done in order to understand the possible causes of rainfall variability over the subcontinent (Lindesay and Jury, 1981; Tyson, 1981; Nyenzi, 1981; Jury and Pathack, 1991; Makarau, 1996). In east Africa the passage of the ITCZ (Inter-tropical Convergence Zone) is associated with two rainy seasons which normally occur during March-May and October- December. Over the southern areas of East Africa only one rainy season is observed which normally occurs from November to March. The ITCZ, over east Africa is a result of low-level convergence of airmass from the two hemispheres which constitute the monsoonal flow. Easterly waves are also associated with precipitation at the coast of East Africa (Lumb, 1966; Nyenzi, 1988). Rainfall in east Africa is also associated with low-level westerly wind (Nakamura, 1968; Mpeta, 1997; Wairoto, 1997). Westerly winds within the tropics at low and middle levels, accompanied with widespread deep convection, are normally associated with passage of the 40-60 day MJO (Madden and Julian, 1971). Southern Africa rainfall variability has been associated with a number of regional circulation anomalies (Miron and Lindesay, 1983; Tyson, 1984; Lindesay and Jury, 1991). These circulation anomalies could be linked to interactions between tropical and westerly wave disturbances, variability in the strength of tropical easterly and temperate westerly disturbances and variability in the intensity of subtropical high pressure systems which controls the strength of the easterly trade winds.

The variability of the 500 hPa circulation field has been linked to precipitation variability over southern Africa (Tyson, 1984). High rainfall amounts over central parts of south Africa is associated with a trough axis over Namibia, Botswana and central Africa. It was also revealed that rainfall variations in southern Africa were associated with the interaction of easterly disturbances from the tropics and temperate westerly disturbances. For example, Lindesay and Jury, (1991) found that interactions between tropical easterly waves, from the south-west Indian ocean and mid-latitude westerly wave disturbance resulted in the floods of February 1988 over south Africa.

1.6.0 Influence of Atlantic and Indian Oceans on African rainfall

Persistently dry and wet periods of several years in the Sahel have been reported by Folland et al., to be accompanied by a global-SST pattern. In a GCM experiment by Palmer (1986) it was found that over the Sahel, the Atlantic and Pacific SST fields induce changes in rainfall whereas the Indian Ocean influence is more limited.

Ward (1998) reported some association between precipitation in Guinea and eastern equatorial Atlantic SST anomalies at the inter-annual time scale. The Indian Ocean SSTs play a more pivotal role in precipitation variability over the highlands of east Africa and a number of studies have indicated this relationship. In their modeling studies Arpe et al., (1998) demonstrated how moderate changes in northern Indian Ocean SSTs affect the Indian summer monsoon. A relationship between summer rainfall in Zimbabwe and Indian ocean SSTs was found by Makarau and Jury, (1997). In their recent modeling study, Reason and Mulenga (1999) have reinforced the observational work which suggests that warm SST anomalies in the south-west Indian ocean are linked with significant rainfall anomalies over southeastern Africa. An association between summer rainfall over some parts of central and eastern south Africa and SST anomalies in the southwest Indian ocean have been revealed by Walker (1990) and Mason (1995). Studies conducted by Ogallo, (1988) have shown an association between the seasonal rains during October-December and SST anomalies in certain oceanic areas. There was however, a relatively weak association between the seasonal rains during March-May and SST anomalies.

1.7.0 Teleconnections

Circulation regimes that alter the preferred location of tropical convection (Harrison, 1986) and the Inter-Tropical Convergence Zone (ITCZ) determine year-to-year fluctuations in rainfall over highlands of tropical Africa. Studies undertaken by Ropelewiski and Halpert, (1987); Janowiak, (1988), have revealed that El Nino-Southern Oscillation warm event in the equatorial Pacific and Indian Oceans are associated with extreme climates over much of Africa. Global ENDO warm events most often influence rainfall in the Austral spring and summer as part of a seasonally dependent response (Meehl, 1988). A strengthening of upper westerly flow throughout the region during warm events, result in a concomitant decline (increase) in moisture confluence over southern (eastern) Africa (Hastenrath *et al.*, 1993). According to Tourre and White, (1995) the tropical Atlantic Ocean can have a delayed response to ENSO, which may induce circulation and convective anomalies over significant parts of Africa with a time lag of the order 12-18 months. According to Cadet, (1985); Jury and Pathack, 1993; Meehl, (1993); Mason, (1995), a warmer tropical Indian Ocean is frequently associated with dry condition over southern Africa. During El Nino conditions, the central Indian Ocean experience changes in wind stress (Hastenrath, *et al.*, 1993) which bring about zonal overturning that spills onto East Africa causing floods. In the equatorial Atlantic, coupled ocean-atmosphere variations have been identified which bear some

resemblance to El Nino events of the tropical Pacific (Weare, 1977; Nicholson and Entekhabi, 1987). Furthermore it has been revealed that Atlantic SST variability affects rainfall over the western half of southern Africa (Jury, 1996). However, there are still many questions to be answered: How does the Atlantic zonal circulation respond to local and remotely driven SST forcing (e.g., ENSO, N-S dipole): How does Congo Basin convection spread across tropical highlands of tropical Africa?

1.8 Forecasting seasonal rainfall over the highlands of tropical Africa

Forecasting of seasonal rainfall is a serious challenge to climatologists all over the world and in particular over the African continent where most countries depend on rain-fed agriculture. The poor state of the economies obliges people to maximise the use of available water resources for hydroelectric power generation. Dynamical and statistical seasonal rainfall forecasting is at an advanced stage on the global level and forecasting results are quite promising. Dynamical or numerical prediction is difficult for most African countries because of the operational resources required. Statistical modelling is within operational capabilities in most national meteorological centres in Africa.

The science of long-range-forecasting started more than one hundred years ago in India when attempts were made to forecast the seasonal monsoon rainfall. The first long range forecast of summer monsoon rainfall over the whole of India and Burma, which was based on the extent of Himalayan snow cover, was issued on June 4, 1886 by Blanford, (1884). Since then the seasonal monsoon rainfall forecasts have been issued by the India Meteorological department every year and efforts have been continued to develop better techniques. Forecasting of seasonal monsoon rainfall over India was the motivation for sir Gilbert Walker's (1923, 1924) pioneering work on the Southern Oscillation. In 1910 he introduced the concept of point-to-field correlation mapping and developed a Multiple Regression model (Walker, 1910) for forecasting the monsoon rainfall over India. Since then, the correlation technique is widely used, in one form or another.

Recent efforts have resulted in the development of new types of LRF models namely, dynamic stochastic transfer (Thapliyal, 1982, 1990), Parametric (Gowariker et al., 1989) and Power Regression (Gowariker, 1989, 1991). Initial attempts at forecasting seasonal rainfall used a single parameter to forecast rainfall. These types of forecasts were later discontinued as they did not exhibit reasonable accuracy. In 1907, Sir Gilbert Walker (1910) introduced an objective method of correlation in seasonal rainfall forecast or LRF (Long Range Forecast). His method was based

on the assumption that the association of various antecedent meteorological factors with the forecast element found in the past by correlation technique, will persist in the future also. The first multiple regression model based on this principal, contained four predictors namely, the Himalayan snow accumulation at the end of May, south American pressure for Spring, Mauritius for May and Zanzibar District rain for April and May. Using the correlation technique, Walker, 1923 embarked on a world wide search for an association between the Indian monsoon rainfall and antecedent weather features in different parts of the world. Despite wide use, the correlation technique has limitations. For example, Thapliyal (1987) found that summer monsoon rainfall forecasts were correct on about 65% of occasions. Thapliyal (1987) attributes this failure to the fact that the model projects the relationship (measured by the correlation coefficient) observed in the past, into the future and this change with time. To account for the ebb and flow of historical relationships, the updating of operational multiple regression-models is done on a regular basis, Thapliyal 1991.

Over southern Africa, many researchers have developed seasonal forecasting models (Jury et al., 1999). The Multiple regression technique is the method of choice, whilst composite and principal component analyses are the main diagnostic tools. Using PCA and correlation mapping Mason, (1992); Jury et al., (1999), identified SST indices for use in multiple regression models to forecast summer rainfall over southern Africa. In East Africa internal efforts have progressed slower. Attempts at creating a seasonal forecasting model in Tanzania have been done by Nyenzi et al., (1997). The parametric model attempted to forecast MAM, OND, and O-A (October to April) rainfall using ENSO and SSTs in two areas of the tropical west Indian and eastern Atlantic Oceans.

The objective of this thesis is to 'underpin' rainfall forecasting models for southern and eastern Africa. Principal component analysis was used to identify coherent patterns in predictand and predictor parameters. This spatially aggregates the variables. The correlation technique employed used to identify predictor parameters which are significantly associated with the respective predictand (target).

1.9 Statistical modelling of rainfall

Some of the common modelling techniques used, are: Persistence, Analogues, quasi-periodic,

multiple regression, Parametric, Dynamic (numerical), canonical correlation analysis (CCA), etc. In this study multiple regression method is used to formulate seasonal forecasting models for the two selected areas, i.e. east and southern Africa. This method, which is basically a linear correlation method, is based on the assumption that the association of various meteorological factors with the forecast element, found in the past by the correlation technique will remain the same in future. Though this technique has demonstrated some skill for some regions and seasons of the world, there is a problem of stability of correlation coefficients used in regression forecasting as these change with time in both magnitude and in their sign (Rao, 1964; Thapliyal, 1986). In order to avoid this problem the India Meteorological Department updates their models every year by dropping unstable predictors and at times, adding a few promising ones. Details of these methods can be found in Thapliyal (1991). Using a similar approach, i.e. of the correlation technique, potential predictors for rainfall over east and southern Africa have been identified in chapter 5 and shall be used to create forecasting models for these areas.

Rainfall variability at the annual time scale over the tropical highlands of Africa is controlled by the north-south movement of the sun. Observations show that the seasonal total is significantly modulated. Similarly the spatial distribution of rainfall is different for different areas due to a number of factors such as differences in topography, prevailing wind regimes, and passing storm tracks. Research work has established that rainfall over a larger part of the tropical highlands of Africa is influenced by the ENSO phenomenon, though its influence is not entirely deterministic. Even in the absence of extreme of ENSO cases drought or flood conditions may be experienced. Hence, other regional features must influence inter-annual rainfall variability.

A number of research works have been done over east and southern Africa on mechanisms of rainfall variability at inter-annual time scale (Nicholson, 1986; Nicholson and Entekhabi, 1987; Nyenzi, 1988; Ogallo, 1989; Walker, 1989; Mason, 1992 and Mulenga, 1998). Most of these studies have put emphasis on the association between rainfall, ENSO and SST over the Atlantic and Indian Oceans. Walker, (1989) analysed SST associations from the south-west Indian and Atlantic Oceans (0°-40S, 20°-70°W). Similarly Mason (1992) studied the association of southern Africa rainfall and SST over the Indian and Atlantic Oceans in the domain 0-50°S, 70°W-70°E. Mulenga (1997) used SST monthly time series data (1950-1991) from the United Kingdom Meteorological Office (UKMO) and performed PCA in the domain 17.5°N-37.5°S, 47.5°W-97.5°E. His work mainly focussed on how the Angola low modulates rainfall over southern Africa and the association of the Atlantic and Indian Ocean to ENSO.

In this study use shall be made of monthly SST and sea level pressure (SLP), zonal (U) and meridional (V) wind components over the Atlantic and Indian Oceans in the domain 20°N-40°S, 70°W-100°E from January 1965 to December 1995. SST and SLP are important in this study because they are appropriate to investigate the hydrostatic interaction between the oceans and atmosphere. From the results action centres are identified for use in modelling the inter-annual rainfall over east and southern Africa.

This study is expected to achieve the following goals:
Find the principal mechanisms responsible for the inter-annual variability of rainfall over the tropical highlands of Africa. Identifying regional/global predictors to be used in seasonal prediction of rainfall over the highlands of tropical Africa. Study the anti-phase relationship between the east Atlantic and west Indian Ocean SST and its influence on convection over the highlands of Africa. Identify the major inter-annual spatial and temporal patterns of climates which can help in the prediction of seasonal rainfall over east and southern Africa.

In chapter two the observational data used to study the mechanisms of inter-annual rainfall variability over the tropical highlands of Africa shall be described. The continuous wavelet transform method, which transforms a time series to a two-dimensional frequency-time domain, will be discussed.

CHAPTER 2

2 .0 Data and Methodology

2.1.0 Data

To study inter-annual climate variability gridded mean monthly rainfall and temperature data over the African continent, from the Climate Research Unit (CRU), and COADS (Comprehensive Ocean Atmosphere Data Set) gridded SST, SLP, U and V surface winds are used. In some cases' NCEP gridded kinematic and thermodynamic data are considered. Station rainfall data from Tanzania are used as a reference, but the even data coverage of the CRU gridded rainfall is advantageous in statistical analysis. The period 1965-1995 was chosen for the study because it was found that there were few missing data in the COADS data set. For climatological studies this 31-year period is acceptable. A short description of the data follows in the next section.

2.1.1 Comprehensive Ocean Atmosphere Data Set (COADS)

The Comprehensive Ocean Atmosphere Data Set (COADS) is an extensive collection of surface marine data available for the world ocean. COADS is a result of a continuing cooperative project in the National Oceanic and Atmospheric Administration (NOAA) – specifically its Environmental Research Laboratories (ERL), National Climate Data Centre (NCDC), and Cooperative Institute for Research in Environmental sciences (CIRES) conducted jointly with the University of Colorado -- and the National Science Foundation's National Centre for Atmospheric Research (NCAR). The parameters used from this data set were Sea Surface Temperatures (SST), Sea Level Pressure (SLP), Zonal (U) Wind Component and Meridional (V) Wind Component. Mean 'enhanced' monthly statistics were extracted from the Indian and Atlantic Oceans in the domain 30°N-40°S, 70°W-100°E for the period 1965-1995. The period 1950-1964 was excluded because of too many missing data. The enhanced statistics, whose record period is from 1950 to 1995, were derived using 3.5 sigma trimming limits (a quality control procedure used to identify outliers with respect to climatological values). The trimming limits still allow for extreme climate events. In order to increase coverage, marine observations from ships, fishing vessels, and surface oceanographic measurements were combined. The data is accumulated into 10°x10° Lat./Lon. grid boxes from which inter-annual patterns are extracted for the Atlantic and Indian Oceans.

2.1.2 Climate Research Unit (CRU) data

Gridded monthly rainfall and temperature data for continental Africa were obtained from the (Climate Research Unit -University of East Anglia, 1998). The 2° latitude/longitude gridded mean monthly precipitation and temperature data for the period 1951 to 1995 were created from 3 minute latitude/longitude grids of mean monthly precipitation and temperature data. The 3 minute latitude/longitude grids were constructed using 2307 stations for precipitation and 1485 stations for temperature. Uniform gridded data were obtained by interpolation of irregular station data. A thin-plate spline technique was used to interpolate the mean climate surfaces as a function of latitude, longitude and elevation. The technique is robust in areas with sparse and irregularly spaced data as is the case in Africa (Wahba, 1979). Hutchinson (1995) provides a theoretical description of its application to surface climate variables such as precipitation.

2.1.3 NCEP data

Kinematic and thermodynamic re-analysis data were obtained from the National Centre for Environmental Prediction (NCEP). The re-analysis project which is a joint project between NCEP and NCAR, (Kalnay et al., 1996) and is aimed at producing a 40-year record of global atmospheric fields. The project is involved in the recovery of land surface, ship, rawinsonde, pibal, aircraft, satellite and other data; quality control and assimilating the data with a system that is kept unchanged over the re-analysis period 1958-1998. This type of approach eliminates perceived climate jumps associated with changes in the data assimilation system. Table 2.1 gives a classification of the selected parameters according to relative influence of observational data and the model on the gridded variable. Mean monthly temperature, geopotential height, zonal and meridional winds, and sea level pressure, and vertical velocity were retrieved for all levels between 1000hPa and 100hPa inclusive, while relative humidity and specific humidity were retrieved between 1000hPa and 300hPa levels inclusive. Stream function and velocity potential were available at two levels, i.e., 850hPa and 200hPa. Other integrated variables like precipitable water were also utilized. These data were retrieved from 1965 to 1995 to match the CRU and COADS data. NCEP data has been used in numerous climatological studies, such as by (Webster et al., 1999; Hastenrath, 1999, 2001).

Table 2.1: Classification of parameters according to observational data and the model on the gridded variable

CLASS A		CLASS B	
PARAMETER	UNIT	PARAMETER	UNITS
Zonal wind	m s^{-1}	Surface pressure	hPa
Meridional wind	m s^{-1}	Specific humidity	
Pressure reduced to msl	hPa		

CLASS A: Indicates that the analysis variable is strongly influenced by observed data and hence it is in the most reliable class (upper-air temperature and wind).

CLASS B: Indicates that although there are observational data that directly affect the value of the variable, the model also has a very strong influence on the analysis value (e.g., humidity and surface temperature).

2.1.4 Station Rainfall data

Station monthly rainfall data for the period 1965-1995 were available from the Tanzania Meteorological Agency listed in table 2.2. The Southwestern area of Tanzania is considered. Station monthly rainfall data is used to cross-check the adequacy of gridded rainfall data from CRU which is used extensively in this study. Monthly station rainfall averages, within the box 30°-36°, 4°S-10°S, were calculated to obtain a time series index which was used to compare with the gridded rainfall data from CRU extracted in the same box (fig 2.0). Stations within the box had uninterrupted data between 1965 and 1995. The correlation coefficient between monthly station rainfall averages and monthly gridded rainfall data obtained in the same box was +0.78, significant at 99% confidence limit.

Fig 2.0: Stations in table 2.2 sampled in the box shown

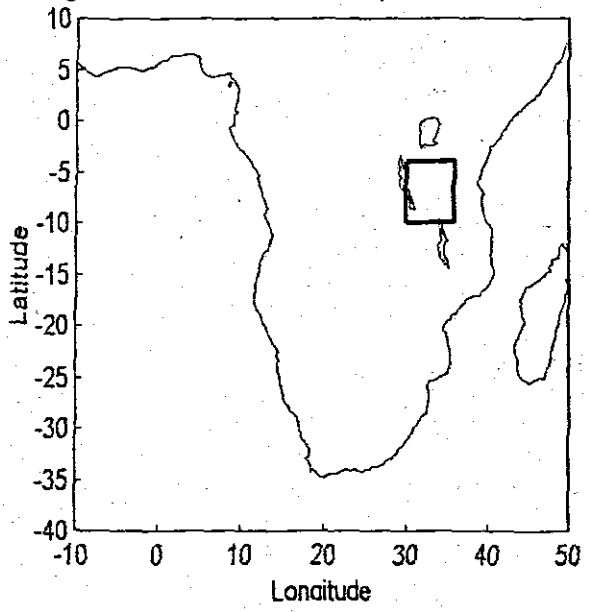

Table 2.2 Rainfall stations used in the comparison with CRU gridded rainfall data

STATION NAME	STATION NUMBER	LATITUDE	LONGITUDE
Nzega Boma	9433000	4.3°	33.2°
Tabora Met	9532012	5.1°	32.8
Mwanhala	9433002	4.4°	33.1°
Mpanda	9631005	6.3°	31.1°
Kigoma Met.	9429018	4.9°	29.9°
Singida	9434001	4.8°	34.7°
Kondoa	9435025	4.9°	55.8°
Manyoni	9534000	5.7°	34.8°
Dodoma Met.	9635001	6.2°	35.8°
Iringa Met.	9735013	7.6°	35.8°
Luponde	9934013	9.5°	34.7°
Ichenge	9934024	9.5°	34.8°
Njombe Wattle	9934015	9.4°	34.7°
Songea	10035010	10.7	35.6
Peramiho	10035006	10.5°	35.5°
Helvetia	9934027	9.6°	35.7°
Igeri Agriculture	9934029	9.7°	35.6°
Njombe bomani	9934001	9.3°	34.8°
Chunya	9833002	8.5°	33.4°
Mbeya Met.	9833001	8.9°	33.5°
Luiga	9835022	8.6°	35.3°
Ifupirra	9835019	8.5°	35.4°
Matuguta	9835034	8.6°	35.3°
Chivanjee	9933016	9.4°	33.7°
Kilima	9835009	8.6°	35.2°
Kyela	9933010	9.6°	33.8°

2.1.5 Teleconnection Indices

2.1.5.1 ENSO

El Nino is an extensive warming of the upper Ocean in the tropical eastern Pacific lasting up to three seasons. The negative, or cool phase of El Nino is called La Nina. El Nino events are linked with a change in atmospheric pressure known as the southern Oscillation (SO), (Glantz, et al., 1991). The Southern Oscillation is characterised by a see-saw in atmospheric pressure between the western and eastern regions of the Pacific Ocean, with one centre of action located south of Indonesia and the other centre located near Tahiti. The SOI, which is an index that measures the magnitude of SO is

obtained by calculating the difference in atmospheric surface pressure anomalies between Tahiti and Darwin Australia. As the SO and El Nino are closely linked with each other, they are collectively known as the *El Nino - Southern Oscillation, or* "ENSO". *Another measure of the magnitude of* El Nino events, is sea surface temperature averaged over a specific region of the Pacific Ocean, such as the Nino3 region which extends from 150°W to 90°W and 5°N to 5°S. The return period of El Nino events is varied, ranging from two to seven years. *The intensity and duration of the event are* also varied yet predictable to some degree. Typically, it lasts anywhere from 14 to 22 months. ENSO events are those in which both El Nino and Southern Oscillation occur together. El Nino often begins early in the year and peaks between the following November and January. *ENSO events are known* to influence rainfall over the African continent (Ropelewski and Halpert, 1987; Ogallo, 1994). The Nino3 SST index from 1965 to 1995 is used in this study.

2.1.5.2 Indonesia sea-level pressure anomalies

The Indonesia sea level pressure anomaly index is the standardized sea level pressure over Indonesia. This index has some ENSO characteristics and has been acquired from the NOAA web site *(http://www.cdc.noaa.gov/), from 1965 to 1995.*

2.1.5.4 Quasi-biennial Oscillation Index (QBO)

The Quasi-biennial oscillation is a zonal stratospheric wind reversed over the tropics with an oscillation period of 24-26 months. In this study use is made of the zonal wind index (m/s) at 30 hPa of Marquardt and Naujokat, (1997). The index is a concatenation of values at Canton Island (3°S, 172°W) for January 1953- August 1967; Gan./Maldives (1°S, 173°E) for September 1967- December 1975; and Singapore (1°, 104°E) from January 1976-February 1999. QBO index data from January 1965-December 1995 is used in this study to match with other data sets. Naujokat (1986) documents the data, uncertainties in the early years due to lack of daily data, change in reference stations, and the general features of QBO.

2.2.0 Methodology

In order to study inter-annual rainfall variability over an area and at the same time to capture mechanisms which cause the variability use is made of indices which help to define rainfall over such

an area. There are many methods which can be used to create indices, among them is principal component analysis which helps to extract coherent patterns in spatial data. Area averages are then calculated for stations falling within these coherent patterns. In this way the number of data is reduced and meso-scale features are filtered out. In order to understand the spectral characteristics of the resulting time series a continuous wavelet analysis is done as described later. Composite analysis is also used to study the thermodynamic and kinematic features associated with dry and wet scenarios for various patterns of rainfall and temperature. Statistical association is also analysed using Pearson's product correlation. These methods are further described in the following section.

2.2.1 Principal Component Analysis (PCA)

Principal Component Analysis (PCA) is a multivariate statistical technique having wide applications in meteorology (Lyons, 1982; Yin, 1984; Basalirwa et al., 1998). The method reduces the number of variables whilst explaining variability within the original record (Jolliffe,1993). PCA is done when the original data contains grid point variables that are spatially correlated, as is in the present study for gridded rainfall and temperature data over Africa; and gridded SST, SLP, U and V wind over the Atlantic and Indian Oceans. Application of PCA thus reduces the original data to subsets ranked in order of importance.

Principal components (PCs) or modes are produced via PCA, each consisting of an eigenvalue that quantifies the variance, a set of loadings (eigenvectors) that describe the spatial distribution (coherent patterns) and a set of time scores that define the evolution. The first PC is a linear function accounting for the highest variance, i.e., the dominant pattern. The second PC is the linear function with the next highest variance subject to being uncorrelated with the first PC. Subsequent PCs are all linear functions ranked in order of decreasing variance which are not correlated with each other or with the first and the second PCs (Jolliffe, 1990). When carrying out PCA the correlation matrix technique was chosen to avoid the analysis being dominated by high variance. This approach enables a focus on relative rather than absolute variability of the variables. The first nine rainfall PCs were retained for further analysis as they explained a large amount of variance (see table) and these could be interpreted easily. Varimax rotation was performed on the remaining nine PCs. Rotation is normally used to simplify the structure of the eigenvectors and facilitate interpretation.

Mathematical details of PCA follows:

Consider having P variables, then the number of parameters to be estimated shall be P- means, P - Variances, and $[(p^2 - p)/2]$ Co-variances; that is a total of $(p^2 - p)/2 + 2p$ parameters. The PCA creates uncorrelated variables such that there remain about $2p$ parameters to estimate, i.e., p-means and p-variances (there are no co-variances between the variables as they are uncorrelated) these could be easy to estimate and interpret. So the relation of any single transformed element of the vector variable to any external criterion variable is independent of relation of any other element to that criterion, and can be interpreted separately and unambiguously. When meteorological/climatological data is collected at different stations over a region, it turns out that the data are usually correlated. If an uncorrelated vector variable is desired, the data need to be transformed. Consider a general linear transformation vector variable z of the form

$$y = V'z$$

where V is a p x n coefficient matrix that carries the p-elements variable z into derived n-element variable y.

The centroid or the mean of y

$$my = v'm_2 = 0 \text{ because } m_2 = 0,$$

and the dispersion of y is

$$D_y = v' D_z v = v' Rv$$

where R is the correlation matrix of z (since the dispersion of a standardized variable is a correlation matrix). To reduce a transformation vector y (principal components) for which the elements are uncorrelated, is the same as saying that a v vector becomes is a diagonal matrix Dy. That is, all off-diagonal elements of Dy must be zero. There is an infinite number of values of v that will yield a diagonal Dy for any given correlation matrix R.

The problem is to "find a unique V such that Dy is diagonal". The next restriction is to maximize the variances of the leading elements of y whose variances are maximized or principal components as they are called by Hotelling (1933).

For the first principal component, which will be the first element of y, and will be explained by the coefficients in the first column of y, and will be defined by the first coefficients in the first column of V (denoted by v_1), a solution is required such that the variances of y_1 will be maximized. The

restriction will be such that the sum of squares of the coefficients in v_l be unity, i.e.,

$$\frac{1}{N}\sum_{i=1}^{N} y_{1i}^2 \Big|_{\max}$$

where $y_{1i} = v_1' z_i$

and $v_1' v_1 = 1$ (Normalizing v_l)

but $$\frac{1}{N}\sum_{i=1}^{N} y_{1i}^2 = \frac{1}{N}\sum_{i=1}^{N} \left(v_1' z_i\right)^2$$

$$= \frac{1}{N}\sum \left(v_1' z_i\right)\left(z_i' v_1\right)$$

$$= v_1' \frac{1}{N}\sum \left(z_i z_i'\right) v_1 = v_1' R v_1$$

we want to maximize $v_1' R v_1$ subject to $v_1' v_1 = 1$

$$\text{Let } \phi_1 = v_1' R v_1 - \lambda_1\left(v_1' v_1 - 1\right)$$

Introducing the restriction on v_l to the function to be maximized via the Lagrange multiplier λ_l. The vector of partial derivatives is

$$\frac{\partial \phi_1}{\partial v_1} = 2Rv_1 - 2\lambda_1 v_1$$

and setting equal to zero, dividing throughout by 2, and factoring gives

$$\left(R - \lambda_1 I\right) v_1 = 0 \quad \text{.....1}$$

which is the problem of Eigen structure of R.

The partial differentiation results in a set of p homogeneous equations which can be written as:

$$\begin{aligned}
v_1(1-\lambda) + \; & v_2 r_{12} + v_3 r_{13} + \ldots + v_p r_{1p} = 0 \\
v_1 r_{21} + \; & v_2(1-\lambda) + v_3 r_{23} + \ldots + v_p r_{2p} = 0 \\
v_1 r_{31} + \; & v_1 r_{32} + v_2(1-\lambda) + \ldots + v_p r_{3p} = 0 \\
& \cdots \\
& \cdots \\
v_1 r_{p1} + \; & v_2 r_{p2} + v_3 r_{p3} + \ldots + v_p(1-\lambda) = 0
\end{aligned}$$

The above equation can also be written as matrices as follows:

$$\begin{bmatrix}
(1-\lambda_i) & r_{12} & r_{13} & \cdots & r_{1p} \\
r_{21} & (1-\lambda_i) & r_{23} & \cdots & r_{2p} \\
r_{31} & r_{32} & (1-\lambda_i) & \cdots & r_{3p} \\
 & & & & \\
r_{p1} & r_{p2} & r_{p3} & \cdots & (1-\lambda_i)
\end{bmatrix}
\begin{bmatrix} v_{1i} \\ v_{2i} \\ v_{3i} \\ \\ v_{pi} \end{bmatrix} =
\begin{bmatrix} 0 \\ 0 \\ 0 \\ \\ 0 \end{bmatrix}$$

Finally, in matrix notation this becomes equation 1

The characteristic equation of R is a polynomial of degree p gotten by expanding the determinant of

$$|R - I\lambda| = 0 \quad \ldots\ldots\ldots\ldots\ldots\ldots\ldots\ldots\ldots\ldots\ldots\ldots\ldots\ldots \quad \mathbf{2}$$

and solving for the roots λ. Specifically, the largest eigenvalue λ_1 and its associated vector v_1 are required. Letting λ_1 be the largest root of the characteristic equation for R, we substitute it and its vector in equation 1 which is expanded and then multiplied by v_1' on the left:

$$\begin{aligned}
& Rv_1 - v_1\lambda_1 = 0 \\
& Rv_1 = v_1\lambda_1 \\
& v_1' Rv_1 = v_1' v_1 \lambda_1 = \lambda_1
\end{aligned}$$

Note: $v_1' v_1 = 1$

So that λ is clearly the variance of the normalized linear component of z that has maximum variance. Next we want to find the normalized linear combination

$$y_2 = v_2' z$$

which, out of all the components of uncorrelated with y_1 has maximum variance. The statistical restriction of uncorrelated ness of y_1 and y_2 is stated as

$$\frac{1}{N}\sum_{i=1}^{N} y_{2i}y_{1i} = 0$$

where

$$\frac{1}{N}\sum y_{2i}y_{1i} = \frac{1}{N}\sum\left(v'_2 z_i\right)\left(v'_1 z_i\right)$$

$$= \frac{1}{N}\sum\left(v_2' z_i\right)\left(z'_i v_1\right)$$

$$= v_2' \frac{1}{N}\sum\left(z_i z'_i\right)v_1$$

$$= v_2' R v_1 = v_2' v_1 \lambda_1$$

but this can be zero only if

$$v_2' v_1 = 0$$

which states the requirement of geometric orthogonality of the eigenvectors.

Introducing a second Langrange multiplier λ2 to get the orthogononality restriction into the calculus problem, it is required to maximize

$$\phi_2 = v'_2 Rv_2 - \lambda_2\left(v_2' - 1\right) - v_1 v_2' Rv_1$$

$$\frac{\partial \phi_2}{\partial v_2} = 2Rv_2 - 2\lambda_2 v_2 - 2v_1 Rv_1$$

and setting equal to zero, dividing out 2, and multiplying on the left by v_1' gives

$$v_1 Rv_2 - \lambda_2 v_1' v_2 - v_1 v_1' Rv_1 = 0$$

which reduces to

$$- v_1 v_1' Rv_1 = 0$$

showing that v_1 must equal zero and λ_1 and v_2 must be the second root of the characteristic equation 2. This process may be continued to get p-1 maximal variances λ_j for components $y_j = v_j' z$

letting L be a diagonal matrix with λ_j in the j[th] position on the diagonal, the full eigen structure of R is given by

$$RV = VL$$

where $V'V = VV' = I$

and $V'RV = L = D_y$

In PCA we normally compute

$$RV = VL$$

So that λ_1 is the maximum value the variance of a component of 2 can have, subject to the normalization of the vector v_1. Then λ_2 is a maximum *given* λ_1, and so on for the remaining eigenvalues. Each component has a maximum variance and of all possible normalized linear functions statistical uncorrelated *and geometrically* orthogonal to the ones preceding.

2.2.2.0 Key areas

2.2.2.1 Selection of key areas and creation of time series indices

The number of PC modes retained to study the annual cycle was two, with the seasonal cycle removed to study inter-annual variability - three modes were retained. In each case, for all parameters, the PCA was done first unrotated, then Varimax rotated. The first and third rainfall PC modes, were picked for further analysis; while the second PC mode was not picked because it was loaded over the Congo/Angola areas where data is known to be unreliable. For SST, SLP data PC 1 to PC3, for both un-rotated and rotated modes, were picked for further analysis. U wind PC 1-3 un-rotated loading areas and PC 1 and PC 3 rotated were picked for analysis. The rotated zonal wind components PC 2 mode was not selected because the loading area was similar to that of PC 2 un-rotated mode. Finally the rotated V wind PC1 to PC3 modes were selected. Key areas were identified from PC modes and time series were created by area averaging of values within maximum spatial loadings from January 1965 to December 1995. For convenience boxes were created to cover large loading values instead of using the non-geometrical shapes of the loading areas. In cases where there are two areas, then the averages from the two areas were calculated and added or subtracted, depending on the sign. In this way time series were created with 372 data points for the target (rainfall and temperature) and predictor (environmental parameters) key areas based on PCA.

2.2.2.2 Correlation coefficients between key areas and respective selected extracted PCs

Principal component analysis was performed on continental gridded rainfall and temperature data and gridded SST, SLP, and U and V wind data with seasonal cycles and without seasonal cycles. Based on these PCs, key areas were chosen for further analysis (see table 2.3). Correlation analysis was done between the selected PCs and respective key area time series (Table 2.4). Key areas are considered to be superior in operational applications - as they are easier to obtain and track over time, and also they represent fixed-area anomalies that do not receive small contributions from outlying areas. In

the following chapters mention will be mainly on key areas rather than PCs

Table 2.3: Description of the PCs for different parameters, their approximate loading areas and their names. The first column gives the parameter name, while the second column provides the PC mode. The third column gives the approximate location with large loading values and the fourth column the name of the key area. The key area name comprises the parameter name and the ocean basin. When large loading areas are over the two oceans simultaneously, the key area name comprises the names of the two oceans with a + or - sign.

Parameter	PC Mode	Key Areas (Lon, Lat)	Key area name
SST	PC1	60°E-90°E,10°N-10°S + 50°W-10°W,20°N-10°S	SST Ind+Atl
SST	PC2	60°W-20°W,10°N-20°N - 30°W-0°,0°-30°S	SST Atldipole
SST	PC3	50°W-0°,10°N-10°S - 40°E-60°E, 0°-30°S	SST Ind-Atl
SST	PC1R	50°E-90°E, 0°-20°N	SST Ind
SST	PC2R	30°W-10°E, 10°N-20°S	SST eastAtl
SST	PC3R	40°W-10°W, 30°N-10°	SST northAtl
SLP	PC1	40°E-100°E,10°N-10°S + 50°W-0°,10°N-20°S	SLP Ind+Atl
SLP	PC2	60°E-90°E,10°N-20°S - 70°W-10°W,0°-30°N	SLPInd-Atl
SLP	PC3	70°W-10°W,10°N-30°N - 30°W-0°W,10°S-30°S	SLP AtlDipole
SLP	PC1R	30°W-0°, 0°-20°S	SLP Atl
SLP	PC2R	70°E-100°E, 0°-30°N	SLPInd
SLP	PC3R	40°W-10°W, 10°N-30°N	SLP NwestAtl
U ZONAL WIND	PC1	60°W-30°W,10°N-20°N + 40°E-90°E,20°S-40°S	U Atl+Ind
U ZONAL WIND	PC2	70°E-100°E,10°N-10°S	U Ind
U ZONAL WIND	PC3	40°W-10°W,10°S-20°S + 50°E-80°E,10°S-20°S	U Atl+Ind2
U ZONAL WIND	PC1R	60°W-10°W, 10°N-10°N	U Atl1
U ZONAL WIND	PC3R	40°W-0°, 10°S-30°S	U Atl2
V MERIDIONAL WIND	PC1R	20°W-10°E, 10°S-40°S	V Atl1
V MERIDIONAL WIND	PC2R	40°W-10°W, 20°N-10°S	V Atl2
V MERIDIONAL WIND	PC3R	40°E-70°E, 20°N-10°S	V Ind

Where R stands for Rotated

Note: PCA spatial loading pattern are illustrated in chapter 4

Table 2.4 CORRELATIONS BETWEEN EXTRACTED KEY AREAS and PCs

		Rfn PC1	Rfn PC3	SST						SLP					
				PC1	PC2	PC3	PC1R	PC2R	PC3R	PC1	PC2	PC3	PC1R	PC2R	PC3R
Southern Africa		-													
E. Africa			0.78												
SST	Ind+Atl			-			-0.9								
	AtlDipole				0.89										
	Ind-Atl					0.75									
	Ind			0.79			-0.7								
	eastAtl							0.34							
	northAtl			-			-0.6	0.60							
SLP	Ind+Atl									-0.9					
	Ind-Atl									-0.8					
	AtlDipole														
	eastAtl												-0.5		
	eastInd													0.79	-0.26
	NwestAtl														

Table 2.4 Continued

		Zonal Wind					Meridional Wind		
		PC1	PC2	PC3	PC1R	PC3R	PC1R	PC2R	PC3R
Zonal Wind	Atl+Ind1	0.86							
	Ind		0.8						
	Atl+Ind2			-0.48					
	Atl1				0.94				
	Atl2					-0.81			
Meridional wind	Atl1								
	Atl2							0.24	
	Ind								-0.2

2.2.3.0 Continuous Wavelet Analysis (CWT)

In studying spectral characteristics of geophysical data which is mainly non-stationary many researchers use standard Fourier techniques that yield spectral coefficients that are averaged over the entire measurement period Meyers and O'Brien (1994). Fourier methods do not produce information on the time evolution of a signal. Wavelet transform (WT) is an analysis tool which is appropriate to the study of multi-scale, non-stationary processes occurring over finite spatial and temporal domains Lau and Weng (1995). This analysis tool is becoming a common tool for analysing localized variations of power within a time series. With the ability of WT to resolve a time series within a time-frequency space, one is able to determine dominant modes of variability and how those modes vary in time, Torrence and Compo (1998). Wavelet transform, which was introduced by Morlet (1983) has found wide application in a wide field of sciences, like image processing, optics, turbulence etc. A number of geophysical studies have used this technique and have produced some interesting results. In recent years wavelet analyses are becoming common into atmospheric and oceanographic literature (Kumar and Foufoula-Georgiou, 1993; Gamage and Blumen, 1993; Weng and Lau, 1994; Meyer and O'Brien, 1994; Gu and Philander, 1995; Gollmer et al., 1995; Wang and Wang,1996; Baliunas et al., 1997 and Kukarin, 2000). In this study wavelet analysis is used to decompose a number of time series into time-

frequency space. Time scores from rainfall and temperature, and environmental parameter key area indices PCA are analysed to enable us determine the dominant modes of variability and how these modes vary in time. The time-frequency space might provide a better picture in understanding the frequency and amplitude modulation within the period of measurement for a number of parameters. A brief introduction to the idea of wavelet transform is presented below; a complete description of geophysical applications can be found in Foufoula-Georgiou and Kumar (1995), while a theoretical treatment of WT is covered in Daubechies (1992)

2.2.3.1 Wavelet Transform Technique (Adopted from Melice, pers com., 2000)

The WT is a mathematical tool which allows the decomposition of the signal $x(t)$ in terms of elementary contributions called wavelets. These wavelets are obtained from a single function φ by translations and dilations:

$$\varphi_{b,a}(t) = \frac{1}{a}\varphi\left(\frac{t-b}{a}\right) \quad \text{..... 3}$$

where a (>0) is the dilation (scale) parameter and b is the translation (position) parameter; both are real variables. As the CWT will be used to filter the data, here the normalisation $1/a$ is chosen instead of the usual $1/\sqrt{a}$ (Delprat et al., 1992). The CWT of the signal $x(t)$ with the analysing wavelet φ is the convolution of $x(t)$ with a set of dilated and translated wavelets:

$$W_x(b,a) = \frac{1}{a}\int_{-\infty}^{\infty} x(t)\varphi^*\left(\frac{t-b}{a}\right)dt \quad \text{..... 4}$$

where * denotes the complex conjugate. The wave is transformed and defined as continuous since a and b may be varied continuously Meyers and O'Brien, (1994). The CWT expands the time series $x(t)$ into a two dimensional parameter space (b, a) and yields a measure of the relative amplitude of local activity (over an interval proportional to a) at scale a and b. The scale parameter a in $W_x(b,a)$ corresponds to wavelength or period if the data is spatial or temporal respectively. The choice of the wavelet φ depends on the signal to be analysed. In this study a wavelet that is well localized in the frequency space such as the Morlet continuous complex wavelet (Morlet, 1983) is selected. This

wavelet is defined by:

$$\varphi(t) = \pi^{-1/4} e^{-t^2/2} e^{i\omega_0 t} \quad \text{..... 5}$$

where $i = \sqrt{-1}$ and $\omega_0 = 5.4$ is chosen large enough to ensure that φ satisfies the admissibility condition:

$$\int_{-\infty}^{\infty} \varphi(t)dt = 0 \quad \text{..... 6}$$

is satisfied. For the Morlet wavelet, it makes sense to identify the inverse of the scale to a frequency. The relation between the scale a and the usual frequency f is given by (Meyers et al., 1993):

$$f = \frac{\omega}{2\pi}\left(\frac{\omega_0}{a} + \frac{\sqrt{2+\omega_0^2}}{\omega_0}\right) \quad \text{..... 7}$$

The Morlet wavelet can in fact be interpreted as a bandpass linear filter of weight $1/a$ centred around $\omega = \omega_0/a$. Finally, the CWT with the Morlet wavelet is a time-frequency analysis where the dilation parameter corresponds to the wavelength or period and the translation parameter corresponds to position or time. Note also that, as the Morlet wavelet is complex, the wavelet transform coefficient $W_x(b,a)$ is also complex and may be expressed in terms of real and imaginary parts, modulus and phase. Generally speaking, the CWT is infinitely redundant: the 1-D original signal being transformed into a 2-D time-frequency image. Nevertheless, the fundamental information can be extracted from the so-called ridges of the CWT. These ridges are made of the points in the time-frequency representation for which the frequency of the dilated-translated wavelet coincides with the local frequency of the signal. More precisely, the ridges are the sets of couples (b, a) for which the relation:

$$\frac{\partial \phi_{b,a}}{\partial b} = \frac{\omega_0}{a} \quad \text{..... 8}$$

is satisfied and where $\phi_{b,a}$ is the phase of $W_x(b,a)$ and ω_0/a is the frequency of the dilated

wavelet. Equation (2) expands a one-dimension time series into the two-dimension parameter space (b, a) and yields a measure of relative amplitude of local activity over an interval proportional to a) at scale a and time b; which contrast the Fourier transform which yields an average amplitude over the entire data set. For equation (2) the inverse transform (Wavelet synthesis) reconstructs *f* from

$$f(t) = C_g^{-1} \int_{+0}^{+\infty} \int_{-\infty}^{\infty} a^{-2} W_x(b,a) \varphi_{ab}(t) dbda \quad \text{.....9}$$

were C_g is the integral of $\left\| \hat{\varphi} \right\|^2 \omega^{-1}$ over all frequencies. The $\hat{}$ indicates Fourier Transform, Meyer and O'Brien, (1994). Altering the limits of integration for a or imposing cutoffs in the value of W(b, a) filter *f*. Using this technique filtering of various time series is done in the following chapters.

2.2.3.2Cross-wavelet spectrum

The relationship between two time series can be investigated in the time-frequency domain by computing their cross-wavelet spectrum. For two time series *x(t)* and *y(t)*, with wavelet transforms W_x and W_y, one can define the cross-wavelet spectrum as

$$W_{xy}(b,a) = W_x(b,a) W_y^*(b,a) \quad \text{..... 10}$$

where $W_x(b,a)$ and $W_y(b,a)$ are the CWT of *x(t)* and *y(t)* respectively and where * denotes the complex conjugate. The complex cross-wavelet coefficient $W_{xy}(b,a)$ may be expressed in terms of real and imaginary parts, modulus and phase difference. Let us recall that if $x_1 = a_1 e^{i\theta_1}$ is a complex number with a modulus a_1 and a phase θ_1 and if $x_2 = a_2 e^{i\theta_2}$ is a complex number with a modulus a_2 and a phase θ_2 then: $x_1 x_2^* = a_1 a_2 e^{i(\theta_1 - \theta_2)}$. Where phase is independent of amplitude. Estimation of the instantaneous time delay between two time series is also possible by integration of the cross-wave spectrum.

In chapter two data to be used in the study and its source was discussed. Also brief discussion was

done on the quality control procedures performed on the data. The main methods to be used in studying the mechanisms of inter-annual variability of the tropical highlands of Africa have been discussed. Short discussion on the methods to be used shall be made further in sections when required. The climatology of tropical Africa is discussed in chapter three. Spatial and temporal variability of annual cycles of rainfall and temperature over the continent, and sea surface temperature, sea level pressure, zonal and meridional wind components are discussed using the continuous wavelet transform technique.

CHAPTER 3

3.0 The climatology and annual cycle of Climates over sub-Saharan Africa

3.1 Introduction

In this chapter the NCEP re-analysis, COADS and CRU gridded data sets are explored to establish a rainfall and temperature climatology over Africa south of 10°N. The kinematic and thermodynamic climatology, in the 70°W to 110°E, 30°N to 60°S, is explained using NCEP re-analysis data. In order that subsequent results have meaningful interpretations, the climatology described by NCEP and CRU data should compare well with results obtained by other researchers using other data sets. The mean patterns are based on 31 years (1965-1995) of monthly climatological data. The discussion will mainly focus on the southern Africa rainy period (November to April). Some of the researchers who have described the mean pattern of climatological parameters over southern Africa are Preston-Whyte and Tyson (1988); Theron and Harrison (1989); Pathak (1993); Rocha (1992); Kabanda (1995) and Mulenga (1997). The main characteristics are the mean position of the ITCZ, the monsoon flow over Africa and the subtropical high pressure systems. Further analysis shall be performed to study the annual spatial and temporal patterns of rainfall and temperature over Africa south of 10°N, and SST, SLP, and U and V wind over the Atlantic and Indian Oceans. PCA shall be performed to extract the annual cycle from respective variables. Wavelet transform is used to evaluate and filter the annual cycles. Descriptions given below are supported with figures, but some of them are not shown.

3.2.0 The climatology of parameters (1965-1995)

3.2.1 Rainfall climatology

The seasonal rainfall climatology over Africa responds to the apparent north-south movement of the overhead sun. In the NDJ (November-December-January) season fig. 3.1 (a) high rainfall values are shown over the Congo basin, Gabon and over Mozambique. The desert area over south west Africa exhibits relatively low rainfall values. During the FMA rainy season fig.3.1 (b) high rainfall values are revealed over the Congo basin, southern Tanzania and Mozambique. Relatively high rainfall values are also indicated over Sudan and Ethiopia during the FMA season. A study of November-April rainfall average over Tanzania, done by Nyenzi et al., (1997) revealed

a similar pattern of heavy rainfall in March and April over the southern highlands of Tanzania.

3.2.2 OLR (Outgoing Longwave Radiation)

The Outgoing Longwave Radiation (OLR) climatology pattern is analysed for NDJ (November-December-January) and FMA (February-March-April). OLR infers areas of deep convection and indicate the position of the ITCZ. OLR measures the amount of radiation reaching the satellite, in W m^{-2}. In warm tropical areas, low values of OLR correspond to large amounts of high, cold clouds while high values of OLR correspond to relatively clear areas or cloudy areas with low warm clouds. It should be noted however, that the extra-tropics OLR values typically decrease with decreasing temperatures.

The OLR mean November-April patterns show the progressive movements of convective areas from north to south as revealed by the rainfall climatology discussed above. Desert areas (the Kalahari and the Sahara) are well depicted. The ITCZ over west Africa is confined north of 4° North, probably due to the relatively cold Atlantic sea surface in the Gulf of Guinea. The OLR pattern over east Africa requires some mention. In November deep convection (ITCZ) can be traced over the Indian Ocean and the Congo Basin. A clearly defined convective zone can be traced from December to March in the Zambezi valley south of Tanzania over the eastern Africa coast. Over the southern hemisphere, the semipermanent southern subtropical high pressure systems are well indicated by relatively high OLR values over the southern Atlantic and Indian Oceans.

3.2.3.0 Wind flow pattern climatology

3.2.3.1 850 hPa level

In the presence of moisture, low-level wind convergence may result in the development of clouds and hence precipitation. We have used the 850 hPa level to represent a low-level flow pattern; this will reduce the effect of high ground over some areas fig. 3.2. In November there is a northeasterly and southeasterly wind convergence off the coast of East Africa. Weak winds and cyclogenic curvature over the Congo basin are observed in November; this flow supports the existence of strong convective activity over the Congo basin. In December the northeasterly monsoon penetrates further south thus converging with southeasterlies north of Madagascar.

Wind convergence at this time can be observed over central Mozambique, and in the great lake region. In January and February northeasterlies recurving to southwesterlies, resulting in diffluent flow, seem to have firmly established over the East Africa. Two cyclonic centres, one over northern Namibia and another over the Mozambique channel, are well established during these two months, which seem to 'hold' the ITCZ in the south. In March the two low pressure centres in the south start filling up and the flow reverses. Over eastern Africa the wind assumes a more easterly flow and the ITCZ shifts northwards. By April the southeasterly flow dominates the whole of east African Coast. The whole of central Africa is swept by a southwesterly flow.

3.2.3.2 200 hPa Level

Diffluent flow over the Congo basin and some parts of east Africa is induced by the simultaneous presence of two anticyclonic circulation systems, north and south of the equator, at about 20°E. By December the ridge in the south retreats southwards and the anticyclone in the north weakens into a ridge. The flow pattern becomes cross-equatorial with the divergence axis oriented in the northwest-southeast. This is the axis where deep convection or high rainfall amounts are observed in the December rainfall pattern over southern Africa. The cross-equatorial flow strengthens in January and February. In March the cross-equatorial flow weakens and the southern subtropical high moves slightly northeastwards. In April the southern subtropic ridge line moves further north to about 2.5°S. The position of this ridge line together with the northern hemisphere ridge line establishes a diffluent flow pattern farther north, at this level, thus supporting vertical motion in the northern hemisphere.

3.2.4 Mean Sea Level Pressure (SLP)

Salient features on the Mean SLP patterns, from November to April, are the semi-permanent subtropical high pressure systems, the Saint Helena and Mascarene in the south and the Azores high in the north. Another important feature is the high pressure system over Asian from November to March, which reverts to a low pressure system from March to April. Over the Indian Ocean a low pressure system, with a trough axis from the coast of east Africa to Indonesia along about 0° latitude in November, moves southward to about 15°S in February. Pressure falls, over the southern Africa subcontinent, is observed from November to February whereas pressure build up are observed from March to April as the low pressure system start shifting northwards.

3.3.0 The annual cycles of parameters

The apparent north-south movement of the sun controls the atmospheric general circulation and therefore rainfall and temperature. The annual cycle of rainfall and temperature over Africa is a direct result of this. However, the ocean, atmosphere and other external systems operate at different spatial and temporal scales. The interaction of these systems at different spatial and time scales results in year to year variation of the climate system. These fluctuations on the other hand cause the year to year variation of annual cycles in rainfall, temperature, etc. over the African continent and elsewhere. In this section the spatial and temporal variability of a number of parameters, which includes rainfall, temperature, SST, SLP and, U and V winds are studied. PCA is performed on the data without removing the respective long-term means which represent the average of the annual variability for different parameters within the tropics. PCs for rainfall, temperature and environmental parameters which exhibit large amplitudes at twelve month periods are discussed below.

3.3.1 Annual spatial and temporal patterns of rainfall over Africa

The first three PCs of rainfall with annual cycles contribute about 64% of the variance. Table 3.1 shows the PC modes (both un-rotated and rotated), the variances they explain, and spatial loading region figs. 3.3 (a-c) for un-rotated PC1-PC3 modes. The three modes show coherent features over Africa, south of 10°N. The first PC mode, with the highest variance contribution of 47%, contains the main annual cycles. Positive loadings are to the north and the extreme southernmost cape of the African continent and negative loadings over southern Africa. Positive loading regions have wet conditions when time scores amplitudes are positive and those with negative loadings have dry conditions. The time score amplitude peaks for this mode occur around August. This mode represents the annual cycles with wet boreal (northern) summer and dry Austral (southern) winter. The second PC mode fig. 3.3 (b) is positively loaded in equatorial Africa. This PC has the second highest variance of about 12%. The time score amplitudes show that equatorial regions experience bimodal rainy conditions from October to April with a short period of reduced rainfall in January-February. May to September is a period with relatively less rainfall. The bimodal rainfall distribution could be a response to the passage of the overhead sun. The third PC mode fig. 3.3 (c) which explains about 5% of the variance is positively loaded over south Africa (after rotation). The time score plot reveals that this PC mode is also bimodal with the first maximum

in August and the second peak in January. The wavelet transform of rainfall PC1 time scores figs. 3.3 (d-g) indicate that the major period of oscillation over the respective loading areas is 12 months. PC2 time scores plot however, reveal that there is a second period of six months having high amplitude. Six month oscillations also exist in the first PC1 mode. PC1 time scores plot reveals amplitude modulation. High amplitudes are shown to occur between 1972 and 1978 fig 3.3 (g)

Table 3.1: Approximate locations and variance explained in percentage for rainfall PC 1-3 modes (unrotated and rotated) with annual cycles.

PC MODE	VARIANCE (%)	Approximate Central Position (Lon, Lat)
PC1	47.6	(20°E, 8°N), (25°E, 15°S)
PC2	11.8	(25°E,20°S & 15°E, 10°N)
PC3	4.6	(20°E, 2°S & 24°E, 32°S), (36°E, 6°S)
PC1R	47.6	(20°E, 10°N)
PC2R	11.8	(20°E, 2°S)
PC3R	4.6	(22°E, 35°S)

R stands for rotated

3.3.2 Annual spatial and temporal patterns of temperature over Africa

The first three PCs contribute about 85% variance of temperature over Africa, south of 10°N. The first PC mode which is negatively loaded in the north explains about 55% of the variance fig. 3.4 (a). The amplitudes of the time score plot indicate maximum values in June (in the north) and small peaks around October. Minimum values are indicated over southern Africa. The second PC mode is positively loaded south of 10°S and negatively loaded north of 10°S and explains about 23% of the total variance. The positively loaded areas, i.e. the south, are hotter in January-December and colder in May-June. The third PC mode which explains 6.7% of the variance is positively loaded over the Congo Basin fig. 3.4 (c). The time score's plot indicates the lower temperatures are indicated in March while high temperatures are indicated in June and September-October. Spectral amplitudes with periods of twelve and six months are revealed by CWT in all three PC time scores except the third PC which has small amplitudes with six month oscillations.

The amplitudes of the PC1 time scores, fig. 3.4 (d-g) do not show much modulation which indicates that the annual variations of temperatures over the domain have remained quasi-stationary during the 1965-1995 period.

Table 3.2: Approximate locations and variance explained in percentage for temperature PC 1-3 modes (un-rotated and rotated) with annual cycles.

PC MODE	VARIANCE (%)	Approximate Central Position (Lon, Lat)
PC1	54.8	(40°E, 10°N)
PC2	23.2	(20°E, 25°S), (20°E, 10°N)
PC3	6.7	(25°E, 8°S)
PC1R	54.8	(40°E, 10°N)
PC2R	23.2	(20°E, 10°N)
PC3R	6.7	(25°E, 8°S)

R stands for rotated

3.3.3 Annual spatial and temporal patterns of SST field over the Atlantic and Indian Oceans

The first two PC modes of SST over the Indian and Atlantic oceans (with annual cycles not removed), explain about 83% of the variance. The first PC mode of SST over the two oceans indicates that positive loadings are in the north and negative loadings in the south fig. 3.5 (a). This PC mode represents the annual SST northern winter signal, with lower SST in around March and higher SST around the August. PC1 time scores plot in fig. 3.5 (f) reveals large variability in annual time scale with little amplitude modulation and small variability in the six month oscillations fig 3.5 (d). The second PC mode of SST, loaded over the Atlantic and Indian Oceans, explains 14% of the total variance. The PC mode is negatively loaded in the equatorial Atlantic and northern Indian Oceans with small positive loadings in the south of the two oceans. The time score amplitudes of this second PC mode reveal a bimodal temporal pattern. Large peaks are shown in February and small peaks in August with low values occurring in June and October. This is in response to the apparent north-south movement of the overhead sun. The CWT of PC2 for SST shows a bimodal temporal pattern. Small amplitudes are indicated between 1977 and 1979.

Table 3.3: Approximate locations and variance explained in percentage for sea surface temperature PC 1-3 modes (un-rotated and rotated) with annual cycles.

PC MODE	VARIANCE (%)	Approximate Central Position (Lon, Lat)
PC1	68.9	(0, 30°S and 60°E,30°S)
PC2	14.2	(30°W, 2°S and 60°, 4°N)
PC1R	68.9	(35°W, 40°S)
PC2R	14.2	(60°E, 10°N)

R - Stands for rotated

3.3.4 Annual spatial and temporal patterns of SLP field over the Atlantic and Indian Oceans

The first two PCs of SLP over the Indian and Atlantic Oceans (with annual cycle) contribute about 58% percent variance of pressure variability over the Indian and Atlantic Oceans figs. 3.6 (a-b). The first PC of SLP explains 45.6 percent of the total variance. This PC represents the annual SLP signal over the two oceans with higher pressures in July, in the south, and low pressures in the north. The second PC, which explains about 12.7% of the variance, is positively loaded over the equatorial Indian Ocean and negatively loaded over the Atlantic Ocean northeast of south America with smaller positive loadings over the southern Atlantic Ocean. Plots of the time scores for SLP PC1 reveal that this PC has mainly annual cycles signals. PC2 of sea level pressure time scores show bimodal temporal patterns with high spectral amplitudes in the 12-month period and relatively small amplitudes in the 6-month period. Some amplitude modulation is revealed in the 12-month oscillation for the two PCs. PC2 has high amplitudes between 1972 and 1978, and between 1988 and 1992.

Table 3.4: Approximate locations and variance explained in percentages for sea level pressure PC 1-3 modes (un-rotated and rotated) with annual cycles.

PC MODE	VARIANCE (%)	Approximate Central Position (Lon, Lat)
PC1	45.6	(10°E, 22°S and 40°E, 22°S), (60°E, 18°N)
PC2	12.7	(90°E, 10°S), (50°W, 18°N)
PC1R	45.6	(60°E, 10°S)
PC2R	12.7	(70°W, 10°N)

R - Stands for rotated

3.3.5 Annual spatial and temporal patterns of zonal wind field over the Atlantic and Indian Oceans

The first two PC modes of zonal wind with annual cycles explain about 41% of the total variance. PC1 mode shows a positive loading between 10°S and 22°S. To the south and north of this latitude band negative loadings are indicated fig 3.7 (a). The amplitudes of the time scores for PC1 indicate that this PC has annual cycles' signals for the zonal wind component. An increase in easterly anomaly flow is indicated, between10°S and 22°S, in July and an increase of westerly anomaly flow north and south of this latitude band. This is normally the time of the southerly monsoons over the west Indian Ocean and the Gulf of Guinea during the boreal summer. The second PC mode which explains about 7% of the variance is negatively loaded over the Gulf of Guinea and Atlantic Ocean to the north of south America. The amplitudes of the time scores suggest that this PC mode is bimodal with two peaks; smaller peaks occurring in May and larger peaks occurring in October. The continuous wavelet transform shows that the first PC mode of the zonal wind component is uni-modal fig. 3.7 (c, f) while the second PC mode is bimodal. In addition to having a 12-month oscillation the second PC mode shows a six-month oscillation. Amplitude modulation is indicated in both PC modes reflecting the variability of the annual cycles in both amplitude and time.

Table 3.5: Approximate locations and variance explained in percentage for zonal wind PC 1-3 modes (un-rotated and rotated) with annual cycles.

PC MODE	VARIANCE (%)	Approximate Central Position (Lon, Lat)
PC1	33.8	(18°S ridge line - Indian and Atlantic Oceans)
PC2	6.9	(0, 10°S & 60°W, 10°N)
PC1R	33.8	(20°W, 10°N & 70°E,15°N)
PC2R	6.9	(60°W, 10°N)

R - Stands for rotated

3.3.6 Annual spatial and temporal patterns of meridional wind field over the Atlantic and Atlantic Oceans

The first two PC modes of meridional wind components over the Atlantic and Indian Oceans, with annual cycles, explain about 44% of the variance. About 34 percent of this is contributed by annual cycles dominated by the monsoon wind circulation over the west Indian Ocean and the Gulf of Guinea figs. 3.8 (a, b). The amplitudes of the time scores plot for the first PC indicates that the northerly wind component occurs in January-February of each year, while the southerly wind component occurs in July. The second PC mode of the meridional wind is positively loaded over the Atlantic Ocean north of south America with the loadings extending to south Atlantic Ocean. In the south the negative-positive-wavy pattern indicates the position of the southern anticyclones fig. 3.8 (b). The amplitudes of the time score plot for PC2 suggest that maximum positive meridional components are attained in October and negative meridional components in February. The plot reveals second smaller peaks around May and low values in July. The first mode of the meridional wind characterises the annual cycle fig. 3.8 (e-f). The CWT analysis shows that the second PC mode of the meridional wind has two oscillation periods, i.e. 6- and 12-month.

Table 3.6: Approximate locations and variance explained in percentage for meridional wind components PC 1-3 modes (un-rotated and rotated) with annual cycles.

PC MODE	VARIANCE (%)	Approximate Central Position (Lon, Lat)
PC1	35.5	(20°W,0; 50°E,0, & 90°E,0)
PC2	8.4	(40°W,10°N), (50°E, 30°S)
PC1R	35.5	(60°E, 15N°)
PC2R	8.4	(40°W,10°N)

R - stands for rotated

3.4 Summary

The analysis in this chapter has mainly focussed on three issues. The first was to find the adequacy of gridded rainfall, temperature and marine data in the study of climate variability at the inter-annual time scale. The secondary issue was the mean patterns for which one could compare with subsequent results in this study. Finally, interest was focussed in understanding the main spatial and temporal characteristics of the annual cycle over the African continent and over the Atlantic and Indian Oceans from 1965 to 1995. Comparisons between gridded CRU rainfall data and station data were promising and that CRU data can be used in climatological studies.

Comparing the partial correlations of the field variables with terrestrial rainfall and temperature shows that the V PC1 is most closely related to the annual cycle of rainfall PC1. Although inter-annual variability is the focus of research here, it is important to place it within the context of the annual cycle which represents 50% of the variance vs 10% for inter-annual fluctuations according to PCA. For example, years with high annual cycles have been corresponding with high inter-annual rainfall amplitudes. Continuous wavelet analysis of the major temporal patterns over the African continent and the Atlantic and Indian Ocean, extracted by PCA, have revealed interesting results. Most of the patterns with loading away from the equatorial belt revealed high amplitudes at 12 month period which reflects movement of the sun. Loading patterns within the equatorial band displayed high amplitudes at two periods one at 12 months and another one at 6 months; these are the areas where the sun crosses twice in a year. Results in this chapter have shown amplitude modulation of annual cycles from year to year.

In the next chapter the analysis concentrates on major spatial and temporal patterns at inter-annual time scale. The data is filtered by removing oscillation periods below 1.5 years using the continuous wavelet transform.

(a)

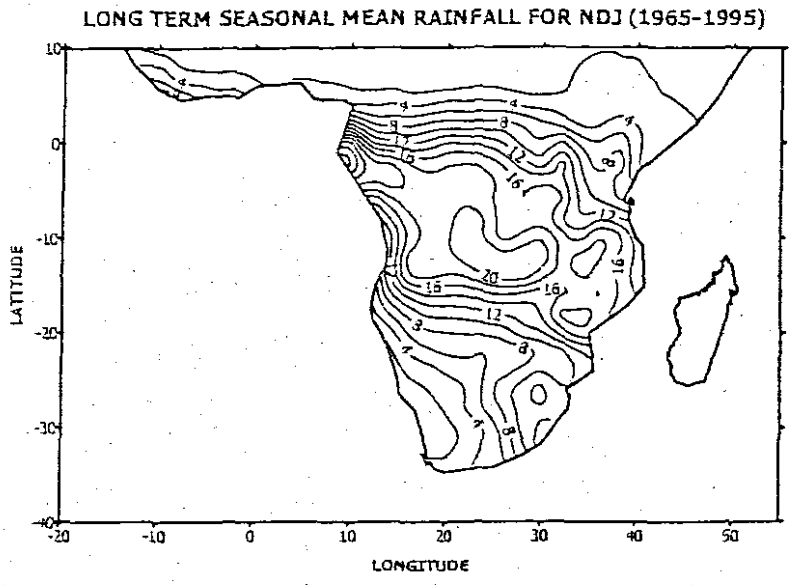

(b)

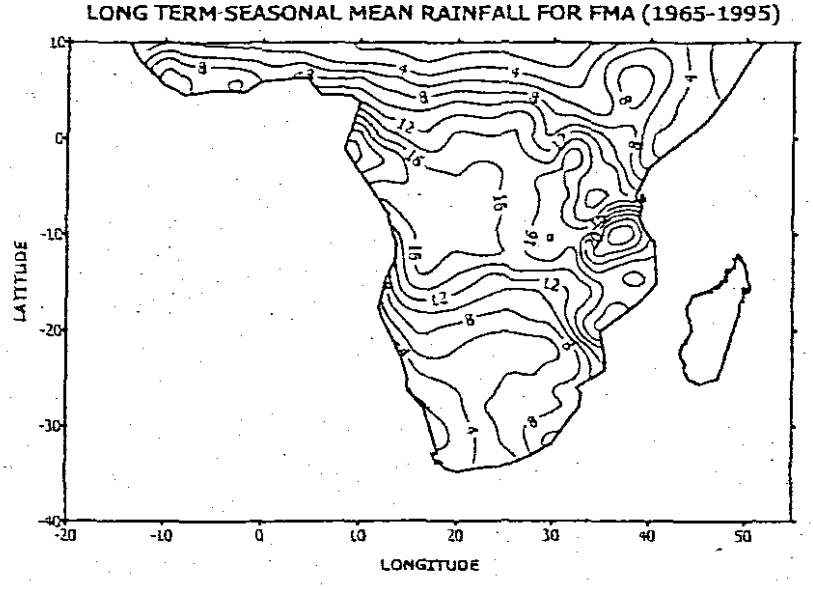

Fig. 3.1: Long term seasonal mean rainfall, (a) NDJ-November-December-January (b) FMA-February-March-April, Interval 2mm day^{-1}

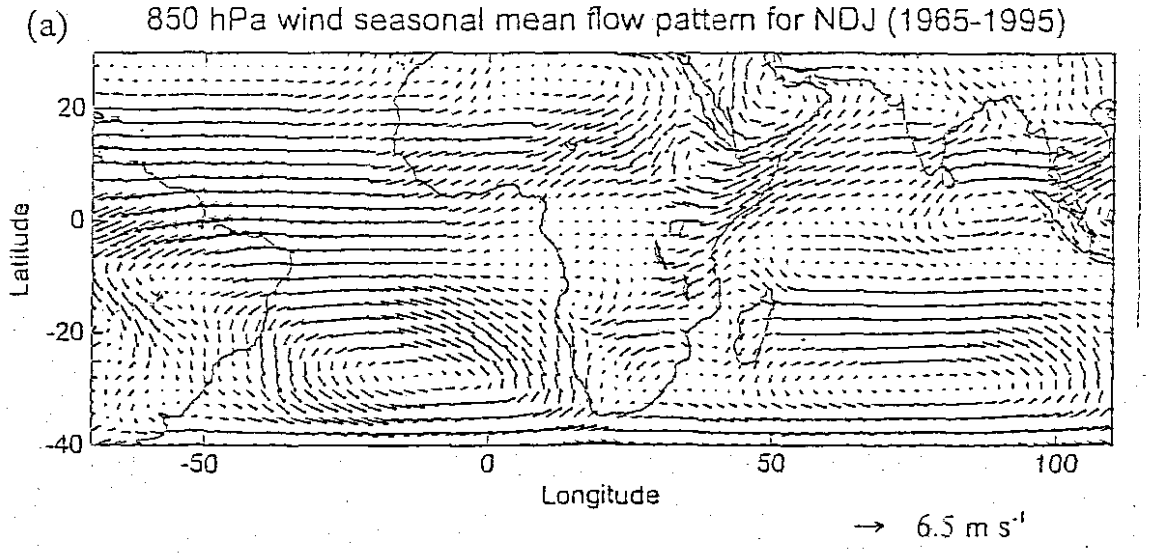

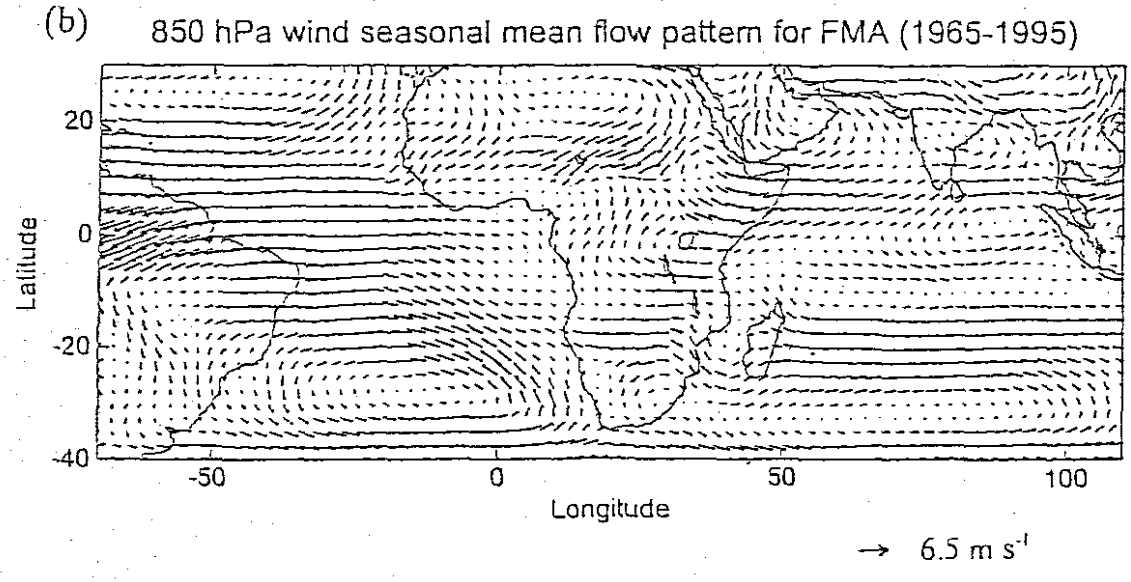

Fig. 3.2: 850 hPa wind pattern long term seasonal mean pattern for (a) NDJ-November-December-January (b) FMA-February-March-April

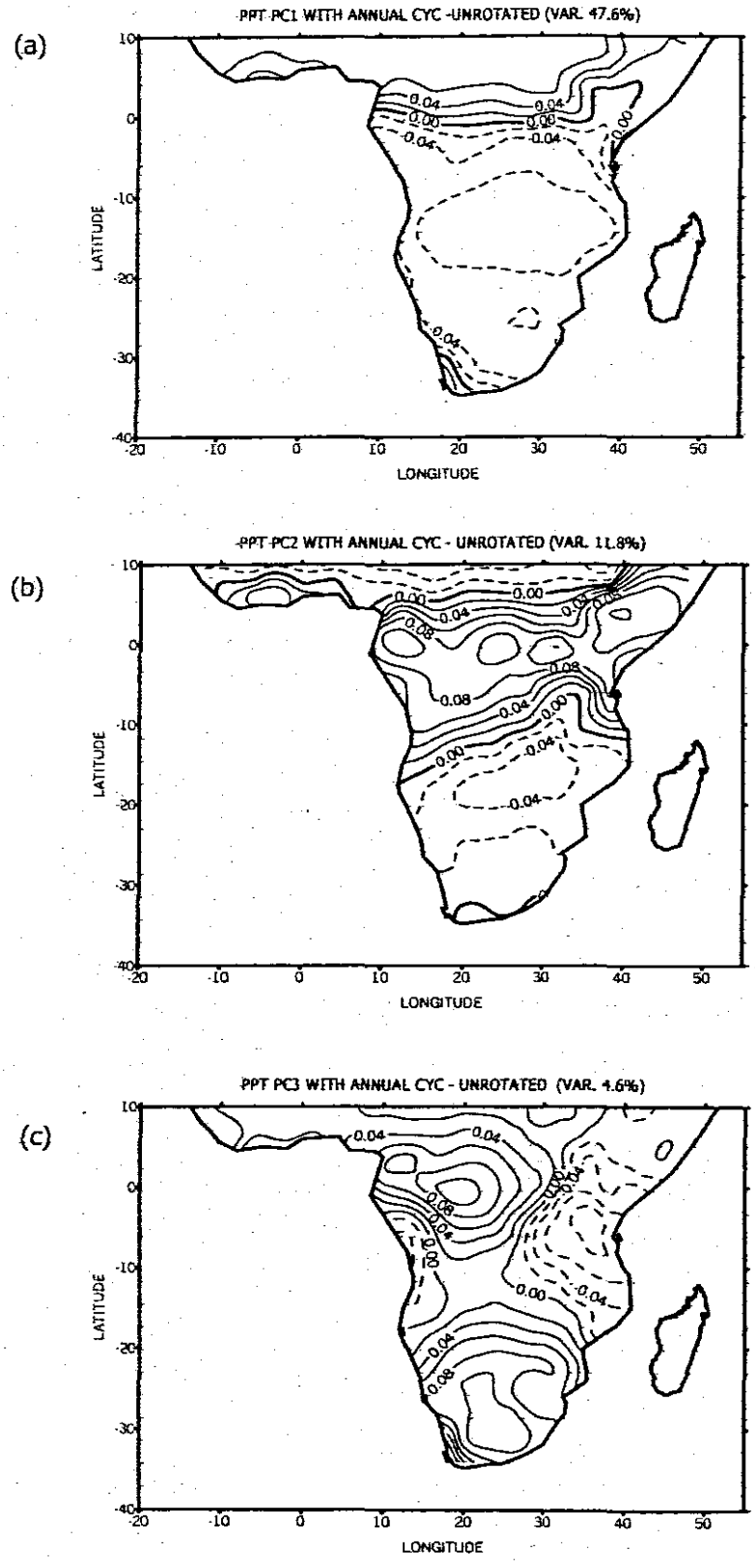

Fig. 3.3: PC 1-3 for rainfall with annual cyle (unrotated)

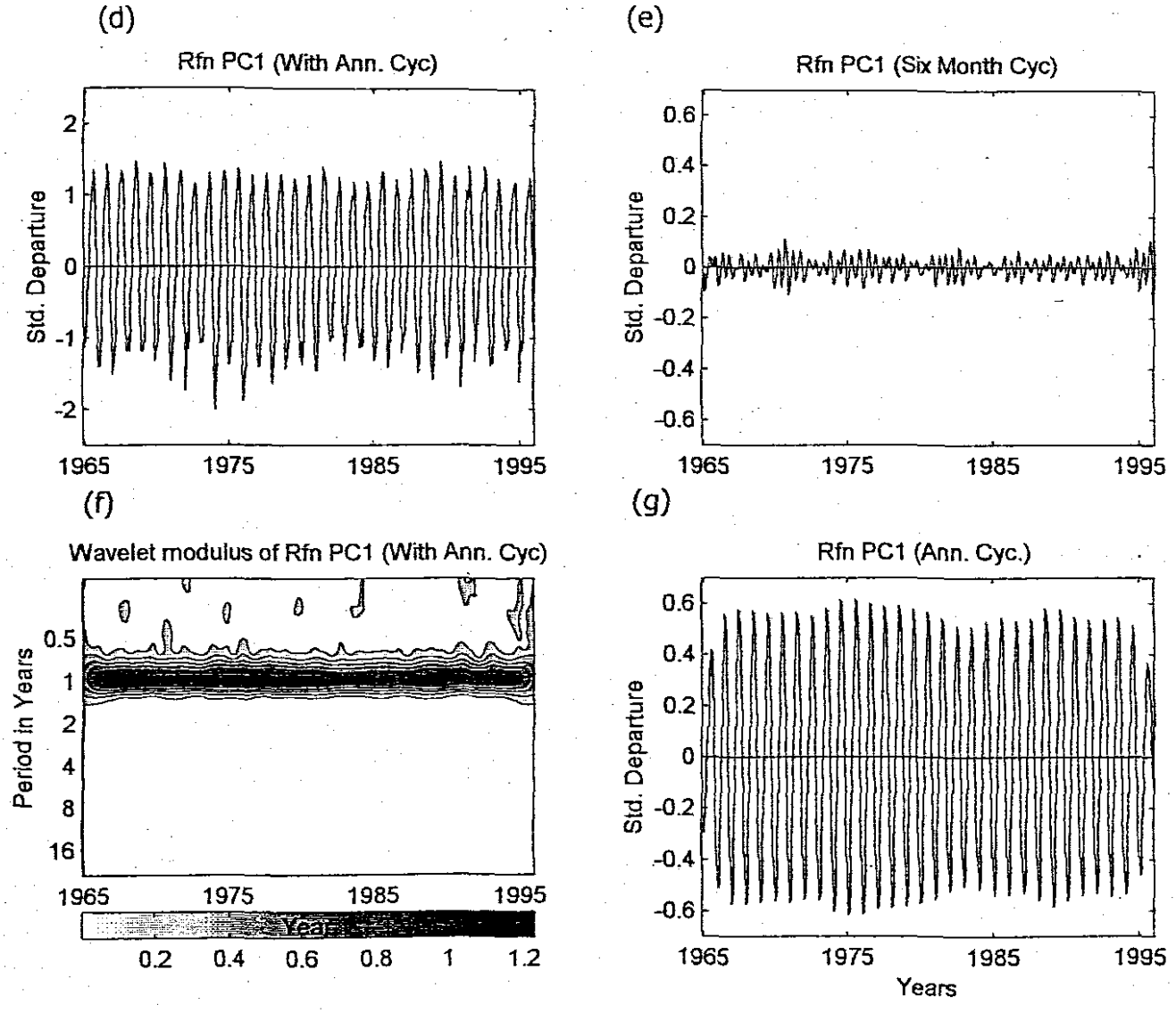

Fig. 3.3: Contd. Time scores of unrotated PCA for gridded monthly rainfall over Africa with annual cycle; (d) plot PC1 time score, (e) plot of 6 month cycle PC1, (f) plot of wavelet modulus of rainfall PC1, (g) plot of annual cycle for rainfall PC1 (time score filtered in the respective periods using the CWT)

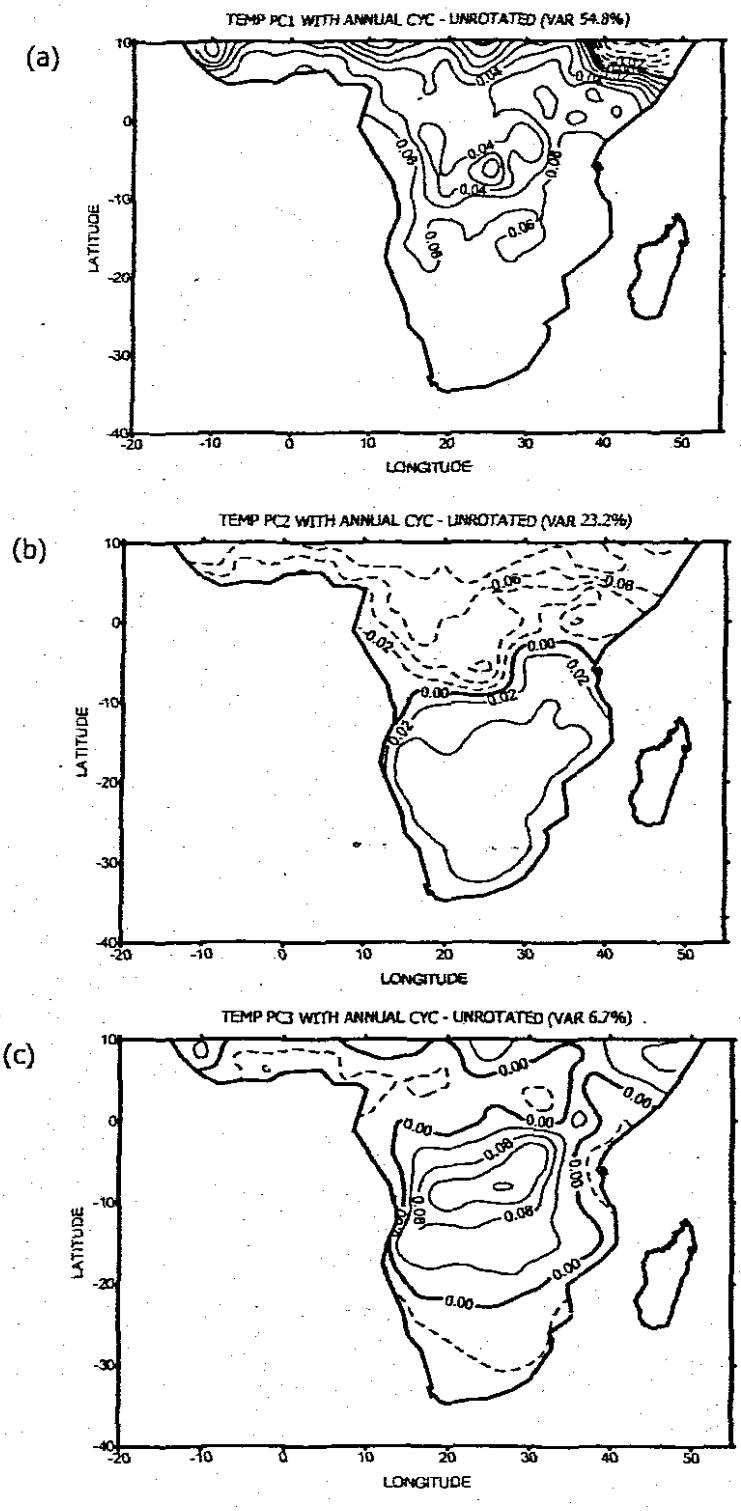

Fig. 3.4: PC 1-3 for temperature with annual cycle (unrotated)

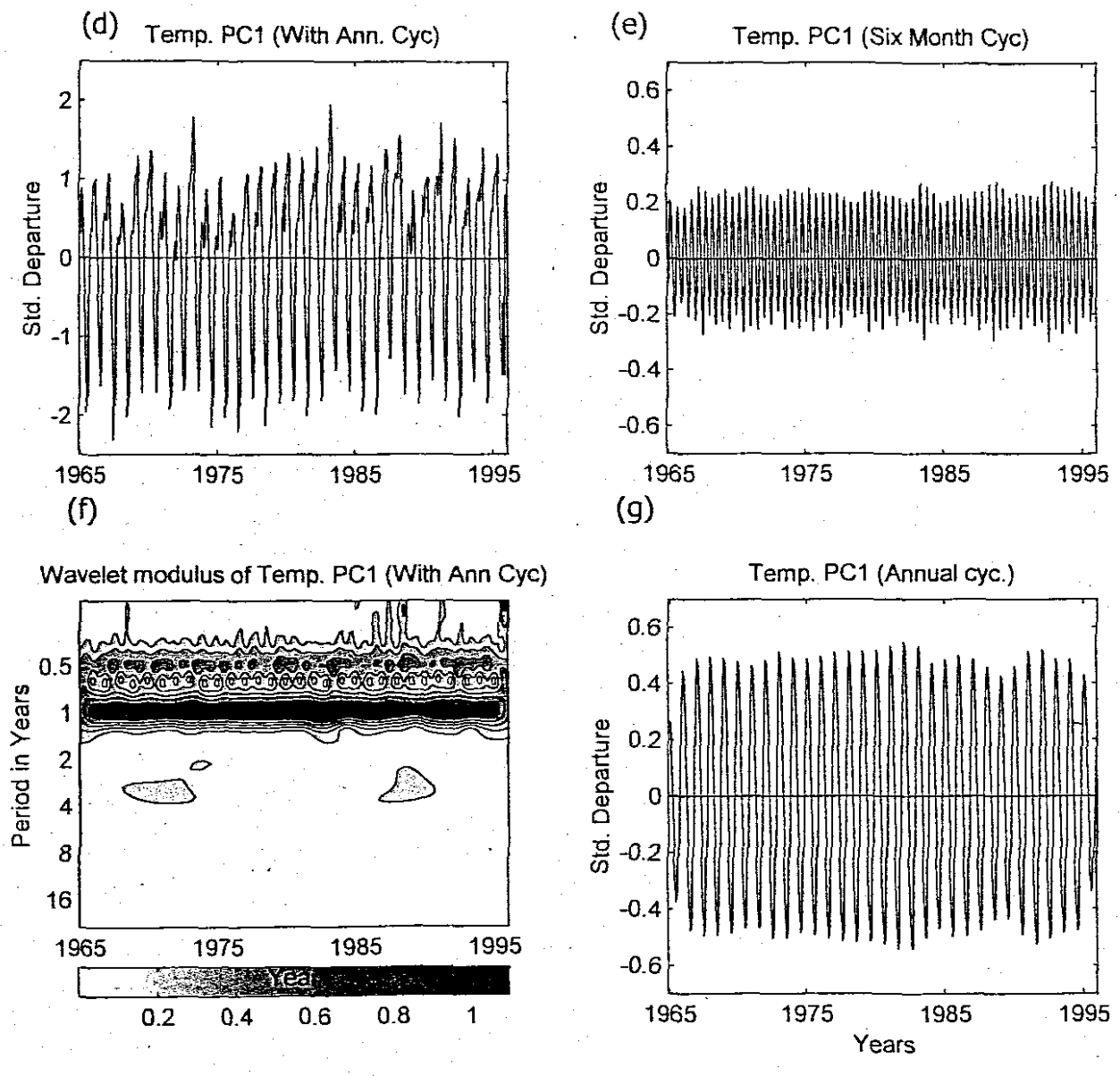

Fig. 3.4: Contd. Time scores of unrotated PCA for gridded monthly Temp. over Africa with annual cycle; (d) plot Temp. PC1 time score, (e) plot of 6 month cycle PC1 (f) plot of wavelet modulus of Temp. PC1, (g) plot of annual cycle for Temp. PC1 (time score filtered in the respective periods using the CWT)

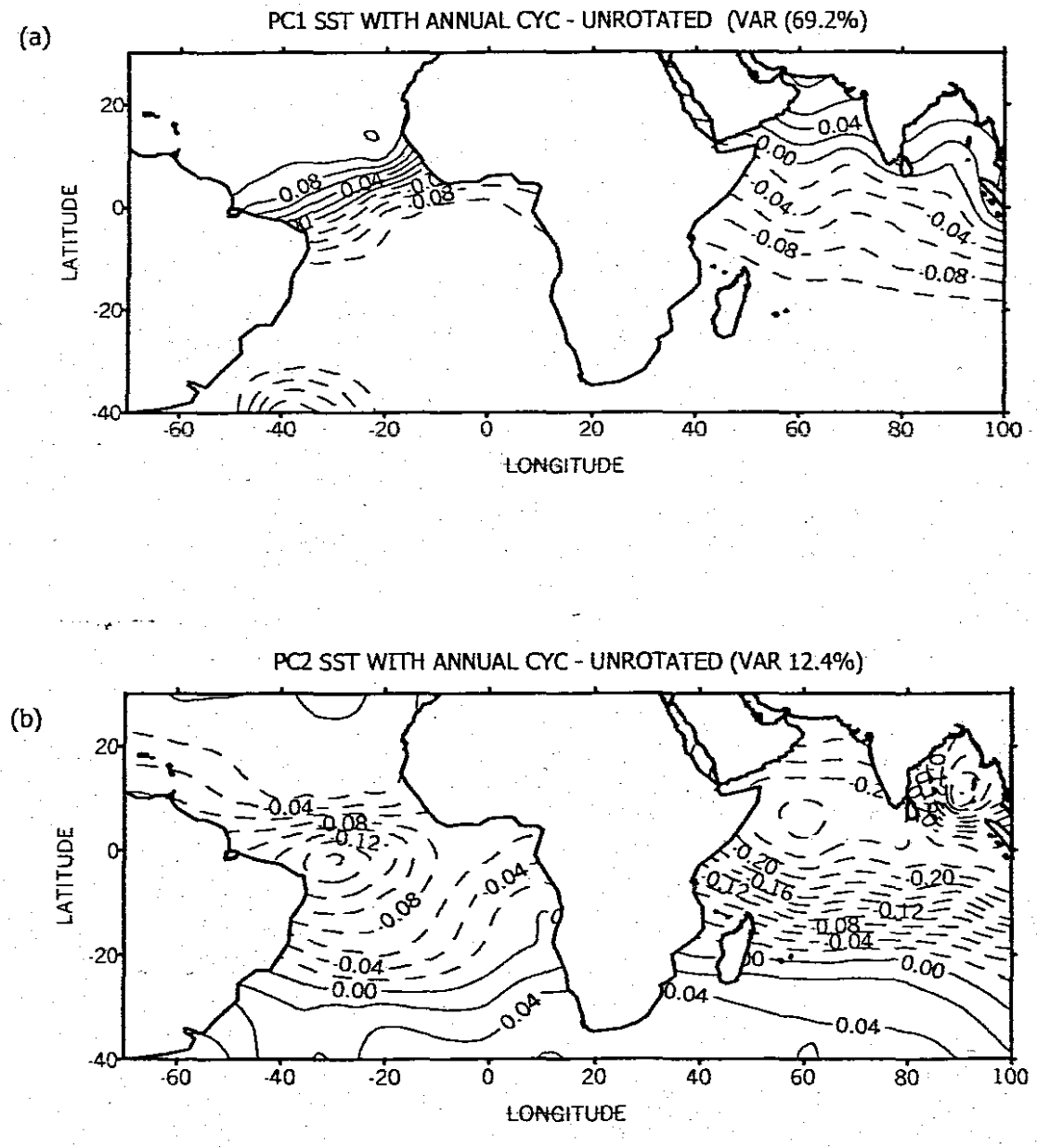

Fig 3.5: PC 1-2 for SST over the Atlantic and Indian Oceans with annual cycle (unrotated)

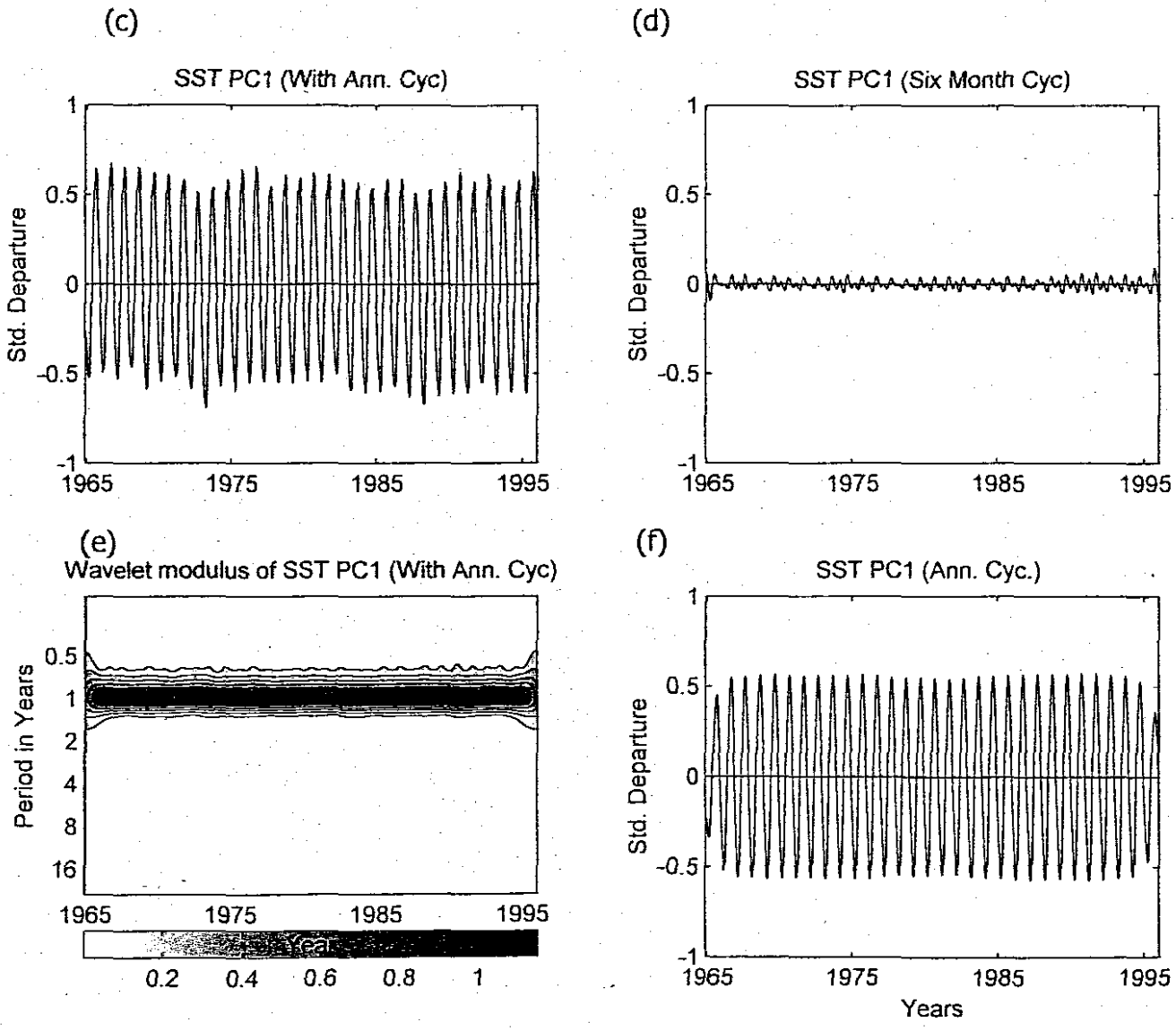

Fig. 3.5: Contd. Time scores of unrotated PCA for gridded monthly SST over the Atlantic and Indian Oceans with annual cycle; (c) plot PC1 time score, (d) plot of 6 month cycle PC1, (e) plot of wavelet modulus of SST PC1, (f) plot of annual cycle for SST PC1 (time score filtered in the respective periods using the CWT)

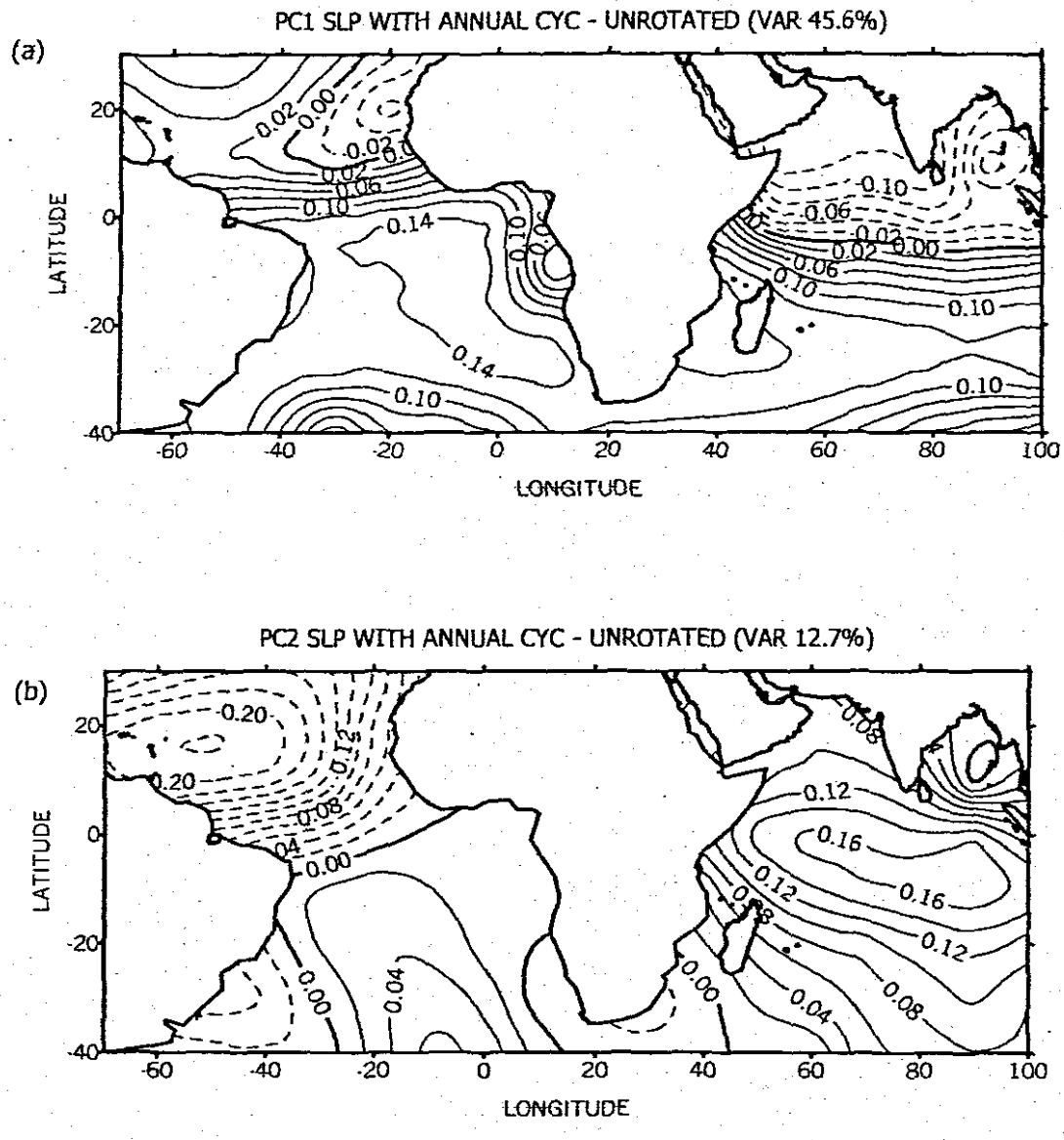

Fig. 3.6: PC 1-2 for SLP over the Atlantic and Indian Oceans with annual cycle (unrotated)

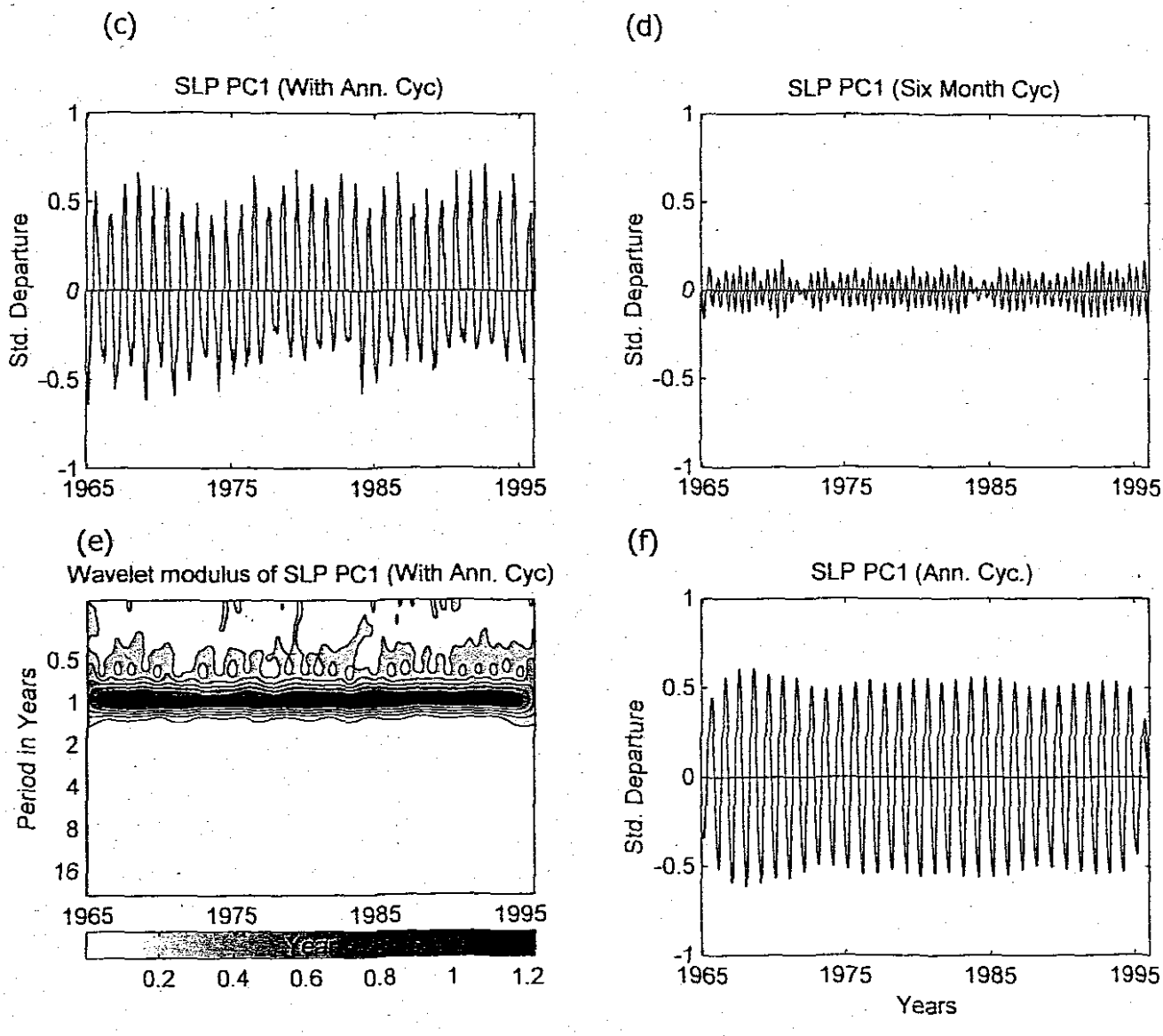

Fig. 3.6: Contd. Time scores of unrotated PCA for gridded monthly SLP over the Atlantic and Indian Oceans with annual cycle; (c) plot PC1 time score, (d) plot of 6 month cycle PC1, (e) plot of wavelet modulus of SLP PC1, (f) plot of annual cycle for SLP PC1 (time score filtered in the respective periods using the CWT)

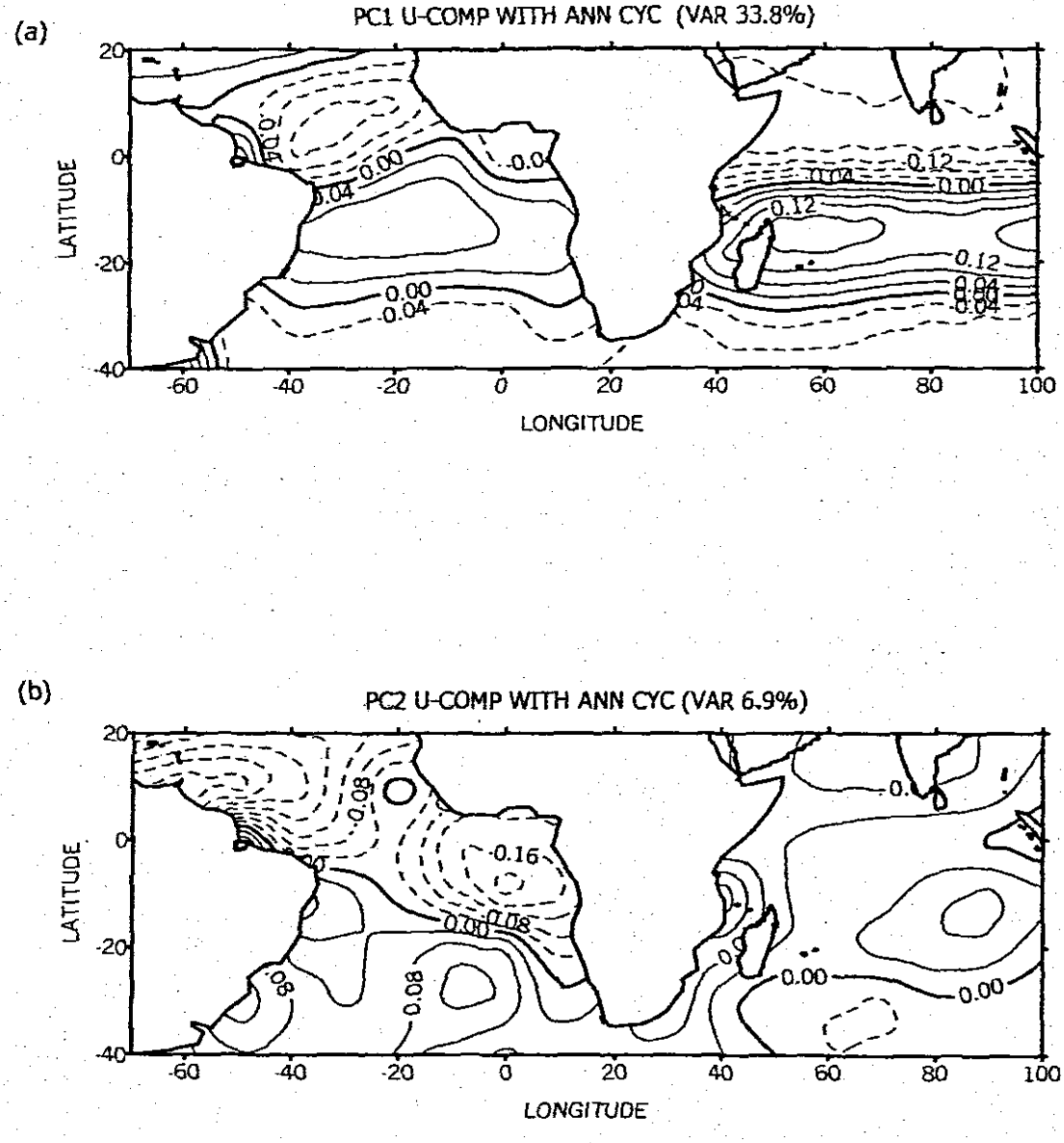

Fig. 3.7: PC1-2 for zonal wind component over the Atalntic and Indian Oceans with Annual cycle unrotated

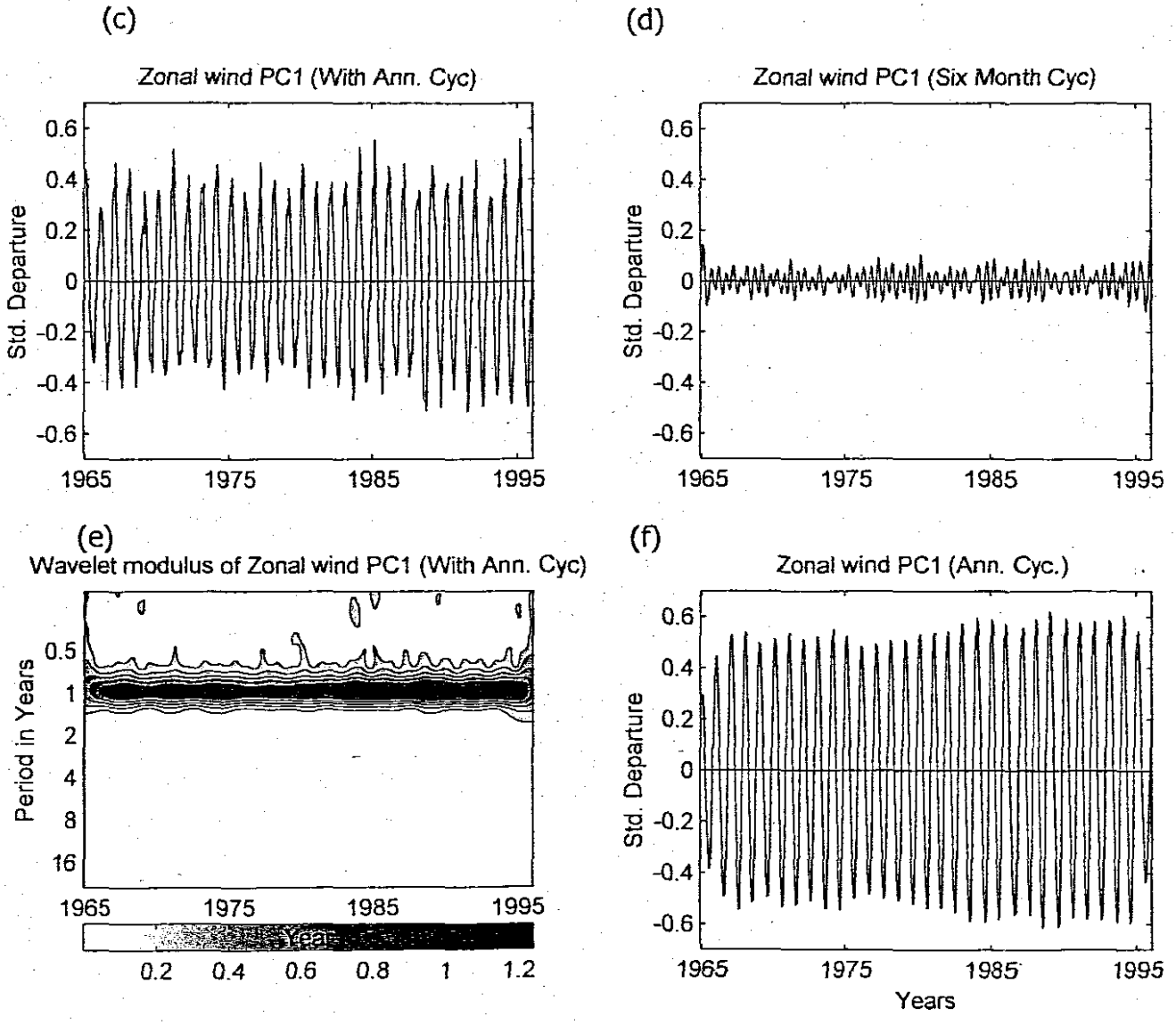

Fig. 3.7: Contd. Time scores of rotated PCA for gridded monthly zonal wind field over the Atlantic and Indian Oceans with annual cycle; (c) plot PC1 time score (d) plot of 6 month cycle PC1 (e) plot of wavelet modulus of zonal wind field PC1 (f) plot of annual cycle for zonal wind field PC1 (time score filtered in the respective periods using the CWT)

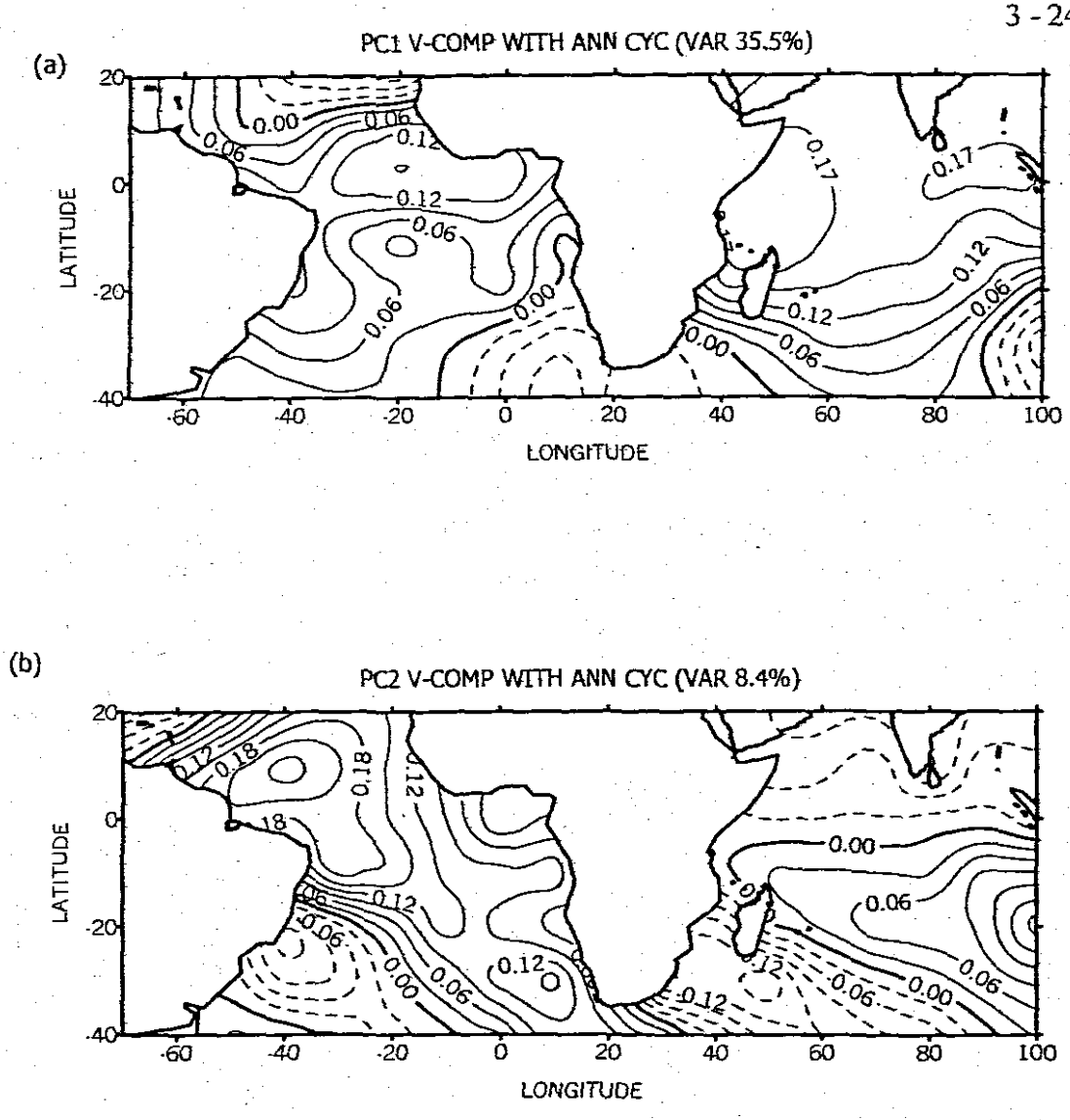

Fig. 3.8: PC1-2 for meridional wind over the Atlantic Oceans with annual cycle (unrotated)

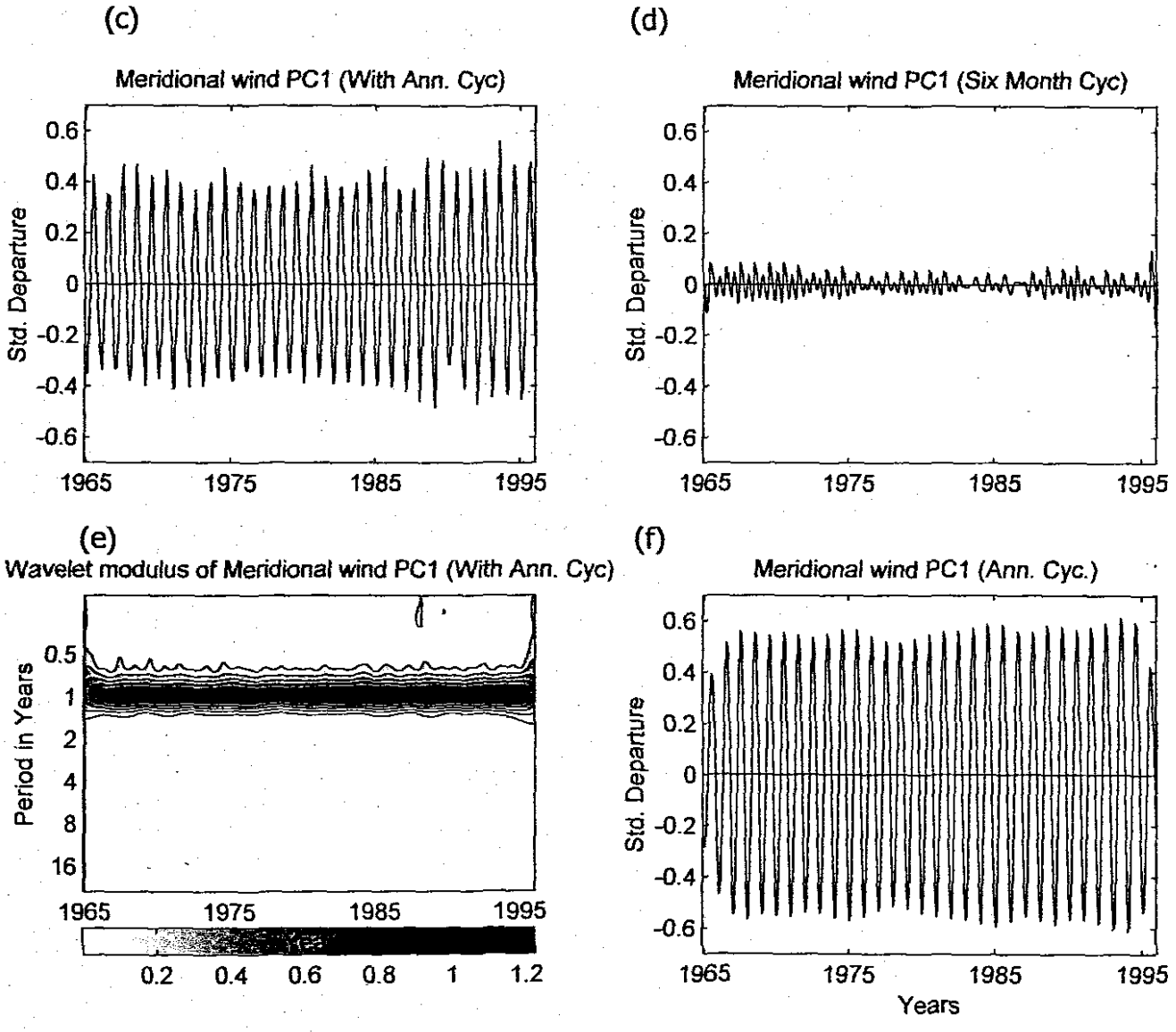

Fig. 3.8: Contd. Time scores of rotated PCA for gridded monthly meridional wind field over the Atlantic and Indian Oceans with annual cycle; (c) plot PC1 time score (d) plot of 6 month cycle PC1 (e) plot of wavelet modulus of meridional wind field PC1 (f) plot of annual cycle for meridional wind field PC1 (time score filtered in the respective periods using the CWT)

CHAPTER 4

4.0 INTER-ANNUAL SPATIAL AND TEMPORAL VARIABILITY

4.1 Introduction

In this chapter the inter-annual spatial and temporal variability of rainfall and temperature, and environmental field parameters (SST, SLP, U and V wind component) are identified and documented using Principal Component Analysis (PCA) and Continuous Wavelet Transform (CWT). PCA is a method which can effectively link the spatial and temporal patterns of a data field (Legler, 1983). The technique partitions the temporal variance of the data into orthogonal spatial patterns called eigenvectors. The eigenvectors are then ranked in decreasing order according to the percent of variance they account for and each respective eigenvector is associated with a series of coefficients in time that modulate it. Coherent patterns are assigned to particular eigenvectors that account for a large fraction of the variance. The method also helps in reducing the number of variables to handle. Many studies have used this method in revealing coherent rainfall patterns in Africa, (Mason, 1992; Mulenga, 1998).

In this study continuous monthly gridded rainfall and temperature data are used as described in chapter 2. The rainfall and temperature data span the period 1965 to 1995. The period has been chosen to correspond with other data sets selected to minimise missing data. Firstly, PCA was performed on continuous monthly data with annual cycles (chapter 3) and secondly, on continuous monthly data with the annual cycles removed using a NAG subroutine (NAG, 1996). The first 3 principal components were retained and then rotated using Varimax. Cut off point for PC modes to retain was decided by using the Scree test. The domain of analysis is 10°N-34°S, 12°W - 44°E or continental Africa south of the Sahara desert excluding Madagascar.

Wavelet analysis was applied to key area time series to reveal instantaneous amplitude variations at different frequencies throughout the entire time series as described in chapter 2. By decomposing a time series into time-frequency space, it is possible to determine both the dominant modes of variability and how those modes vary with time. The continuous wavelet transform gives a two Dimensional frequency representation of a time series, and can also be used to filter the time series

to the required time scales. Here the CWT is used to remove oscillations with periods less than 1.5 years, to remain with estimates of inter-annual variability. Annual cycles are also plotted to reveal amplitude modulations with time.

The selection of PCs, as given in table 2.3, is based on a number of reasons. The rainfall PC1 and PC3 were selected because of the stated intention to understand inter-annual rainfall variability over the highlands of Africa. PC2 on the other hand was not selected because this mode is loaded over an area with poor data quality. Additionally PC2 and PC3 of temperature are explored. The focus will be on inter-annual time scales when discussing the CWT results of rainfall, temperature and oceanic/atmospheric parameters. This is important because these are the immediate moisture sources for the African continent and perhaps greatly influence the rainfall climatology of the tropical highlands of Africa. PCA and CWT were applied to gridded COADs data (SST, SLP, U and V wind) over the Atlantic and Indian Oceans in the domain 20°N-40°S, 70°W-100°E. Similarly PCA was performed on monthly data with annual cycles (chapter 3) and with annual cycles removed (chapter 4). Potential predictors are extracted from PC1 to PC3 patterns in the environmental fields.

4.2.0 Inter-annual spatial and temporal variability of rainfall and temperature over Africa

4.2.1.0 Rainfall PCs

In the following section we shall describe un-rotated and rotated PCs derived from continuous monthly data with annual cycles removed. About 22% of the variance is contributed by the first three PC modes. However, the main focus of discussion will be PC1 and PC3. PC2 is not discussed because of data problems over the Democratic Republic of the Congo and Angola, where it is loaded. The table below shows the PC modes and variances they explain. Their spatial patterns are given in fig. 4.1.

Table 4.1: Rainfall PC modes

Mode	Variance (%)	Approximate Location (Longitude/latitude)
PC1	9.4	22°S, 25°E southern Africa
PC3	7.2	2°N, 38°E east Africa
PC1R	9.4	25°S, 25°E southern Africa
PC3R	7.2	5°N, 40°E east Africa

R - Stands for rotated

4.2.1.1 The southern Africa rainfall mode (PC1-Variance 9.4%)

The first PC mode of inter-annual rainfall over Africa explains 9.4% of the variance. Fig. 4.1 (a) show the rainfall PC1 mode with negative loading over southern Africa centred at (22°S, 25°E). The rotated PC1 mode is shown in fig 4.1 (b) with loadings over the same area. A small positive loading is found over northern Mozambique and Malawi. Fig. 4.1 (g-i) shows the temporal inter-annual variability for PC1 rainfall mode. The standardized inter-annual southern Africa rainfall time series plot reveals that the southern Africa region is characterised by year to year rainfall variation throughout the 1965-1995 period except the period 1980-1987 when relatively drier conditions were experienced. High rainfall variability is however, revealed in the 70's. Annual cycles of southern Africa rainfall are shown to be modulated. High amplitudes are indicated between 1973 and 1977 and low amplitudes between 1979 and 1985, fig. 4.1 (h). 79 percent of rainfall variability, in the region covered by PC1 mode, is contributed by the annual variability and about 8% is a contribution from the inter-annual variability. The wavelet transform of the southern Africa key area rainfall time series shows that rainfall over southern Africa oscillates with dominant periods of 2-4 and 8-12 years, figs. 4.1 (i). Relatively strong spectral power is indicated between 1973 and 1977 with oscillation period of 1.5-3 years indicating a strong QBO signal. The oscillation at about 2-year period in the early 70's modulates to a 2-4 year period in the 80's.

4.2.1.2 The east Africa rainfall mode (PC3 -Variance 7.5%)

The third PC mode (un-rotated and rotated) for the rainfall with annual cycles removed explain 7.5% of the variance. Large positive loadings for this PC are found over northeastern Africa, fig 4.1 (e, f). Maximum positive values are centred at about 2°N, 38°E and small negative and positive values are revealed elsewhere particularly over Angola for the un-rotated PC mode. The inter-annual time series plot, fig. 4.1 (k) indicate that the east African region had relatively low rainfall between 1970 and 1976 and between 1984 and 1991. The annual cycle contributes about 19% of the east Africa rainfall and 12% is a contribution from the inter-annual time scale. The time series plot, fig. 4.1 (l), shows high rainfall variability in the region between 1973 and 1984. Fig. 4.1 (m) reveals that amplitudes of the annual cycles are modulated with low amplitudes between 1971 and 1974 and between 1984 and 1986. The wavelet transform plot, reveals relatively high spectral power with oscillations period

between 2 and 4-years fig. 4.1 (m); with large spectral amplitudes between 1965 and 1971, between 1982 and 1994, and between 1990 and 1995.

4.2.2.0 Temperature PCs

PCA was also done for monthly temperature over Africa south of 10°, from 1965 to 1995, with seasonal cycles removed. The leading 3 PC modes were retained and rotated fig 4.2 However, only the first three PC modes (rotated) are discussed. The variance explained by each mode and the location of high values are tabulated in table 4.2.

Table 4.2: Temperature PC modes

Mode	Variance (%)	Approximate Location (Lon./Lat.)
PC1	30.2	6°S-20°S, 20°E-32°E Zambezi and Congo
PC2	10	16°S-28°S, 22°E-34°E Zimbabwe
PC3	6.8	6°N-12°S, 30°E-42°E east Africa

The total variance accounted by the first 3 PCs is 60%. The individual PCs except PC1 are discussed below.

4.2.2.1 The Southern Africa temperature mode (PC2 - variance 10.6%)

The second PC mode, which explains 10.6% variance for the monthly temperature data without the seasonal cycle, is loaded over southern Africa with its center at 31°S, 22°E figs. 4.2 (a, b). The time series obtained by area averaging of temperature in the box shown in fig 4.2 (h) is plotted and reveals that there is relatively large inter-annual temperature variability over southern Africa fig. 4.2 (e-g). High temperatures are shown to have occurred in 1976 and lower temperatures in 1973. Relatively low temperatures are revealed between 1976 and 1995. Large spectral power with oscillations period between 2 and 4 years is revealed. However, relatively high amplitudes are revealed in the years 1965-1975 and 1985-1993.

4.2.2.2 The east Africa temperature mode (PC3 - variance 6.8%)

Centered at 22°S, 22°E, is the third PC mode figs. 4.2 (c, d), which explains 6.8% variance of monthly temperature data without annual cycles. Negative values cover almost the whole southern Africa except the extreme southwestern tip of the Continent. Amplitudes of the time series plot shows high temperature variability figs. 4.2 (i-k). The time series is obtained by area averaging of temperatures in the box in fig 4.2 (l). The positive loading over the southwestern tip of the continent could be associated with westerly frontal wave intrusions in the southern hemisphere. High month to month temperature variability could be attributed to the influence of westerly waves. The wavelet transform of the key area time series in the box in fig 4.2 (l) reveals variability of spectral power with a period of 2 to 4 years. Relatively high spectral power is indicated between 1975 and 1994; Short period variability contains more spectral power for this mode.

4.3.0 Inter-annual spatial and temporal variability of environmental field parameters

4.3.1.0 Sea Surface Temperature PCA

Coherent patterns were found in monthly SST over the Atlantic and Indian Ocean. The location and variance explained by each mode are tabulated in table 4.3. The time series used in the analysis are created by calculating the box area averages in the PC loading regions (key areas). Time series plots for PC1 only are illustrated. Plots for other PCs were also done and some of them are shown in the appendix.

Table 4.3: Sea Surface Temperature PC modes

Mode	Variance (%)	Approximate Location (Lon./Lat.)
PC1	16.7	0°,30°W and 0°,80°E (Atlantic + Indian) SST Atl + Ind
PC2	8.8	15°N,38°W and - 20°S,10°W SST AtlDipole
PC3	6.3	10°S,50°E and -10°N, 20°W (Ind - Atl) SST Ind-Atl
PC1R	16.7	21°N, 61°E Arabian Sea SST Ind
PC2R	8.8	2°S, 10°W Equatorial Atlantic Ocean SST eastAtl
PC3R	6.3	30°N, 20°W SST northAtl

4.3.1.1 SST PC1 mode (Variance 16.7%)

The first PC mode reveals loadings over the Atlantic and Indian Oceans fig. 4.3 (a, b). The un-rotated PC1 mode show relatively large negative loadings centered at 0°, 30°W over the Atlantic Ocean and 0°, 80°E over the Indian Ocean fig 4.3 (a). The rotated PC1 mode is negatively loaded over the Arabian Sea fig 4.3 (b). The key area time series for PC1 mode (un-rotated), obtained by calculating the average of the key area means in the two boxes shown in fig 4.3 (j), indicates high inter-annual variability and relatively small annual variability, figs. 4.3 (g) and 4.3 (h). The wavelet power spectrum of this time series reveals relatively large amplitudes in the 2-4 and 7-12 year period bands' fig. 4.3 (i). The amplitudes in the 2-4 period band, which coincides with the ENSO signal, were weaker between about 1972 and 1980. Small annual variability with little amplitude modulations are revealed.

4.3.1.2 SST PC2 mode (Variance 8.8%)

The second PC mode for the monthly SSTs without the annual cycles explains 8.8% of the variance fig app4a (c, d). PC2 mode (un-rotated) is a dipole in the Atlantic Ocean centered at 15°N, 38°W and 20°S, 10°W negatively loaded over the Gulf of Guinea is centered at 5°S, 10°W after rotation. The plot of the SST time series, fig. app4a (a, b), which is the difference between the positive and negative loading key areas (PC2 un-rotated) fig. app4a (d), indicates small inter-annual variability but large annual variability with small amplitude modulation. The plot time series, fig. app4a (a), indicates that SST over the central Atlantic was cooler than SSTs between the west and east south Atlantic north of 5°N between 1977 and 1984 and warmer between 1969 and 1976. The plot of the SST time series (figure not shown), obtained by calculating the area average of the SST in the box 30°W-10°E, 10°N-20°S where PC2R (rotated) is loaded (the Gulf of Guinea) reveals generally low SSTs between 1974 and 1984 and a decreasing SST trend between 1985 and 1994, fig. app4a (a). Modulation of the annual SST variability is small, fig app4a (b). The wavelet spectral amplitudes for the two time series are similar as both contain relatively high amplitudes with 1.5 to 2 year and 8 to 14 year oscillation periods, fig. app4a (c)

4.3.1.3 SST PC3 mode (Variance 6.3%)

The third PC mode for the monthly SSTs without the seasonal cycle explains 6.3% of the variance

fig 4.3 (d, e). The third PC mode (un-rotated) is positively loaded over the western Indian Ocean, in the box 50°W-0°, 10°N-10°S and negatively loaded over the central Atlantic Ocean, in the box 40°E-60°E, 0°-30°S after rotation. The plot of the time series, calculated as the difference of area averages of SSTs in the 50°W-0°,10°N-10°S and 40°E-60°E, 0°-30°S boxes, shows a high annual and inter-annual variability. Amplitude modulation is revealed in the annual SST variability between 1982 and 1986. The continuous wavelet transform of the time series reveals relatively high spectral amplitudes with oscillation periods of 1.5-3 and 5-8 years.

4.3.2.0 Sea Level Pressure PCA

Similar principal component analysis was performed on sea level pressure over the Atlantic and Indian Ocean basins with the annual cycles removed in the 1965-95 data. The first three PCs explain about 43% of the variance. Table 4.4 lists the variance and approximate location of the loadings.

Table 4.4: Sea Level Pressure PC modes

Mode	Variance (%)	Approximate Location (Lon./Lat.)
PC1	24.1	5°S, 80°E and 5°S,20°W Ind+Atl
PC2	12.1	10°S, 80°E and 20°N,50°W Ind-Atl
PC3	7.2	30°N, 50°W and 20°S,20°W AtlDipole
PC1R	24.1	15°S, 20°W eastAtl
PC2R	12.1	17°N, 95°E eastInd
PC3R	7.2	30°N, 18°W northAtl

4.3.2.1 SLP PC1 mode (Variance 24.1%)

The first PC mode for sea level pressure without annual cycles explains 24.1% of the variance. This PC mode is negatively loaded over the equatorial Atlantic and Indian Oceans and centered at (5°S, 20°W) and (5°S, 80°E) respectively fig 4.4 (a). The plot of the SLP time series, figs. 4.4 (g and h), obtained by calculating SLP area average in the boxes in fig. 4.4 (j) shows high SLP variability at both the annual and inter-annual time scales fig 4.4 (g) and 4.4 (h) respectively. The wavelet

transform of this time series, fig 4.4 (i), indicates relatively large spectral power with oscillations period of 1.5-5 and 8-12 years.

4.3.2.2 SLP PC2 mode (Variance 12.1%)

The second PC mode, for the sea level pressure over the two oceans without the seasonal cycle, explains 12.1% of the variance. The second SLP PC mode (un-rotated) fig. 4.4 (c), is positively loaded over the Indian ocean (10°S, 80°E) and negatively loaded over the Atlantic ocean (20°N, 50°W) in different latitude bands. The time series, obtained by calculating the difference of area averages in the 60°E-90°E,10°N-20°S and 70°W-10°W,0°-30°N boxes, is plotted and reveals high SLP variability at the inter-annual and annual time scale. High amplitude modulation is revealed in the annual cycles. The two time series indicate relatively high spectral energy with 2-5 and 8-12-year oscillations period.

4.3.2.3 SLP PC3 mode (Variance 7.2%)

The third PC mode (un-rotated and rotated) of monthly SLP over the two oceans without the seasonal cycle explains 7.2% of the variance table 4.4. The third SLP PC mode (un-rotated) is a N-S dipole loaded over the Atlantic ocean with a positive centre at 30°N, 50°W and a negative centre at 20°S, 20°W, fig. 4.4 (e). These are the areas of the Azores and St. Helena anticyclones respectively. The difference of the monthly area averages for the two key areas represent the temporal variability of SLP in the PC loading region. The area averages are calculated in the boxes shown in fig. app4b (d). The plot of filtered time series, fig.app4b (a) and fig app4b (b), reveals high SLP variability at both annual and inter-annual time scales. Amplitude modulation of annual cycles is noted in the time series plot fig. app4b (b). The plot shows a general decreasing trend in the amplitude throughout the whole period of 1965 and 1995. The continuous wavelet analysis of the third SLP PC suggests the existence of relatively large spectral amplitudes with periods 1.5 to 5 years and 8 to10 years. Relatively high amplitudes at the period 1.5 to 6 years are revealed throughout the period with modulations in some years fig. app4b (c).

4.3.3.0 Zonal Wind Component PCA

Coherent patterns which were extracted from the zonal and meridional wind components, with the seasonal cycle removed, are discussed in this section. The zonal and meridional wind component fields are analyzed separately. The domain remains the same as in SST and SLP. Table 4.5 gives the central location and variance explained by each PC for U wind field.

Table 4.5: Zonal Wind PC modes

Mode	Variance (%)	Approximate Location (Lon./Lat.)
PC1	8.3	32°S, 50°E and 15°N, 50°W Atl + Ind
PC2	6.5	0°, 80°E Ind
PC3	5.7	20°S, 20°W and 20°S, 60°E Atl +Ind2
PC1R	8.3	20°N, 30°W Atl1
PC3R	5.7	20°S, 20°W Atl2

4.3.3.1 Zonal wind PC1 (Variance 8.3%)

The first PC mode for zonal winds without the seasonal cycle explains 8.3% of the of variance. The zonal wind PC1 mode (un-rotated) has large positive loadings over the north Atlantic and south Indian Oceans centred at 15°N, 50°W and 32°S, 50°E respectively. The zonal wind time series is obtained by calculating area averages over the two boxes as shown in fig.app4c (d). The plot of this time series, shows high inter-annual variability and relatively small annual variability with irregular amplitude modulation figs. app4c (a, b). The continuous wavelet transform analysis reveals relatively strong spectral amplitudes with oscillation period between 1.5 and 3 years, and 3 and 7 years. Strongest amplitudes are revealed between 1982 and 1994. The continuous wavelet analysis of the time series indicates relatively high spectral amplitude with oscillation periods between 2 and 6 years and between 8 and 12 years.

4.3.3.2 Zonal wind PC2 (Variance 6.5%)

The second PC mode for zonal wind without the annual cycles explains 6.5% of the variance fig 4.5 (c). As the un-rotated and rotated loading areas for PC1 are almost the same only the rotated one

will be discussed. Positive loading values, for the the second PC are loaded over the central Indian Ocean fig. 4.5 (c). The filtered time series created by calculating the area average over the box 10°N-10°S, 70°E-100°E over the Indian Ocean are plotted in fig. 4.5 (f and g) and reveals small inter-annual zonal wind variability and large annual zonal wind variability over this region. Wavelet analysis of rotated PC2 of zonal wind component indicate oscillation at a period of inter-annual time scale, 4.5 (h). Spectral amplitude with oscillation periods between 2-3, 4-6 and 8-12-years are indicated between 1970 and 1990.

4.3.3.3 Zonal wind PC3 mode (Variance 5.7%)

The third PC3 mode for zonal wind with annual cycles removed explains about 5.7% of the variance. The un-rotated third PC mode is negatively loaded in the subtropical high pressure areas of the southern hemisphere fig. 4.5 (d). The zonal wind time series is obtained by calculating the mean of the appropriate areas of the Atlantic and Indian Oceans. The plot of this time series indicates relatively large inter-annual and annual zonal wind variability with large amplitude modulation at the annual time scale. Small amplitudes are revealed between 1973 and 1983. The wavelet transform of PC3 for zonal wind shows relatively large spectral amplitudes with oscillation periods between 1.5 and 3 years and between 4 and 6 years.

4.3.4.0 Meridional wind PCA

PCA has also been performed on the meridional wind after removing the annual cycles. The domain of analysis is the same as that for zonal wind, SST and SLP. Table 4.6 gives the central location and variance explained by each PC. The first three modes for the meridional wind components without the annual cycles explain about 27% of the variance. The rotated modes are similar to the un-rotated, so only they are retained for analysis.

Table 4.6: Meridional wind PC modes

Mode	Variance (%)	Approximate Location (Lon./Lat.)
PC1R	6.2	33°S, 5°W Atl1
PC2R	5.7	15°N, 27°W Atl2
PC3R	4.8	10°N, 45°E Ind

4.3.4.1 Meridional wind PC1 mode (Variance 6.2%)

The first PC mode (rotated) for the meridional wind without the annual cycle explains 6.2% of the variance. This mode PC is positively loaded over the south Atlantic Ocean with its centre at about 30°S, 5°W fig 4.6 (a). Small positive loadings are also indicated over the northwest and south central Indian Ocean while small negative loading are over the southwest Atlantic Ocean and southwest Indian Ocean. The meridional wind component time series,is obtained by calculating the area average over the southern Atlantic, fig. app4d (d). The plot of the time series show high inter-annual variability of meridional wind wind component over the south east Atlantic Ocean fig. app4d (a). Annual variability is relatively small with amplitude modulation fig. app4d (b). relatively large spectral amplitudes with oscillations period of 2-3 and 4-6 years are revrealed between 1965 and 1982 and 1985 and 1995 respectively, fig app4d (c).

4.3.4.2 Meridional wind PC2 mode (Variance 5.7%)

The rotated PC2 mode (PC2R) for meridional wind component, which is located off the coast of west Africa, is centred at 15°N, 25°W fig. 4.6 (b). This PC mode for meridional wind with the annual cycle removed explains 5.7% of variance. The time series plot, (not shown) created by area averaging of meridional wind component in the box 40°W-10°W, 20°N-10°S, reveals large inter-annual. Large variability is also observed at the annual time scale with relatively small amplitude modulation. The spectral resolution of the inter-annual time series reveals high energy with periods between 2 and 6 years and also between 9 and 12 years.

4.3.4.3 Meridional wind component PC3 mode (Variance 4.8%)

The third PC mode (rotated) is located over the northwest Indian Ocean centred at 10°N, 45°E fig.

4.6 (c). The third PC mode for meridional wind without the annual cycles explains 4.8% of the variance. The time series is obtained by calculating the area average in the box, fig 4.6 (g). The plot of the filtered time series reveal relatively small inter-annual variability and large annual variability with small amplitude modulation figs 4.6 (d, e). Large variability of the meridional wind over the region indicated could be due to the monsoon wind system over the central western Indian Ocean. Oscillations with periods between 2 and 4 years are found to have relatively high spectral energy.

4.4.0 CWT analysis of the teleconnection indices

4.4.1Quasi-Biennial Oscillation

The quasi-biennial zonal wind anomaly time series plot, fig. 4.7 (a) shows relatively large variability at the inter-annual time scale and small variability at the annual time scale, fig. 4.7 (b). Oscillation periods of the QBO, as revealed by continuous wavelet analysis, are between 2 and 3 years as expected. An interesting feature of the frequency-time display is the amplitude modulation of the QBO with time. There are time spans when the QBO amplitude is strong and others when the amplitude is weak.

4.4.2 Nino3 SST and Indonesia SLP anomalies

The time series plots of the Nino3 SST index, fig. 4.8 (a), (area average of SST in the box 150°W-90°W, 5°N-5°S over the Pacific Ocean fig. 4.8 (d)) and the Indonesia sea level pressure anomalies (fig. app4e) (anomalies in the box 90°E-140°E, 5°N-5°S) both show relatively high variability at the inter-annual time scale. The difference between the two indices is revealed in the annual variability. At the annual time scale Nino3 has larger variability, fig. 4.8 (b), than the Indonesia sea level pressure anomalies, fig.app4e (b). The continuous wavelet transform of the two time series reveals similarities in the inter-annual time scale but some differences at the decadal time scale. Relatively high amplitudes, with oscillation period between 8 and 12 year, are revealed in the Indonesia SLPa than the Nino3 time series.

4.5 Summary

In chapter two, it was demonstrated that conversion of PC loadings to key areas is acceptable. as correlation coefficients between PC time scores and respective time series extracted over the parameter loading regions were significant. Parameters over the selected key areas may therefore, be assigned physical meaning. The analysis of the key area time series has revealed evolution of annual cycles and also annual and inter-annual variability of various parameters over diffrent key areas. Frequency-time representation of the key area time series sheds light on the stability climate. Some key areas maintained similar frequency patterns for the whole period, whilst others have shown disjointed frequency patterns. Dominant frequencies are in the range 2-4 years and in many cases, the amplitudes evolve similarly for rainfall and SLP.

Correlation analysis is done in the next chapter to establish the association between potential predictors and predictant key areas. The results help understand mechanisms governing east and southern Africa rainfall.

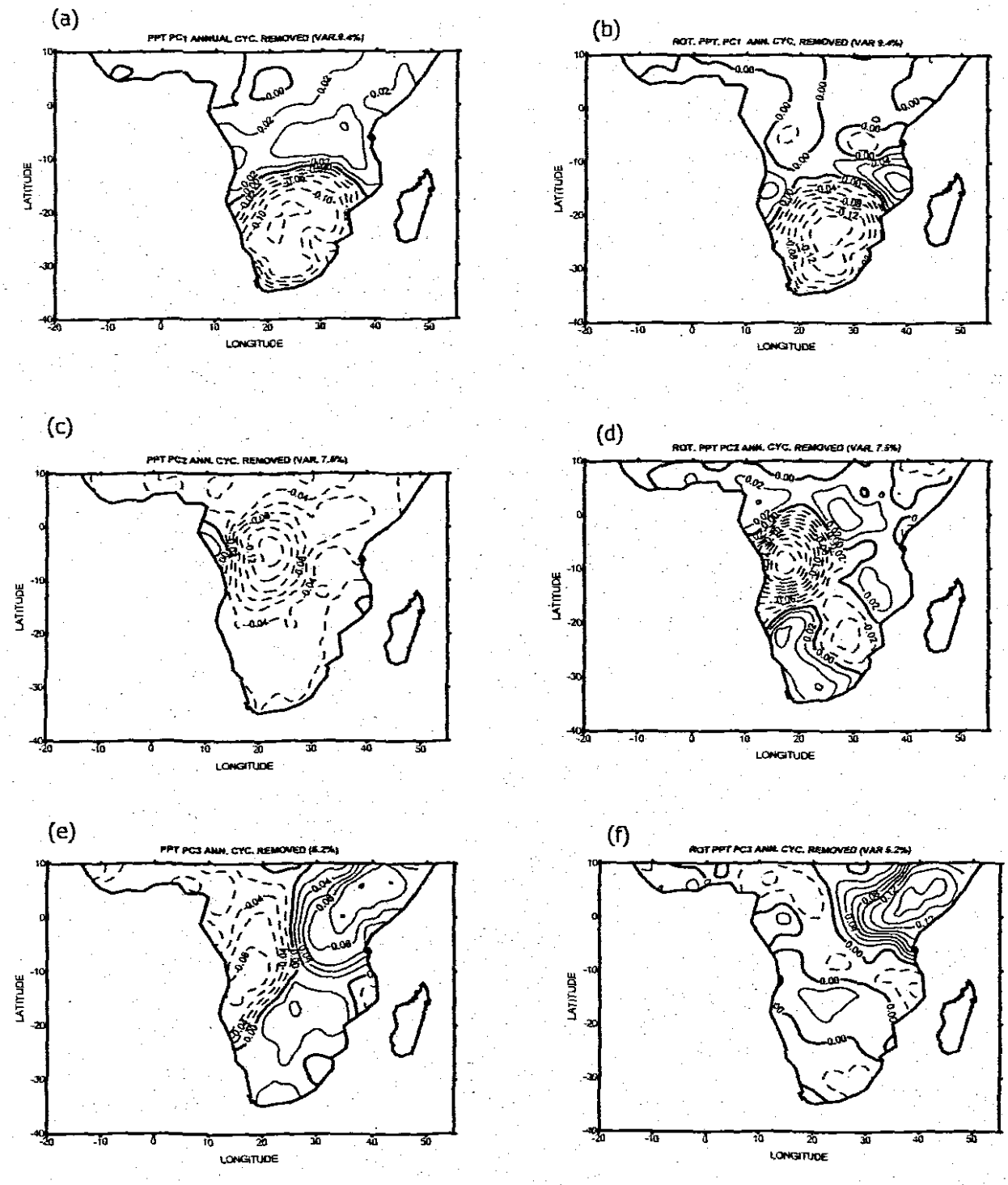

Fig. 4.1: Loading patterns for continental rainfall (a, c, e) unrotated PC1-PC3 modes; (*b,d,f*) rotated PC1-PC3. PCA performed after removing annual cycles from rainfall data at each grid point using wavelet transform.

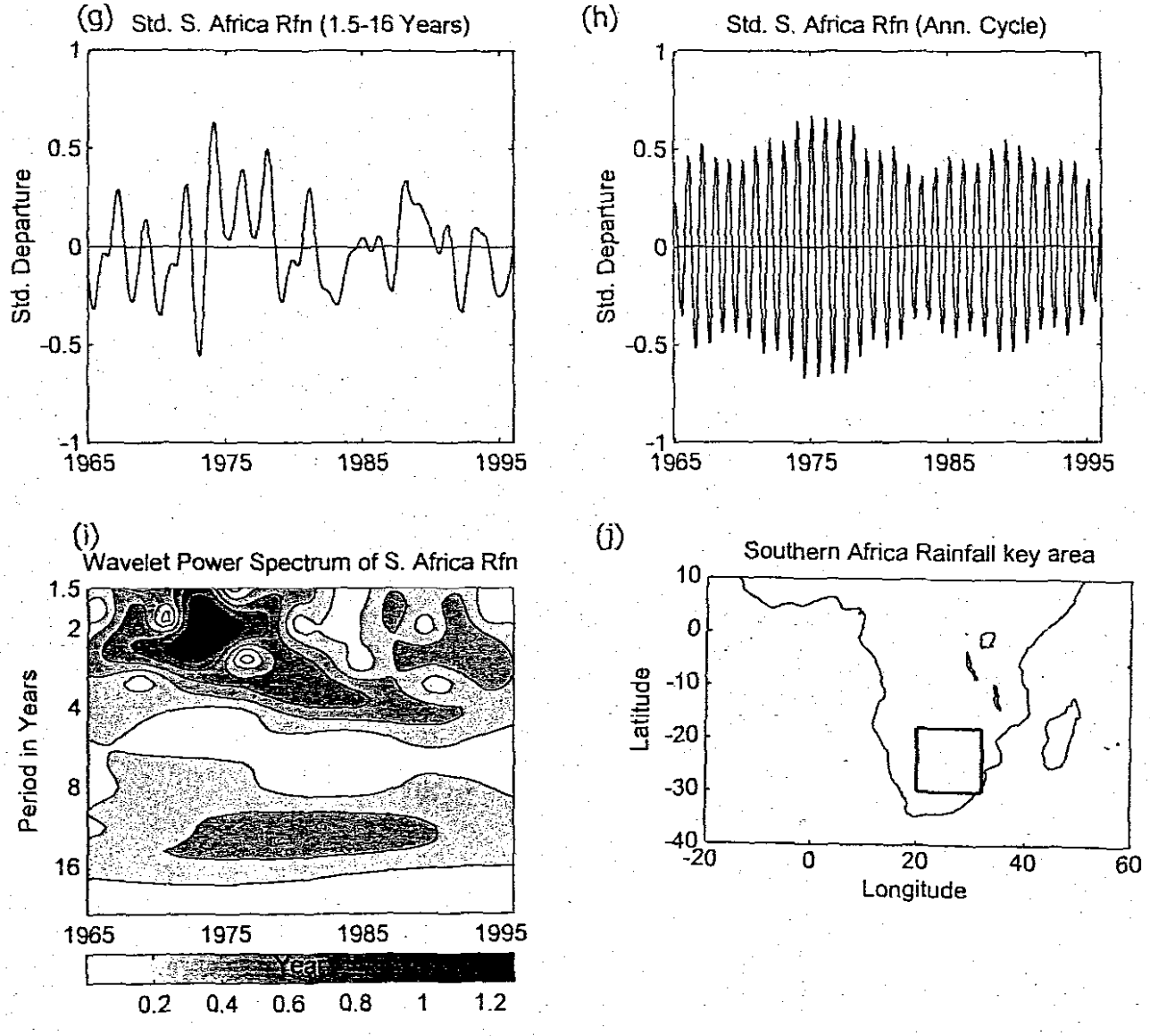

Fig. 4.1: Contd. Plots of: (g) Inter-annual southern Africa rainfall time series index (top left), **(h)** annual variability of southern Africa rainfall (top right), **(i)** modulus of the wavelet transform coefficient for inter-annual variability of southern Africa rainfall (bottom left), **(j)** box for southern Africa key area (bottom right)

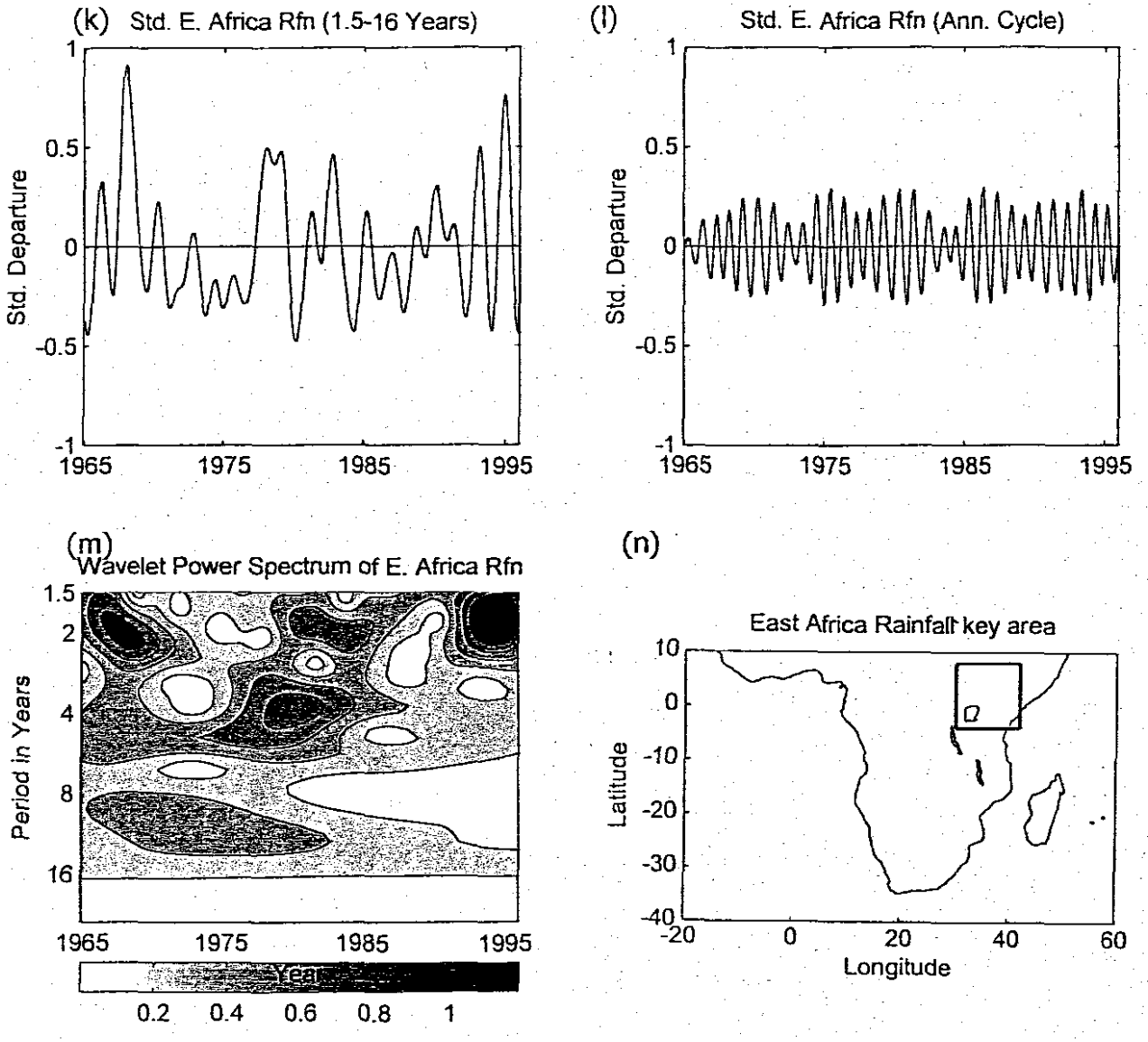

Fig. 4.1: Contd. Plots of: (k) Inter-annual east Africa rainfall time series index (top left), **(l)** annual variability of east Africa rainfall (top right), **(m)** modulus of the wavelet transform coefficient for inter-annual variability of east Africa rainfall (bottom left), **(n)** box for east Africa rainfall key area (bottom right).

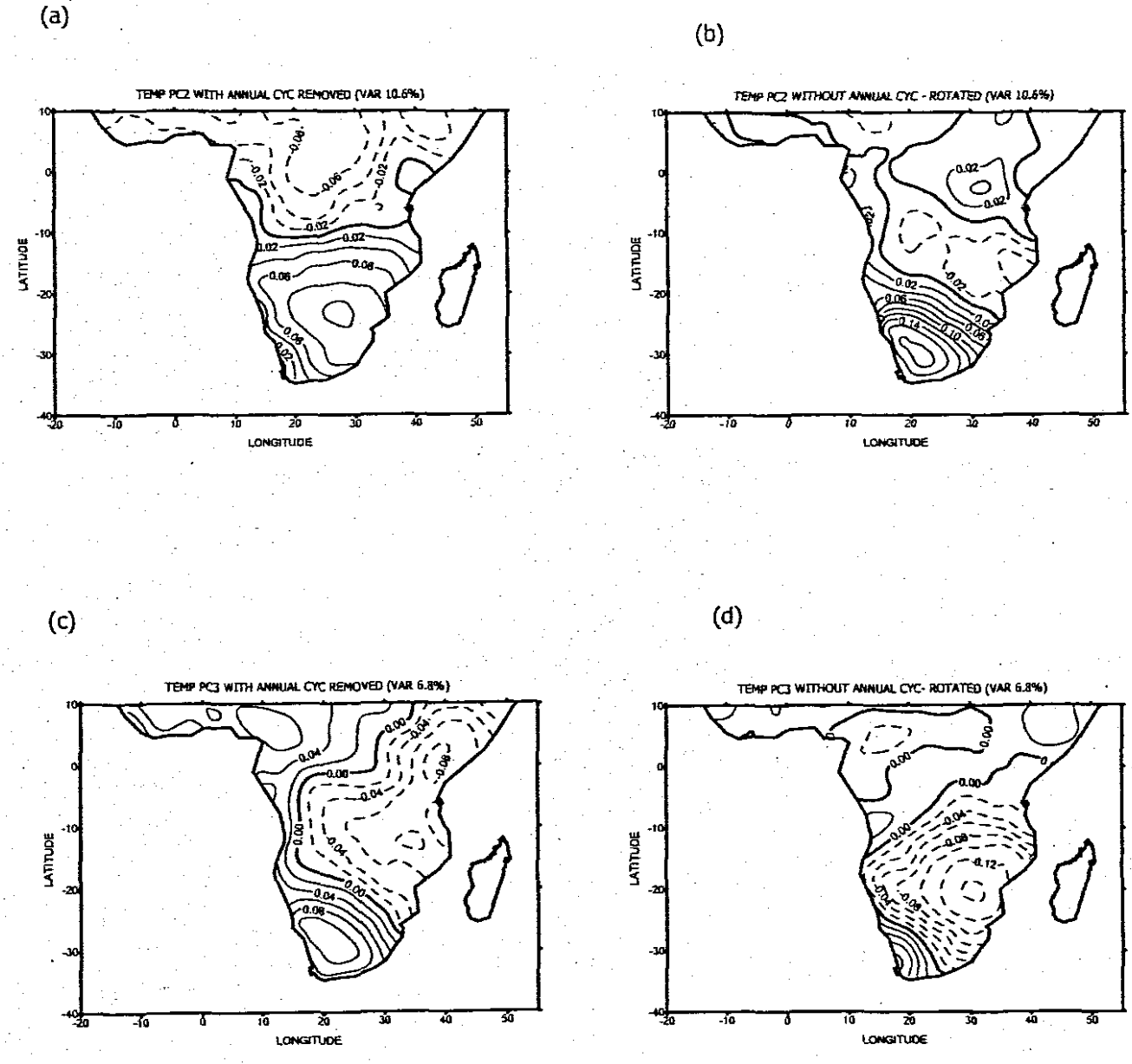

Fig. 4.2: Loading patterns for continental temperature (a,c) unrotated PC2 -PC3 modes; (b,d) rotated PC2-PC3. PCA performed after removing annual cycles from temperature data at each grid point using wavelet transform

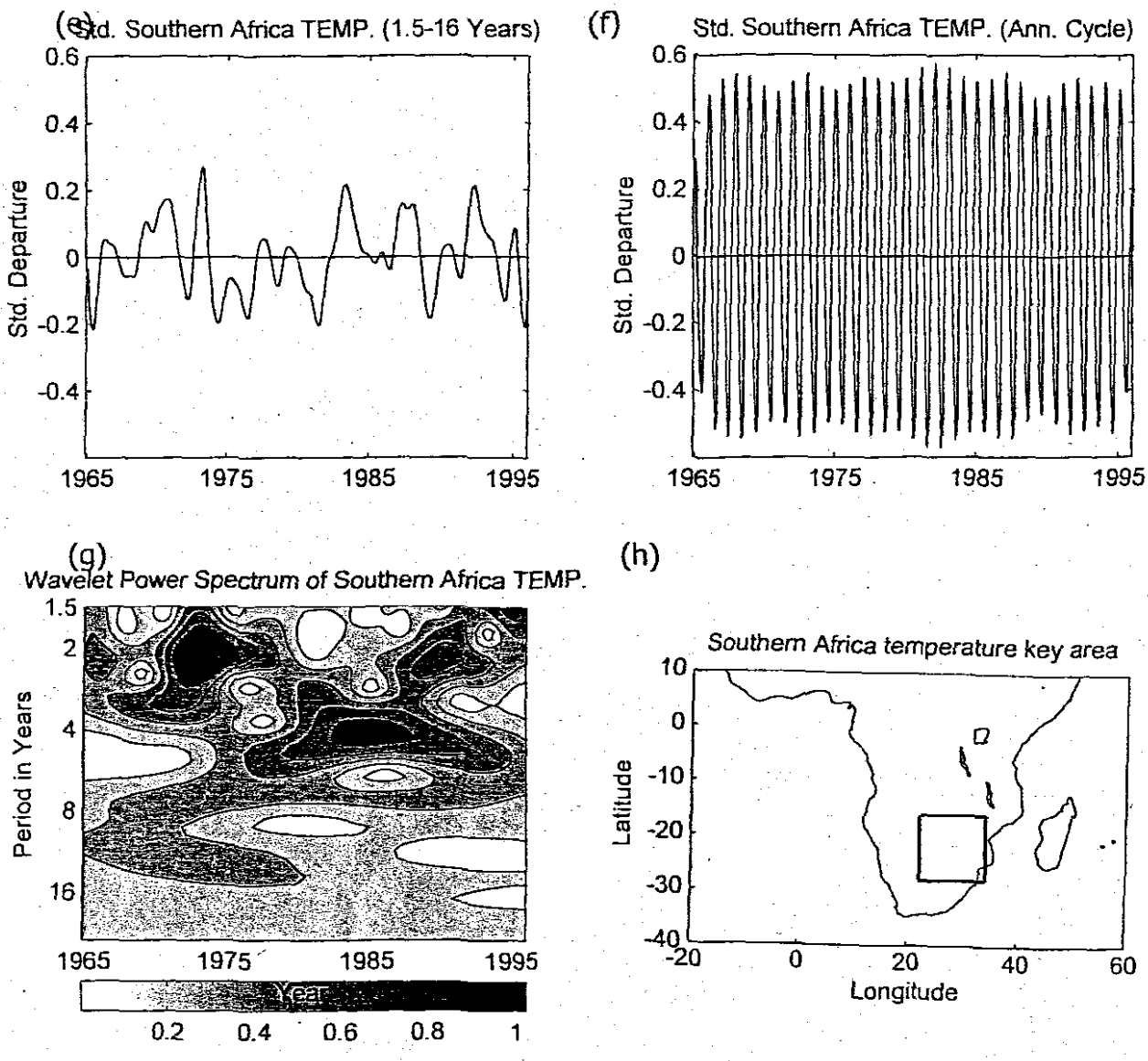

Fig. 4.2: Contd. Plots of: (e) Inter-annual southern Africa temperature time series index (top left), **(f)** annual variability of southern Africa temperature (top right), **(g)** modulus of the wavelet transform coefficient for inter-annual variability of southern Africa temperature (bottom left), **(h)** box for southern Africa key area (bottom right); for the period 1965-95.

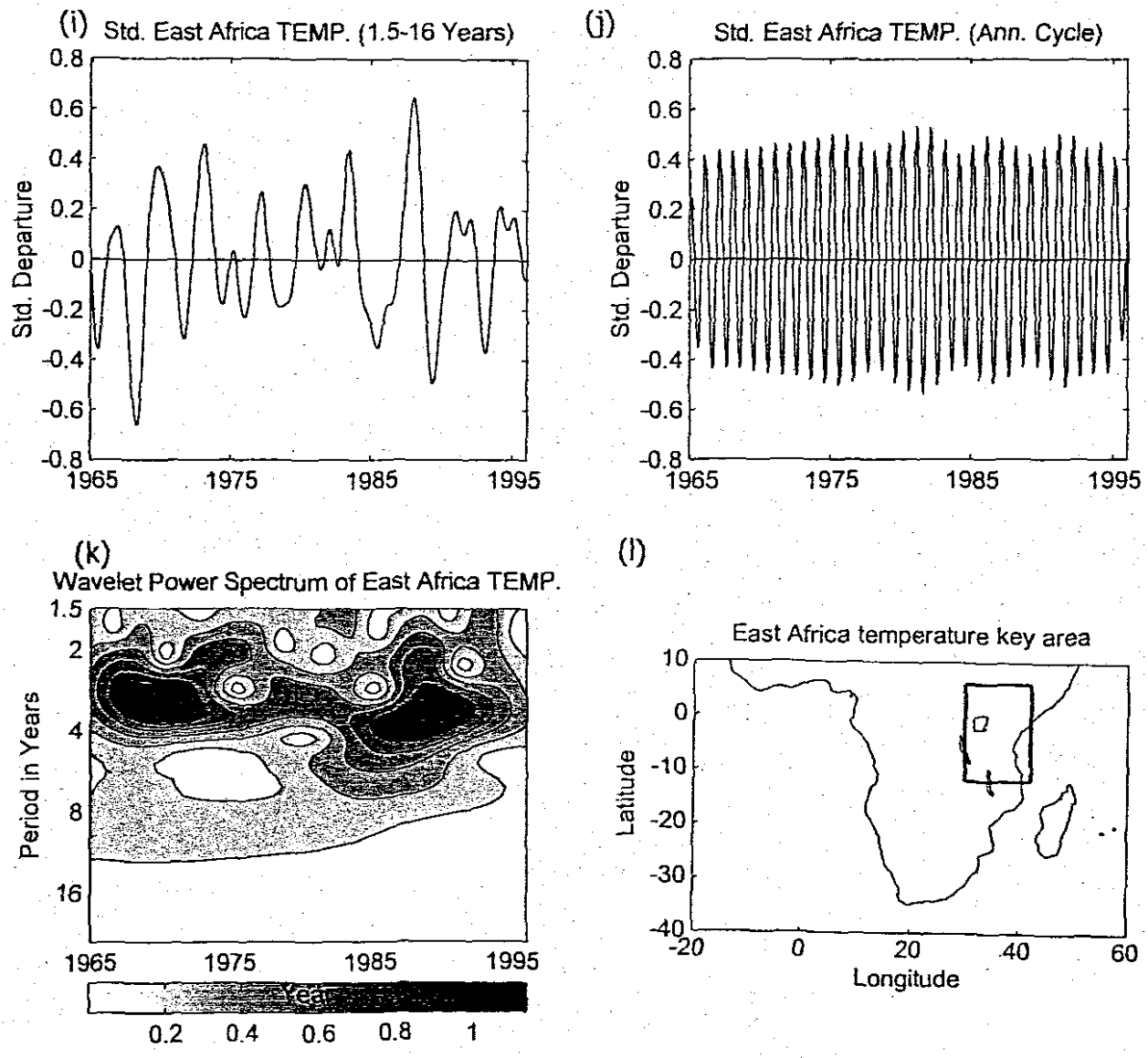

Fig. 4.2:Contd. Plots of: (i) Inter-annual east Africa temperature time series index (top left), **(j)** annual variability of east Africa temperature (top right), **(k)** modulus of the wavelet transform coefficient for inter-annual variability of east Africatemperature (bottom left), **(l)** box for east Africa temperature key area (bottom right)

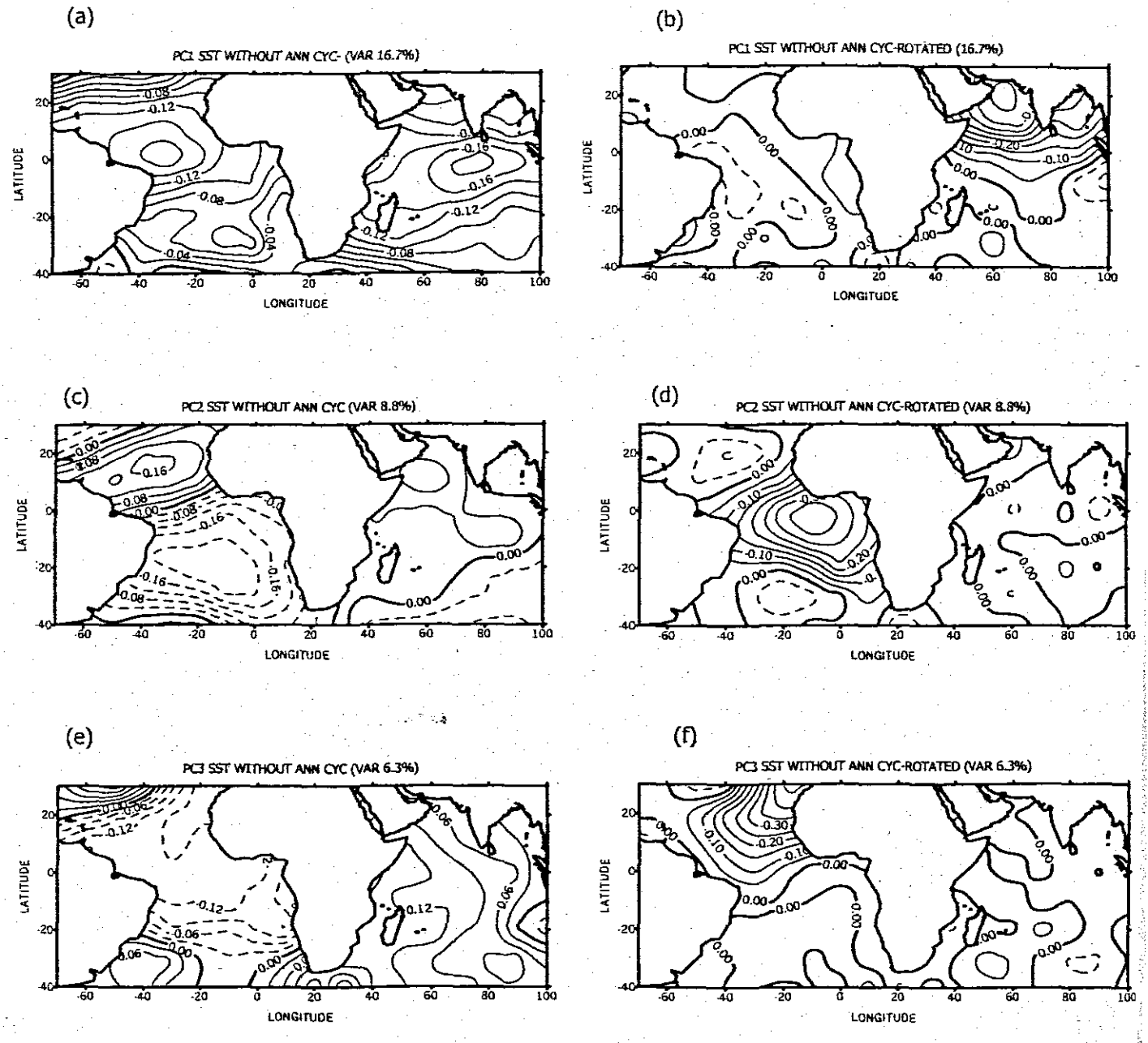

Fig. 4.3 Loading patterns for SSTs over the atlantic and Indian Oceans (a, c, e) unrotated PC 1-3 modes; (b, d, f) rotated PC 1-3. PCA performed after removing annual cycles from SST data at each grid point using wavelet transform

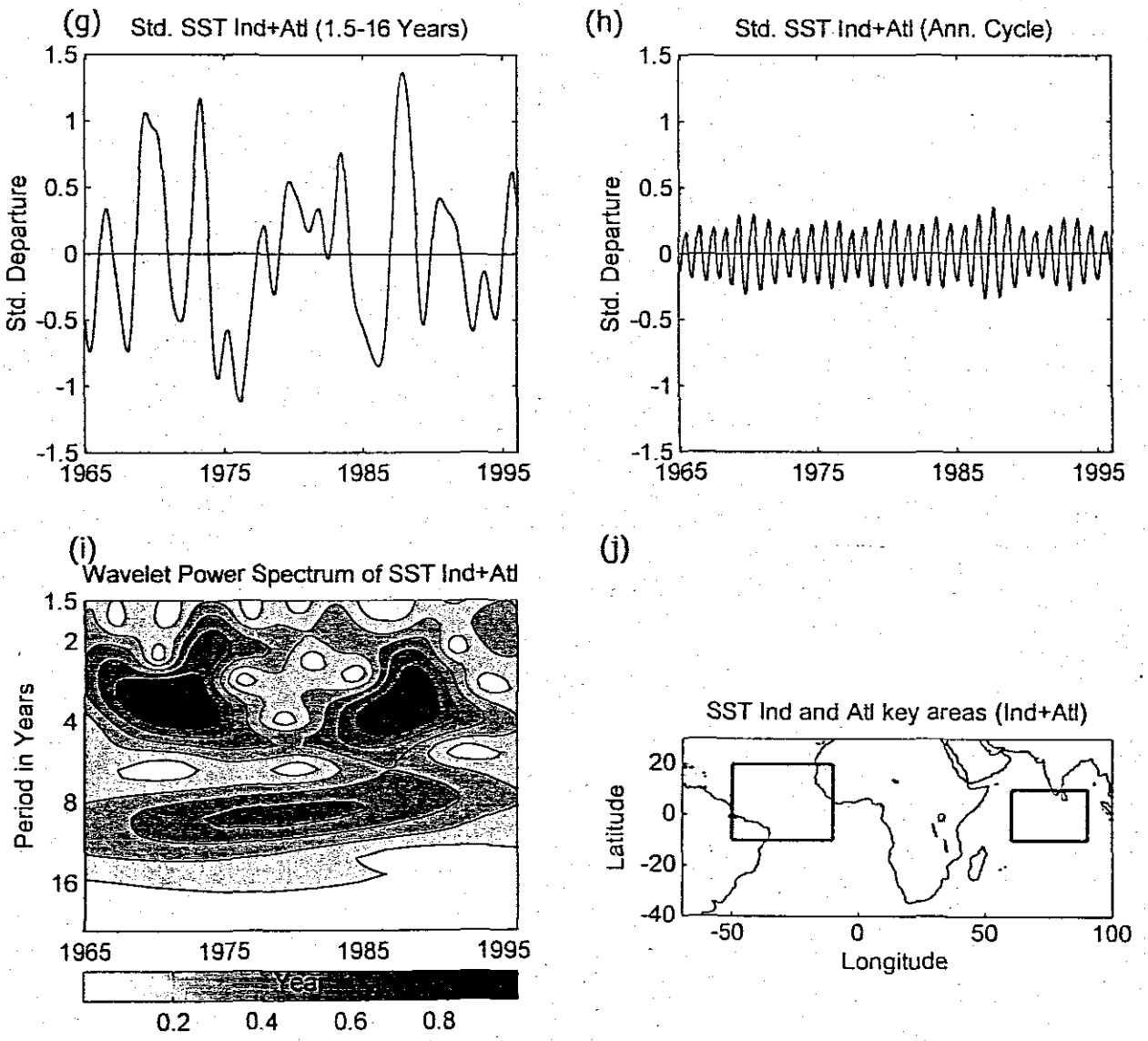

Fig. 4.3: Contd. Plots of: (g) Inter-annual SST Ind+Atl time series index (top left), **(h)** annual variability of SST Ind+Atl (top right), **(i)** modulus of the wavelet transform coefficient for inter-annual variability of SST Ind+Atl (bottom left), **(j)** box for SST Ind+Atl key area (bottom right).

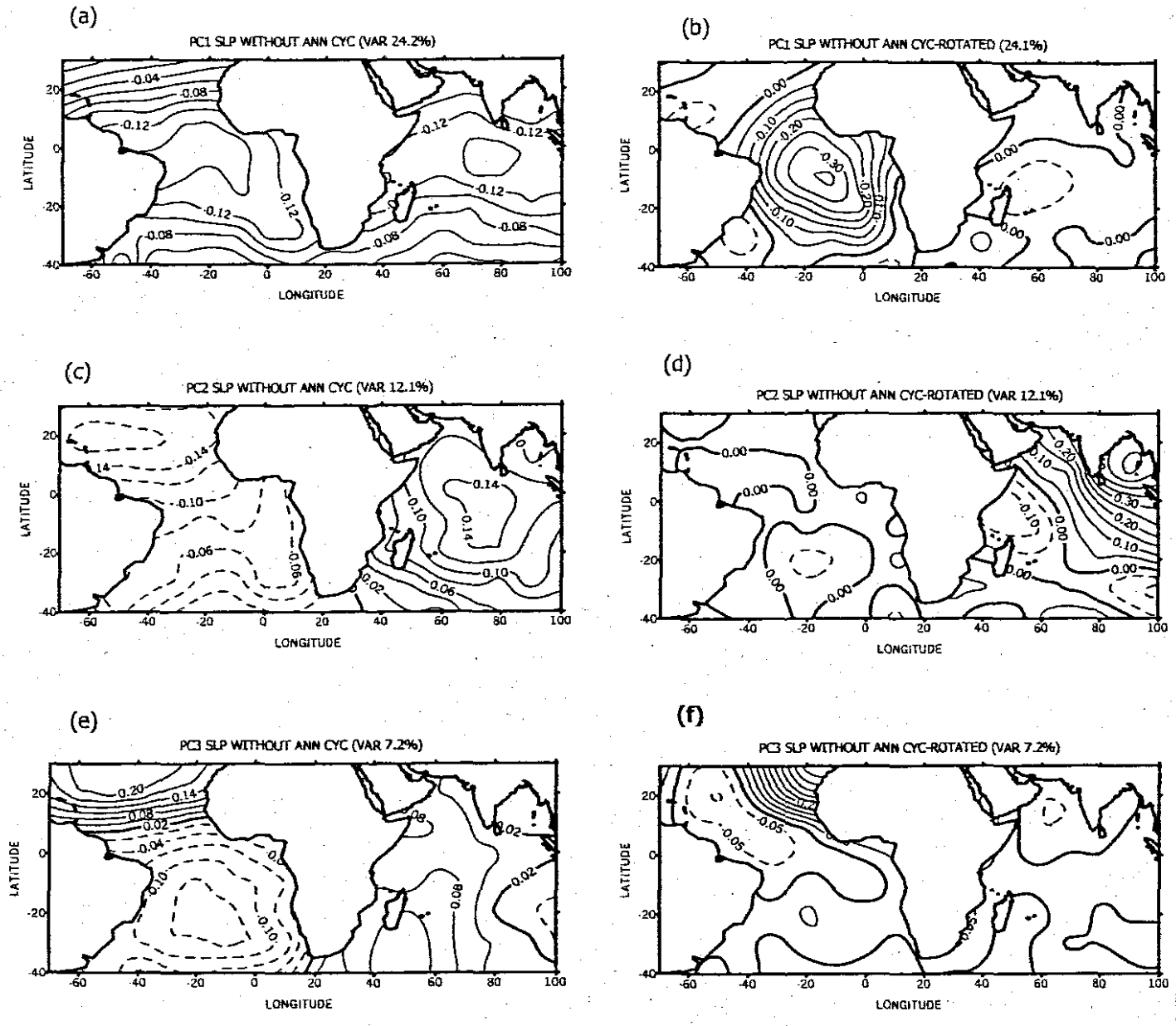

Fig. 4.4: Loading patterns for SLPs over the Atlantic and Indian Oceans (a, c, e) unrotated PC 1-3 modes; (b, d, f) rotated PC 1-3. PCA performed after removing annual cycles from SLP data at each grid point using wavelet transform

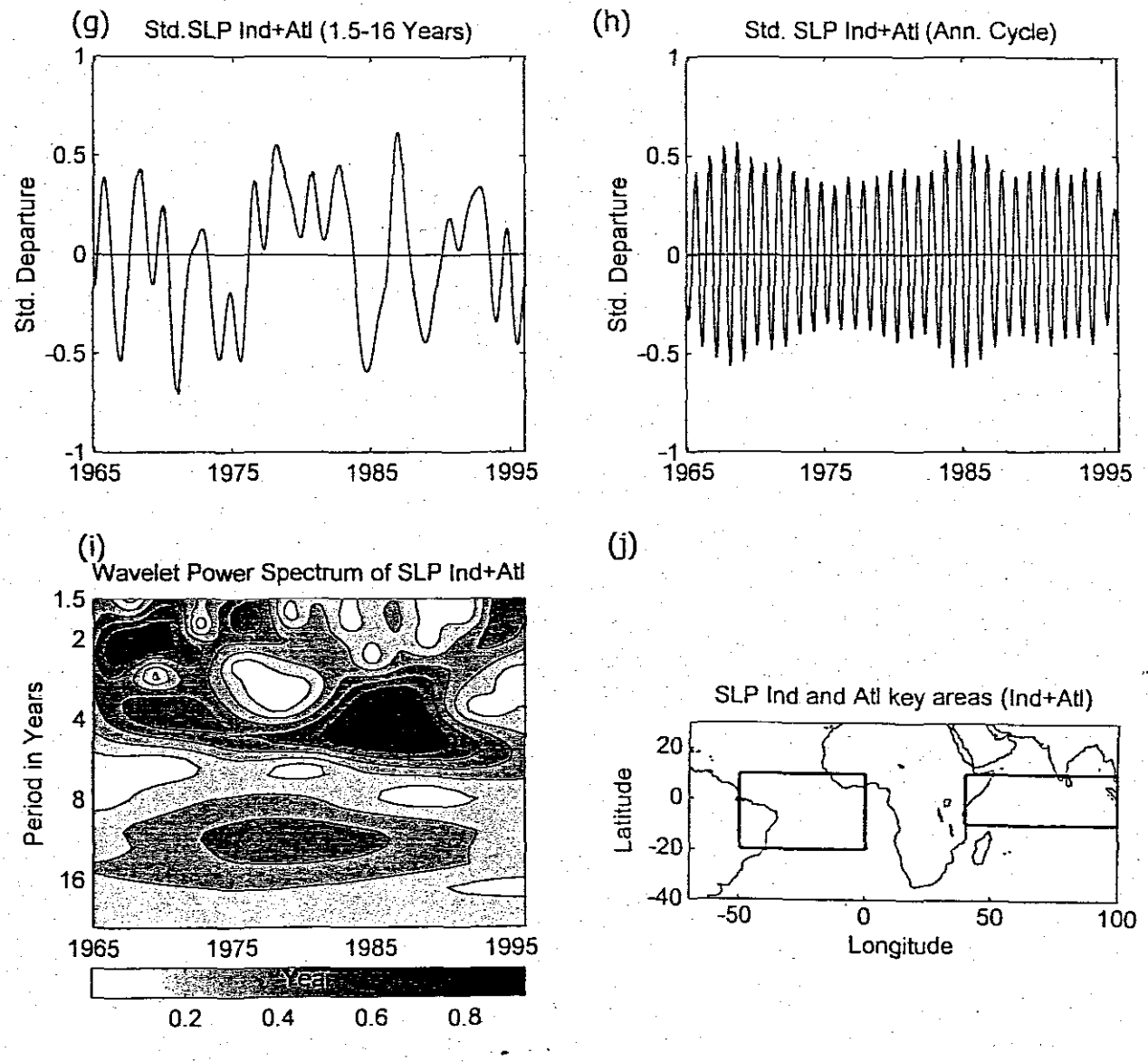

Fig. 4.4: Contd. Plots of: (g) Inter-annual SLP Ind+Atl time series index (top left), **(h)** annual variability of SLP Ind+Atl (top right), **(i)** modulus of the wavelet transform coefficient for inter-annual variability of SLP Ind+Atl (bottom left), **(j)** box for SLP Ind+Atl key area (bottom right).

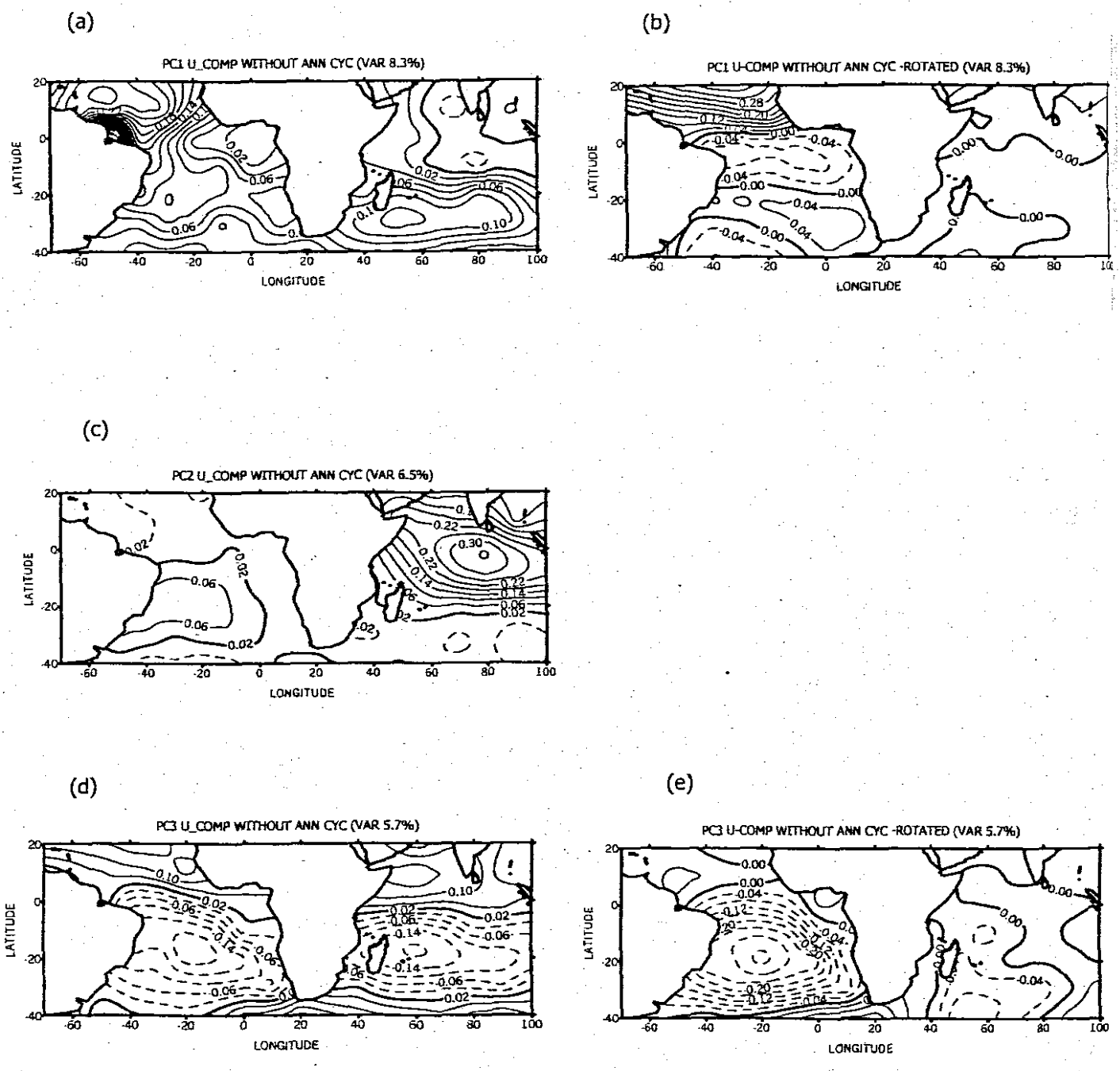

Fig. 4.5 Loading patterns for U wind component field over the atlantic and Indian Oceans (a, c, d) unrotated PC1-PC3 modes; (b, e) rotated PC1, PC3. PCA performed after removing annual cycles from zonal wind data at each grid point using wavelet transform.

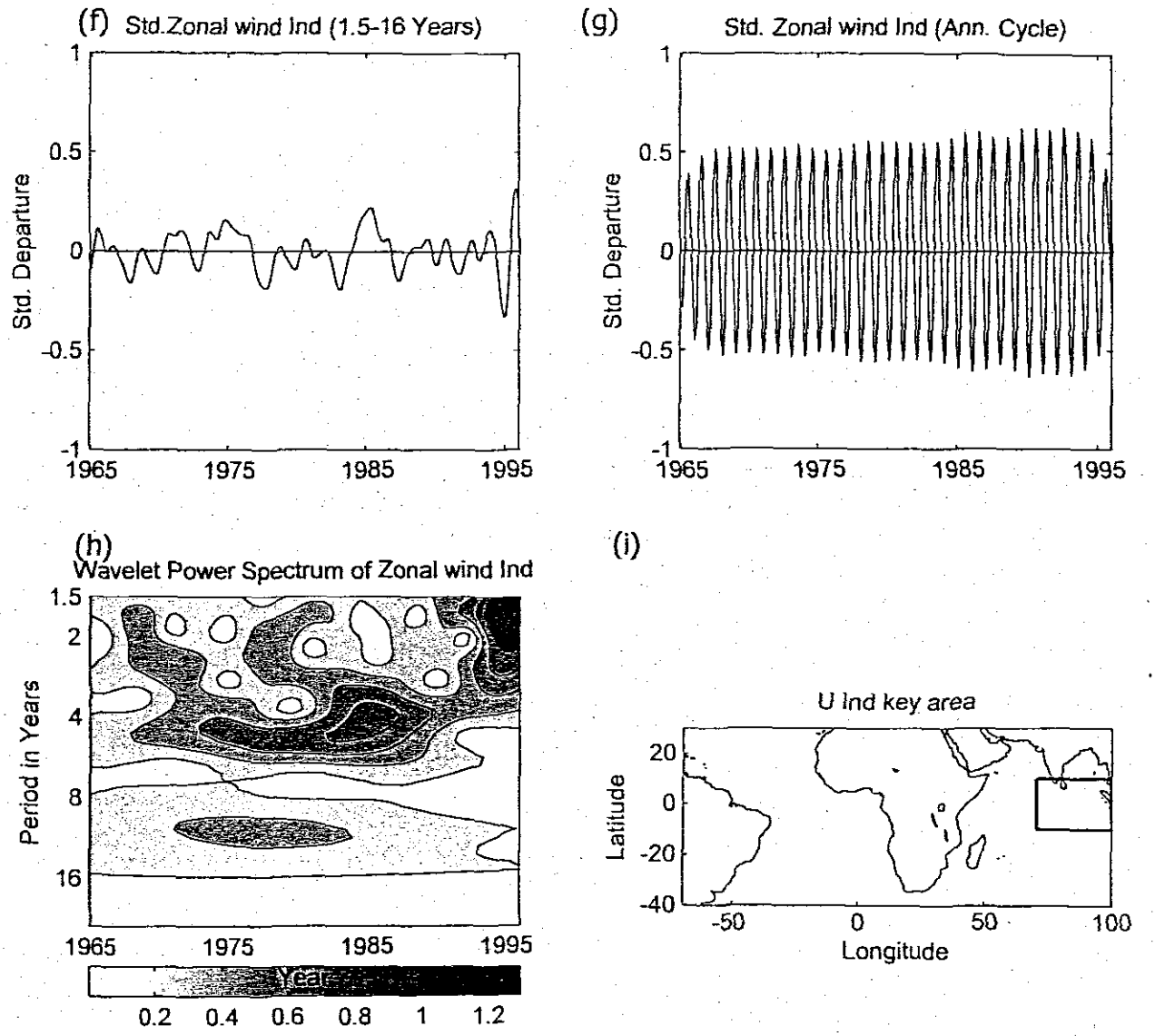

Fig. 4.5: Contd. Plots of: (f) Inter-annual Zonal wind Ind time series index (top left), **(g)** annual variability of Zonal wind Ind (top right), **(h)** modulus of the wavelet transform coefficient for inter-annual variability of Zonal wind Ind (bottom left), **(i)** box for Zonal wind Ind key area (bottom right).

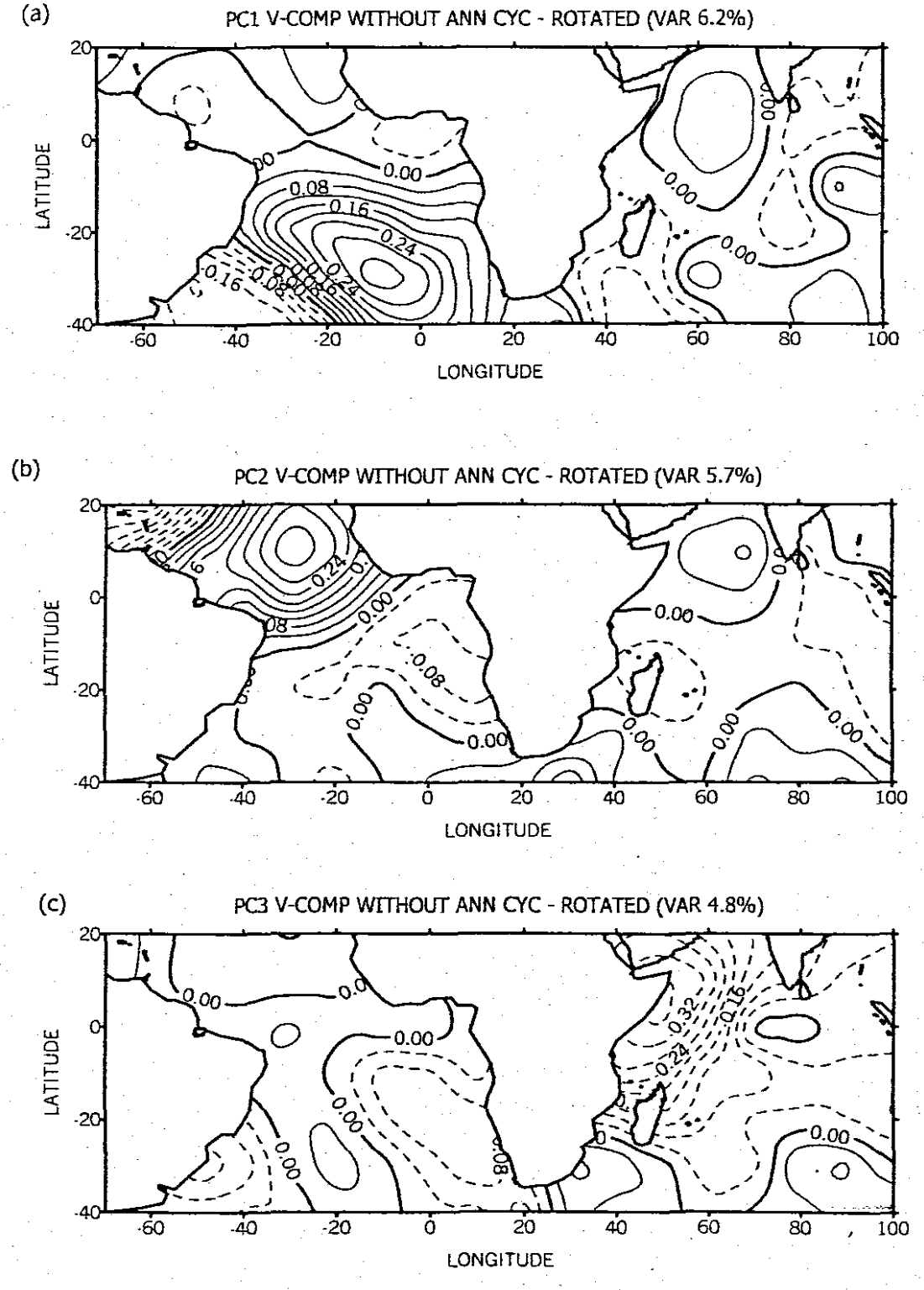

Fig. 4.6 Loading patterns for meridional wind (V) field over the atlantic and Indian oceans (a, b, c) rotated PC1-PC3 modes. PCA performed after removing annual cycles from meridional wind data at each grid point using wavelet transform

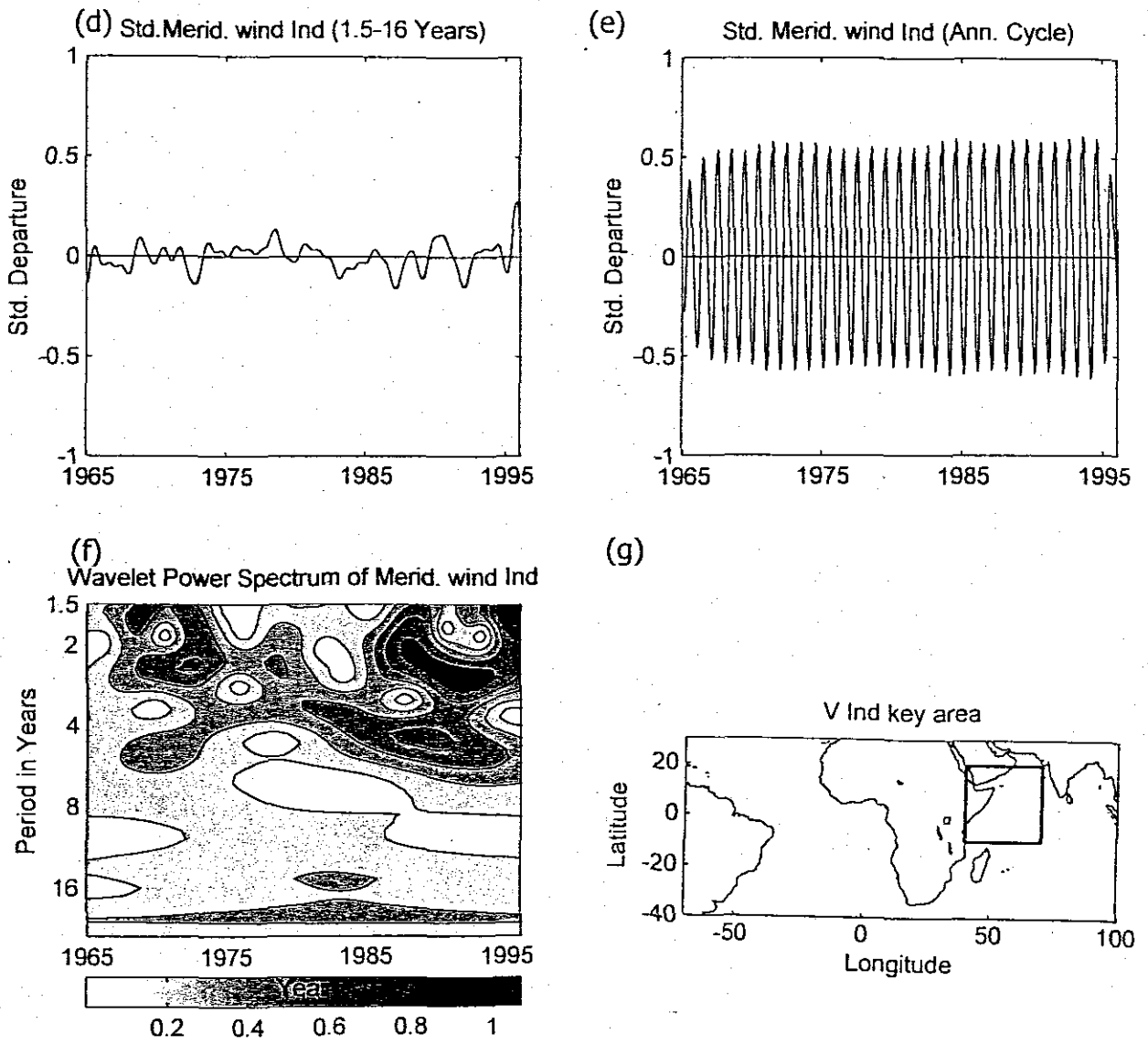

Fig. 4.6: Contd. Plots of: (e) Inter-annual Meridional wind Ind time series index (top left), **(f)** annual variability of Meridional wind Ind (top right), **(g)** modulus of the wavelet transform coefficient for inter-annual variability of Meridional wind Ind (bottom left), **(h)** box for Meridional wind Ind key area (bottom right).

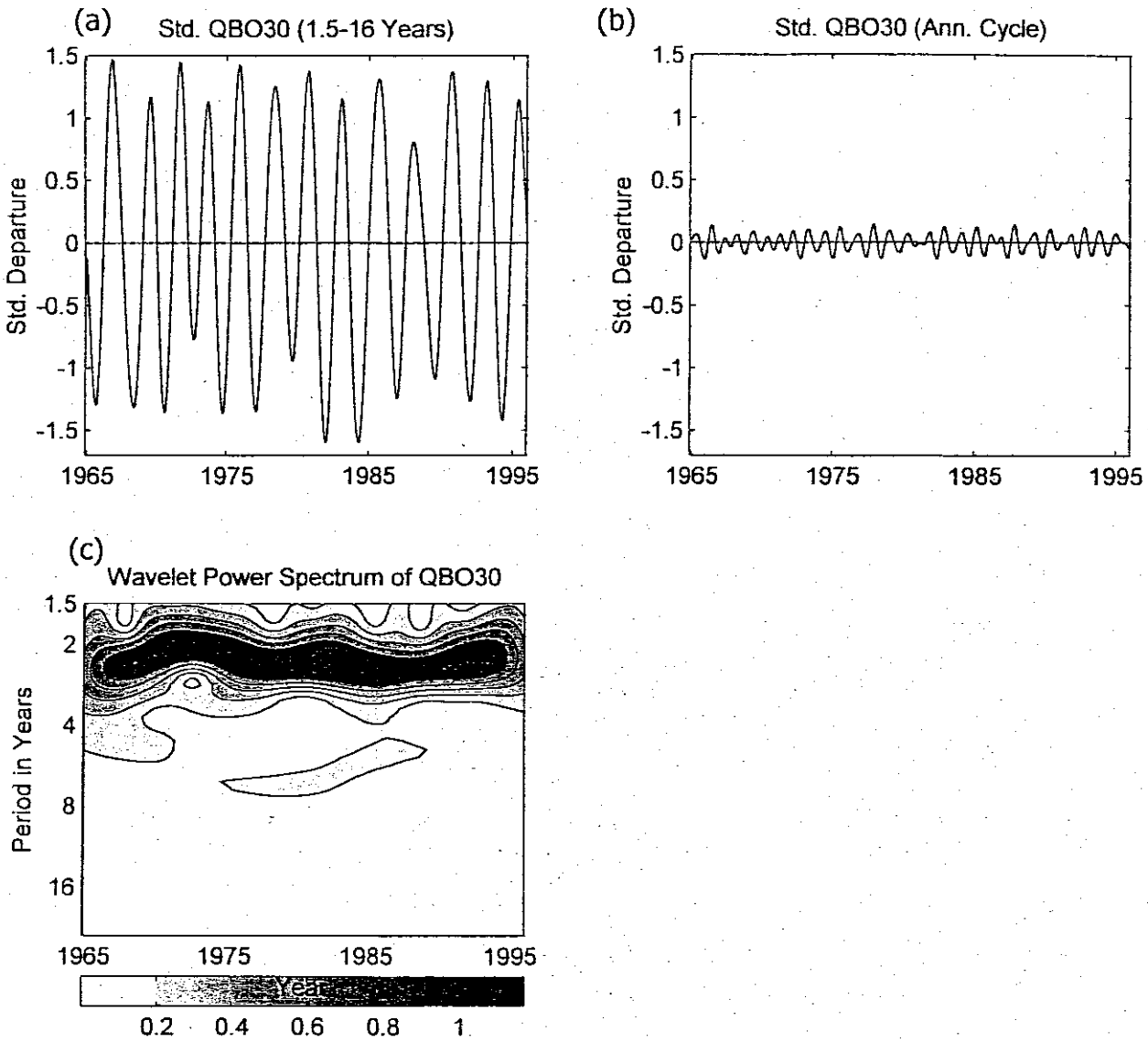

Fig. 4.7: Plots of: (a) Inter-annual QBO30 time series index (top left), **(b)** annual cycles of QBO30 index (top right), **(c)** modulus of the wavelet transform coefficient for inter-annual variability of QBO30 index (bottom left).

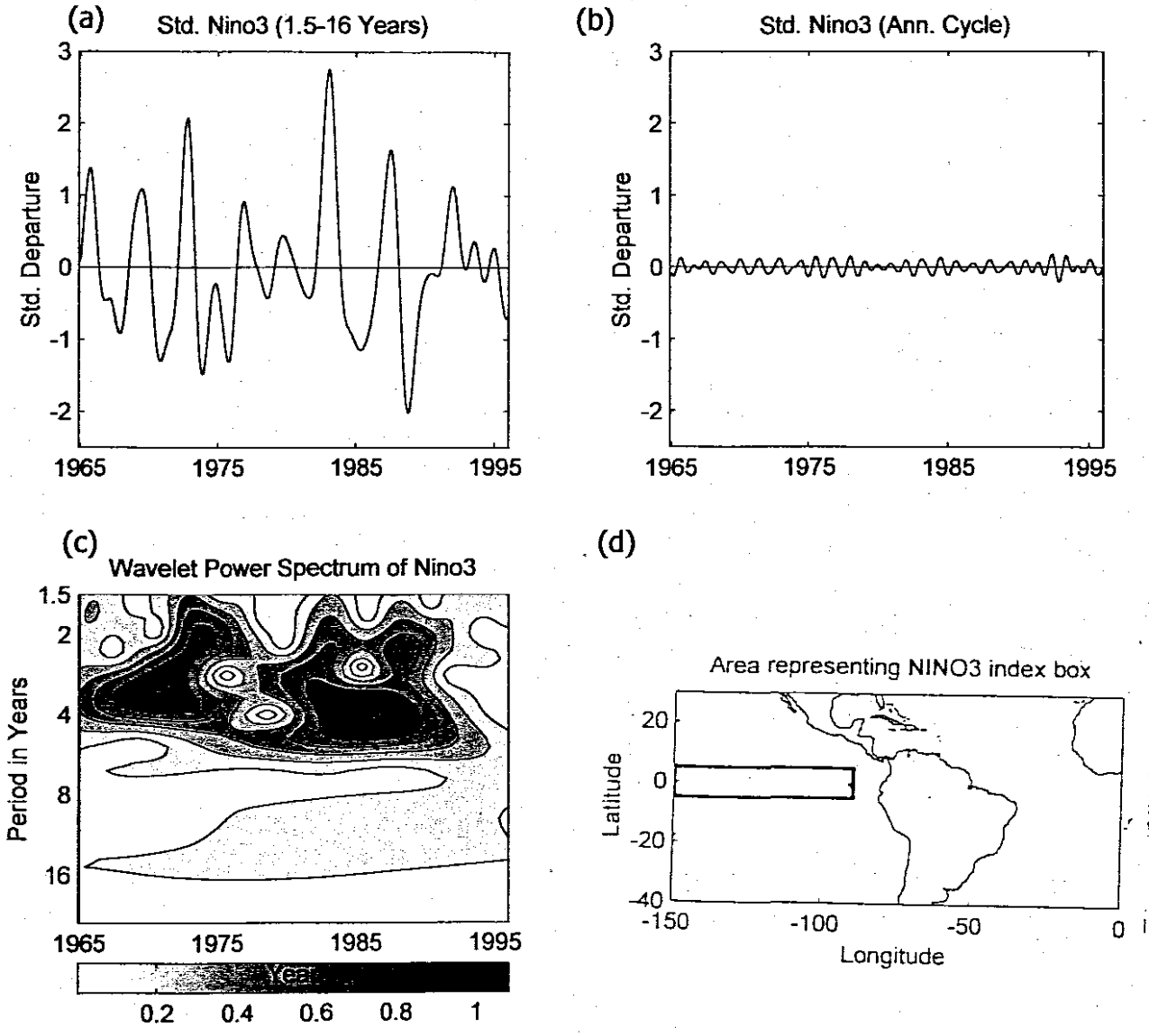

Fig. 4.8: Plots of: (a) Inter-annual SST Nino3 time series index (top left), **(b)** annual variability of SST Nino3 index (top right), **(c)** modulus of the wavelet transform coefficient for inter-annual variability of SST Nino3 index (bottom left); **(d)** box for SST Nino3 index key area (bottom right).

CHAPTER 5

5.0 CORRELATION ANALYSIS

5.1.0 Introduction

One of the objectives of this study is to look into the rainfall predictability potential over tropical highlands of Africa using statistical forecasting method. Statistical forecasting techniques require one to know the historical association between the predictant and the potential predictors or to forecast a meteorological variable from observations of the same or other meteorological variables at a previous time. Here predictor and predictant indices are created by area averaging of data informed by PCA modes outlined in chapter 4. Physical meanings are attached to the extracted PC mode to help establish the mechanism of rainfall variability over the highlands of tropical Africa. The continental Africa rainfall and temperature PCs are the targets or predictants, while the SSTs, SLP, and zonal and meridional winds over the Atlantic and Indian Oceans are the predictors. Rainfall and temperature modes are correlated with environmental patterns or modes in order to identify potential predictors at specified lead times. This approach has been used before by many researchers among them are; (Graham et al., 1987; Barnston and Ropelewski, 1992; Thacker and Lewandowicz, 1996) where the predictor indices are determined by empirical orthogonal functions (EOFs) and extended empirical functions (EEOFs). Many researchers have looked into the teleconnection of East African rainfall with ENSO (Ogallo, 1988, Hastenrath, 1993) and found coupling during the OND season. However, the relation between ENSO and MAM rainfall is reported to be poor. Currently a number of statistical models are in use operationally for forecasting short rains in East Africa. However, few reliable predictors have been identified to predict the long rains.

To describe the relationship between SST, SLP, zonal and meridional winds and terrestrial climate, the simple linear correlation coefficient method is used. First simultaneous correlations between key predictor area and target areas are calculated. Secondly maps of correlation between target areas and environmental parameters over the Atlantic and Indian Oceans are calculated at lag zero using both continuous monthly and seasonal series, and at 3-month lead time using only seasonal time series. In all cases the CWT filter is applied to knock out all variability with cycles less than 1.5 years.

5.2.0 Simultaneous Correlations of monthly data

The degree of association between rainfall/temperature key areas times series and regional/global atmospheric key area indices provide an indication of climatic components modulating the climate over the highlands of tropical Africa. The results from these calculations suggest which key areas and environmental parameters hold the potential of predicting rainfall over the highlands of tropical Africa and therefore, should be used to create rainfall forecast models over the two rainfall key areas of east and southern Africa. For discussion purposes the selected environmental key areas have been assigned names as shown in table 2.3. Correlation coefficients above 0,20 will be discussed, which for 93 degrees of freedom is significant at 95% limit after the data have been filtered using CWT. Filtering data using CWT do not reduce the number of data points. However, the edge effects, which are a factor of the wavelet scale, and the auto-regressive nature of filtered (estimated inter-annual) time series, results in the reduction of the number of degrees of freedom. For geophysical data the number of degrees of freedom (or the number of independent measurements) is much less than the number of data points Sciremammano, (1979) (due to the auto regressive nature of geophysical data). The number of degrees of freedom can be given by (372-1)/4, where 372 is the number of data points and 4 is the number of lags in months, at which auto-correlation are significant at 95% level (auto-correlation coefficients for most key area indices were significant at 95% level at an average of 4 months lag).

5.2.1 South African rainfall association with environmental parameter key areas indices

Correlation coefficients between Southern Africa rainfall key area and potential atmospheric and oceanographic parameters and global teleconnection indices are given in tables 5.1a - 5.1d. Table for correlation coefficients between rainfall and meridional wind components is not shown. Rainfall over the southern Africa key area is negatively associated with SSTs over the tropical Atlantic Indian Oceans (Ind and Atl) key areas. Simultaneous warming/cooling of the equatorial Indian and Atlantic Ocean is associated with the weakening/increasing of pressures over the tropics and a possible withholding of moisture in the equatorial band. The warming of SSTs over northwest Indian Ocean is associated with a (reduced $\partial T/\partial x$) weakening of the Arabian ridge and hence weak northeasterly monsoon. The correlation coefficients between rainfall over the southern Africa key area and key areas (SLP Ind+Atl, eastAtl and eastInd) are all negative. High pressures over the equatorial regions (Atl+Ind) of the Atlantic and Indian Oceans are associated with less rainfall over southern Africa. Relatively high pressures over the south Atlantic Ocean

suppresses convection over southern Africa. Note the extension of the loading towards the Benguela cold up-welling over the Atlantic Ocean (Ind+Atl), fig. 4.4a. Pressures over the northeastern Indian Ocean region Ind are negatively associated with rainfall over the Southern Africa key area. The physical explanation for this association is however, not clear. Zonal wind over the Atlantic and Indian Oceans Atl+Ind, Atl1 and Atl2 key areas are negatively associated with southern Africa rainfall while zonal wind over the Indian key area (Ind) is positively associated with the rainfall over the Southern Africa rainfall. Easterlies over the Atlantic and Indian Oceans key areas (Atl and Ind) are associated with wet conditions over the southern Africa. Strong easterlies suggest strong Azores and Mascarene anticyclones, hence evaporative cooling of the oceans there. Similarly easterly zonal winds over the tropical Atlantic Ocean and central south Atlantic Ocean are associated with more rainfall over the southern Africa key area. Positive zonal wind anomalies (westerlies) over the equatorial east Indian ocean are associated with increased rainfall over southern Africa. This association is similar to those found by Mason, (1992). Rainfall over southern Africa is positively associated with meridional wind over the north west Indian Ocean key area V Ind (correlation coefficient +0.325). This suggests that increased southerlies over the west Indian Ocean are associated with increased rainfall over the southern Africa, though the physical explanation is not clear. The westerly phase of QBO30 is positively associated with rainfall over the southern Africa key area, i.e. positive zonal winds at 30 hPa are associated with an increase of southern Africa rainfall. Similar results have also been found by Mason, (1992). The two ENSO indices are negatively associated with rainfall over the Southern Africa key area rainfall. Negative pressure anomalies over Indonesia and negative SSTs over Nino3 are associated with an increase of rainfall over the southern Africa key area. This event corresponds to La Nina.

Table 5.1a: Correlation coefficients between Rainfall and SST key areas

		Rainfall key areas	
		Southern Africa	East Africa
SST KEY AREAS	Ind+Atl	-0.238	
	AtlDipole		0.231
	Ind-Atl		0.380
	Ind	-0.233	
	eastAtl		-0.237

5.2.2 East Africa rainfall association with Environmental key area indices

The SST indices AtlDipole and Ind-Atl are positively associated with rainfall over the east Africa key area and the eastAtl index is negatively associated with rainfall over this key area. A positive AtlDipole index requires that SST over the north Atlantic be warmer than SST over the southern Atlantic. With this temperature set-up the southeasterlies over the southeast Atlantic and the recurved westerlies over the western Atlantic Ocean and Congo Basin become stronger thus pushing moist Congo airmass over the east African highlands. A negative AtlDipole index results in the reversal of pressure gradient thus weakening the westerlies over the eastern Atlantic Ocean and the Congo Basin which may result in reducing rainfall over East Africa.

Table 5.1b: Correlation coefficients between Rainfall and SLP key areas

		Rainfall key areas	
		Southern Africa	East Africa
SLP KEY AREAS	Ind+Atl	-0.297	0.414
	Ind-Atl		0.323
	AtlDipole		0.361
	eastAtl	-0.234	0.423
	easInd	-0.380	0.299

A positive SST index Ind-Atl implies warmer west Indian ocean (hence low pressure anomaly) and colder east Atlantic Ocean (high pressure anomaly). This setup suggests a west-east pressure gradient which allows ageostrophic westerlies from the tropical Atlantic Ocean to penetrate into east Africa crossing the moist Congo Basin. The moist Congo air orographic uplift results in convective activities over east Africa. An increased easterly flow from the Indian ocean can also improve chances for rain. The SLP indices Ind+Atl, Ind-Atl, AtlDipole, eastAtl, eastInd is all positively associated with east Africa rainfall. This pattern of pressure supports an easterly flow over the Indian Ocean. The U indices Ind and Atl+Ind2 are negatively associated with east Africa rainfall while U Atl1 index is positively associated with east Africa rainfall. Together these suggest large-scale convergence. Easterly anomalies (negative zonal wind) over the southern Indian Ocean and southern Atlantic Oceans suggest active southern subtropical anticyclones.

Table 5.1c: Correlation coefficients between rainfall and zonal wind key areas

		Rainfall PCs (Rotated without seasonal cycles)	
		Southern Africa	East Africa
ZONAL WIND	Atl+Ind	-0.229	
	Ind	0.243	-0.535
	Atl+Ind2		-0.207
	Atl1	-0.289	0.214
	Atl2	-0.211	

In such a situation there will be relatively strong southeasterly trade over the Indian Ocean and also southeasterly winds over the Atlantic Ocean which recurves to westerlies into the Congo Basin. This flow pattern supports an increase of rainfall over east Africa. Positive U Atl1 index anomalies suggest a strong push of moist air from the Azores' anticyclone shifting the ITCZ towards east Africa. The meridional wind indices show no significant association with rainfall over the east Africa key area.

The Indonesia sea-level pressure anomaly index is positively associated with the east Africa rainfall. Positive Indonesia SLP anomalies suggest a pressure build-up over Indonesia and therefore air-outflow from Indonesia (strengthening easterlies over the equatorial Indian Ocean) across the Indian Ocean into east Africa. Studies conducted by (Hastenrath et al., 1993) have established that high pressure anomalies over Indonesia are accompanied by low pressure anomalies over the western Indian Ocean. This setup suggests a general westward moisture advection from the Indian Ocean into east Africa. Both QBO30 and Nino3 indices have poor correlation with continuous east Africa rainfall. The Nino3 index association with east Africa rainfall appear to be seasonally locked as shown in chapter 6.

Table 5.1d: Correlation coefficients between rainfall key areas and Global indices

INDICES	Rainfall key areas	
	Southern Africa	East Africa
QBO30	0.317	
IndSLPa	-0.427	0.307
Nino3	-0.470	0.047

5.2.3.0 Temperature key area indices associations with environmental key area indices

5.2.3.1 Southern Africa temperature and Environmental key areas

Most of the oceanic and atmospheric parameter indices over the Atlantic and Indian Oceans appear to be positively associated with the temperature index over the southern Africa key area table 5.2. Indices which indicate negative association with this temperature index are zonal wind index Ind, and meridional wind indices Atl1 and Ind. The correlation between SST indices Ind+Atl and Ind, and the southern Africa temperature index indicate high correlation coefficient values.

5.2.3.2 East Africa temperature and Environmental key area

Almost all of the environmental parameter indices are positively associated with temperature over east Africa except the zonal wind index Ind. All correlation coefficient values which are not significant at 95% level are not shown in the table in table 5.2. The two SST indices Ind+Atl and Ind indicate relatively higher association with the east Africa temperature key area index. These indices, seem to highly influence temperature variability over east Africa. Correlating environmental parameter key area indices with temperature provide higher correlation coefficients than correlating environmental parameter key area indices with rainfall. This perhaps could be attributed to the continuous nature of temperature records as opposed to rainfall records

5.3.0 Spatial correlations

5.3.1.0 Environmental key areas and global indices associations with gridded continental Africa rainfall

In this section environmental key area and global indices associations with gridded continental Africa rainfall are mapped (i.e. inwardly). Correlation coefficients are calculated between an environmental parameter key area index and rainfall time series at each terrestrial grid point over the African continent. Low period signals, with periods less than 1.5 years, are removed to retain the inter-annual variability, using CWT as explained in chapter two. The idea here is to see how inter-annual rainfall, over different regions of Africa, associates with oceanic and atmospheric patterns.

Table 5.2: Correlations between temperature key areas and environmental key areas

Temperature	Southern Africa	East Africa
SST Ind+Atl	0.56	0.75
SST Ind-Atl	0.25	0.28
SST Ind	0.55	0.80
SST northAtl	0.29	0.48
SLP eastInd	0.27	
U Atl+Ind	0.24	0.27
U Ind	-0.36	-0.32
U Atl1	0.20	
U Atl2	0.24	
V Atl1	-0.39	
V Ind	-0.39	
IndSLPa	0.43	0.37
Nino3	0.43	0.48

5.3.1.1 SST key area indices associations with gridded continental Africa rainfall

The SST index Ind-Atl is positively associated with rainfall over east Africa and the Congo basin, and negatively associated with rainfall over southern Africa, fig. 5.1 (c). It should be noted however, that the SST index Ind-Atl is always (>0°C) during the 1965-1995 period; which suggest that temperatures over the Indian Ocean were always higher than those over the Atlantic Ocean. This implies that relatively warmer SST over the western Indian Ocean and relatively cooler over the Atlantic ocean favours more rainfall over east Africa and less rainfall over southern Africa in agreement with Hastenrath, (1993). The SST indices Ind+Atl and Ind are negatively associated with rainfall over Namibia, Angola, Mozambique, Malawi and Zambia figs 5.1 (a, b).

5.3.1.2 SLP key area indices associations with and gridded continental Africa rainfall

The continental gridded rainfall correlation coefficient patterns with SLP indices Ind+Atl and Ind-Atl are similar. These two indices are positively associated with the inter-annual rainfall over east Africa and negatively associated with rainfall over southern Africa, fig. 5.2 (a) and fig.app5a (a). Positive SLP index Ind+Atl means high pressures over the Indian Ocean, in the box 40°E-100°E, 10°N-10°S and high pressures over the Atlantic Ocean, in the box 50°W-0°, 10°N-20°S. A positive SLP index Ind-Atl suggests higher pressures over the Indian Ocean than over the Atlantic Ocean. The east-west pressure gradient favours an east west flow of warm moist air from the

Indian Ocean, to the coast of east Africa which may result in rainfall over east Africa due to orography. The SLP index AtlDipole shows a positive association with rainfall over the coastal areas of east Africa, Angola and Congo, fig. app5a (b). The SLP indices eastInd and eastAtl also reveal a similar correlation pattern over eastern and southern Africa fig. 5.2 (b, c). Positive anomalies of these indices are associated with wet conditions over east Africa and less rainfall over southern Africa.

5.3.1.3 Zonal wind key area indices associations with gridded continental Africa rainfall

The zonal wind component index Atl+Ind1 is shown to be negatively associated with rainfall over Angola, Namibia, southern South Africa and Mozambique fig 5.3 (a). Negative (positive) association is revealed between zonal wind component index Ind and rainfall over northeast (southern). These associations suggest that easterlies over the Indian Ocean, in the box 70°E-100°E, 10°N-10°S, favours more rainfall over east Africa and less rainfall over southern Africa while westerlies have the opposite result fig. 5.3 (b). The zonal wind component index Atl1, is negatively associated with rainfall over southwestern Africa and positively associated with rainfall over eastern Africa (not shown).

5.3.1.4 Meridional wind key area indices associations with gridded continental Africa rainfall

Rainfall over east South Africa shows a positive association with the meridional wind component index Atl1. Out of the three meridional wind component indices selected only the meridional wind component index Ind that shows a reasonable association with southern Africa rainfall. This meridional wind index is shown to be positively associated with rainfall over the south eastern Africa fig 5.3 (c). What is suggested is that stronger northerly anomalies over the west Indian Ocean, in the box 40°E - 70°E, 20°N-10°N, are revealed to be associated with a decrease of rainfall to the southeast of Africa whereas southerlies over the region have an effect of increasing rainfall over the same areas. The stronger inter-hemispheric transfer of momentum retains convection in the equatorial band through monsoon re-curvature.

5.3.1.5 QBO30 index association with gridded continental Africa rainfall

The QBO30 index shows good association with rainfall over southern Africa. The positive association suggests that wet conditions over southern Africa may be expected during the

westerly phase of QBO30, fig 5.4 (a). Similar results have also been revealed by Mason, (1992). Generally weak positive association is revealed over northeastern Africa.

5.3.1.6 *Indonesia SLPa and Nino3 indices association with gridded continental Africa rainfall*

The IndSLPa and the Nino3 indices are discussed together as they are very closely associated and also give similar correlation coefficient patterns. The Nino3 and IndSLPa indices are shown to be positively associated with inter-annual rainfall over east Africa and negatively associated with inter-annual rainfall over southern Africa, fig. 5.4 (b, c). Similar results have been revealed by other researchers (Ogallo, 1988; Mason, 1992; Hastenrath, 1993).

5.3.2.0 East and southern Africa key areas rainfall associations with gridded oceanic and atmospheric parameters over the Atlantic and Indian Oceans

Associations between area-averaged rainfall indices, over east and southern Africa, and oceanic/atmospheric parameters over the Atlantic and Indian Oceans are determined by calculating correlation coefficients. Correlation coefficients are calculated between a rainfall index and an oceanic/atmospheric parameter time series, for the data between 1965 and 1995, at each grid point over the Atlantic and Indian Oceans. Correlation coefficients (90 values over the two oceans) are mapped to obtain correlation maps. A low pass filter is done to all time series (to remove short-term fluctuations with period less or equal to 1.5 years) using wavelet transform. Areas with high correlation coefficient values indicate that the particular parameter over an area has good association with the respective rainfall index. Three and six-month lag correlation coefficients shall be calculated in the next section to see the potential of predicting rainfall over the two selected areas, i.e. east and southern Africa

5.3.2.1 East Africa rainfall key area associations with oceanic and atmospheric parameters

Rainfall over the east Africa key area is shown to be positively associated with SSTs over the western central Indian Ocean and negatively associated with SSTs over the Atlantic Ocean, east of south America. Rainfall over east Africa key area is also shown to be negatively associated with SSTs over southeastern Indian ocean, in the box 85°E-100°E, 10°S-35°S, fig 5.5 (a). It is further revealed that high pressure anomalies over the eastern Indian Ocean and Atlantic Ocean east of south America are positively associated with rainfall over the east Africa key area, fig 5.5 (c). The

coefficients between SST indices northAtl, eastAtl and Ind-Atl are not shown.

5.3.3.2 SLP key area *indices associations with gridded continental* Africa temperature

With the hydrostatic balance holding, it should be expected that with a rise/fall in temperature there should be a fall/rise in pressure. Therefore, the discussion in this section will be done with this simple principal in mind. The SLP indices Ind+Atl and Ind-Atl are shown to be oppositely related with temperatures over the western and eastern sides of the continent and directly associated with temperatures over the central part of the continent figs 5.7 (a). Pressure rises over the key areas could partly be a result of temperature falls while pressure fall could be partly explained warming. The mapping of correlation coefficients between SLP indices AtlDipole, eastAtl and NwestAtl and continental temperatures are similar fig 5.7 (b). Interesting patterns in these maps are the negative correlation coefficient values over the western parts of Africa and weak positive correlation coefficient values over southern Africa and central Africa. Figure 5.7 (c) reveals that the SLP index eastInd is shown to be positively associated with temperatures over southern and central Africa and negatively associated with temperatures over northeast and western Africa. Correlation maps for other indices are not shown.

5.3.3.3 Zonal wind key area indices associations with gridded continental Africa temperature

The Zonal wind component index Atl+Ind is shown to be positively associated with positive temperatures over the southeast and central Africa fig 5.8 (a). This association suggests that weaker Azores and Mascarene anticyclones may result in higher temperatures over the southeast and central Africa. Stronger anticyclones support stronger south-easterlies from the colder southern hemisphere to penetrate into the tropics. The correlation map of fig 5.8 (b) suggests that westerly wind over the Indian Ocean, in an area associated with the zonal wind component index Ind, generally results in falling temperatures over the continent. With westerly anomalies over the Indian Ocean cooler air from the Cooler Atlantic Ocean penetrates into the continent thus cooling it. Associations of zonal wind component indices Atl+Ind2, Atl1 and Atl2 with continental gridded temperatures are patchy and are not discussed.

5.3.3.4 Meridional wind key area indices associations with gridded continental Africa temperature

It is revealed that the associations between the meridional wind component index Atl1 and temperatures over the southern and eastern Africa are negative. The association suggests that a stronger St. Helena anticyclone with southerly winds components (positive V), to the right of the anticyclone, may result in temperature fall over southern and eastern Africa fig. 5.9 (a). Similarly positive meridional wind components over the western side of the Indian Ocean results in temperature falls over southern and eastern Africa, fig. 5.9 (c). Southerly wind components suggest cold air advection from the southern hemisphere. Positive meridional wind components over the V Atl2 key area are associated with temperature falls over the western and southern tip of Africa. It is further revealed that northerlies over this key area are associated with temperature rises over central and southeast Africa.

5.3.3.5 Association between QBO30 index and gridded continental Africa temperature

The association between the zonal wind component Index (QBO30) and temperatures over the African continent are shown to be patchy. However, large correlation coefficient values are shown over the southeastern Africa. This relationship implies that the westerly phase of QBO30 is associated with temperatures rises over the southeastern Africa fig 5.10 (a).

5.3.3.6 Association between Indonesia SLPa and ENSO-Nino3 indices and gridded continental Africa temperature

As stated in previous sections the Indonesia SLPa and ENSO-Nino3 indices represent a similar signal as they are highly correlated. The correlation coefficients between gridded continental Africa temperatures and the IndSLPa and ENSO-Nino3 indices reveal similar patterns which imply that these two indices have a similar effect on temperatures over the continent fig 5.10 (b, c). Positive/negative pressure anomalies over Indonesia have a positive/negative response in temperatures over central and southern Africa while there is a negative association between pressure anomalies over Indonesia and temperatures over the west coastal strip of Africa and northeastern Africa. Continental Africa temperatures respond to Nino3 in a similar manner. In short one could say that temperatures over central and southern Africa respond positively to Nino3 while temperatures over the coastal strip of west Africa and northeastern Africa respond negatively.

5.3.4.0 Temperature over the eastern and southern Africa key areas associations with gridded oceanic/atmospheric parameters over the Atlantic and Indian Oceans

The variability of oceanic and atmospheric parameters, at the inter-annual time scales, can have an influence on the variability of temperatures over the continent. In order to understand the association between area-averaged temperature indices of east, central and southern Africa and oceanic and atmospheric parameters over the Atlantic and Indian Oceans a correlation analysis at zero is done. Correlation coefficients are calculated between a temperature index and an oceanic/atmospheric parameter time series, for the data between 1965 and 1995, at each grid point. All the time series are low-pass filtered, using the continuous wavelet transform to obtain a data series with oscillation period greater than 1.5 years. Correlation coefficients (90 values over the two oceans) are then mapped. Areas with significant correlation coefficients indicate that the particular parameter has an association with the respective temperature index. Three and six month lag correlation coefficients have not been calculated as is the case with rainfall. Discussion of results will be done simultaneously in this section for both the east and southern Africa because the correlation coefficient mappings obtained are very similar.

5.3.4.1 Association between temperatures over east and southern Africa key area indices and oceanic/atmospheric parameters

The mapping of correlation coefficient values between temperature over the east and southern Africa key areas and gridded SST over the Atlantic and Indian Oceans, at the inter-annual time scales, reveal similar patterns as shown in figs 5.11 (a, b). The difference between the two is in the magnitude of the correlation value. It is generally shown that temperatures over the two areas are positively associated with sea surface temperatures over the equatorial Atlantic and Indian Oceans and also the southern hemisphere subtropical Atlantic and Indian Oceans. Temperatures over the Benguela upwelling region are directly associated with temperatures over the two continental areas. Figs 5.11 (c, d) shows the mapping of correlation coefficient values between the east and southern Africa key areas and sea level pressures over the Atlantic and Indian Oceans. Temperatures over the two key areas are shown to be positively associated with SLP over the south-central Atlantic and central eastern Indian Oceans, while sea level pressures over the southern central Indian Ocean and southern and southwestern Atlantic Ocean are negatively associated with temperatures over the east and southern Africa key areas. Temperatures over east and southern Africa key areas are shown to be negatively associated with zonal wind field over

the equatorial Atlantic and Indian Oceans and positively associated with zonal wind field over southern Atlantic Ocean figs 5.11 (e, f). Temperatures over the east and southern Africa key areas are negatively associated with meridional wind field over southeast and northwest Indian and southern Atlantic Oceans and positively associated with meridional wind field over the Indian Ocean south of Madagascar and over the equatorial Atlantic ocean figs 5.11 (g, h). Southerly (positive) cold wind anomaly field, from the cold southern hemisphere, injects cold temperatures into the southern and southeastern parts of the continent.

5.4.0 Inter-annual relationships between rainfall and environmental parameter key area indices

Linear correlation analysis performed in the preceding chapter between rainfall over east and southern Africa, and environmental key area indices have indicated that some indices have good association with some rainfall key area indices. Regional as well as global indices have been used in the calculation of these correlation coefficients. The results make us speculate that some part of the variability of rainfall over east and southern Africa may be partly explained by these regional/global climatic indices. Table 5.3 gives the list of environmental key area indices which have shown good relationship with rainfall over these areas and are considered for further analysis. It should be noted however, that high correlation does not necessarily imply causation. It has been shown, in chapter four, that a number of the environmental indices selected in table 5.3 exhibits oscillations at inter-annual time scale.

Table 5.3: Selected environmental parameter key area indices subjected to further analysis

Parameter	Index	Correlation Coefficients	
		Southern Africa	East Africa
SST	Ind+Atl	-0.24	
	Ind-Atl		0.38
	eastAtl		-0.24
SLP	Ind+Atl	-0.30	
	eastAtl		0.42
	eastInd	-0.38	0.38
U	Ind	0.24	-0.54
	Atl1	-0.29	0.21
V	Ind	0.33	
U	QBO30	0.32	
SLP	IndSLPa	-0.43	0.31
SST	Nino3	-0.47	

The relationships between these indices and rainfall are further investigated graphically to help in the interpreting results. To achieve this, three analyses are made and results shown in figs 5.12 - 5.22. Throughout these analyses the focus shall be on oscillations with period between 1.5 and 8-year period bands, the inter-annual time scale band. The environmental parameter - rainfall indices relationship shall be made in this band. To achieve this high frequency signals with oscillation period less than 18 months (1.5 years) are filtered using an 18-month Gaussian filter leaving low frequency signals (In the wavelet space between 1.5 and 16-year). Seven months of data are lost at the beginning and end of the time series due to the nature of the Gaussian filter. The standardised low frequency components are displayed in figures 5.12-5.22 (top, bold line for rainfall and thin line for environmental parameter indices). The relationship between two series is also investigated in the time frequency domain by computing their cross-wavelet spectrum calculated using equation (9) in chapter 2, $x(t)$ as a low frequency component of rainfall time series and $y(t)$ as the low frequency component of an environmental parameter index time series. The cross-wavelet spectral modulus of the two time series is presented in figures 5.12-5.22 (middle). Finally analysis is made on the instantaneous time delay between two time series (adopted from Melice 2000 personal communication).

5.4.1 Relationship between southern African rainfall and SST index Ind+Atl

The SST index Ind+Atl is plotted against the southern Africa rainfall key area time series as shown in fig 5.12 (top). The time series plot of the two indices show that rainfall over southern Africa is shown to be negatively associated with SST index Ind+Atl. The middle plot of fig 5.12 displays the cross-wave spectral modulus of southern Africa rainfall and the SST index Ind+Atl. The plot indicates high cross-wavelet spectral modulus values from 1971 to 1977 in the 1.5 to 4-year period band, and from 1982 to 1991 in the 2 to 4-year period band. Relatively small cross-wavelet spectral modulus values are also noted in the 8 to 12-year period band between 1970 and 1993. The bottom plot of fig 5.13 displays the instantaneous time delay between rainfall over southern Africa and SST index Ind+Atl time series. Positive values indicate rainfall is leading (in months) and negative values the SST index Ind+Atl is leading. The plot shows that between 1966 and 1984 rainfall was leading the SST index Ind+Atl between 1 to 4 months and at times there were simultaneous responses between the two. Between 1985 and 1990 rainfall was leading the SST index Ind+Atl index by about 10 months while between 1991 and 1994 the SST index Ind+Atl was leading rainfall by about 12 months.

5.4.2 Relationship between southern Africa rainfall and SLP index Ind+Atl

The plot of SLP index Ind+Atl time series against the southern Africa rainfall time series is displayed in fig. 5.13 (top). This plot indicate that rainfall over southern Africa is negatively associated with the SLP index Ind+Atl for a greater part of the time between 1965 and 1995. The rainfall over southern Africa and SLP index Ind+Atl have shown coupling at different period bands between 1965 and 1995 as indicated fig. 5.13 (middle plot). The cross-wavelet spectrum plot indicates high cross-wavelet spectral modulus values between 1965 and 1978 in the 1.5 to 3-year period band, between 1980 and 1991 in the 3 to 5 year period band and between 1970 and 1990 in the decadal period band. The instantaneous time delay plot fig. 5.13 (bottom) shows that the SLP index Ind+Atl time series leading almost throughout by an average of between 15 and 22 months.

5.4.3 Relationship between southern Africa rainfall and SLP index Ind

The relationship between the southern Africa rainfall and the SLP index Ind time series is revealed in fig. 5.14. The SLP index Ind time series is plotted against the southern Africa rainfall time series fig. 5.14 (top), which reveals that southern Africa rainfall is negatively related with the SLP index Ind. The cross-wavelet spectrum of rainfall over southern Africa and the SLP index Ind

indicates high cross-wavelet spectral modulus values between 1970 and 1980 in the 1.5 to 3-year period band, and from 1980 to 1993 in the 3 to 4-year period band. From 1970 to 1980 oscillations period modulates from 3 to 4-year period to 1.5 to 2-year period. Some small cross-wavelet spectral modulus amplitudes are indicated from 1974 to 1993 in the decadal period band. The instantaneous time delay between the southern Africa rain and the SLP index Ind time series is shown in fig. 5.14 (bottom). This plot reveals that the SLP index Ind leading rainfall for a longer time period from 1965 to 1985 with an average period of about 2 to 4 months.

5.4.4 Relationship between southern Africa rainfall and U index Ind

The relationship between the southern Africa rainfall and U index Ind time series is shown in fig. app5b. The top plot displays the plot of the southern Africa rainfall time series against the U index Ind time series. This plot show that rainfall over southern Africa is positively associated with the U index Ind time series for most of the time from 1965 to 1995. The cross-wavelet spectrum between the southern Africa rainfall and the U index Ind time series reveals relatively large spectral amplitudes from 1967 to 1980 in the 1.5 to 3.5-year oscillation period; and from 1977 to 1993 in the 2 to 5-year oscillation period. In the 8 to 12-year oscillation period some relatively large spectral amplitudes are indicated from 1968 to 1990. The plot of instantaneous time delay between the two time series indicates that the U index Ind time series lead southern Africa rainfall for most of the time between 1965 and 1995 with an average time of about 5 months except from 1886 to 1990 when rainfall was leading.

5.4.5 Relationship between southern Africa rainfall and U index Atl1

The relationship between the southern Africa rainfall and the U Atl1 index is graphically displayed in fig. 5.15. The U Atl1 index plotted against southern Africa rainfall is shown in fig. 5.15 (top) and reveals the opposite association between the two time series. Fig. 5.15 depicts the cross-wavelet spectrum of the southern Africa rainfall and the U Atl1 index time series. Relatively large cross-wavelet spectral modulus values are indicated between 1966 and 1995 in the 2 to 4-year period. The 2-year period in 1966 is shown to have modulated to 4 year period in 1995. Also revealed are the relatively large cross-wavelet spectral modulus values between 1966 and 1990 in the 8 to 15-year oscillation period. Fig. 5.15 (bottom) displays the instantaneous time delay between two time series. This plot shows southern Africa rainfall leading the U Atl1 index time series for most of the time from 1966 to 1995 except from 1983 to 1990 and from 1993 to 1995 with an average time of about 20 months.

5.4.6 Relationship between southern Africa rainfall and V index Ind

The southern Africa rainfall is shown to be positively related to the V index Ind and coupled in the 1.5 to 4-year oscillation period as indicated in fig. 5.16. Fig. 5.16 (top) shows the plot of the V Ind index against the southern Africa rainfall time series. The plot indicates that the southern Africa rainfall is positively associated with the V index Ind. The cross-wavelet spectrum of the southern Africa rainfall and the V Ind index time series shows relatively high cross-wavelet spectral modulus between 1967 and 1994 in the 2 to 4-year oscillation period. It is noted however, that the 2-3 year period in 1967 to have modulated to 3-4 year oscillation period. Relatively weak cross-wavelet spectral modulus values are indicated between 1975 and 1990. The V Ind index is shown to lead southern Africa rainfall from 1966 to 1976 and southern Africa rainfall to lead the V index Ind from 1976 to 1992. The average time in both cases is about 5 months (bottom).

5.4.7 Relationship between southern Africa rainfall and QBO30 index

The southern Africa rainfall is shown to be positively associated with QBO, fig.5.17 (top). The two time series are shown to couple in the 1.9 to 2.9-year period (middle). Relatively high cross-wavelet spectral modulus values are revealed almost throughout the whole time in the 1.9 to 2.9-year period. Lower amplitudes however, are indicated between 1983 and 1986 (middle). The plot of instantaneous time delay between the southern Africa rainfall and the QBO30 index (bottom) shows that there has been alternating leadership in the two time series.

5.4.8 Relationship between southern Africa rainfall and Nino3 and IndSLPa indices.

The regional index over the eastern Indian Ocean, IndSLPa and the global index, Nino3 over the Pacific Ocean are discussed in the same section as all are ENSO signals. The two ENSO indices are shown to be positively associated with the southern Africa rainfall figs. 5.18 and app5c (top). The cross-wavelet spectrum between the southern Africa rainfall and IndSLPa, and Nino3 reveal high cross-wavelet spectral modulus values from 1968 to 1977 in the 2 to 4 year period and from 1978 to 1993 in the 3 to 5 year period fig. 5.18 and app5c (middle). The difference between the IndSLPa and Nino3 indices is in the cross-wavelet spectrum results shown in figs. 5.18 and app5c (middle). It is shown that there are relatively high cross-wavelet spectral modulus values between the southern Africa rainfall and IndSLPa than the southern Africa rainfall and Nino3 in the 10 to 12-year period. This suggests that the IndSLPa index has high amplitude in the decadal time scale than Nino3. Both indices show similar characteristics when it comes to instantaneous time delay

analysis. Both indices lead rainfall between 1965 and 1978 with lead a time of about 5 months. Between 1980 and 1995 rainfall leads the two indices with an average time of about 2-3 months figs. 5.18 and app5c (bottom).

5.4.9 Relationship between east Africa rainfall and SST index Ind-Atl

East Africa rainfall is shown to be positively associated with SST index Ind-Atl for most of the time between 1965 and 1995 fig app5d (top). The cross-wavelet spectrum of the two time series fig. app5d (middle) indicates relatively high spectral modulus from 1965 to 1975, 1980 to 1987 and 1993 to 1995 in the 1.8 to 3-year period band. In the 3 to 5-year period band relatively high spectral values are indicated from 1974 to 1993. Fig. app5d (bottom) shows the instantaneous time delay between the two time series. The SST index Ind-Atl index leads the east Africa rainfall from 1965 to 1982 with an average lead time of about 4 to 6 months. From 1982 to 1991 east Africa rainfall leads the SST index Ind-Atl with an average lead time of about 5 to 10 months. For the remaining time the SST index Ind-Atl leads rainfall with an average time of about 5 months

5.4.10 Relationship between east Africa rainfall and SST index eastAtl

Fig. 5.19 (top) shows that the SST index eastAtl index to be positively associated with the east Africa rainfall. The cross-wavelet spectrum of the two time series, fig. 5.19 (middle) shows the two time series coupling in the 1.9-3, 4 to 7 and 9 to 15 year period bands. Relatively high spectral values are indicated between 1967 and 1987 in the 4 to 7-year period band, and between 1966 and 1990 in the 9 to 12-year period band. From 1965 to 1983 and 1990 to 1995 the east Africa rainfall is shown to lead the SST index east Atl with an average lead time of about 20 months (fig. 5.19- middle). Between 1983 and 1990 the SST index eastAtl leads east Africa rainfall.

5.4.11 Relationship between east Africa rainfall and SLP index eastInd

For most of time the east Africa rainfall is shown to be positively associated with the SLP index eastInd fig. 5.20 (top). Relatively larger spectral amplitudes are indicated from 1965 to 1993 in the 3 to 5 year period band and also from 1965 to 1975 relatively high spectral amplitudes are indicated fig 5.20 (middle). The east Africa rainfall is shown to lead the SLP index eastInd for most of the time between 1965 and 1995 with an average lead time of about 12 to 4 years except between 1985 and 1993 when the lead time is between 5 and 20 months (fig. 5.20-bottom).

5.4.12 Relationship between east Africa rainfall and U index ind

The U index Ind is shown to be negatively associated with the rainfall over east Africa (fig. 5.21 (top); the U index Ind is multiplied by -1 for plotting purposes). The cross-wavelet spectrum of the east Africa rainfall and the U index Ind time series is shown in fig. 5.21 (middle). The plot shows relatively high spectral amplitude from 1970 to 1990 in the 3 to 5-year oscillation periods. The U index Ind is shown to lead the east Africa rainfall from 1996 to 1980 with a lead time of about 0 to 4 months. From 1980 to 1995 the east Africa rainfall leads the U index Ind with a lead time of about 0 to 7 months. The plot shows high spectral amplitude from 1970 to 1990 in the 3-5-year oscillations period band.

5.4.13 Relationship between east Africa rainfall and U index Atl1

In fig. app5e (top) the U index Atl1 time series is plotted against the east Africa rainfall time series. This plot shows that the U index Atl is positively associated with the east Africa rainfall. The cross-wavelet spectrum fig app5e (middle) shows relatively high spectral values in the 2 to 4-year period band from 1965 to 1995 and also relatively high spectral values are shown in the 8 to 12-year period band from 1965 to 1985. The east Africa rainfall leads the U index Atl1 by an average lead time of about 5 months.

5.4.14 Relationship between east Africa rainfall and IndSLPa index

Positive association is indicated in the plot of east Africa rainfall against the Indonesia SLP anomaly index IndSLPa. The cross-wavelet spectrum of the two time series fig 5.22 (middle) shows relatively high spectral amplitudes in the 1.9 to 3, 3 to 6 and 9 to 14 year period bands. In the 1.9 to 3-year period band relatively high spectral values are found between 1967 and 1974, and 1982 and 1987. Relatively high spectral amplitudes are also indicated between 1965 and 1993 in the 3-5- year oscillations period band. The instantaneous time delay plot, fig. 5.22 (bottom) shows the east rainfall leading the IndSLPa index between 1965 and 1995 with an average lead time of 0 to 5 months; the lead time increases to 10 months between 1985 and 1993.

5.5 Summary

Results from the correlation analysis in this chapter have revealed that a number of environmental parameters, represented by key areas, are associated with rainfall over east and southern Africa. Although a high correlation between an environmental index and rainfall doesn't imply causality, it is important to speculate on the mechanisms involved. These mechanisms are expected in the

lower atmosphere, but it should be understood that there is an interaction with the ocean and the upper atmosphere (e.g. zonal winds, ocean ekman divergence and changes in SST). Changes in the heat content of the ocean are transferred into the atmosphere by convection and modulate the circulation. Bearing in mind, the physical importance of the environmental key areas and the degree of association with rainfall over east and southern Africa, speculations of mechanisms responsible for the inter-annual rainfall variability over the tropical highlands of Africa are given in chapter 7.

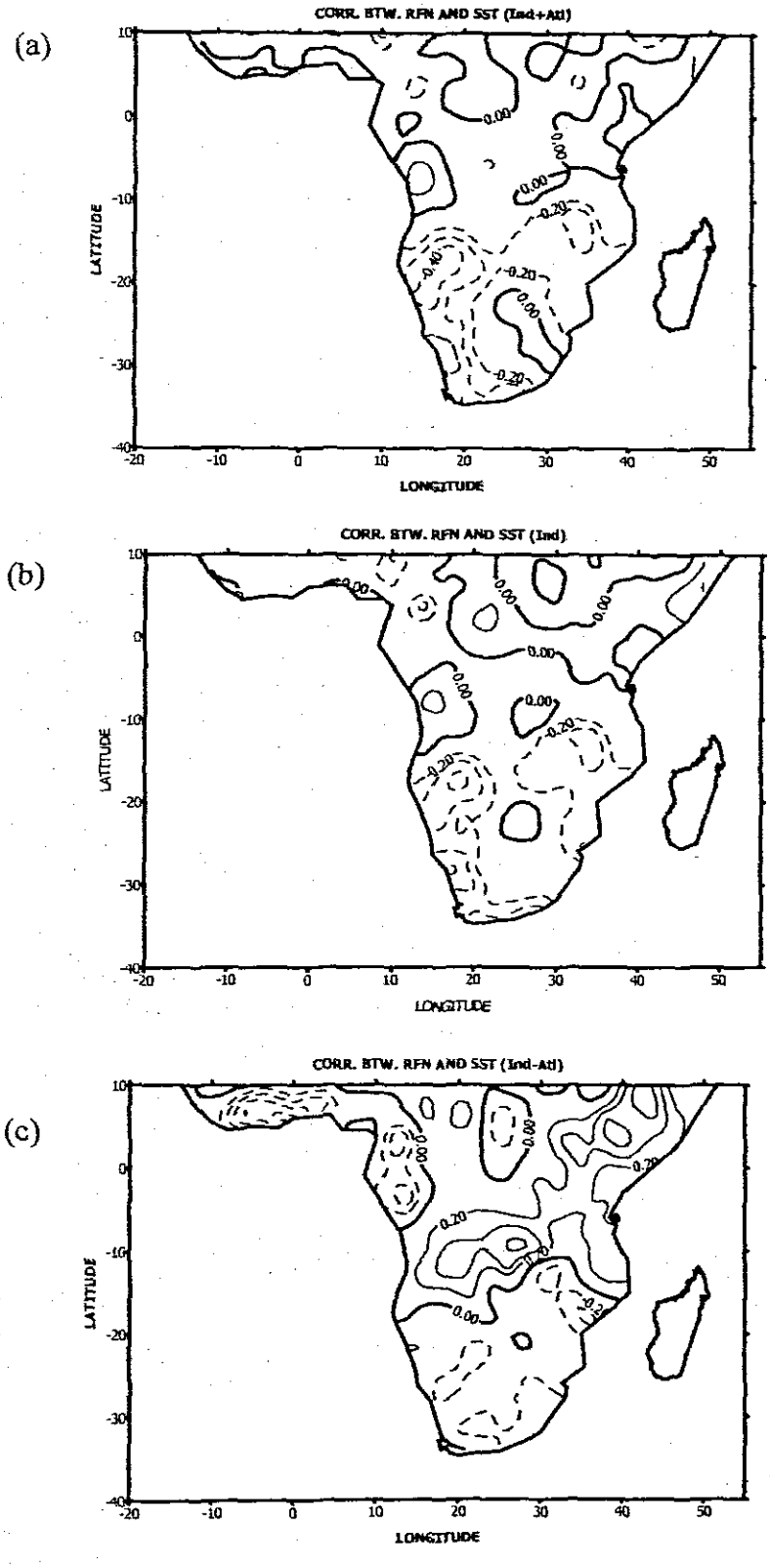

Fig. 5.1: Correlation between continental Africa gridded rainfall and environmental indices. Dashed (continuous) lines represent negatives (positive) correlation coefficients. (a) Correlation btw rainfall and SST Ind+Atl, (b) Correlation btw rainfall and SST Ind (c) Correlation btw rainfall and SST Ind-Atl

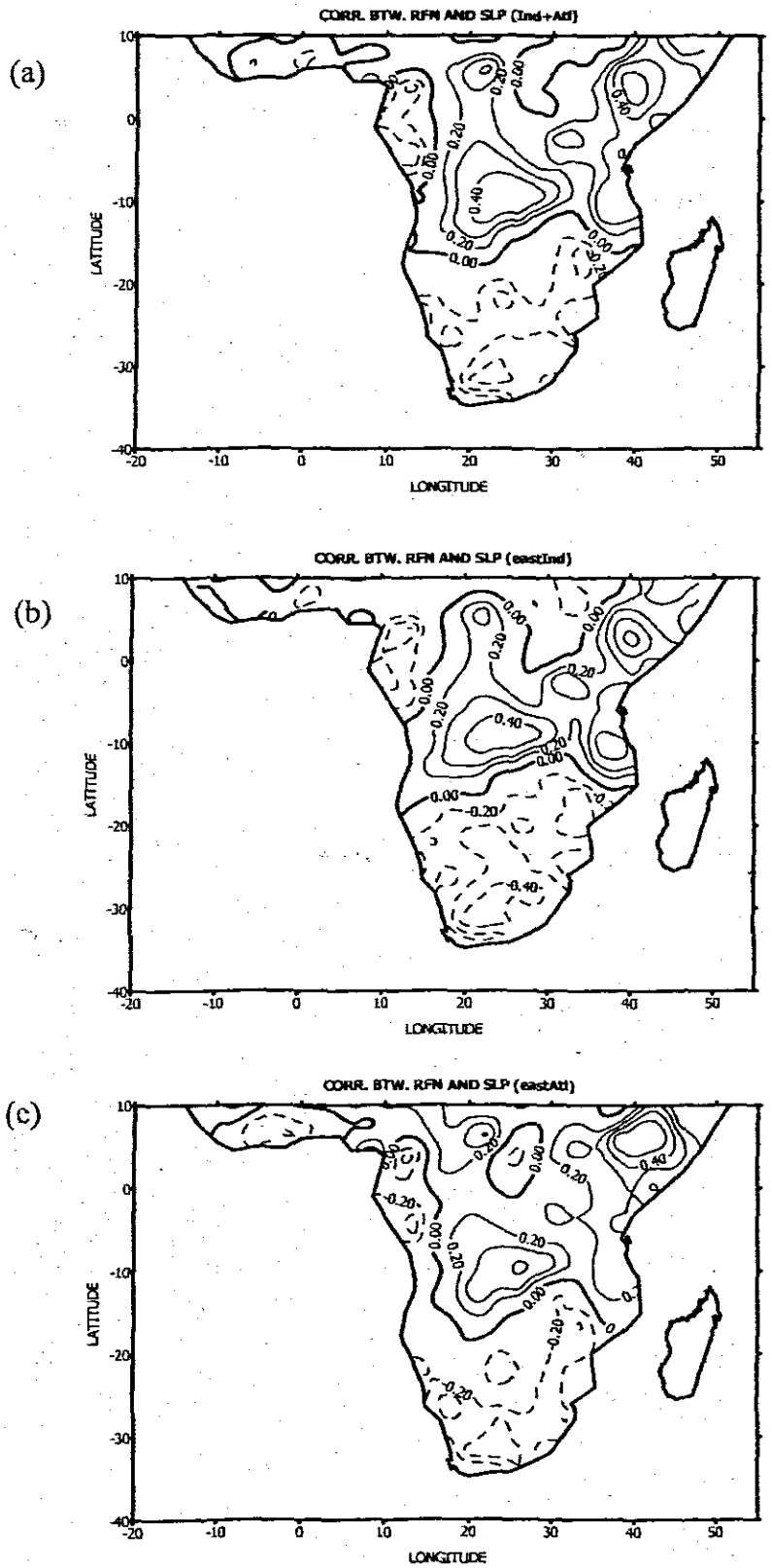

Fig. 5.2 Correlation between continental Africa gridded rainfall and environmental indices. Dashed (continuous) lines represent negative (positive) Correlation coefficients (a) Correlation btw rainfall and SLP Ind+Atl, (b) Correlation btw rainfall and SLP eastInd (c) Correlation btw rainfall and SLP eastAtl

(a)

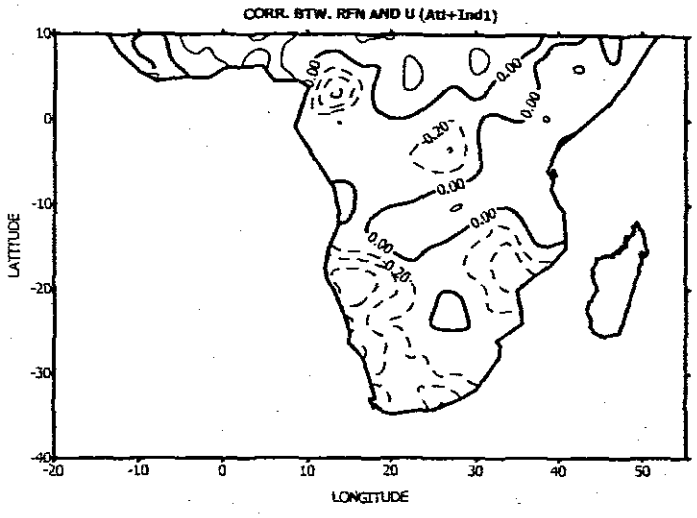

(b)

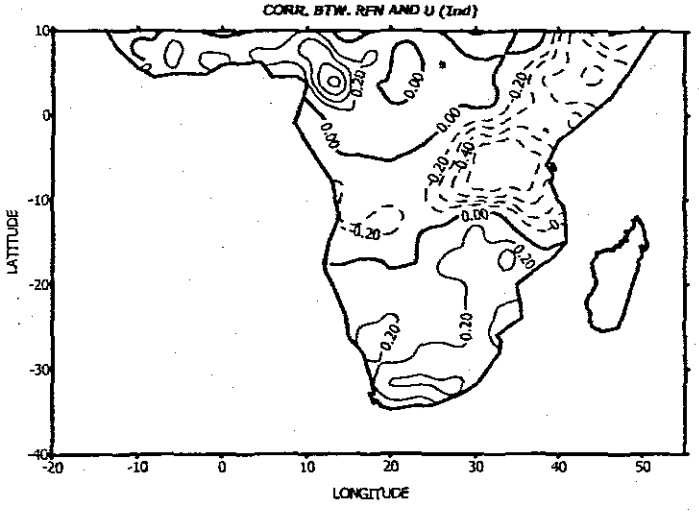

(c)

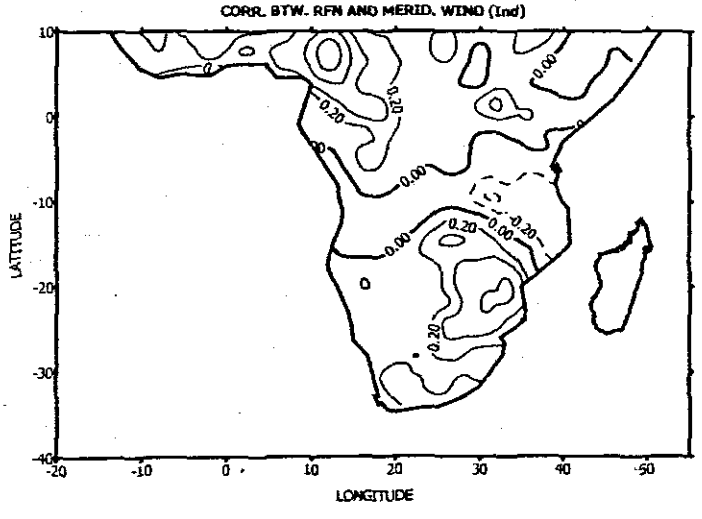

Fig. 5.3 Correlation between continental Africa gridded rainfall and environmental indices. Dashed (continuous) lines represent negative (positive) correlation coefficients. (a) Correlation btw rainfall and U Atl+Ind1, (b) Correlation btw rainfall and U Ind (c) Correlation btw rainfall and V Ind

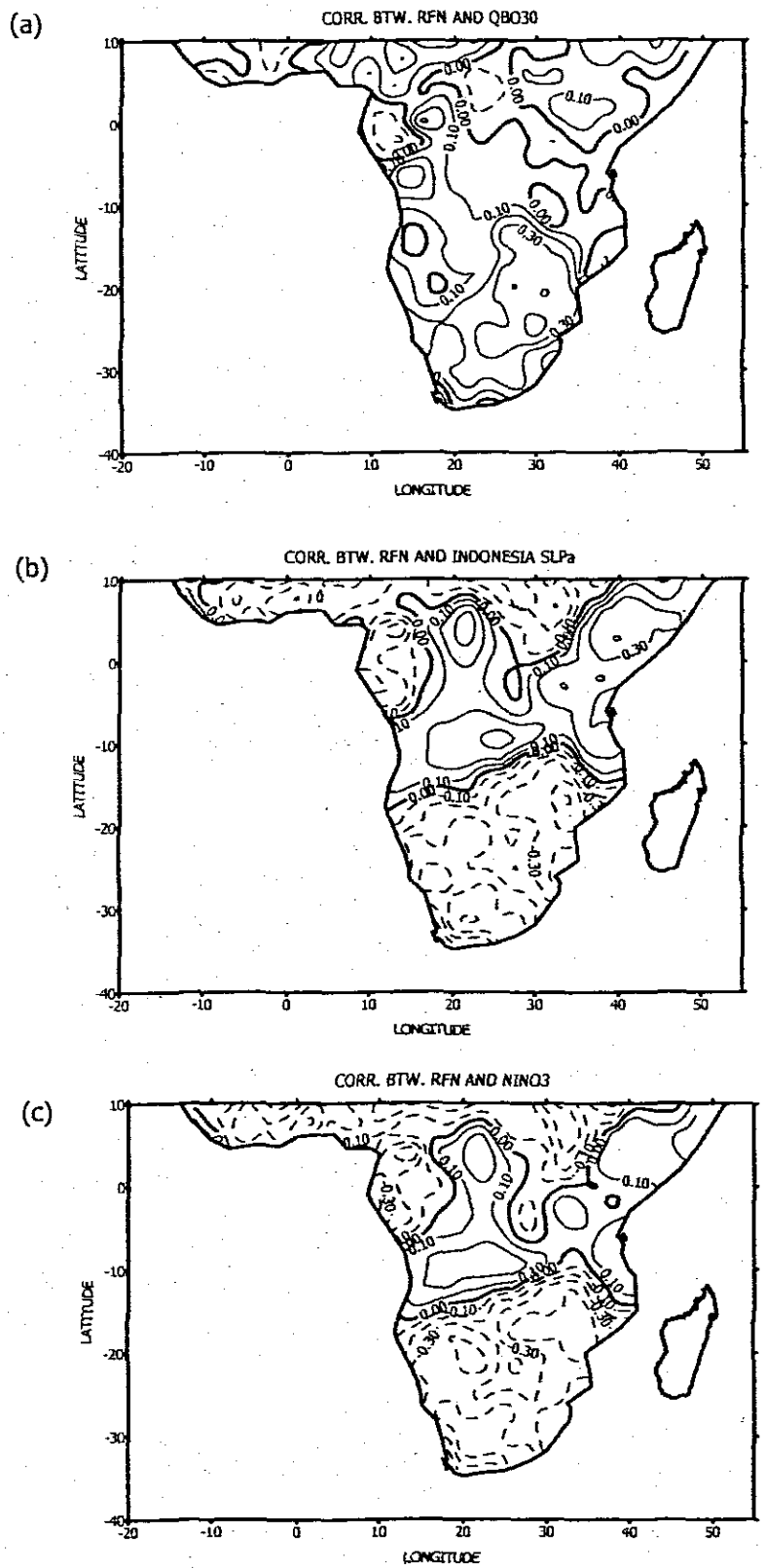

Fig. 5.4: Correlation between continental Africa gridded rainfall and environmental indices. Dashed (continuous) lines represent negative (positive) correlation coefficients. (a) Correlation btw rainfall and QBO, (b) Correlation btw rainfall and UIndSLPa, Correlation btw rainfall and Nino3

(a)

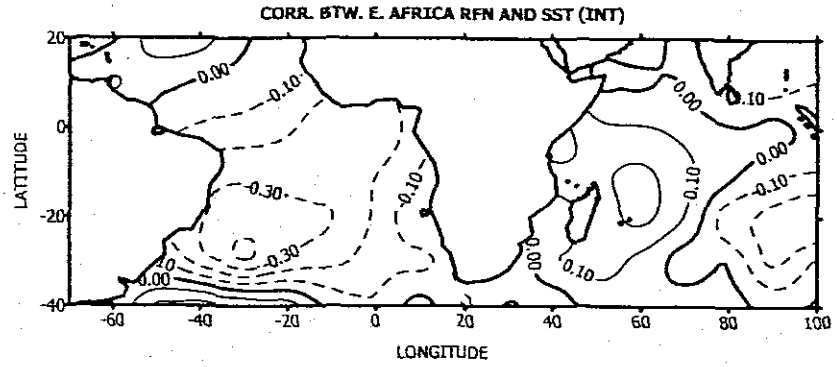

(b)

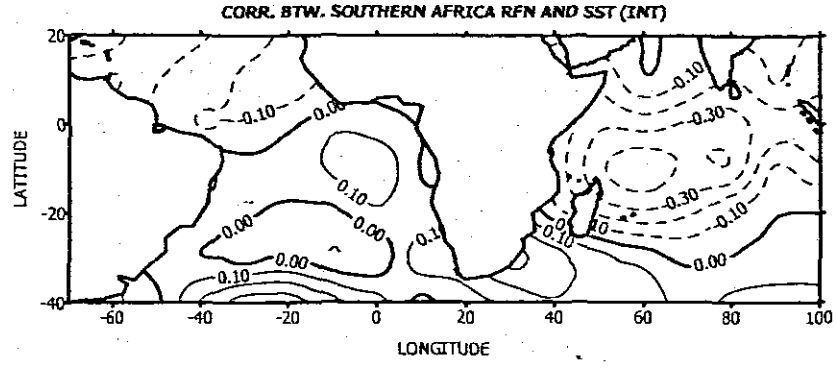

(c)

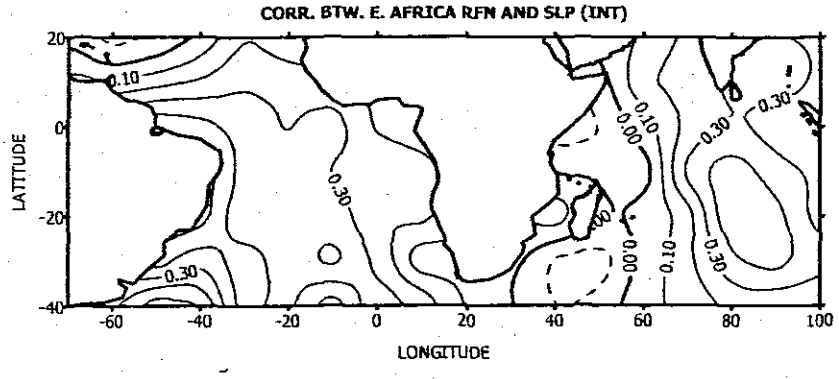

(d)

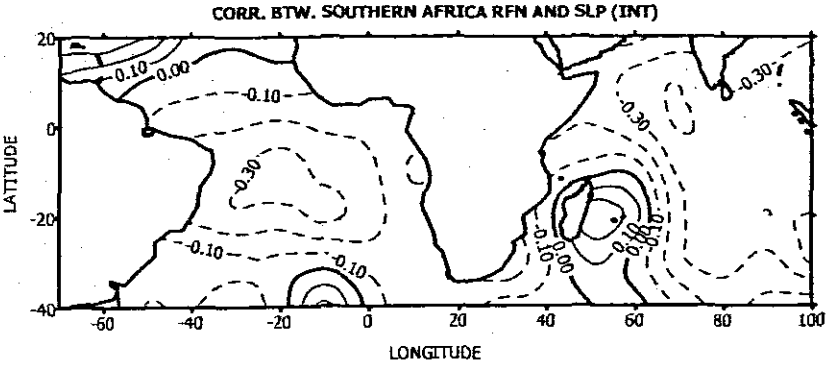

Fig. 5.5: Correlation between east and southern Africa rainfall and environmental parameters over the Atlantic and Indian Oceans. Correlation coefficients calculated after removing period less than 1.5 years using wavelet transform. Correlation between east Africa rainfall and SST (b) Correlation between southern Africa rainfall and SST

(e)

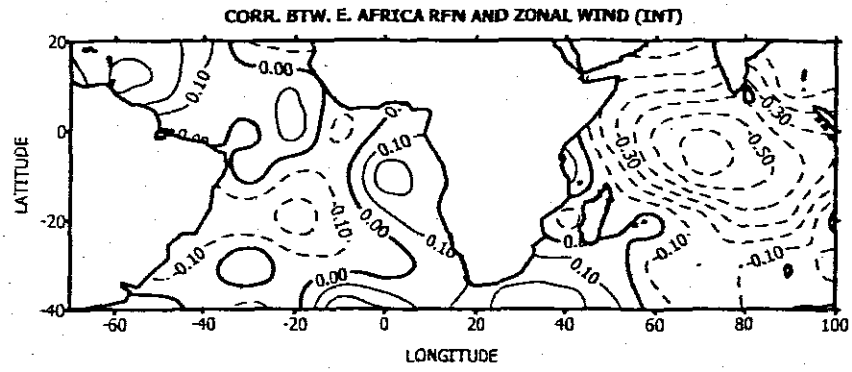

(f)

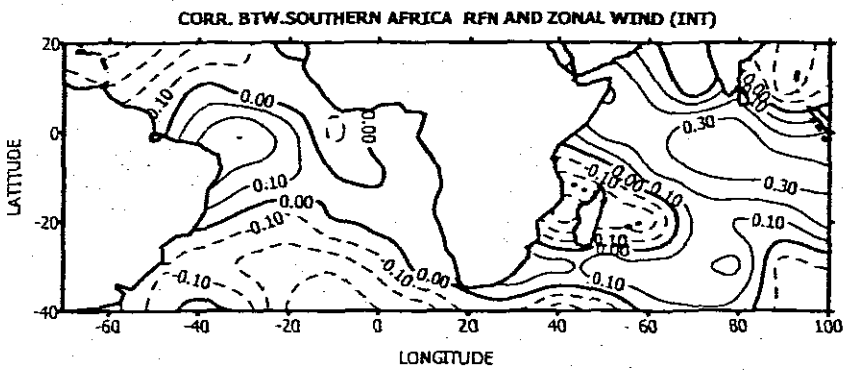

(g)

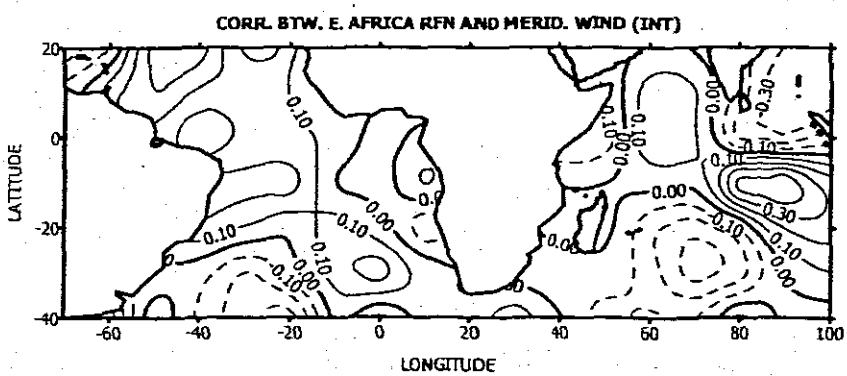

(h)

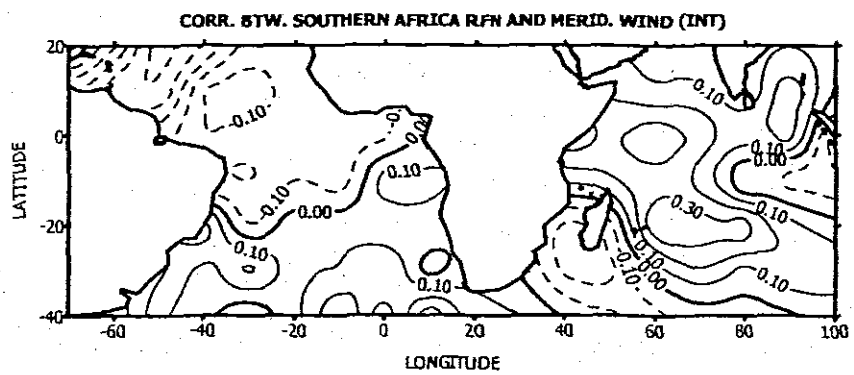

Fig. 5.5: Contd. (c) Correlation between east Africa rainfall and SLP (d) Correlation between southern Africa rainfall and SLP (e) Correlation between east Africa rainfall and U (f) Correlation between southern Africa rainfall and U (g) Correlation between east Africa rainfall and V (h) Correlation between southern Africa rainfall and V

(a)

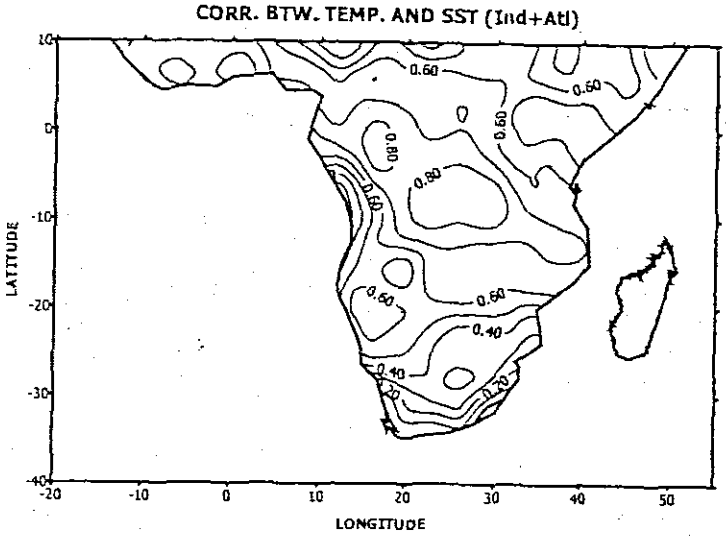

(b)

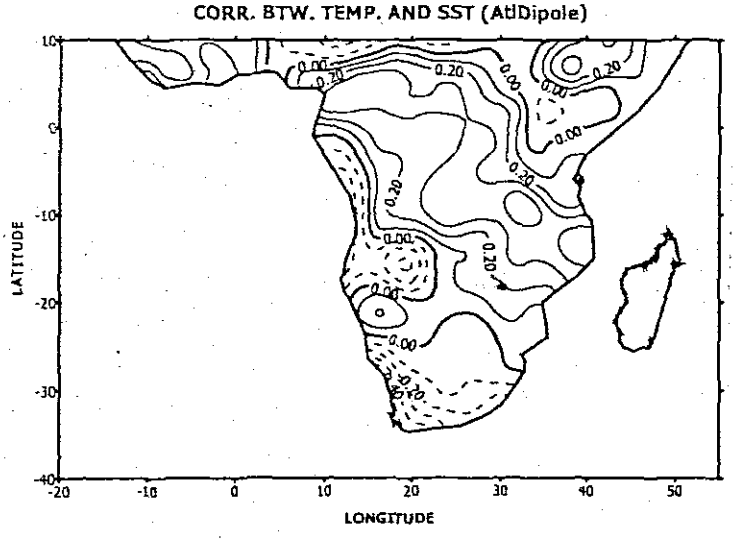

(c)

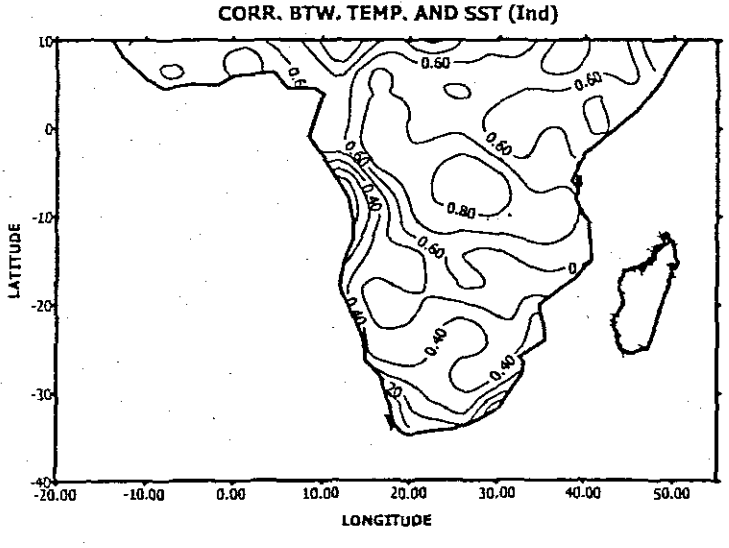

Fig. **5.6:** Correlation between Africa gridded Temp. and SST indices. Dashed (*continuous*) lines represent negatives (positive) correlation coefficients. **(a)** Correlation btw Temp. and SST Ind+Atl, **(b)** Correlation btw Temp. and SST AtlDipole **(c)** Correlation btw Temp. and SST Ind

(a)

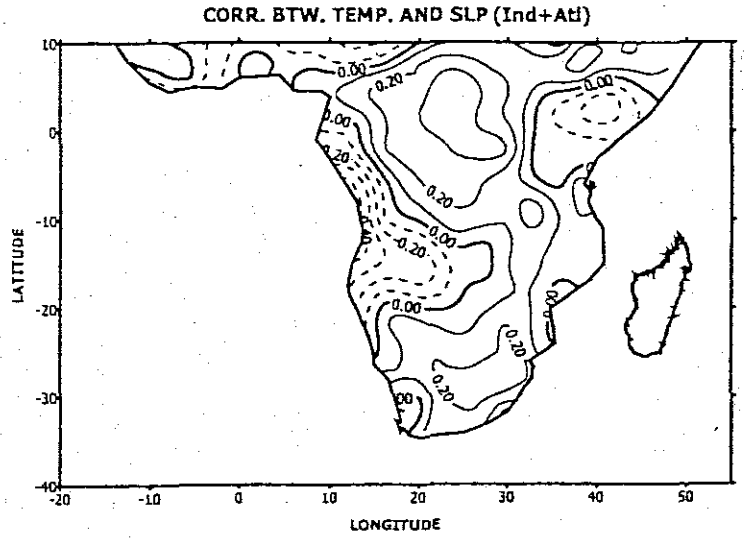

(b)

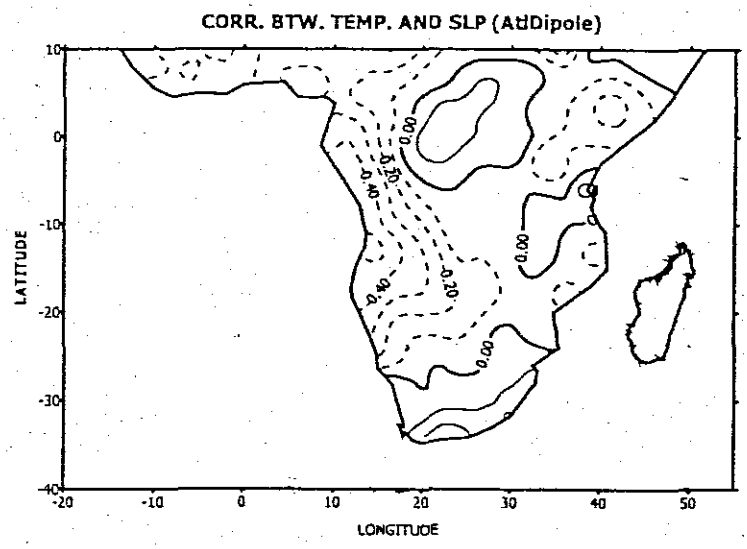

(c)

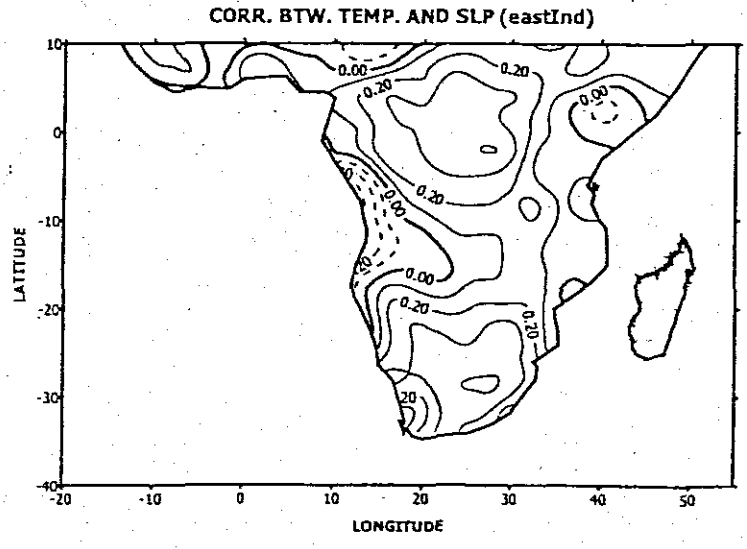

Fig. **5.7:** Correlation between Africa gridded Temp. and SLP indices. Dashed (continuous) lines represent negatives (positive) correlation coefficients. **(a)** Correlation btw Temp. and SLP Ind+Atl, **(b)** Correlation btw Temp. and SLP AtlDipole **(c)** Correlation btw Temp. and SLP Ind

(a)

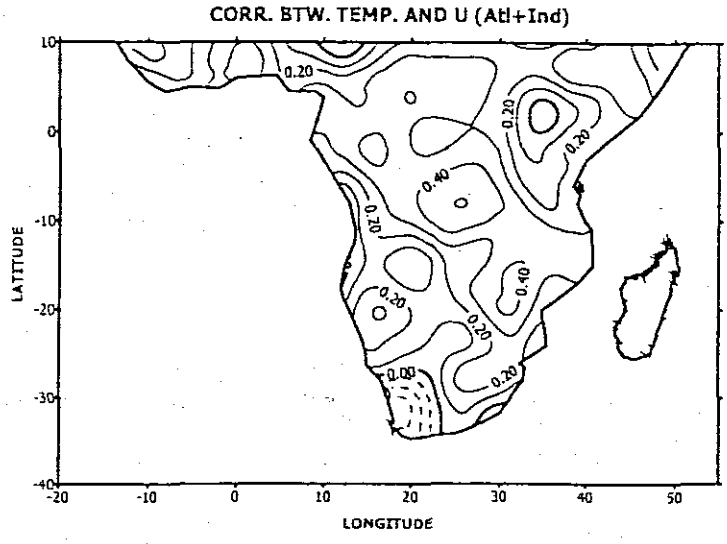

(b)

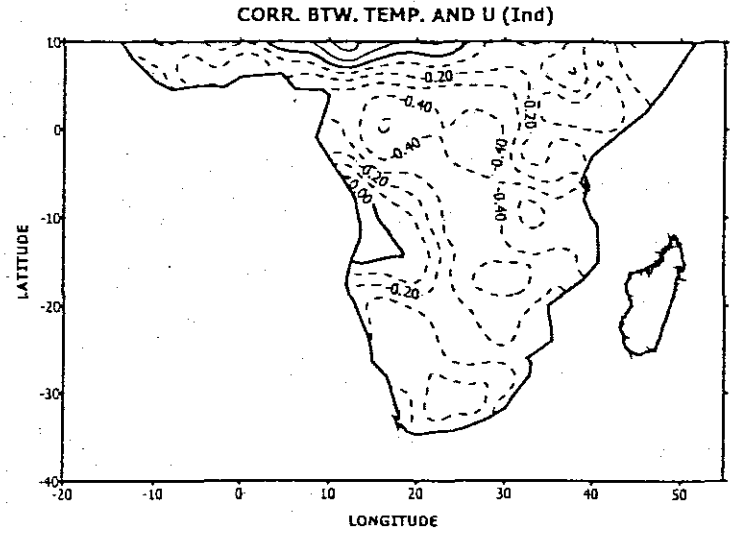

(c)

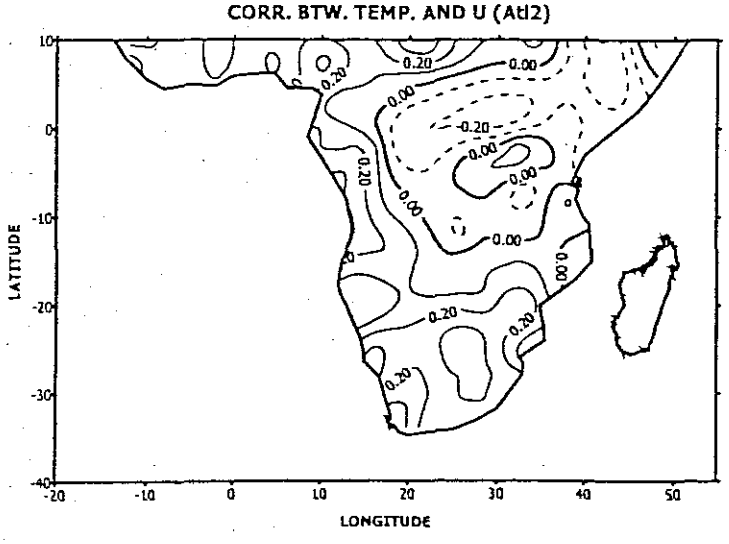

Fig. **5.8:** Correlation between Africa gridded Temp. and U indices. Dashed (continuous) lines represent negatives (positive) correlation coefficients. **(a)** Correlation btw Temp. and U Ind+Atl, **(b)** Correlation btw Temp. and U Ind **(c)** Correlation btw Temp. and U Atl2

(a)

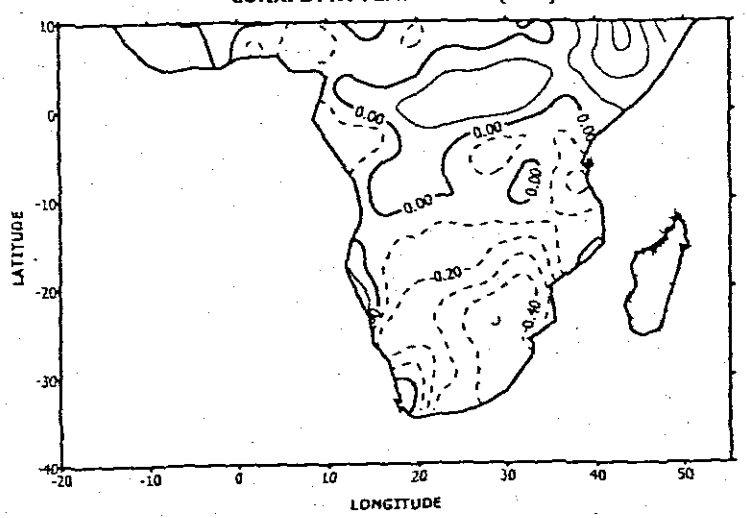

(b)

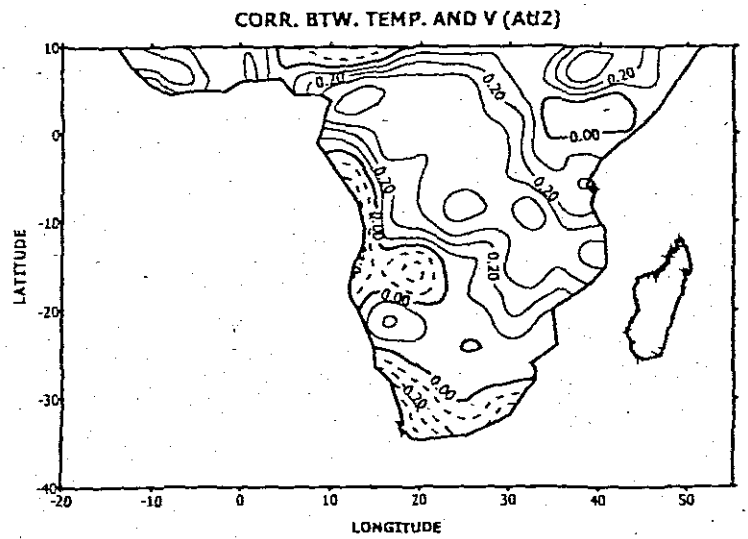

(c)

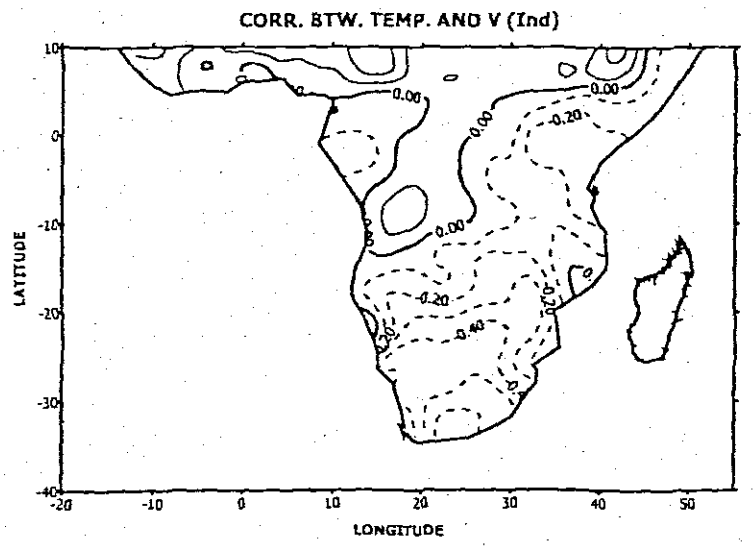

Fig. **5.9:** Correlation between Africa gridded Temp. and V indices. Dashed (continuous) lines represent negatives (positive) correlation coefficients. **(a)** Correlation btw Temp. and V Atl1, **(b)** Correlation btw Temp. and U Atl2 **(c)** Correlation btw Temp. and V Ind

(a)

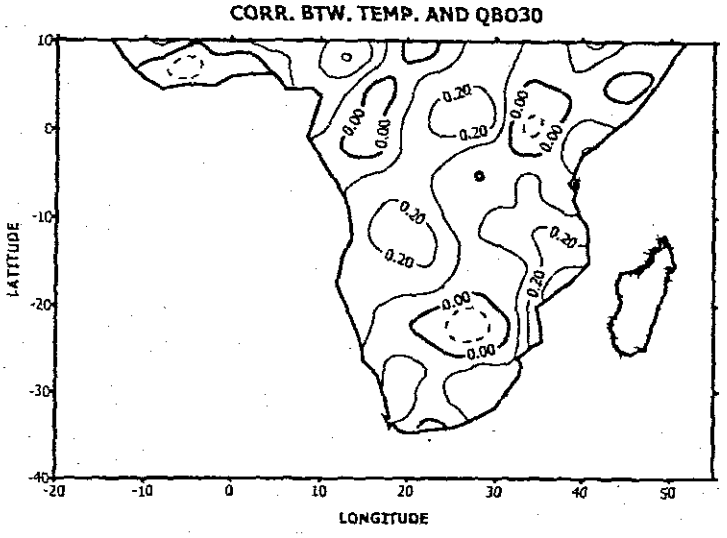

(b)

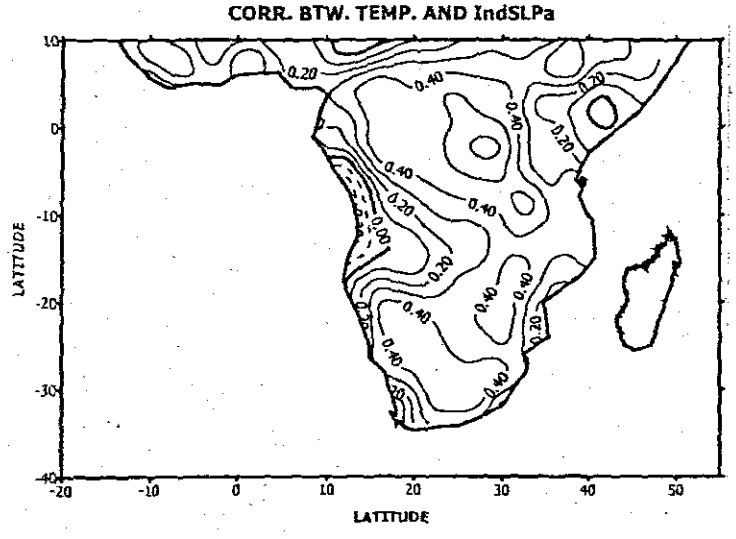

(c)

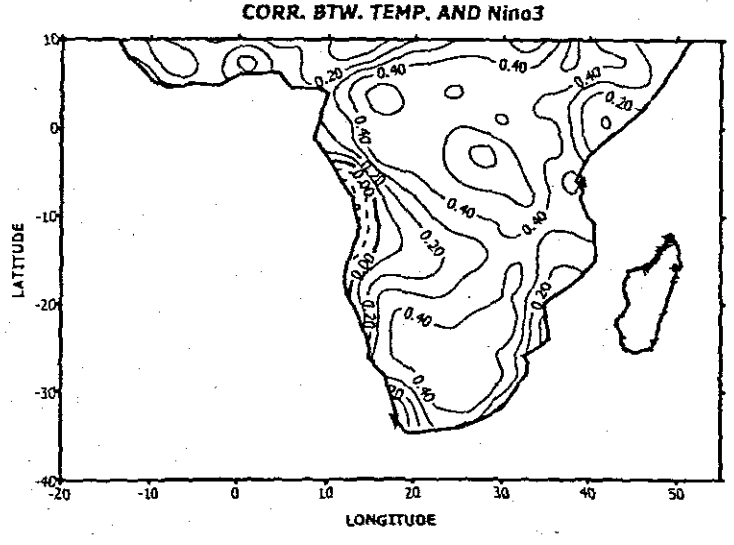

Fig. **5.10:** Correlation between Africa gridded Temp. and teleconnection indices. Dashed (continuous) lines represent negatives (positive) correlation coefficients. **(a)** Correlation btw Temp. and QBO30 index, **(b)** Correlation btw Temp. and IndSLPa index **(c)** Correlation btw Temp. and Nino3 index

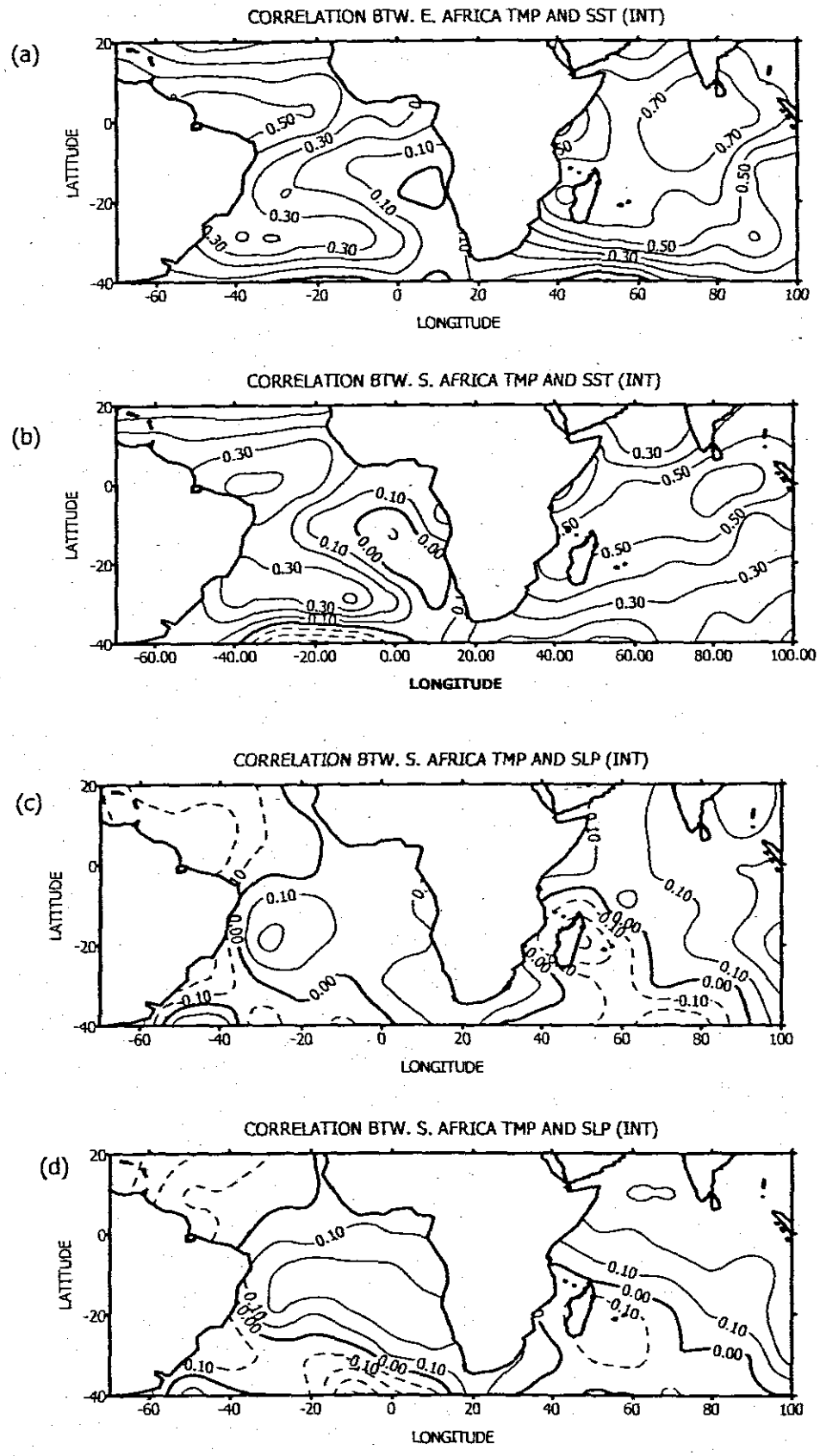

Fig. 5.11: correlation between east and southern Africa temperatures and environmental parameters over the Atlantic and Indian Oceans. *Correlations coefficents calculated after removing periods less than 1.5-years using* wavelet transform. (a) Correlation between east Africa temperature and SST (b) Correlation between southern Africa temperature and SST

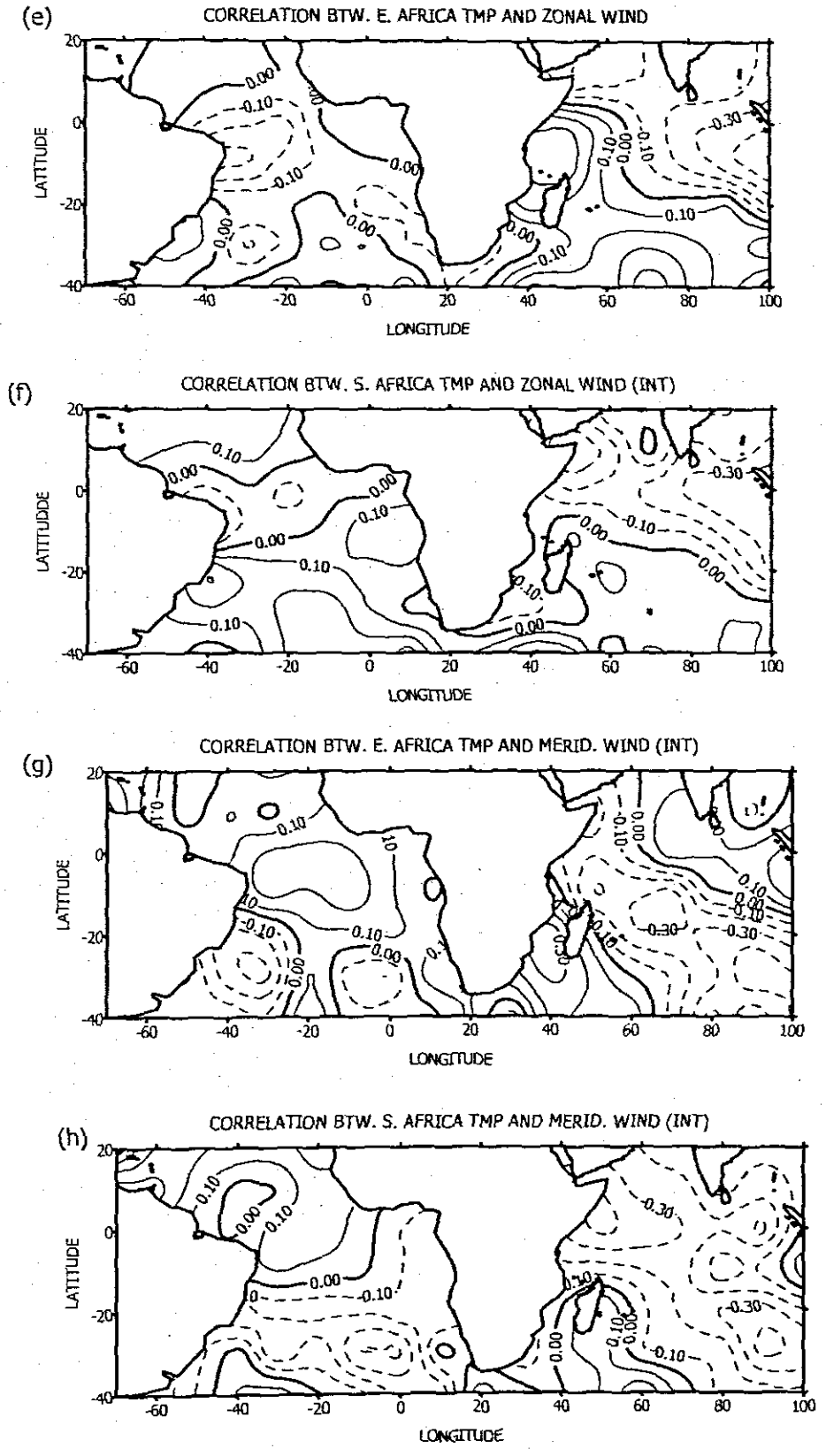

Fig. 5.11: Contd. (c) Correlation between east africa Temperature and SLP; (d) Correlation between southern Africa temperature and SLP; (e) Correlation between east africa temperature and U wind component; (f) Correlation between southern Africa temperature U wind component; (g) Correlation between east Africa temperature and V wind component; (h) Correlation between southern Africa temperature and V wind component.

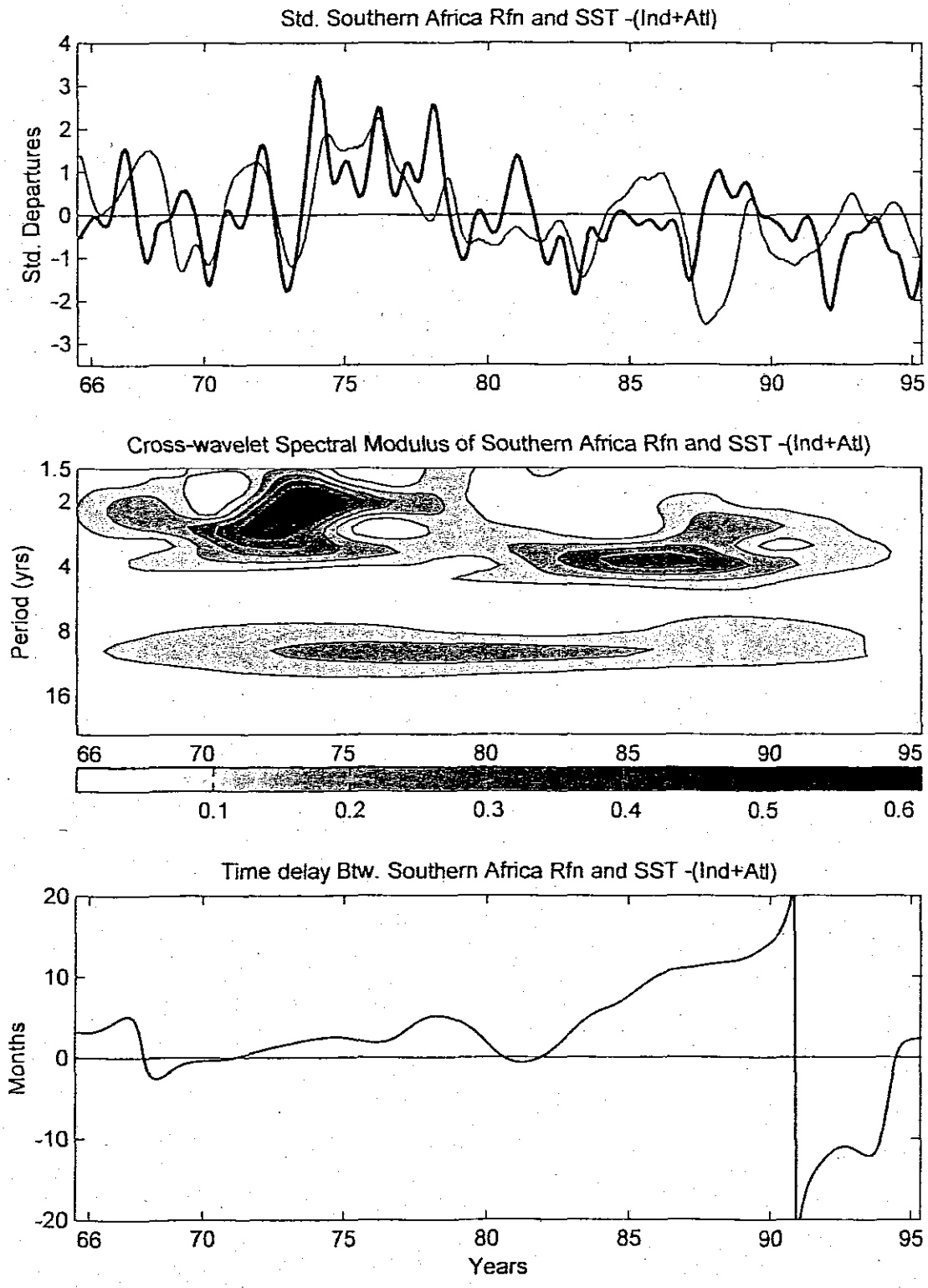

Fig. 5.12: Low frequency variability of southern Africa rainfall (Filtered using an18-month Gaussian filter) (bold) and SST -(Ind+Atl) (thin) for the period August 1965-May 1995. Modulus cross-wavelet spectrum coefficients of southern Africa rainfall and SST -(Ind+Atl); comparing cycles in the two time series middle). Time delay between southern Africa rainfall and SST -(Ind+Atl) (bottom), where SST -(Ind+Atl) leading is -ve

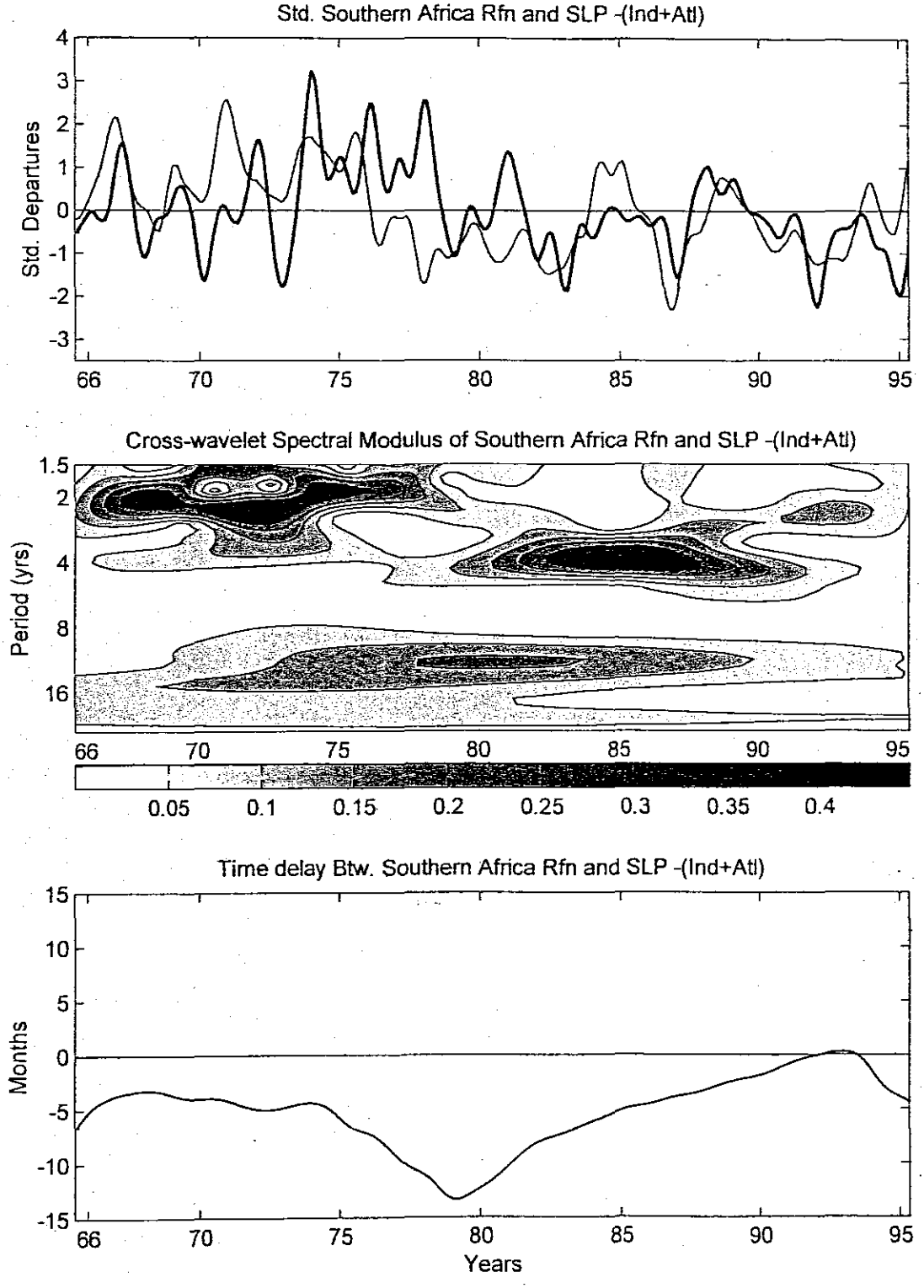

Fig. 5.13: Low frequency variability of southern Africa rainfall (Filtered using an 18-month Gaussian filter) (bold) and SLP -(Ind+Atl) (thin) for the period August 1965-May 1995. Modulus cross-wavelet spectrum coefficients of southern Africa rainfall and SLP -(Ind+Atl); comparing cycles in the two time series (middle). Time delay between southern Africa rainfall and SLP -(Ind+Atl) (bottom), where SLP -(Ind+Atl) leading is -ve

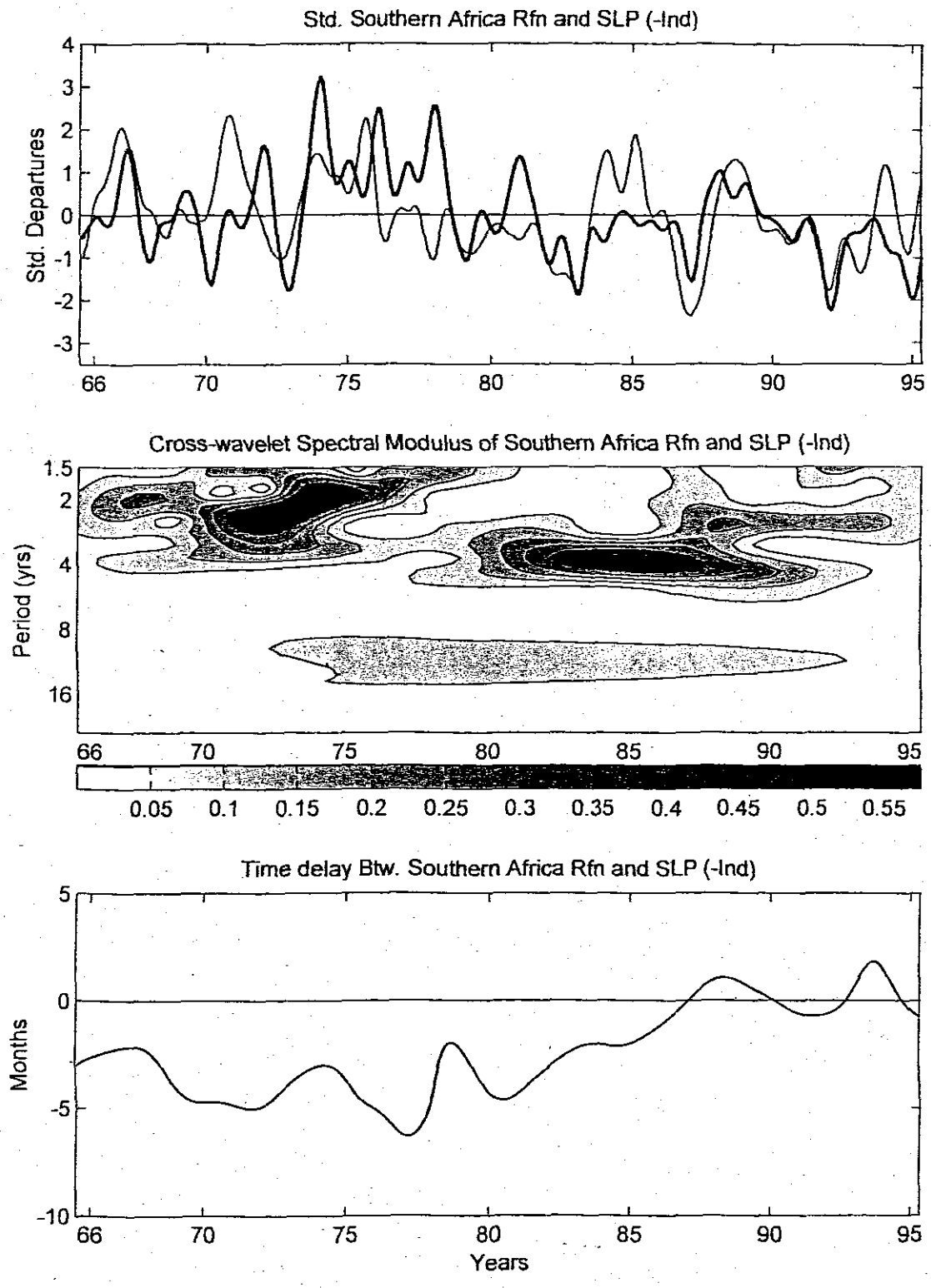

Fig. 5.14: Low frequency variability of southern Africa rainfall (Filtered using an 18-month Gaussian filter) (bold) and SLP -(Ind) (thin) for the period August 1965-May 1995. Modulus cross-wavelet spectrum coefficients of southern Africa rainfall and SLP -(Ind); comparing cycles in the two time series (middle). Time delay between southern Africa rainfall and SLP -(Ind) (bottom), where SLP -(Ind) leading is -ve

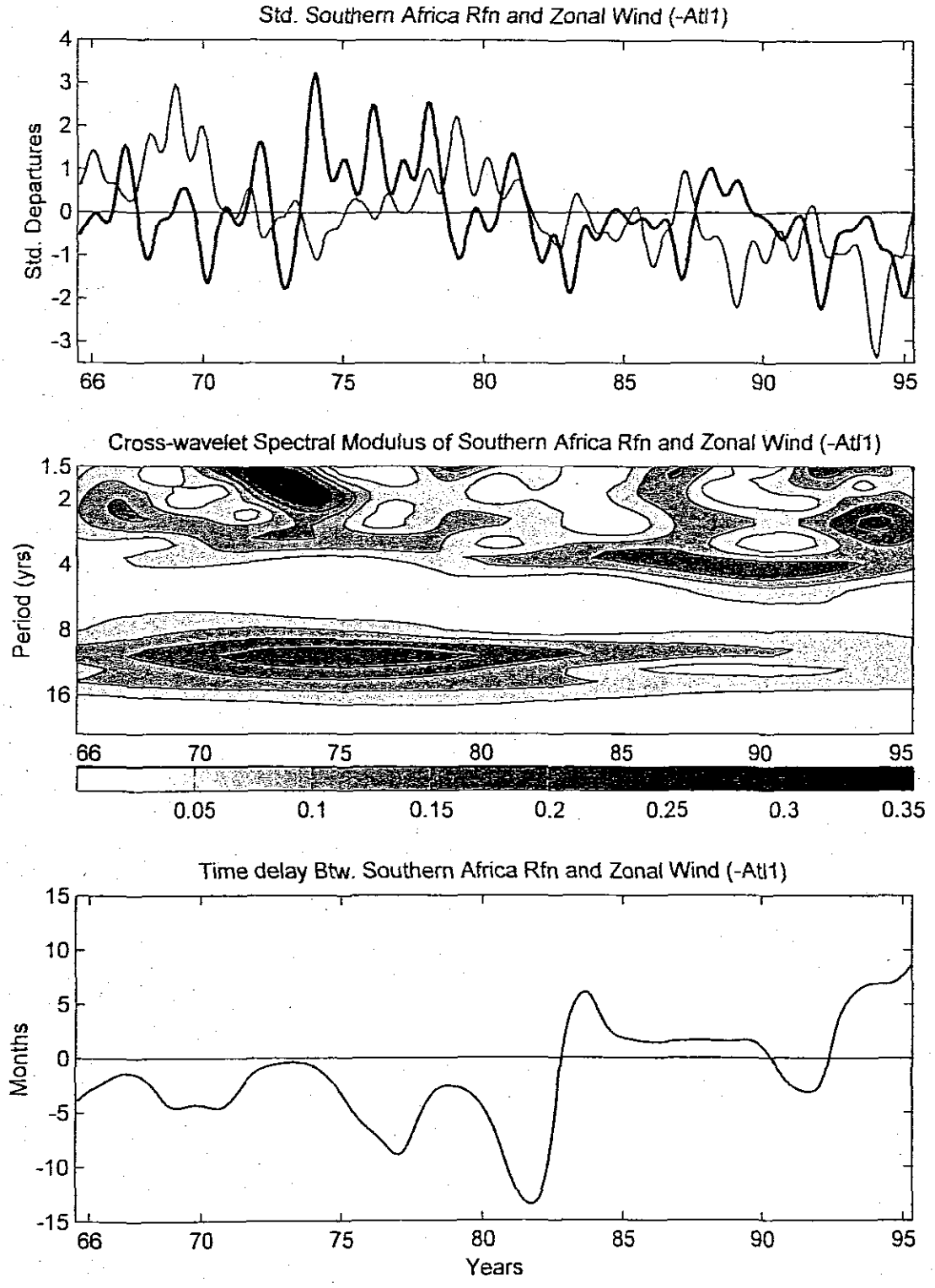

Fig. 5.15: Low frequency variability of southern Africa rainfall (Filtered using an 18-month Gaussian filter) (bold) and U –(Atl1) (thin) for the period August 1965-May 1995. Modulus cross-wavelet spectrum coefficients of southern Africa rainfall and U –(Atl1); comparing cycles in the two time series (middle). Time delay between southern Africa rainfall and U –(Atl1) (bottom), where U –(Atl1) leading is -ve

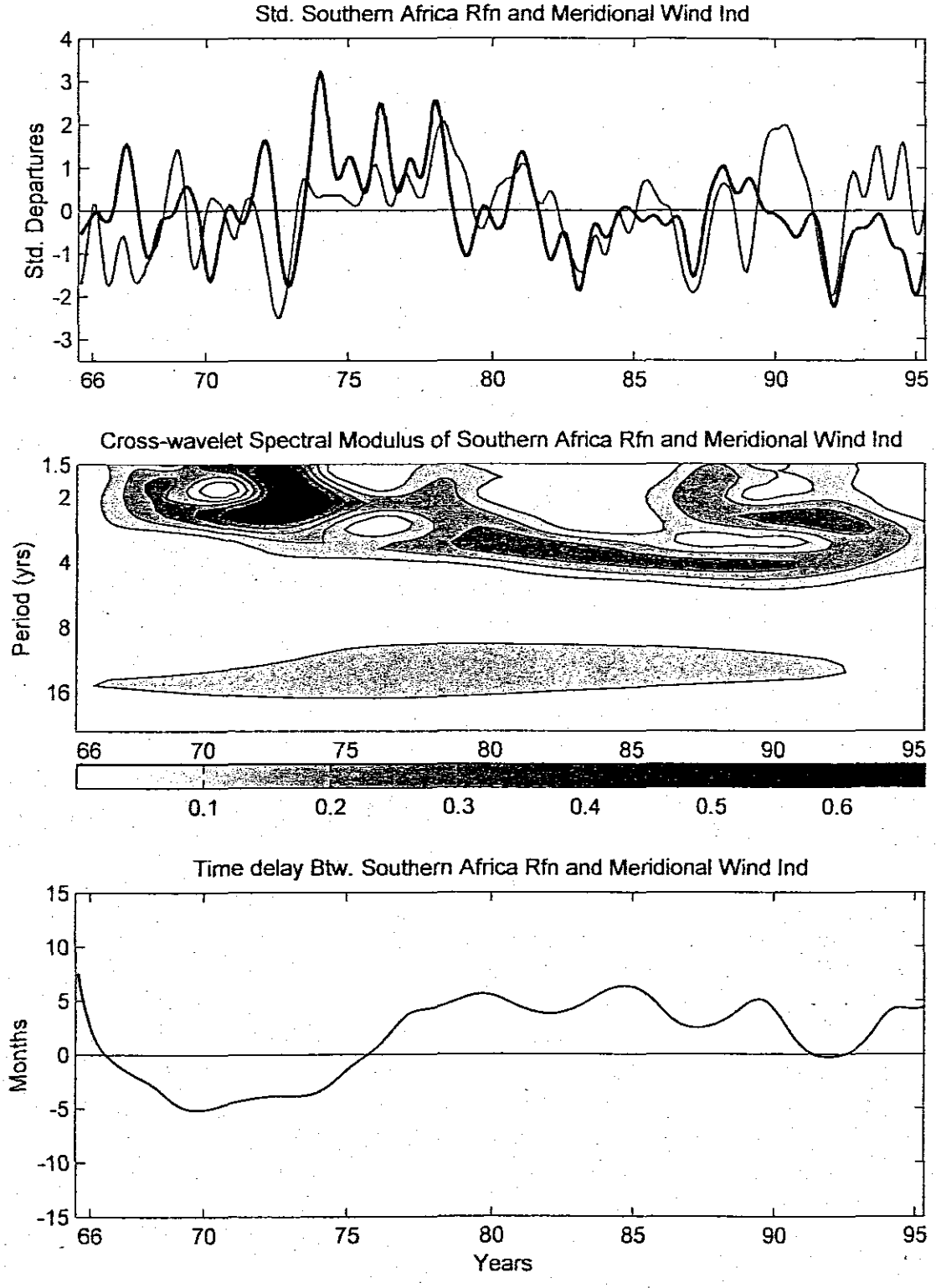

Fig. 5.16: Low frequency variability of southern Africa rainfall (Filtered using an 18-month Gaussian filter) (bold) and V Ind (thin) for the period August 1965-May 1995. Modulus cross-wavelet spectrum coefficients of southern Africa rainfall and V Ind; comparing cycles in the two time series (middle). Time delay between southern Africa rainfall and V Ind (bottom), where V Ind leading is -ve

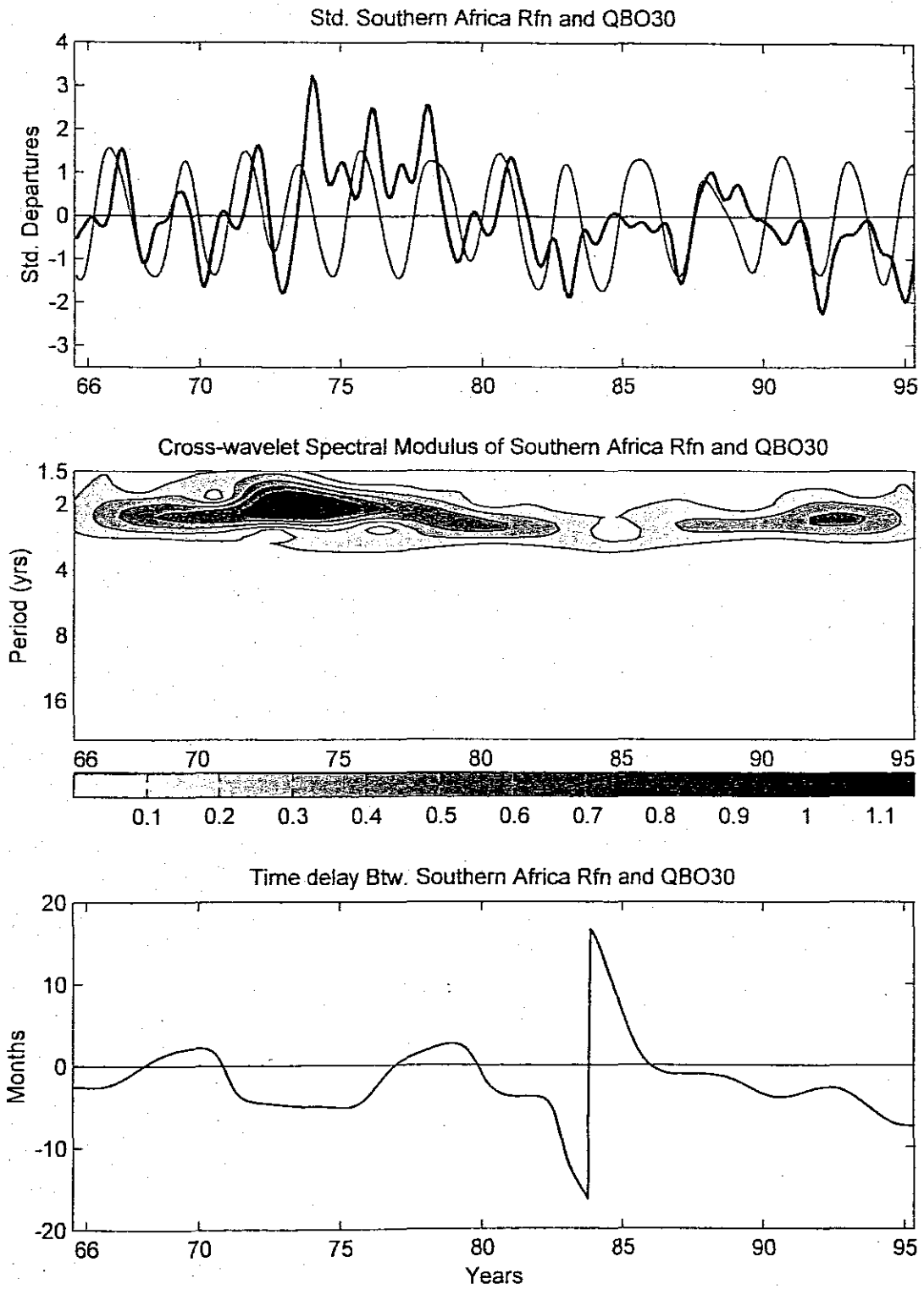

Fig. 5.17: Low frequency variability of southern Africa rainfall (Filtered using an 18-month Gaussian filter) (bold) and QBO30 (thin) for the period August 1965-May 1995. Modulus cross-wavelet spectrum coefficients of southern Africa rainfall and QBO30; comparing cycles in the two time series (middle). Time delay between southern Africa rainfall and QBO30 (bottom), where QBO30 leading is -ve

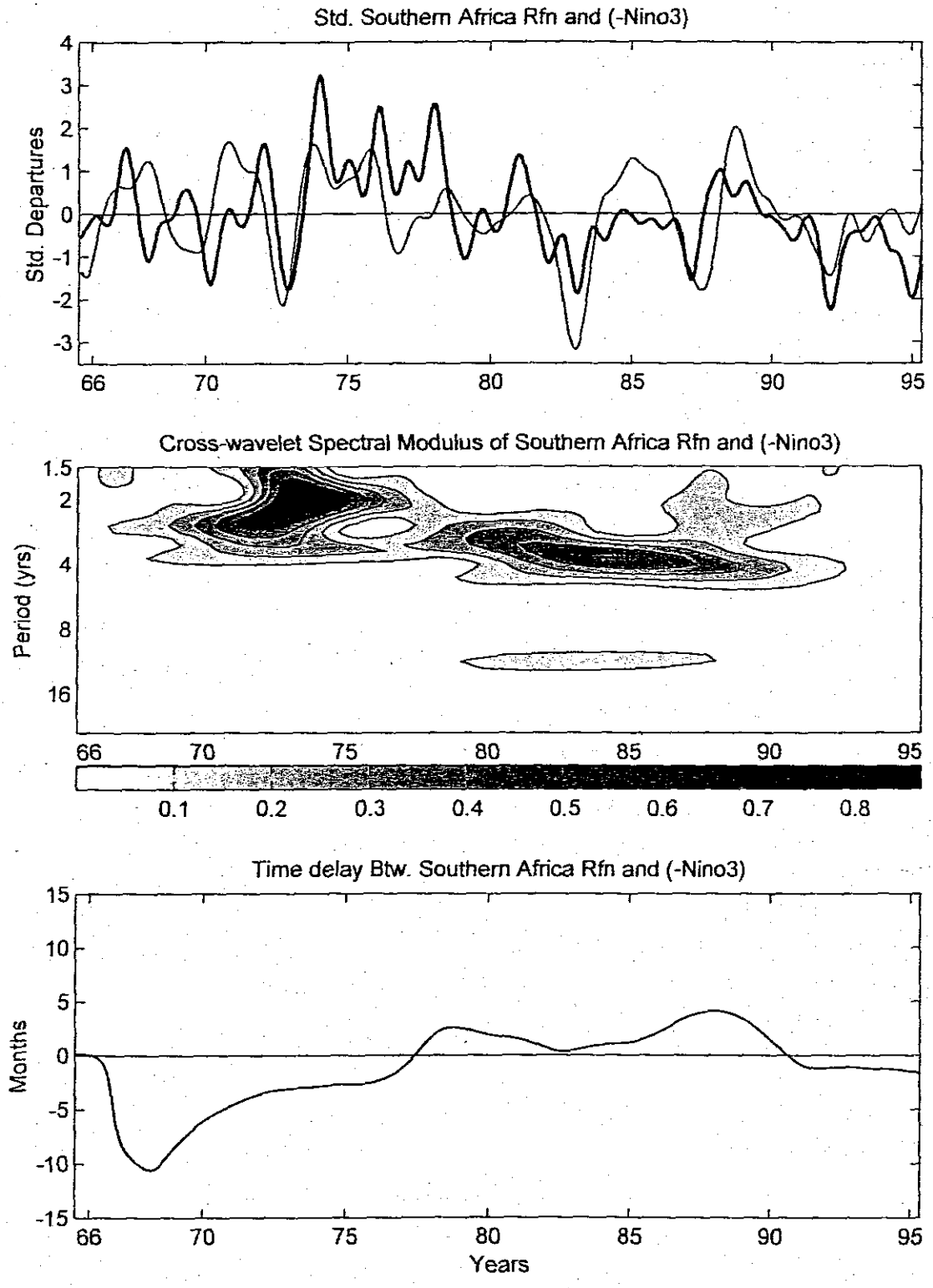

Fig. 5.18: Low frequency variability of southern Africa rainfall (Filtered using an 18-month Gaussian filter) (bold) and -Nino3 (thin) for the period August 1965-May 1995. Modulus cross-wavelet spectrum coefficients of southern Africa rainfall and -Nino3; comparing cycles in the two time series (middle). Time delay between southern Africa rainfall and -Nino3 (bottom), where -Nino3 leading is -ve

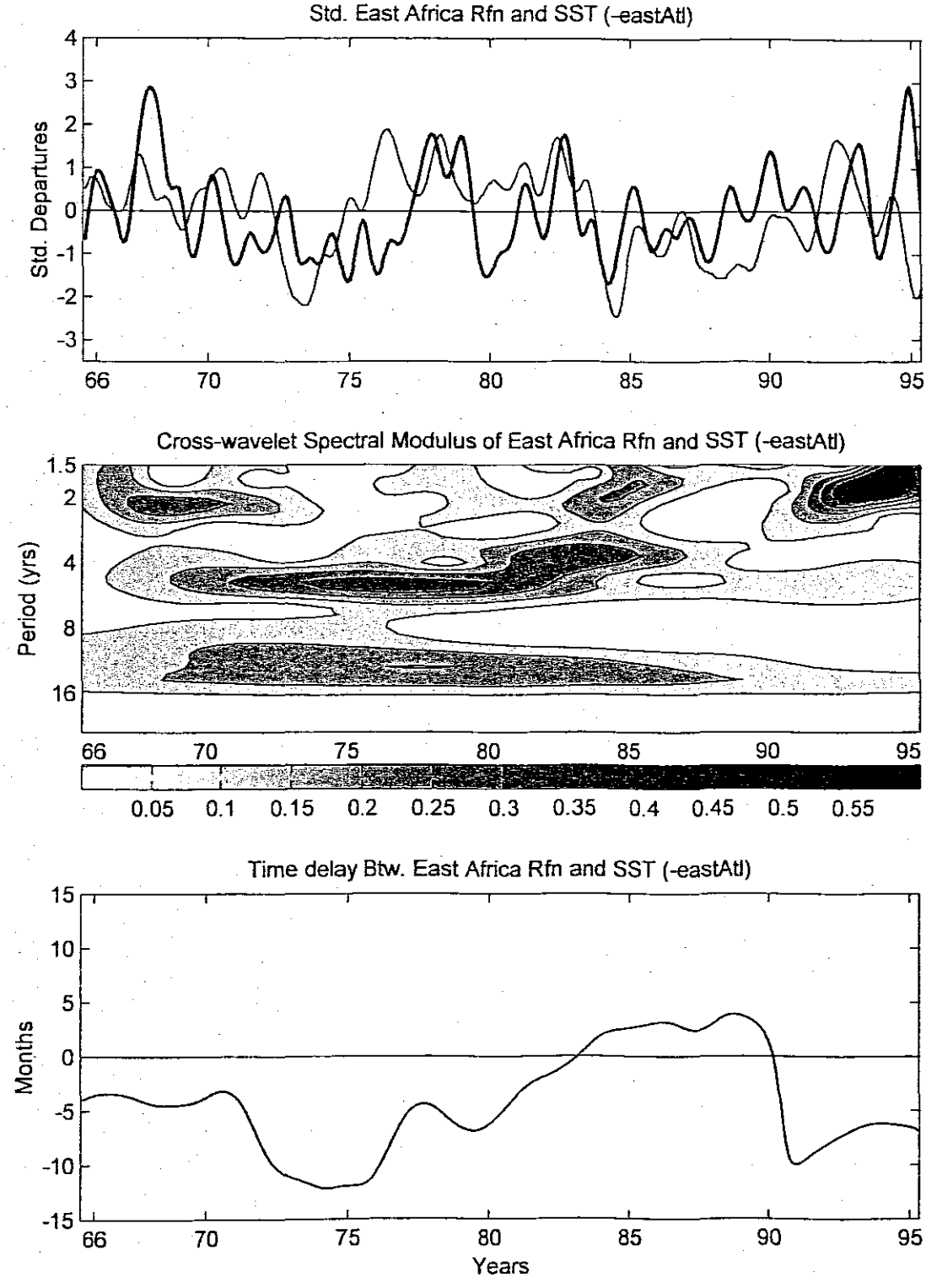

Fig. 5.19: Low frequency variability of east Africa (Filtered using an 18-month Gaussian filter) (bold) and SST –(eastAtl) (thin) for the period August 1965-May 1995. Modulus cross-wavelet spectrum coefficients of east Africa rainfall and SST –(eastAtl); comparing cycles in the two time series (middle). Time delay between east Africa rainfall and SST –(eastAtl) (bottom), where SST –(eastAtl) leading is -ve

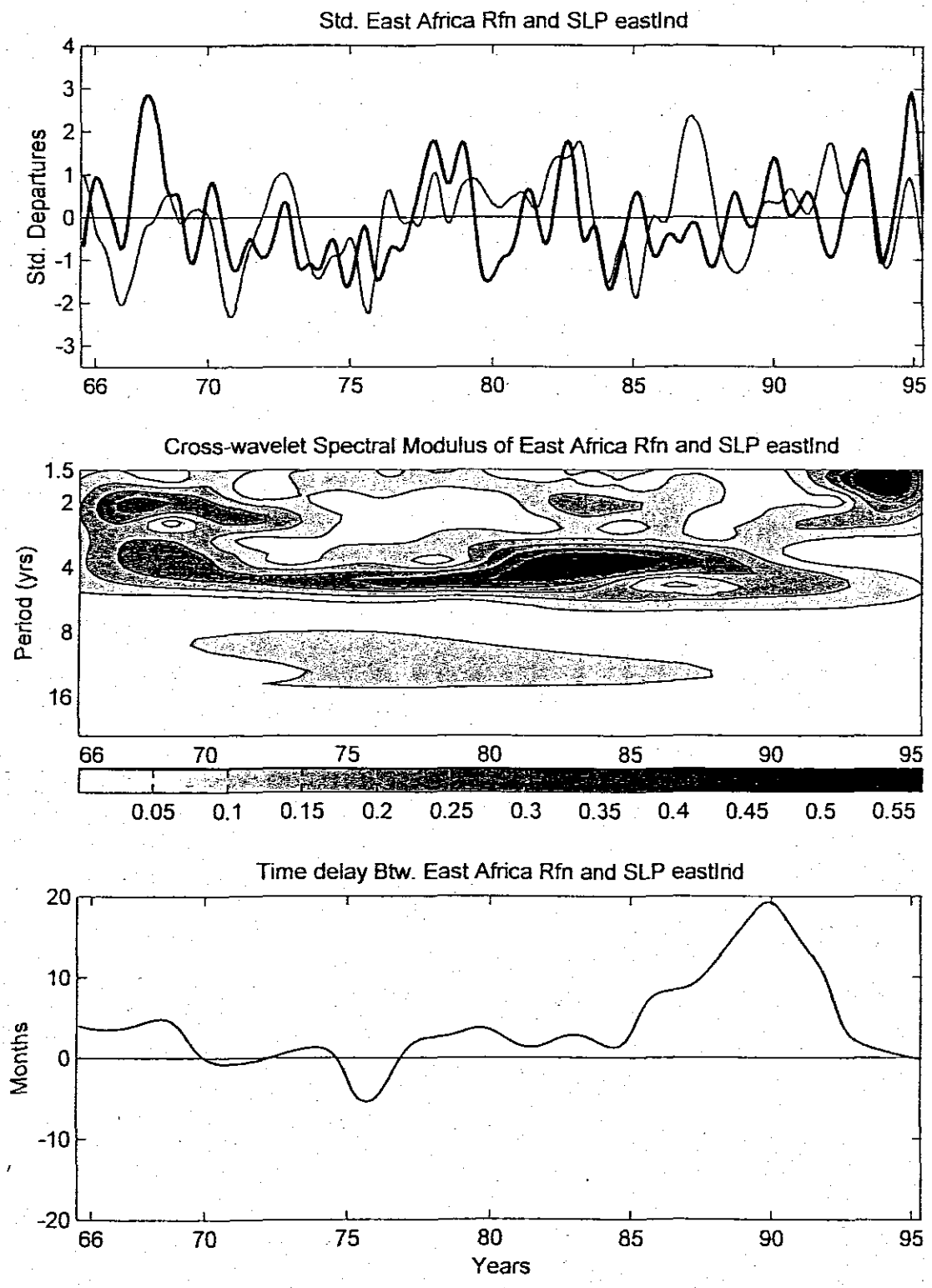

Fig. 5.20: Low frequency variability of east Africa (Filtered using an 18-month Gaussian filter) (bold) and SLP eastInd (thin) for the period August 1965-May 1995. Modulus cross-wavelet spectrum coefficients of east Africa rainfall and SLP eastInd; comparing cycles in the two time series (middle). Time delay between east Africa rainfall and SLP eastInd (bottom), where SLP eastInd leading is -ve

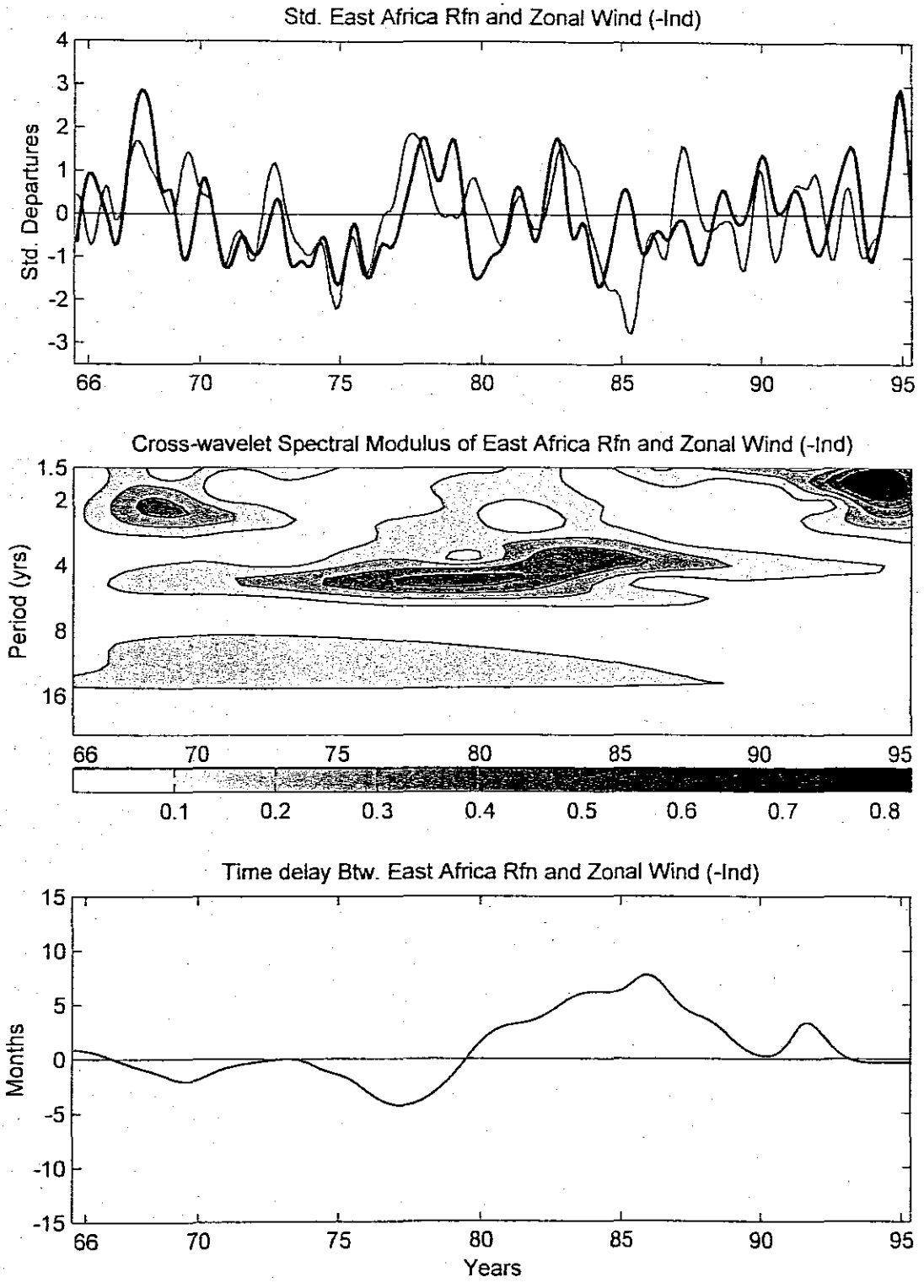

Fig. 5.21: Low frequency variability of east Africa (Filtered using an 18-month Gaussian filter) (bold) and U –(Ind) (thin) for the period August 1965-May 1995. Modulus cross-wavelet spectrum coefficients of east Africa rainfall and U –(Ind); comparing cycles in the two time series (middle). Time delay between east Africa rainfall and U –(Ind) (bottom), where U –(Ind) leading is -ve

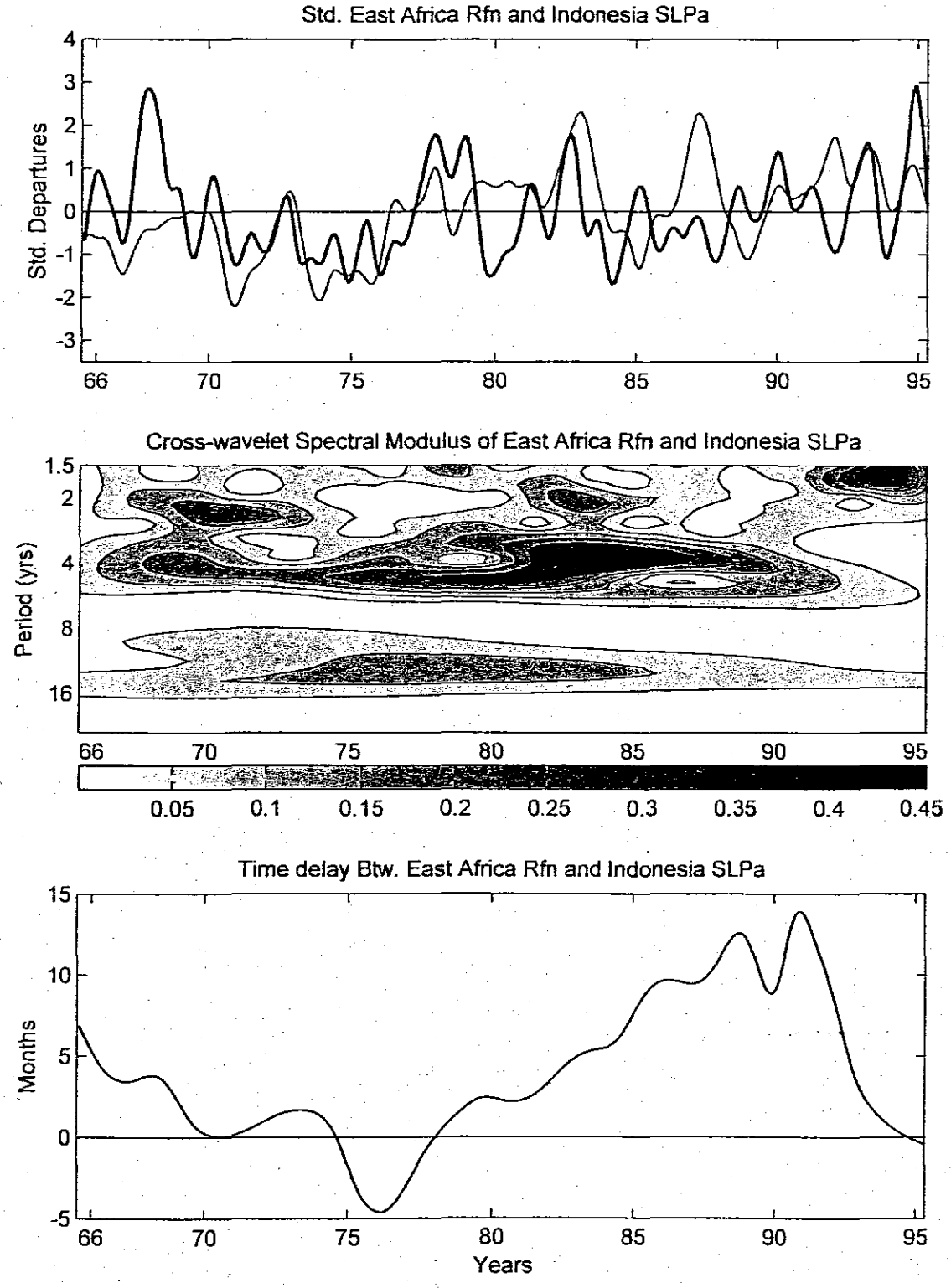

Fig. 5.22: Low frequency variability of east Africa (Filtered using an 18-month Gaussian filter) (bold) and Indonesia SLPa (thin) for the period August 1965-May 1995. Modulus cross-wavelet spectrum coefficients of east Africa rainfall and Indonesia SLPa; comparing cycles in the two time series (middle). Time delay between east Africa rainfall and Indonesia SLPa (bottom), where Indonesia SLPa leading is -ve

CHAPTER 6

6.0 Forecasting Potential

6.1 Introduction

The rate of population growth of many African countries is faster than the rate at of food production. This imbalance is partly due floods and floods. Frequent droughts and floods in recent years have affected agricultural production and have left many African countries with a deficit of food to feed their citizens. A way should be sought to address this problem. One way of addressing this problem is through using accurate and time seasonal forecasts. Seasonal rainfall forecasts may help farmers increase food and cash crops production to support economic growth in their respective countries. Other sectors which may also benefit from seasonal rainfall forecasts in the planning of their activities are water, financial, resource consumption, recreation, health and livestock.

Analysing continuous monthly data in previous chapters, some atmospheric/oceanographic parameters over action centres over the Atlantic and Indian Oceans have been identified. Some of these have shown promising association with rainfall over some parts of the tropical highlands of Africa. Correlation analysis between rainfall and temperature and other oceanic/atmospheric parameters at various lags were performed. A good association of a predictant and predictor at three or six months lead-time implies that a predictor maybe useful in operational forecast. Correlating rainfall data with continuous parameters, e.g. SST, SLP, etc. has some disadvantages. The first disadvantage is that rainfall data, particularly over highlands of tropical Africa, is not continuous, i.e., rainfall is absent 6-7 months of the year. The discontinuity is brought by the fact that rainfall is recorded as zero, in a dry season, similar to dry months, in a rainy season. The second problem with this method is that the correlation coefficient does not have a time reference, i.e. it is not assigned to any particular month or season. To address these problems then rainfall as well as predictor parameters are aggregated into three-month values to produce seasonal time series. Eventually specific predictant seasonal series of interest are correlated with particular seasonal values of predictors. The rainy period over the tropical highlands of Africa is between October and June of the following year. In this study two rainy seasons for both east and southern Africa have been selected to investigate the predictability potential. The seasons, which have been selected, are DJF and MAM. In order to have a reasonable lead-time to forecast DJF rainfall JJA, SON and DJF oceanic/atmospheric parameters are used to identify predictors. Similarly,

association between MAM rainfall and SON, DJF and MAM oceanic/atmospheric parameters are investigated. Correlation analysis between oceanic/atmospheric parameters over the designated action centres and gridded rainfall over the continent shall be done and coefficient mapped as in chapter 5 (inward mapping). In order for a forecast to have any benefit to farmers and other users, a sufficiently long lead-time is required such that forecasts can be used in strategic planning of their activities. For example, farmers can prepare agricultural activities as well as choose the right variety of crops to grow. Similarly water resources or energy managers can release water from their reservoirs if flood forecast is given or use the reservoirs' water carefully if a drought forecast is given. A useful predictor is one which has high correlation with the predictant index at season lags zero, one (three months) and two (six months); that is a degree of persistence.

The following properties are important for predictors: persistence, stability and useful lead-time. Persistence in this context refers to slow evolution; for example, one would require a parameter's auto-correlation function to be high for at least one to six month lags and a stable predictor parameter should be the one which has high and non varying correlation coefficients with a predictant over years. For example, the correlation coefficients between rainfall and Nino3 calculated between 1930 and 1960 and between 1961 and 1990 should be similar. It is also important for the predictor to consistently lead the predictand, i.e. changes in a predictor should occur first before those in a predictand. In this chapter the predictability potential of seasonal rainfall over the tropical highlands of Africa is studied by investigating oceanographic/atmospheric parameters which show persistence, stability and have useful lead time with seasonal rainfall over east and southern Africa. In section 6.2, lag correlation coefficients between African seasonal rainfall and environmental parameters will be discussed while in section 6.3 correlation coefficients between rainfall over Africa and environmental parameters at season lags one and two will be presented. Potential predictors are tabulated in table 6.3 and 6.4 and summarised in section 6.3.5. Section 6.2 gives the correlation coefficient at three and six-month lags with respect to filtered continuous monthly data. It should be noted however, that results do not focus on a particular month or season. Section 6.3 investigates the forecasting potential of the east and southern Africa rainfall at one and two season lags. If the potential is high then operational multi-variate statistical models can be developed using non-collinear predictors

6.2 Three and six-month lagged correlation

Table 6.1 provides correlation coefficients for east and southern Africa key areas at three and six month lags and sheds some light on predictability potential. The results indicate that the two rainfall indices are oppositely associated with a majority of environmental parameter indices and correlation coefficients are higher at three month lag than at six month lags (zero lag is discussed in chapter 5) for a number of indices. Environmental parameter indices that show good associations with rainfall over the two key areas at three and six month lags are discussed. For rainfall over the southern Africa key area a number of environmental parameter indices have shown some promising results though the degrees of associations are not very high. The IndSLPa and Nino3, (which are ENSO signals) and QBO30 demonstrates good association with rainfall over southern Africa at three and six months lags. The IndSLPa, and Nino3 however, hold some limited forecasting potential for rainfall over east Africa. The SLP pressure index which links the simultaneous activity over the Atlantic and Indian Oceans indicate that they have good association with rainfall over the east Africa key area. These results suggest that rainfall over east Africa is most responsive to SLP over the Atlantic Ocean. A number of regional environmental indices hold predictive potential for east Africa rainfall at 3- and 6-month lead time.

6.3.0 Mapping of season lag correlation coefficients

Rainfall indices are created by aggregating three-month values to obtain DJF and MAM seasons; the predictant seasons. Seasonal data for environmental parameter indices are also created for corresponding zero, three and six month lags. Correlation analysis is then performed between rainfall indices and environmental indices at these seasons' lags.

6.3.1.0 Sea surface temperature

6.3.1.1 Relationships between continental Africa rainfall and index SST Ind+Atl

Attention is given to peak rainfall seasons when discussing correlation coefficients over east and southern Africa: DJF and MAM (figures for DJF season not shown). DJF rainfall over western Angola and some parts of the Democratic republic of the Congo (DRC) is shown to be positively associated with the SST index Ind+Atl index at all lags. Negative association is revealed between the DJF SST index Ind+Atl and DJF rainfall over southern Africa while east Africa DJF rainfall is shown to be positively associated.

Table 6.1: Three and six-month lagged Correlation

Environmental Key areas	Southern Africa		East Africa	
	CORRELATION COEFFICIENTS			
	3 Mon. lag	6 Mon. lag	3 Mon. lag	6 Mon. lag
SST Ind+Atl			-0.17	-0.2
SST AtlDipole			0.27	0.25
SST Ind-Atl	-0.3	-0.30	0.38	0.22
SST Ind	-0.15			-0.13
SST eastAtl	0.15	0.27	-0.37	-0.39
SST northAtl		0.13	-0.14	-0.15
SLP Ind+Atl	-0.34	-0.31	0.39	0.23
SLP Ind-Atl	-0.23	-0.24	0.38	0.27
SLP AtlDipole	-0.12	-0.17	0.47	0.41
SLP eastAtl	-0.29	-0.28	0.45	0.34
SLP eastInd	-0.42	-0.36	0.2	
SLP NwestAtl			0.28	0.24
U Atl+Ind	-0.17			0.2
U Ind	0.33	0.3	-0.44	-0.22
U Atl+Ind2		0.16	-0.31	-0.25
U Atl1	-0.19			-0.16
U Atl2	-0.13		-0.19	-0.18
V Atl1	0.12			0.17
V Atl2	-0.17	-0.17	0.14	
V Ind	0.41	0.33		
QBO30	0.4	0.31		
Indslpa	-0.42	-0.33	0.19	
SST Nino3	-0.48	-0.36		

Environmental parameters that show association with rainfall over east and southern Africa at three and six month lags. Rainfall as well as environmental parameter time series were filtered to remove all signals with periods lower than 1.5 years using the CWT. All correlation coefficients above are significant at 95% level. (Monthly data used)

During the JJA and SON seasons the SST index Ind+Atl is poorly associated with the DJF rainfall over southern Africa. Over the Congo basin and Sudan DJF seasonal rainfall is negatively associated with the JJA seasonal SST index Ind+Atl. The MAM season rainfall over southern Africa is shown to be negatively associated with the SON, DJF, and MAM seasonal SST index Ind+Atl; relatively higher correlation coefficients are revealed over the western parts of southern Africa and southeastern Africa fig. 6.7. North of 10°S the correlation coefficients between MAM season rainfall and SST index Ind+Atl are weak and patchy.

6.3.1.2 Relationships between continental rainfall and SST index Ind-Atl

DJF rainfall over Southern Africa is negatively associated with the SST index Ind-Atl index at season lags zero, one, and two. The index is shown to be non-negative throughout the1965-1995

period suggesting that SSTs over the Atl key area was lower than over the Ind key area. In order to have a high positive (Ind-Atl) index either SSTs over Ind should be higher than SSTs over Atl. To have lower positive (Ind-Atl) index SSTs over Ind should be cooler and SSTs over the Atl key area should be warmer but not exceeding SSTs over the Ind key area. Relatively higher SSTs over the Indian Ocean and relatively cooler temperatures over the Atlantic Ocean suggests higher pressures over the Atlantic ocean than over the Indian Ocean key area. This SST pattern favours an increase of rainfall over Angola, the Congo and eastern Africa and a suppression of DJF rainfall over southern Africa, fig 6.1 (a-c). This pattern of warm west Indian Ocean and simultaneously cool east Atlantic Ocean is consistent with the uptake of global El Nino.

6.3.2.0 Sea level pressure

6.3.2.1 Relationships between continental Africa rainfall and SLP index Ind+Atl

The JJA, SON and DJF SLP index Ind+Atl is shown to be negatively associated with the DJF rainfall over southern Africa, fig 6.2 (a-c). Positive association is revealed between SLP index Ind+Atl during SON and DJF seasons and DJF seasonal rains over east Africa. Relatively higher pressures over the Atlantic Ocean supports westerly flow over the eastern Atlantic to the Congo basin. Similarly relatively higher pressures over the central Indian Ocean may strengthen easterly flow towards Africa. The convergence, which results from the two wind regimes may result in rainfall over east Africa. Relatively higher pressures over the Atlantic suppress rainfall over southern Africa as mentioned above. The correlation patterns for MAM rainfall and SLP index Ind+Atl at all lags are weak and patchy.

6.3.2.2 Relationships between continental Africa rainfall and SLP index Ind

Rainfall during the DJF season over southern Africa is shown to be negatively associated with the SLP index Ind during the JJA, SON, DJF seasons, fig 6.3 (a-b); correlation coefficients are higher during the SON season, fig 6.3 (e). The SLP index Ind at seasons SON and DJF are positively associated with eastern and central Africa DJF season rainfall; again the correlation coefficient is highest in SON. The SLP index Ind during the SON, DJF and MAM seasons is negatively correlated with DJF seasonal rains; though the correlation coefficients are patchy during the SON and MAM seasons. The SLP index Ind during the SON, DJF and MAM seasons is negatively associated with MAM seasonal rains over the southern Africa. At season lag zero, i.e. MAM

Season, the SLP index Ind is negatively associated with MAM rainfall to the west of east Africa and southeast Africa fig. app6c (c).

6.3.3.0 Zonal wind field

6.3.3.1 Relationships between rainfall and zonal wind component index Ind over east Indian Ocean

Zonal winds over the eastern Indian Ocean during SON and DJF, represented by the zonal wind component index Ind are shown to be negatively associated with DJF rainfall over east Africa, Angola, and the Congo basin and positively associated with the DJF rainfall over southern Africa. Westerly wind (positive), over the eastern Indian Ocean, induces an outflow from east Africa and hence divergence which results in reduced rainfall during the DJF season (Hastenrath, 2000). Easterly winds on the other hand during the SON and DJF seasons favour reduced rainfall over southern Africa during the DJF season. An easterly wind towards east Africa brings warm moist air and convective activities fig. 6.4 (a-c). In the SON, DJF and MAM seasons positive zonal wind over the east Indian Ocean key area is negatively associated with MAM rainfall over eastern Africa and positively associated with MAM rainfall over Mozambique and Zimbabwe and Zambia fig. 6.8 (a-c). Recent research suggests that this wind induces ocean Rossby waves to travel westward across the Indian Ocean causing changes in SST that shift convection over Africa.

6.3.3.2 Relationships between continental rainfall and zonal wind component index Atl2 over the Atlantic Ocean

The westerly wind, zonal wind component index Atl2, during the JJA and SON seasons are shown to be negatively associated with DJF rainfall over eastern and central west Africa and positive association is revealed over the Central African Republic (figure not shown). During the DJF Season this wind index is shown to be positively associated with eastern Africa rainfall and negatively associated with southern Africa rainfall. The association between MAM rainfall over Africa and the zonal wind component index Atl2 is poor and patchy.

6.3.4.0 Meridional wind field

6.3.4.1 Relationships between continental Africa rainfall and meridional wind component index Ind over the northwestern Indian Ocean

At season lag 2 i.e. JJA season the meridional wind component index Ind over northwestern Indian Ocean is shown to be positively associated with DJF seasonal rains over northeast Africa and east Africa while negative association is indicated over southeastern Africa, Angola and the Democratic Republic of the Congo (DRC) fig. app6a (a). The DJF seasonal rainfall over Sudan, Zimbabwe Angola, southwestern Zambia, and Mozambique, Congo basin is positively associated with meridional wind component index Ind over the northwest Indian Ocean at season lag zero fig. app6a (c). Positive association is indicated over Sudan, southwest Africa, Zambia and Zimbabwe between SON meridional wind component index Ind and rainfall fig. app6a (b). Positive meridional winds off the coast of east Africa causes upwelling and hence cooling the sea surface off the coast of east Africa. Relatively high pressures, which are introduced due the cool SST, strengthen the Arabian ridge. A relatively stronger Arabian ridge has the effect of reducing rainfall over east Africa and favouring more rainfall over the Congo basin and further south. Reduced rainfall over east Africa is due to the diffluent nature of the Arabian ridge, while more rainfall over southern Africa and the Congo Basin is a result of convergence of northeasterly flow and southeasterly flow in the south, and westerly flow from the Atlantic Ocean. A positive meridional wind component index over the northwestern Indian ocean, during SON, and DJF and MAM seasons show positive association with MAM rainfall over Zimbabwe, Zambia, Botswana and eastern South Africa, Gabon and Cameroun fig app6d (a-c). The MAM rainfall over Ethiopia and Central Africa are positively associated with the Meridional wind component index Ind fig. app6d (b).

6.3.5 Relationships between continental Africa rainfall and QBO30 index

DJF rainfall over Gabon and Cameroun is shown be negatively associated with the (westerly phase) QBO30 index at season lags zero and one while over southern Africa DJF rainfall is positively associated with QBO30 at season lags zero, one and two with relatively high association at season lag two, fig 6.5 (a-c). The westerly phase of the QBO favours more DJF rainfall over southern Africa while east Africa shows almost no relationship with the QBO30 index at season lag zero except at season lags one and two. Similar results have also been revealed by Mason, (1992). The westerly phase of the QBO during SON, DJF and MAM seasons is shown to be positively associated with MAM rainfall over Zambia, Zimbabwe and eastern South Africa, fig. 6.9 (a-c); while it is negatively associated with MAM rainfall over Gabon, Angola and Zaire at lag two (i.e. SON and DJF seasons) fig 6.9 (a).

6.3.6 Relationships between continental Africa rainfall, and Nino3 and Indonesia sea-level pressure anomaly (IndSLPa) indices

Mappings of correlation coefficients between DJF rainfall and JJA, SON and DJF Nino3 and IndSLPa indices are very similar and therefore they will be discussed together. It is revealed that Nino3 and Indonesia SLP anomaly indices, which are all ENSO signals, are negatively associated with rainfall over southern Africa, Cameroun and the Sahel at season lags zero, one and two, figs 6.6 (a-c) and app6b (a-c). The IndSLPa index shows higher positive correlation coefficients with rainfall over east Africa at season lags zero and one figs. 6.6 (b, c) and app6b (b, c). The association between DJF rainfall over east Africa and JJA Nino3 index is weakly positive and patchy while the association between DJF rainfall and SON IndSLPa is positive. Over Angola and the Congo basin DJF rainfall is positively associated with JJA, SON and DJF Nino3 and IndSLPa indices. MAM rainfall over southern Africa, Mozambique, northern part of Zambia and western parts of the Congo basin is negatively associated with Nino3 SST and IndSLPa indices during SON, DJF seasons, though the association is weak and patchy over some areas figs. 6.10 and app6e (a-c). At season lag zero, i.e. MAM Season, the IndSLPa and Nino3 are negatively associated with rainfall over southern and southeastern Africa, Gabon and Cameroun and positively associated over central Africa and northeastern Africa. Very poor association is revealed between rainfall over east Africa and the two ENSO indices, mainly because of seasonal decoupling of the Indian Ocean monsoon (Hastenrath, 2000).

6.4 Relationships between DJF gridded Africa rainfall and June-Sept all India rainfall index

The DJF rainfall over the eastern, southeastern and southwestern Africa is positively associated with the June-September all India rainfall index. Positive association is also indicated over west African in the Gulf of Guinea countries. The June-September all India index is negatively associated with DJF rainfall over Angola and the Democratic Republic of the Congo fig. 6.11. Heavy rains during the June-September summer monsoon may result in cooler ocean temperatures due to decreased insolation because of cloudiness. This on the other hand lead to higher pressures over the northern Indian Ocean and the Arabian sea and thus relatively stronger Arabian Ridge.

6.5 Persistence

A number of climatological variables exhibit some degree of persistence, i.e. a tendency for climate anomalies to continue to exist for longer period than might be expected if the variables were randomly distributed in time, (Thapliyal, 1984). This persistence is normally due to inertia or carry over process in physical systems. For example, the slow variability of sea surface temperatures over the central Pacific Ocean due to the heat content with depth and heat capacity (memory) of water (high values tend to follow high values and low values tend to follow low values). The data set which portray this attribute is normally positively auto-correlated. A geophysical data series has high predictability potential if it possesses the following properties: (1) Strong positive auto-correlation and (2) the decreasing auto-correlation function or plot is linear with little noise. This section looks into the persistence of the key area indices using the auto-correlation function; which is calculated at two, four and six month lags, the results being tabulated in table 6.5 (calculated using the STATGRAPHIC statistical package); results are tabulated to reduce the number of figures. Auto-correlation is calculated after removing respective long term mean annual cycles. The tabulated values are significant at 5% level. Out of all the indices analysed, only the Nino3, IndSLPa, QBO30 and SST key areas were persistent and significant at 5% level up to six months lag while a few others showed persistency up to two months lag with low auto-correlation values.

6.6 Tabulation of stability for selected seasonal predictors

Table 6.3 and 6.4 summarises the stability of predictors for the tropical highlands over Africa. The stability could be looked into this way: When the correlation coefficients between a predictant and predictor parameter at lags zero, one and two have significant large values and same sign the predictor is said to be relatively stable with respect to the predictant. Results of the stability analysis have shown that there is a predictability potential of rainfall over the tropical highlands of Africa. Sit is further revealed that some parameters over key regional centres could be used to issue forecasts six months in advance. Global oceanic/atmospheric indices (Nino3 and QBO) have also shown that rainfall over some areas over the tropical highlands over Africa have the potential of being forecast up to six months in advance.

Table 6.3: Two, one and zero seasons lag correlation coefficients - Predictor stability for DJF rainy season; summarised from figures 6.1 - 6.7

Parameter	Predictor Index	Comment
SST	Ind+Atl	Unstable predictor
	Ind-Atl	Stable predictor over southern Africa
	Ind	Stable predictor starting at season lag one
	eastAtl	Unstable predictor; changing correlation coefficient signs at season lag zero
	NorthAtl	Patchy
	AtlDipole	Patchy correlation coefficients over southern and east Africa
SLP	Ind+Atl	Stable predictor
	Ind-Atl	Unstable predictor; changing sign at season lag zero
	AtlDipole	High correlation coefficients at season lag two decreasing at season lag one and increasing at season lag zero
	eastAtl	Stable predictor; same sign and about the correlation coefficients at all season lags
	eastInd	Stable predictor starting at season lag two
	NwestAtl	Patchy correlation coefficients
U	Atl+Ind	Patchy but high correlation coefficients over east Africa at season lag zero
	Ind	Stable predictor starting at season lag one; negative correlation coefficients over east Africa and positive over southern Africa
	Atl+Ind2	Unstable predictor; changing sign at lag season zero
	Atl1	Patchy Correlation coefficients over the target areas
	Atl2	Patchy and unstable
V	Atl1	Stable predictor for south Africa starting at season lag one
	Atl2	Stable predictor for southern tip of Africa.
	Ind	Stable predictor starting at season lag one
QBO30	Singapore	Stable predictor for southern Africa; weak correlation coefficients over east Africa
IndSLPa	Indonesia	Stable predictor for the two rainfall key areas
SST	Nino3	stable predictor for southern Africa

Table 6.4: Two, one and zero seasons lag correlation coefficients- Predictor stability MAM rainy seasons; summarised from figures 6.8 - 6.14

Parameter	Predictor Index	Comment
SST	Ind+Atl	Stable predictor over southern Africa
	Ind-Atl	Patchy correlation coefficients
	Ind	Stable predictor for southern Africa
	eastAtl	Stable predictor over central and east Africa
	NorthAtl	Stable predictor over Angola and Namibia; patchy over east Africa
	AtlDipole	Patchy correlation coefficients over southern and east Africa
SLP	Ind+Atl	Correlation coefficients decreasing from season lag two to season lag zero over southern Africa
	eastAtl	Stable predictor over both east and southern Africa though correlation coefficients are small at season lag zero
	eastInd	Patchy and unstable over east and southern Africa but stable over Mozambique
	NwestAtl	Stable predictor at season lag one to season lag zero over southern Africa
U	Atl+Ind	Patchy and unstable
	Ind	Stable predictor over east Africa but unstable over southern Africa
	Atl+Ind2	Patchy correlation coefficients and unstable
	Atl1	Patchy Correlation coefficients and unstable
	Atl2	Patchy Correlation coefficients and unstable
V	Atl1	Patchy Correlation coefficients
	Atl2	Patchy Correlation coefficients
	Ind	Stable predictor starting at season lag one to season lag zero
QBO30	Singapore	Stable predictor for Zambia, Zimbabwe and eastern South Africa; weak correlation coefficients over east Africa
IndSLPa	Indonesia	Stable predictor for southern Africa and central eastern Mozambique
SST	Nino3	Stable predictor for southern Africa and western parts of east Africa; weak correlation coefficients over the coastal strip of east Africa.

Table 6.5: Auto-Correlation Coefficients at lags 2, 4 and 6

PARAMETER		Auto-correlation at lag		
		2	4	6
Rainfall	Southern Africa	0.21		
	East Africa			
SST	Ind+Atl	0.78	0.62	0.48
	AtlDipole	0.71	0.49	0.38
	Ind-Atl	0.55	0.36	0.23
	Ind	0.60	0.45	0.34
	eastAtl	0.62	0.42	0.31
	northAtl	0.66	0.40	0.29
SLP	Ind+Atl	0.33	0.23	0.19
	Ind-Atl	0.28		
	AtlDipole	0.31		
	eastAtl	0.38	0.28	0.28
	eastInd	0.26		
	NwestAtl			
Zonal Wind	Atl+Ind	0.17		
	Ind	0.17		
	Atl+Ind2			0.16
	Atl1			
	Atl2			
Meridional Wind	Atl1			
	Atl2	0.35	0.14	
	Ind	0.18		
QBO30		0.83	0.53	
SLP Indonesia		0.94	0.81	0.38
SST	El Nino3	0.83	0.62	0.39

6.7 Summary

In this chapter the association of seasonal rainfall over the tropical highlands over Africa has been considered. Seasonal oceanic/atmospheric parameters have been analysed into at lags 0, 1 and 2 seasons using cross-correlation amplitude as an indicator. Results found in this chapter suggest that there is a potential of predicting rainfall over the highlands of tropical Africa and also that these forecasts can be given up to six months in advance using ocean/atmospheric parameters over certain action centres in the tropical Atlantic and Indian Oceans. Most importantly this methodology represents a shift away from 'apriori' rainfall targets and has mapped many of the Ocean climate influences 'inward' across Africa. A rainy summer monsoon suggests good rains over the tropical highlands of Africa.

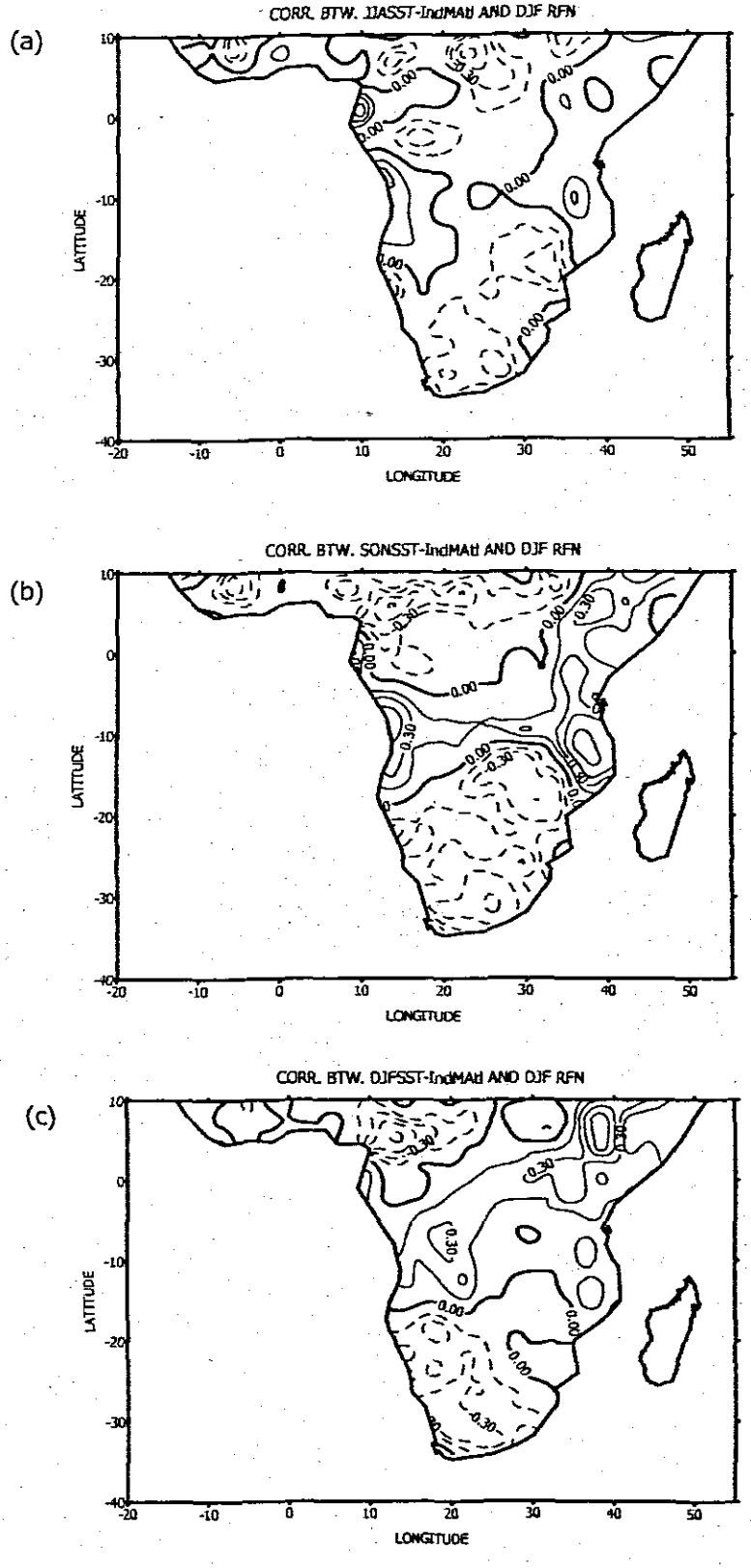

Fig. 6.1 Correlation between continental Africa gridded DJF rainfall and environmental parameter indices. Dashed (continuous) lines represent negative (positive) correlation coefficients. (a) Correlation btw rainfall and JJA SST over Ind-Atl; (b) Correlation btw rainfall and SON SST over Ind-Atl; (c) correlation btw rainfall and DJF SST over Ind-Atl

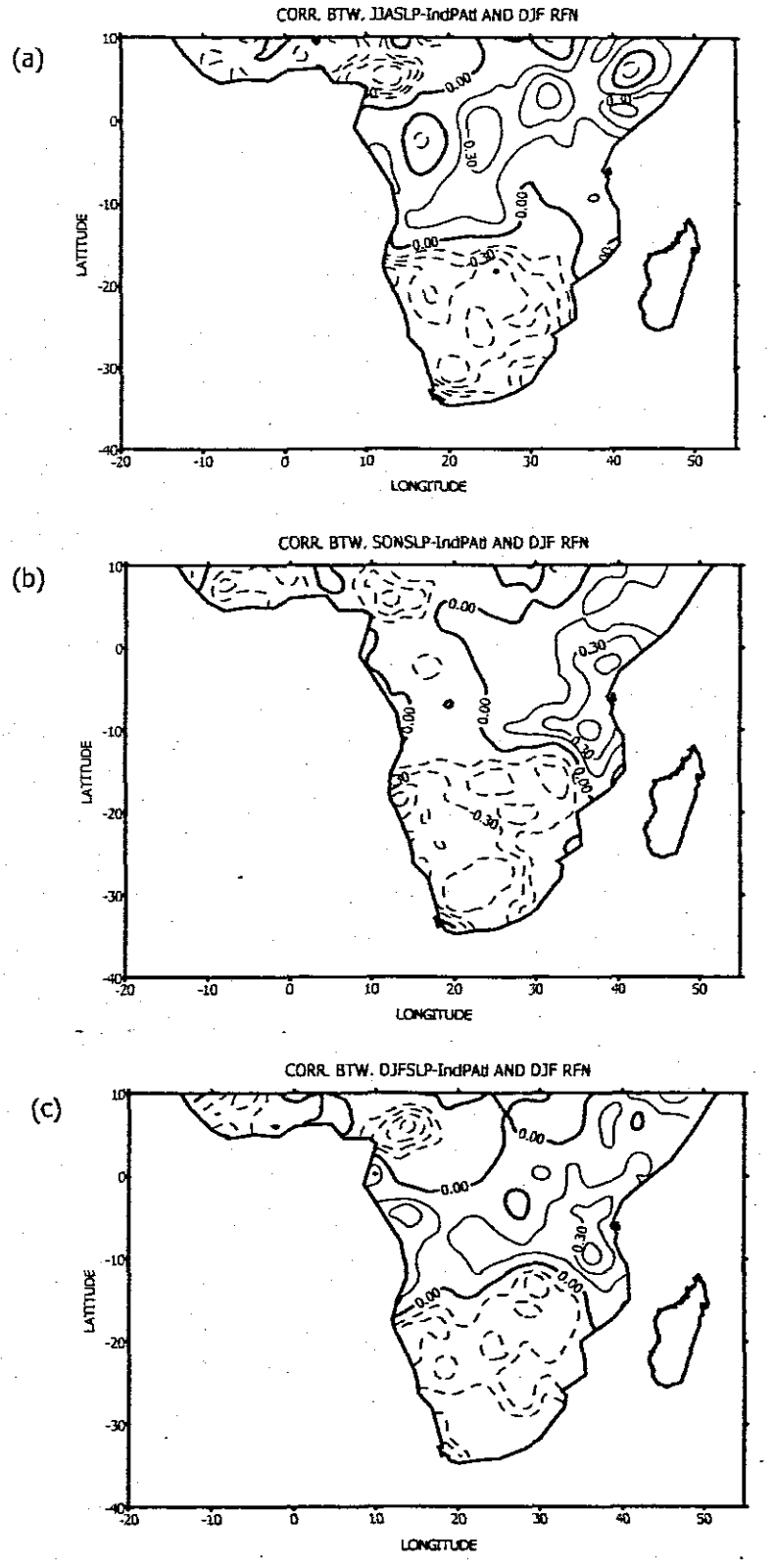

Fig. 6.2 Correlation between continental Africa gridded DJF rainfall and environmental parameter indices. Dashed (continuous) lines represent negative (positive) correlation coefficients. (a) Correlation btw rainfall and JJA SLP over Ind+Atl; (b) Correlation btw rainfall and SON SLP over Ind+Atl; (c) correlation btw rainfall and DJF SLP over Ind+Atl

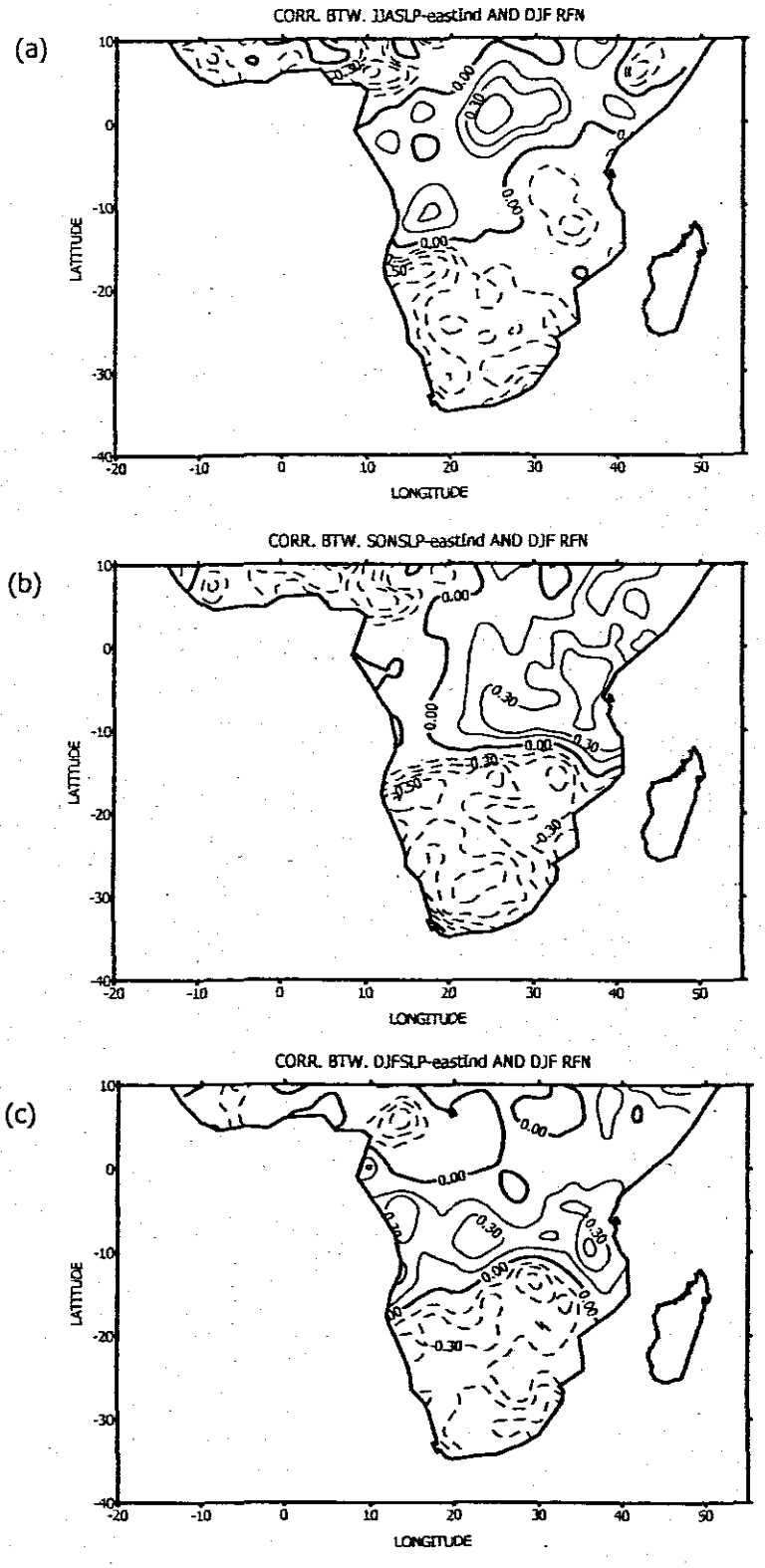

Fig. 6.3: Correlation between continental Africa gridded DJF rainfall and environmental parameter indices. Dashed (continuous) lines represent negative (positive) correlation coeficients. (a) Correlation btw rainfall and JJA SLP over eastInd; (b) Correlation btw rainfall and SON SLP over eastInd; (c) Correlation btw rainfall and DJF SLP over eastInd

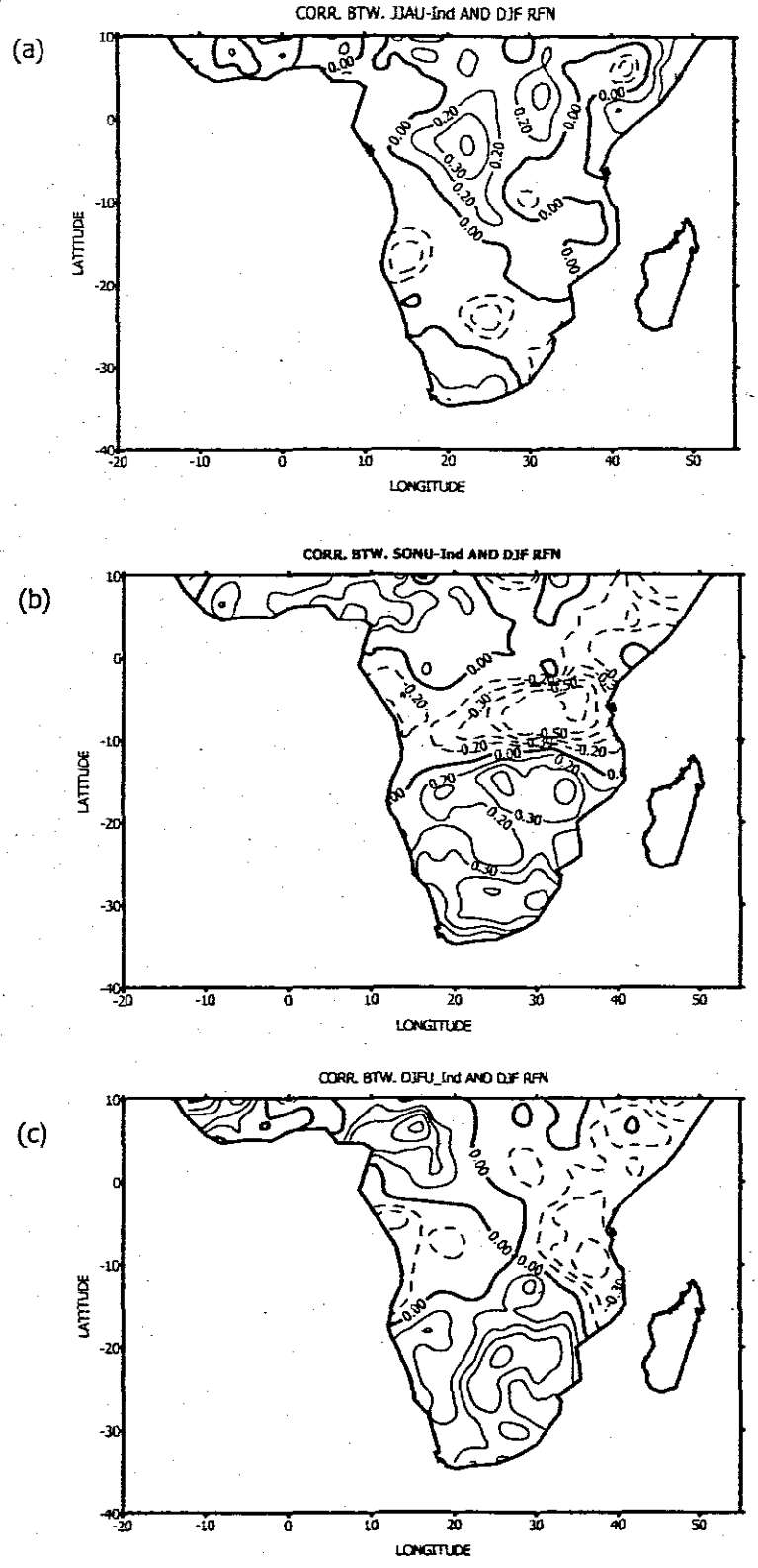

Fig 6.4: Correlation between continental Africa gridded DJF rainfall and environmental parameter indices. Dashed (continuous lines represent negative (positive) correlation coefficients. (a) Correlation btw rainfall and JJA U wind component over Ind; (b) Correlation btw rainfall and SON U wind component over Ind; (c) Correlation btw rainfall and DJF u wind component over Ind

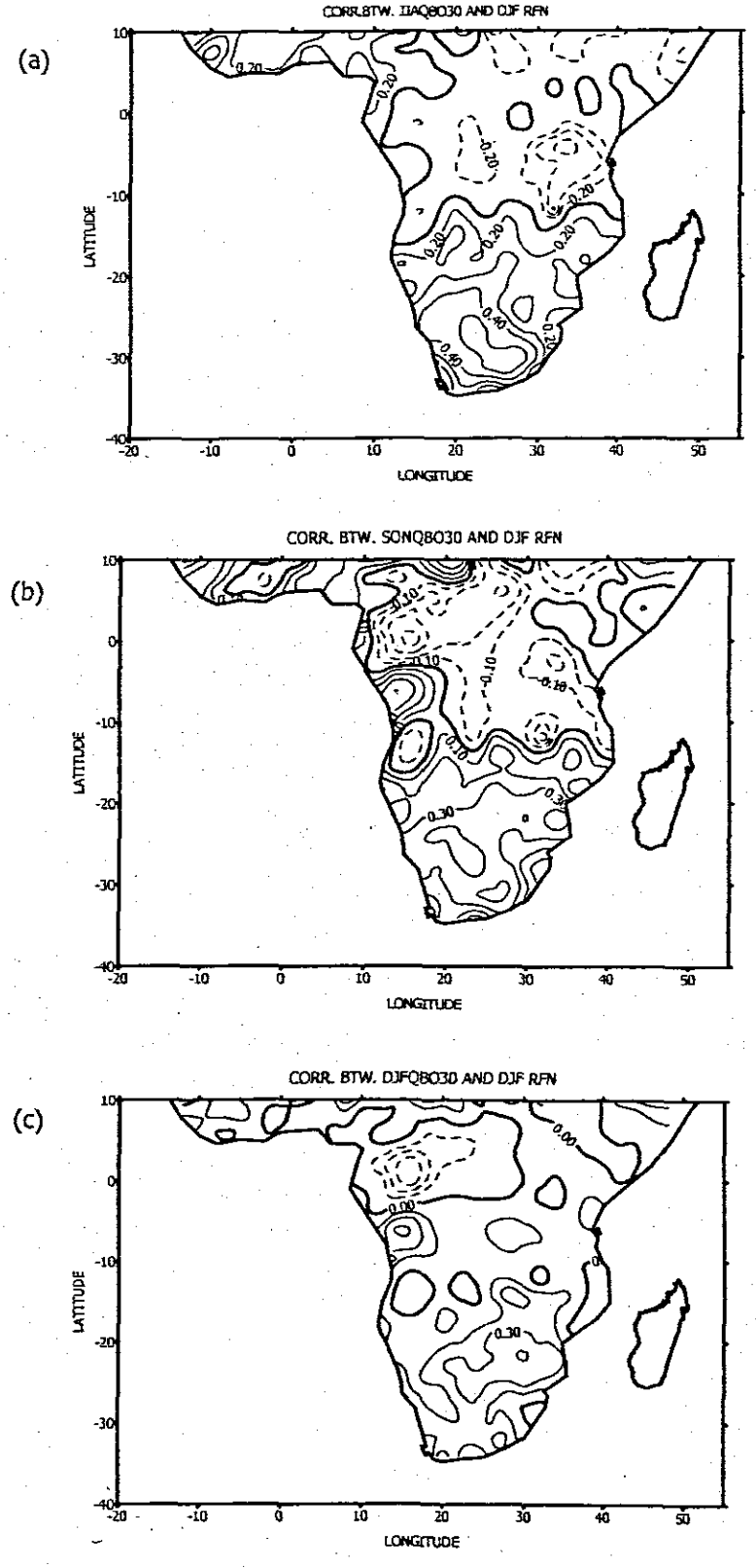

Fig. 6.5: Correlation between continental Africa gridded DJF rainfall and environmental parameter indices. Dashed (continuous) lines represent negative (positive) correlation coefficients. (a) Correlation btw rainfall and JJA QBO30) index; (b) Correlation btw rainfall and SON QBO30 index; (c) Correlation btw rainfall and DJF QBO30

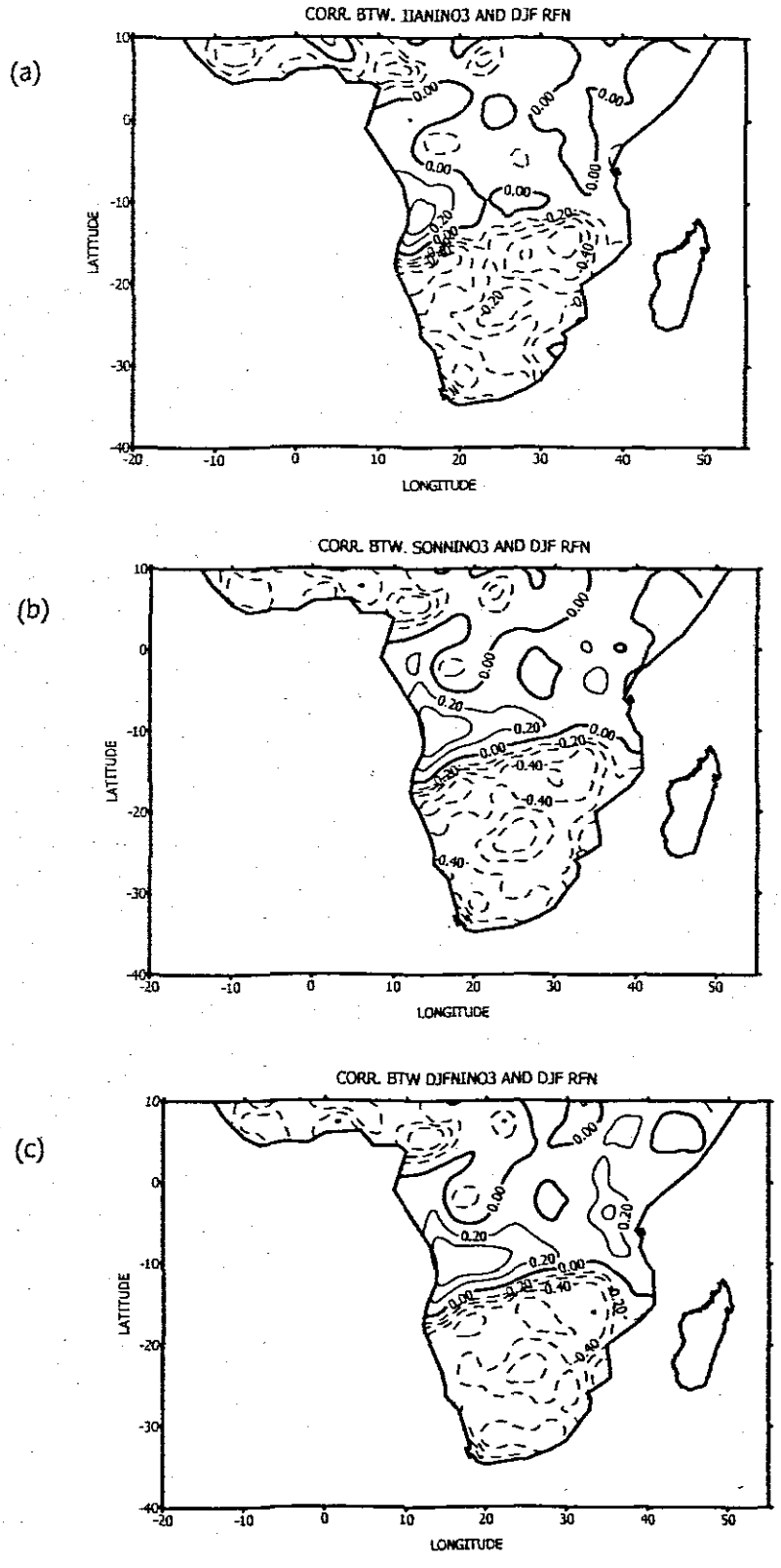

Fig. 6.6: Correlation between continental Africa gridded DJF rainfall and environmental parameter indices. Dashed (continuous) lines represent negative (positive) correlation coefficients. (a) Correlation btw rainfall and JJA SSTs over NINO3; (b) Correlation btw rainfall and SON SSTs over NINO3; (c) Correlation btw rainfall and DJF SSTs over NINO3

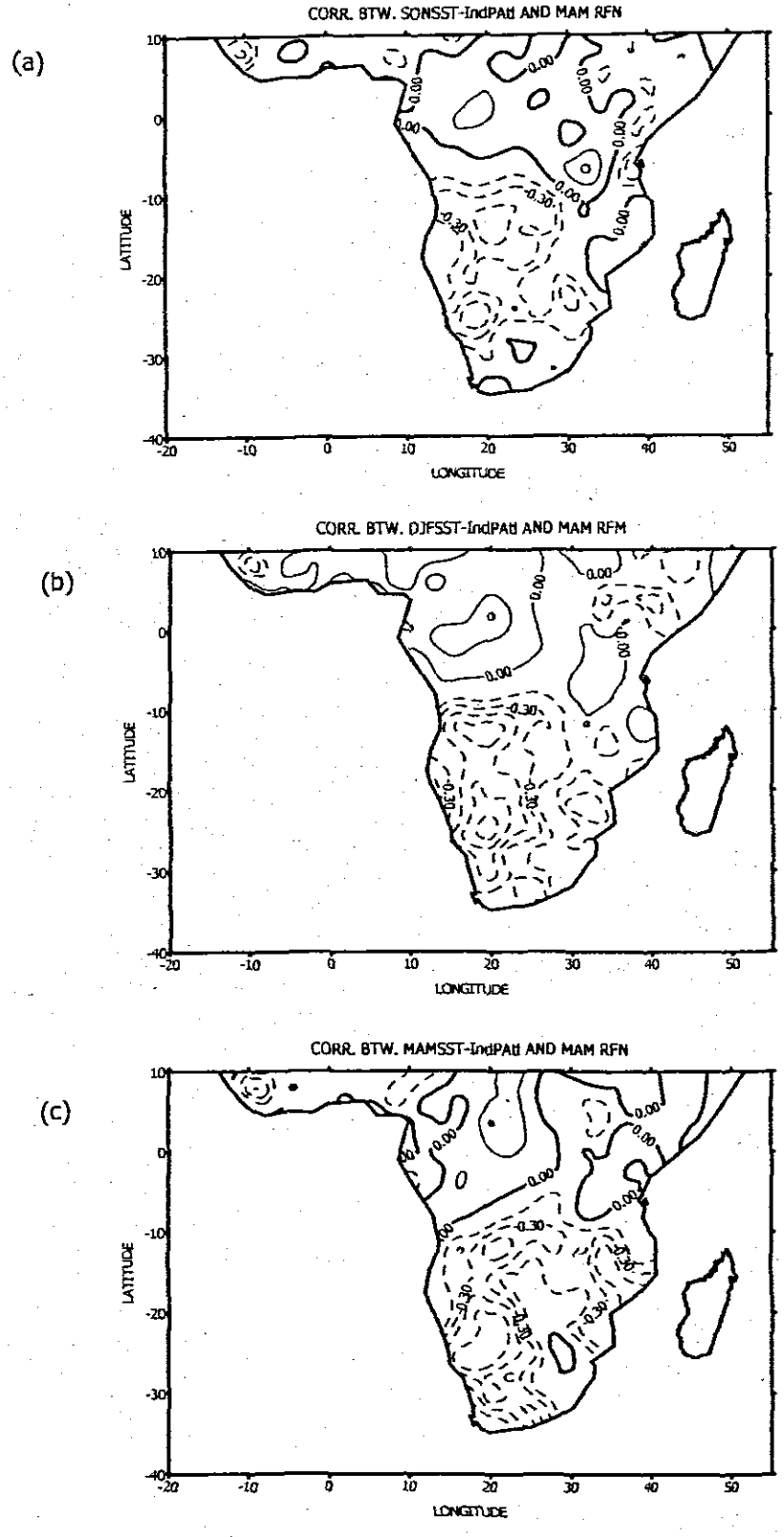

Fig. 6.7: Correlation between continental Africa gridded MAM rainfall and environmental indice. Dashed (continuous) lines represent negative (positive) correlation coefficients. (a) Correlation btw rainfall and SON SSTs over Ind+Atl; (b) Correlation btw rainfall and DJF SSTs over Ind+Atl; (c) Correlation btw rainfall and MAM SSTs over Ind+Atl

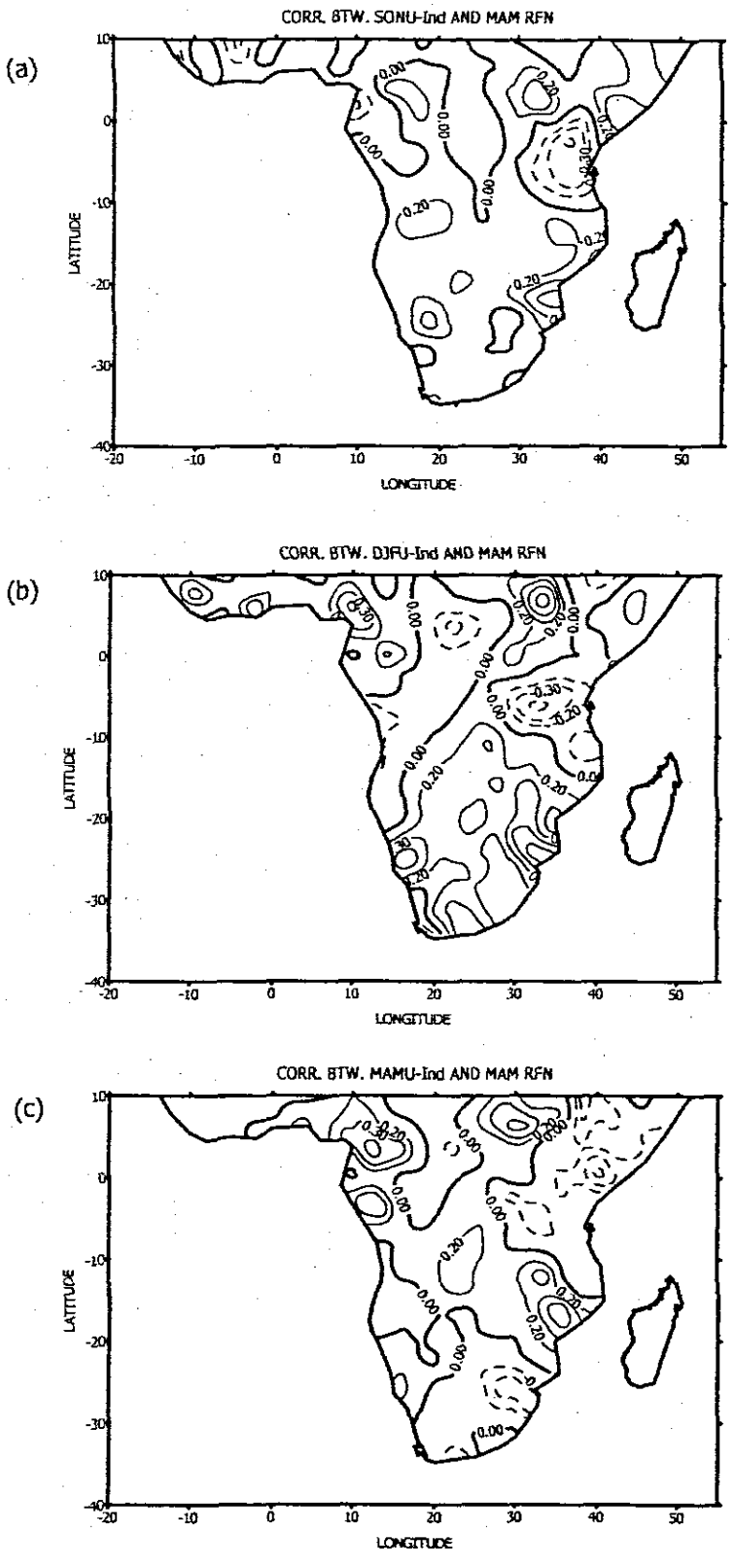

Fig 6.8: Correlation between continental Africa gridded MAM rainfall and environmental parameter indices. Dashed (continuous lines represent negative (positive) correlation coefficients. (a) Correlation btw rainfall and SON U wind component over Ind; (b) Correlation btw rainfall and DJF U wind componentover Ind; (c) Correlation btw rainfall and MAM u wind component over Ind

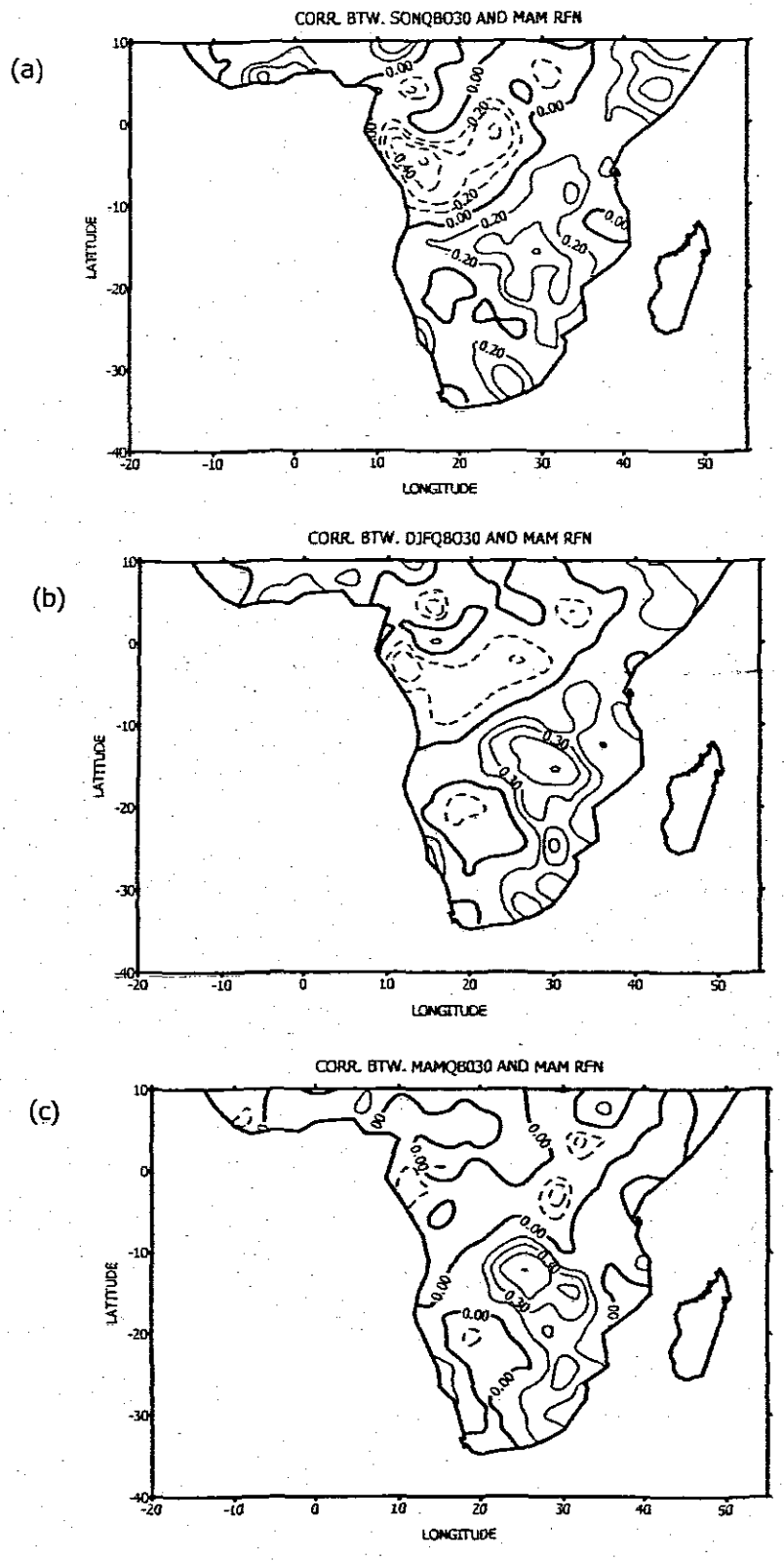

Fig. 6.9: Correlation between continental Africa gridded MAM rainfall and environmental parameter indices. Dashed (continuous) lines represent negative (positive) correlation coeffuicients. (a) Correlation btw rainfall and SON QBO30) index; (b) Correlation btw rainfall and DJF QBO30 index; (c) Correlation btw rainfall and MAM QBO30

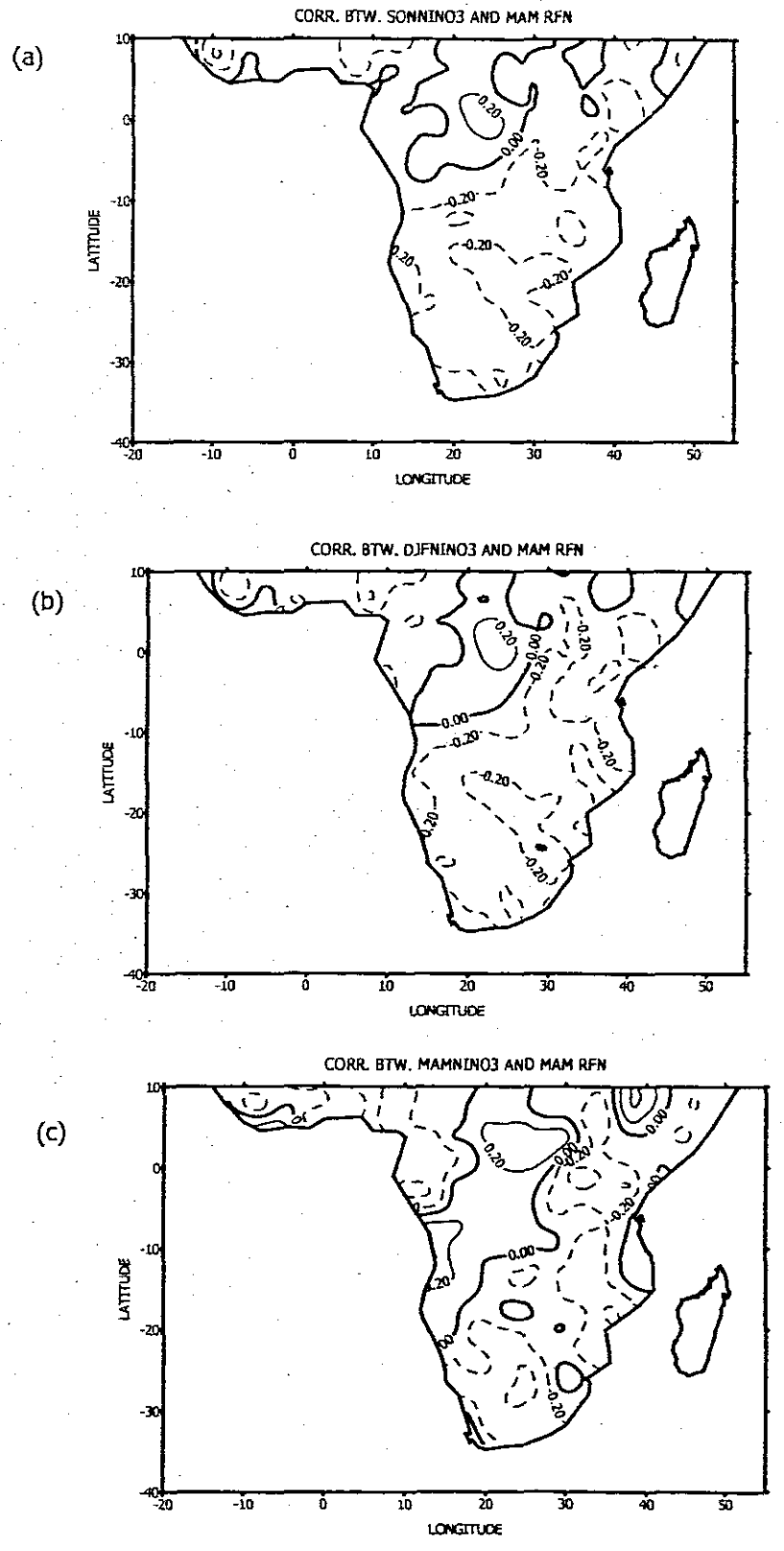

Fig. 6.10: Correlation between continental Africa gridded MAM rainfall and environmental parameter indices. Dashed (continuous) lines represent negative (positive) correlation coefficients. (a) Correlation btw rainfall and SON SSTs over NINO3; (b) Correlation btw rainfall and DJF SSTs over NINO3; (c) Correlation btw rainfall and MAM SSTs over NINO3

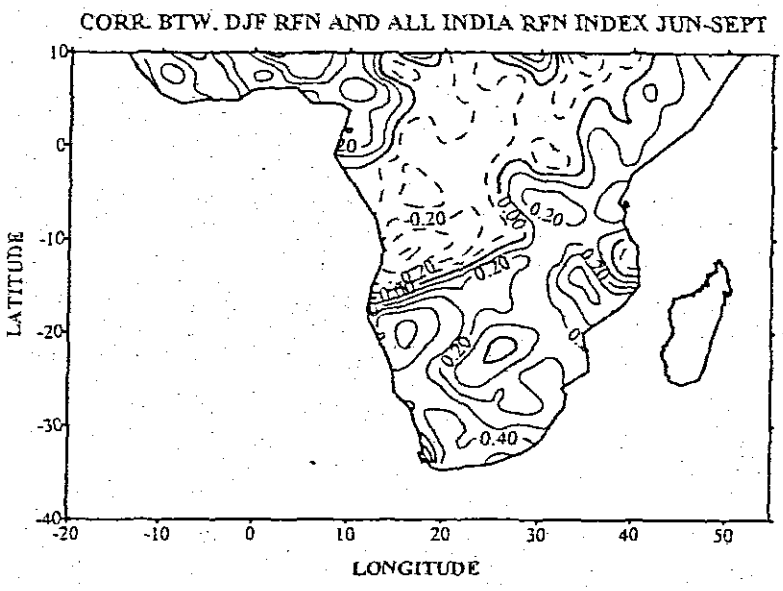

Fig. 6.11: Correlation between gridded continental Africa rainfall and June-September Summer Monsoon rains (1965 -1995). Dashed (continuous) line represent negative (positive) correlation coefficients

CHAPTER 7

7.0 Summary and conclusion

7.1 Introduction

Rainfall is one of the major components of the climate system, which support life. For human beings rainfall supports a number of socio-economic activities including industries, agriculture, construction, livestock, health, hydro-power generation etc. Excessive deficient in rainfall may result in the disruption of these activities and hence the socio-economic well being of the concerned population. The economies of many African countries, particularly those poor sub-Saharan countries, depend mainly on rain-fed agriculture as irrigation is outside their reach. The spatial and temporal distribution of tropical Africa rainfall unfortunately varies from year-to-year. Floods and drought conditions may result in the disruption of many socio-economic activities. Shortage of rains for a longer period may result in a drought which may lead to a serious shortage of food and pasture for livestock. On the other hand heavy rains persisting for a long time period may result in low lying farmlands or settlements being inundated with water thus destroying crops and infrastructure. For example, floods in Tanzania in 1997/98, disrupted agricultural activities, destroyed food and cash crops, and infrastructures. The total cost to infrastructures was estimated to be TShs72bil. (Equivalent to US$70 million) (Kanemba, personal comm., 2001). Due to the variable nature of rainfall over tropical Africa and dependency of countries concerned, planners must be aware of the vagaries of the climate of Africa in order to get prepared.

Is it the year-to-year fluctuations of the seasonal rainfall that is of major concern? Yes, indeed together with these fluctuations which at times are extreme, resulting in floods or droughts, it would be necessary to know in advance the behaviour of the coming seasonal rains. Part of the aim of this study therefore, was to understand the inter-annual patterns and mechanisms of rainfall variability over the tropical highlands of Africa and its predictability potential in the context of key tropical ocean/atmosphere parameters. A number of international researchers have done studies on rainfall variability over Africa at different time scales and its association with global teleconnection indices with aims of first understanding its variability and mechanisms thereof and second to be able to predict these rains. Few studies however, have been done by local scientists on the behaviour of the climate system over the tropical highlands of Africa and its association

with surrounding ocean-atmosphere system. An effort is made therefore, to create this understanding locally.

It is anticipated that seasonal rainfall over some areas of Africa is modulated by global oceanic and atmospheric phenomena (ENSO, QBO, etc) and their variable 'uptake' in regional oceanic/atmospheric thermodynamic and circulation patterns. Firstly, efforts have been made to identify and document the spatial and temporal pattern of rainfall and temperature over the continent of Africa. Secondly to identify and document the spatial and temporal pattern of the oceanic and atmospheric parameters (at low levels) over the tropical Atlantic and Indian Oceans. Association between temperature and rainfall over Africa, and marine environmental indices have been investigated. Finally the predictability potential of inter-annual rainfall over the tropical highlands of Africa using the identified environmental parameter key areas has been explored. In carrying out this study different data sets and data analysis methods have been used. A recently introduced technique, the Wavelet Transform (WT) was employed to study spectral characteristics of different time series. In this study a number of findings have been made, a summary of which is made below:

7.2.0 Summary

7.2.1 The climatology and annual cycle of climates over sub-Saharan Africa

The adequacy of gridded monthly rainfall and temperature data from CRU was investigated. The CRU data was found to compare well with observed station rainfall data or ground truth between 1965-1995. Gridded rainfall data was compared with station rainfall data extracted in the same box for the 1965-1995 period. The correlation coefficient between the two time series was found to be 0.79 significant at 95% level. The NCEP re-analysis long term seasonal patterns, in the area 70°W-110°E, 30°N-40°S, has also shown to compare well with previous COADS data used in other studies. The NCEP re-analysis was also used to study the climatology of tropical Africa thermodynamic and circulation climatology over the Atlantic and Indian Oceans (Mulenga, 1999). By sampling a few modes of rainfall variability results show that about 50% of rainfall variability is due to the annual cycle and 10% due to inter-annual variability. Patterns with loading away from the equatorial belt have shown high amplitudes at an oscillation period of 12 months; which reflects movement of the sun. Loading patterns within the equatorial band displayed relatively

high amplitudes at two periods; one at 12 month period and another one at 6 month period. These are the areas where the sun crosses twice in a year. Further it has been shown that there are periods when annual amplitudes are high and other periods when they are low. It is proposed that inter-annual variability "modulate" the annual cycle.

7.2.2 Inter-annual spatial and temporal variability

In chapter two, it was demonstrated that conversion of PC loadings to key areas is acceptable. The selected PC modes may therefore, be assigned physical meaning. Analyses of the key area time series have revealed annual and inter-annual variability of different parameters. Frequency-time representations of key area time series have shed light on the stability of climate systems. Some key areas maintained similar frequency patterns for the whole period, whilst others have shown disjointed frequency patterns. Dominant frequencies are in the range 2-4 years and in many cases, amplitudes evolve similarly for rainfall and SLP as expected. Synoptic features associated with the major modes of climates around Africa have been identified. Principal mechanisms responsible for these major modes have been speculated and explanations as to how they influence inter-annual rainfall variability over the tropical Africa have been given.

The PCA analysis on rainfall, temperature, SST, SLP and U and V wind components with annual cycles yielded a number of homogeneous regions with their first mode depicting annual cycles. PCA (with annual cycles) yielded 12 and 7 homogeneous rainfall and temperature regions, over the African continent south of 10°N, which explained a total of 81 and 91 variance respectively. PCA on marine environmental parameters over the Atlantic and Indian Ocean revealed a number of homogeneous regions, some of which could be associated with synoptic systems. Similarly PCA was performed on the above data after removing the annual cycle. Coherent SST, SLP, U and V wind patterns were identified over the Atlantic and Indian Oceans. These patterns were derived using principal component analysis on data after removing seasonal cycles. The fact that similar spectral patterns could be found in target and environmental data it could be proposed that an interrelationship between the climate component do exist.

Most of the environmental parameter coherent patterns are located over the tropical belt of the Atlantic and Indian Oceans. In some cases they simultaneously evolve over the two oceans. Air

temperature and rainfall coherent patterns depict the nature and seasonality of climates of tropical Africa, south of 10°N between 1965 and 1995.

Many of these patterns have shown oscillation periods between 2-6 years. SST and U wind field patterns over the central east Indian Ocean in the equatorial belt, have shown strong/large amplitude in the 2-4 year period which is similar to ENSO signals. Coherent patterns over the tropical Atlantic Ocean meanwhile, have shown high amplitudes in the 2-6 and 8-12-year oscillations period. Most patterns in the tropics do not show high amplitudes in the decadal range, except a few in the Atlantic Ocean (periods above 10 years should be treated with caution because of the length of record used). It has been shown that southern Africa rainfalls have amplitude in the 2-4, 4-6 and 8-14 year period while rainfall over east Africa has amplitudes in the 2-4 and 4-6 period bands which may suggest that rainfall over southern Africa could have stronger influence from tropical Atlantic Ocean than rainfall over east Africa.

7.2.3 Relationships between inter-annual rainfall and temperature, and environmental parameters over the Atlantic and Indian Oceans

Direct factors in rainfall variability are the SSTs in the more proximate oceans that in turn respond to Pacific ENSO events. Associations between targets and environmental parameters are sought to help in the identifications of potential predictors. Results from correlation analyses revealed a number of environmental parameters, over some key areas, to be associated with rainfall over some areas of tropical Africa. Teleconnection indices, like QBO, ENSO have shown good association with southern Africa rainfall at lag zero. But the relationship is not good with east Africa rainfall.

'Pockets' of relationships between environmental parameters, over key areas and continental Africa gridded rainfall have been identified. Some environmental parameters have revealed good association with rainfall and temperature over some areas of the tropical highlands of Africa. Some indices have shown correlation patterns similar to those of ENSO. The behaviour of temperature variability over the west coast of Africa and the Congo basin seems to be closely associated with temperature variability over the Atlantic Ocean. With a cold Atlantic Ocean over the Benguela area and the Gulf of Guinea, cold temperatures over the west coast of Africa, including Angola, Gabon and the Democratic Republic of the Congo are expected. High

pressures over the Benguela and the Gulf of Guinea are related to cooler temperature there and therefore these cooler temperatures affect the thermodynamic situation over west Africa. Nino3 and IndSLPa are positively correlated with temperatures over central and southern Africa and are negatively associated with temperatures over the west coast of Africa.

Correlation coefficient patterns revealed by the outward correlations suggest typical scenarios which could bring about wet and dry conditions over the tropical highlands of Africa. These modes, over tropical equatorial belts of the Atlantic and Indian Oceans, have been shown to explain rainfall up to about 25% over some areas of Africa south of 10°N. Temperatures over the continent are well correlated with SST modes over the equatorial tropical oceans and some of these explain more than 64% of temperature variability over some areas of the continent

The graphical comparison between time series of rainfall target key areas and environmental parameter key areas have shed some more light on the potential of predictability of rainfall over the tropical highlands of Africa. Cross-wavelet spectral results over the two areas have revealed that coupling of rainfall and environmental parameters over some key areas occur in the 2-3, 4-8, 10-12 year period bands. The time delay results indicate that there is no clear picture as to which parameter leads. The oscillations are not always in phase nor exhibiting constant lags. The unharmonious nature of these features could sometimes undermine predictability in statistical context. So the idea of reviewing predictor relationships in a time varying manner is well justified.

An explanation of physical associations between rainfall over the tropical highlands of Africa and environmental parameters over the designated action centres is proposed in the following section. Scenario for wet and dry situation are proposed using the diagrams in fig 7.1 and 7.2. In fig 7.1 the West Indian Ocean (WIO) is relatively warm and the East Indian Ocean (EIO) area is cool as well as the East Atlantic Ocean (EAO) is cool. The thermodynamic state of the Ocean sectors above suggests relatively lower and higher pressures over the western and eastern Indian Ocean sector respectively. This setup establishes an east-west pressure gradient and hence easterly anomalies over the Central Indian Ocean (EIO). Low SSTs over the east Atlantic Ocean sector suggests high pressure and a possibility of strengthening of westerly anomalies. A convergence of moist easterly wind anomaly from the Indian Ocean and westerly wind anomalies from the

Atlantic Ocean is expected over the West India Ocean and eastern Africa. The southern Africa region is less active at this time due to a possible eastward shift of convergence due to the warmer west Indian Ocean fig 7.1. Fig 7.2 depicts a situation when eastern Africa is dry and southern Africa is wetter. This second scenario is such that the western Indian Ocean is cooler and the east Indian Ocean is warmer. The Atlantic Ocean which is relatively warmer maintains a relatively weak westerly wind anomaly. The cooling over the western Indian Ocean could be attributed to the upwelling off the Somali coast. In this situation a west-east pressure gradient is established resulting in having westerly wind flow anomalies over the central Indian Ocean thus drying eastern and the western Indian Ocean. Southern Africa is wet during this time due to convergence of moist air from the Indian Ocean and the Atlantic Ocean.

7.2.4 Predictability of rainfall over the tropical highlands of Africa

Auto-correlation analyses of predictors and predictants indices revealed persistence of up to six months. Seasonal lag correlations between seasonal gridded rainfall and seasonal oceanic/atmospheric indices show good association of up to three month lags. Over southern Africa more environmental parameters show good association than over east Africa. This suggests that rainfall over southern Africa is more predictable than that over east Africa. The MAM seasonal rainfall over east Africa indicates stable association for up to about six months with SST anomalies over Nino3 region and zonal wind anomalies over the eastern Indian Ocean.

Results of correlations between seasonal data at season lags zero, one and two are higher than when monthly data were used. This could be due to the inherent nature of monthly rainfall data not being continuous.

7.3 Conclusions

A number of features over the Atlantic and Indian Oceans have shown good association with some areas over the African continent. This is reasonable because the direct factors of rainfall variability are SSTs in the more immediate Oceans. Very few patterns have shown persistence and stability up to six months lag. Rainfall over east Africa is difficult to predict especially during the MAM season. Nino3 and zonal wind over the eastern parts of the Indian Ocean have shown stability in respect to rainfall over the east Africa key area. It could be said that there is an

interplay between the components of the climate system. There exist oceanic/atmospheric parameters, over homogeneous regions in the equatorial Atlantic and Indian Oceans which can be used to forecast seasonal rainfall up to three months in advance.

7.4 Recommendations for further work along these lines

Efforts should be done to increase more marine observations over the Atlantic and Indian Oceans and studies to forecast SSTs over these ocean basins done, as is over the Pacific Ocean. Numerical studies should be enhanced to better understand processes involved in the ocean basins adjacent to the African continent.

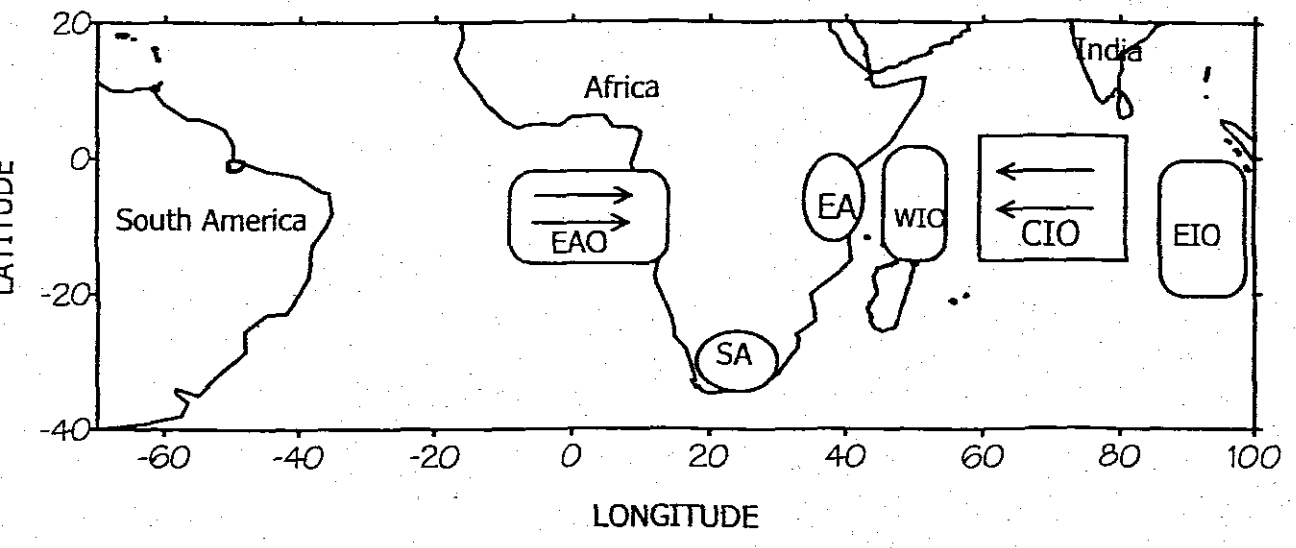

Figure 7.1 depicts the case when the east Africa region is wet and the southern africa region is dry

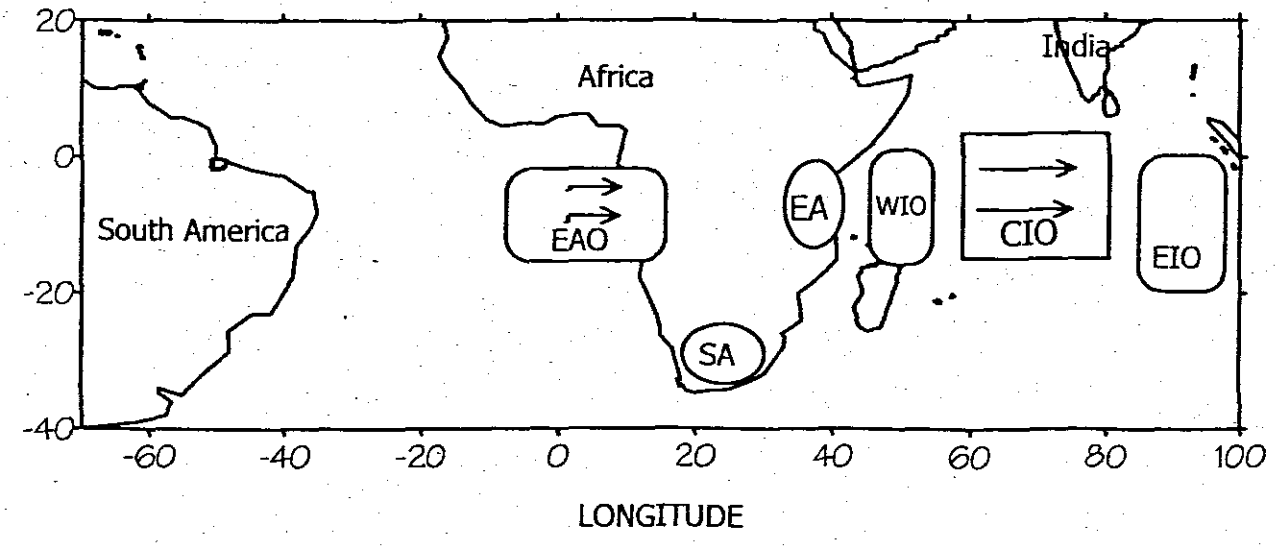

Figure 7.2 depicts the case when the east Africa regipn is dry and the southern Africa region is wet

References

Alusa, A., and M. Mushi, 1973: A study of the onset, duration and cessation of the rains in East Africa. Proceedings of the fifth specialist Meeting on Applied Meteorology in East Africa, Nairobi, Kenya, 133-140.

Anderson, T.W. 1958: An Introduction to Multivariate Statistical analysis, New York: Wiley, 240pp

Arpe, K., L. Dumenil, and M. A. Giorgetta, 1998: Variability in the Indian Monsoon in the ECHAM3 model: Sensitivity to sea-surface temperature, soil moisture, and the stratospheric quasi-biennial oscillation. J. Climate, 11, 1837-1858

Barnston, A. G., and C. F. Ropelewiski, 1992: Prediction of ENSO episodes using canonical correlation analysis. J. Climate, 5, 1316 - 1345.

Barnston, A. G. and Livezey, R. E., 1987: Classification, seasonality and persistence of low-frequency atmospheric circulation patterns, Mon. Wea. Rev., 115, 1083 - 1126

Basalirwa, C.P.K., Odiyo,O.J., Mngodo, R.J. and Mpeta, E.J., 1999: The climatological regions of Tanzania based on the rainfall characteristics, Int. J. Climatol., **19**, 69-80

Blanford, H. N., (1884): On the connection of Himalayan snow with dry winds and seasons of droughts in India. Proc. Roy. Soc. London, **37**, 3-22

Burt, J. E., and G. M. Barber, 1996: Elementary Statistics for geographers, The Guilfor Press, pp 640

Cadet, D. L., 1985: The Southern Oscillation over the Indian Ocean. J. Climate, **5**, 189-212.

Critchfield, H. J., 1975: General Climatology, Prentice-Hall of India, New Delhi, 368pp.

CRU/SAMRC, 1998: African Monthly climate data CD-ROM. Climate research Unit and the Mapping Malaria Risk in Africa Initiative. Available from the Climate Research Unit -NR4 7TJ, United Kingdom.

Daubechies I., 1992: Ten lectures on wavelets. SIAM Philadephia.

Delprat N., Escuide B., Guillemain P., Kronland-Martnet R., Tchamitchian P and Torresan., 1992: Asymptotic wavelet and Gabor analysis: Extraction of instantaneous frequencies. IEEE transactions on information theory, **38**, (2), pp 644-664

Dyer, T.G. J., 1981: A description of inter-annual rainfall variance over space and time for South Africa: 1921-1975, Transactions of the Royal Society of South Africa, **44**, 453-464

EAMD, 1963: Climatic seasons of East Africa, East African Meteorological Department. Report No. **8**, 4pp.

Ebdon, D., 1997: Statistics in Geography, Basil Blackwell. pp. 232.

Folland, C. K.; Palmer, T. N. and Parker, D.E; 1986: Sahel rainfall and world-wide sea surface temperature, *Nature*, ***320***, *602-607*

Foufoula-Georgiou, E., and P. Kumar, Eds., 1995: Wavelets in Geophysics. Academic Press, 373 pp

Gamage, N., and W. Blumen, 1993: Comparative analysis of low level cold fronts: Wavelet, Fourier, and empirical orthogonal function decompositions. Mon. Wea. Rev., **121**, 2867-2878.

Glantz, M.; R. Katz, and N. Nicholls, eds., 1991: Teleconnections Linking Worldwide Climate anomalies: Scientific Basis and Societal impacts, Cambridge University Press, 534pp.

Gowariker,V., Thapliyal, V. Sarkker, R.P., Mandal, G.S., Sen Roy, and Sikka, D.R.,1991: A power regression model for long range forecasting of monsoon rainfall in India, Mausam, **42**, pp125-130

Gowariker,V.,Thapliyal,V., Sarker, R.P., Mandal,G.S. and Sikka, D.R.,1989: Parametric and power regression models: New approach to long range forecasting of monsoon rainfall in India, Mausam, **40**, pp115-122

Graham, N. E., J. Michaelson, and T. P. Barnett, 1987: An Investigation of the El Nino- Southern Oscillation cycle with statistical models. Part 1: Predictor filed characteristics, J. Geophys. Res., **92**, 14 251 - 14 270.

Griffiths, J., 1959: The variability of Annual rainfall in East Africa. Bull. of American Society, **44**, 361-362.

Gu, D., and S. G. H. Philander, 1995: Secular changes of annual and inter-annual variability in the tropics during the past century. J. climate, **8**, 864-876

Harrison, M. S. J., 1986: A synoptic climatology of South African rainfall variability. Unpublished Ph.D. Thesis, University of the Witwatersrand, 341pp

Hastenrath, S., 2000: Zoanl circulations over the equatorial Indian Ocean. Journal of Climate: Vol. 13, No. 15, pp 2746-2756

Hastenrath, S., 2001: In search of zonal circulations in the equatorial Atlantic sector from the NCEP-NCAR re-analysis, Int. J. Climatol. **21**, 37-47

Hastenrath, S., A. Nicklis and L. Greishar, 1993: Atmospheric-hydrospheric mechanisms of climate anomalies in the western Indian Ocean. J. Geophys. Res., **98**, 20219-20235.

Hotelling, H., 1933: Analysis of a complex of statistical variables into principal components. Journal of Educational Psychology, **24**, 417-441, 498-520.

Hutchinson, M.F., 1995: Interpolating mean rainfall using thin plate smoothing splines. Int. J. Geog. Inf. Sys. **9**, 385-403.

Janowiak, J. E. 1988: An investigation of inter-annual rainfall variability in Africa. J. Climate, **1**, 240-255.

Johnston, R. J. 1992: Multivariate statistical Analysis in Geography, Longman Scientific Technical. John Wiley and sons, Inc. New York 280pp

Jolliffe, I.T., 1990: Principal component analysis; Royal Met. Soc., **45**, 375-382

Jury, M. R., and B. M. R. Pathack, 1993: Composite climatic patterns associated with extreme modes of summer rainfall over southern Africa: 1975-1984. Theoretical and Applied Climatology, **47**, 137-145.

Jury, M. R., 1996: Regional teleconnection patterns associated with summer rainfall over South Africa, Namibia, and Zimbabwe. Int. J. Climatology, **16**, 135-153.

Jury, M. R. and Pathack, B., 1991. A study of weather variability over the tropical southwest Indian Ocean, Meteorol. Atmos. Phys., **47**, 37-48

Jury, M. R., McQueen., 1993: Correlation atlas of climatic determinants for Tanzania

Kabanda, T.A., 1995: Seasonal and intra-seasonal dynamics and precusors of rainfall over northern Tanzania. Msc. Thesis, Oceanogr. Dept. University of Cape Town.

Kalnay et al., 1996: the NCEP/NCAR 40-year re-analysis project. Bull. Amer. Meteor. Soc., **77**, 437-471

Keen, C.S., and Tyson, P.D., 1973: Seasonality of south African rainfall: a note on its seasonal delimitation using spectral analysis, Arch. Meteor. Geophy. Bioklimat., **21**, 207-217

Kulkarin, J.R., 200:Wavelet Analysis of the Association between the southern Oscillation and the Indian summer monsoon, Int. J. Climatol., **20**, 89-104

Kumar, P., and E. Foufoula-Georgiou, 1993: A new look at rainfall fluctuations and scaling properties of spatial rainfall using orthogonal wavelets. J. Appl. Meteor., **32**, 209-222

Lau, K.-M., and H.-Y Weng, 1995: Climate signal detection using wavelet transform: How to make a time series sing. Bull. Amer. Meteor. Soc., **76**, 2391-2402

Legler, D.M., 1983: Empirical orthogonal function analysis of wind vectors over tropical Pacific region, Bull. Amer. Soc., vol. **64**, No. 3, 234-241

Lumb, F. E., 1966: Synoptic disturbances causing rainy periods along the East African coast, Met. Mag., 150-159.

Lyons, S. W., 1982: Empirical Orthogonal function analysis of Hawaiian rainfall, J. Appl. Meteol., **21**, 1713-1729

Madden, R. A.; and P.R. Julian, 1971: Description of a 40-50 day oscillation in the zonal wind in the tropical Pacific, J. Atmos. Sci., **28**, 702-708

Makarau, A. and M. R. Jury, 1997: Predictability of Zimbabwe summer rainfall. Int. J. Climate, **17**, 1421-1432.

Mallat S., 1998: A wavelet tour of signal processing. Academic Press, San Diego, CA. 200pp

Marquadt, C., and B. Naujokat, 1997: An update of equatorial QBO and its variability. 1st SPARC Gen. Assemb., Melbourne, Australia, WMO/TD-No. **814**, Vol.**1**, 87-90

Mason, S.J. and Lindesay, J. A., 1993 A note on the modulation of Southern Oscillation - southern African rainfall oscillations and the quasi-biennial Oscillation. J. Geophys. Res. **98**, 8847-8850.

Mason, S. J. and Tyson, P. D., 1992: The modulation of sea surface temperature and rainfall association over southern Africa with solar activity and the quasi-biennial oscillation, J. Geophys. Res., **97**, 5847-5856

Mason, S.J., and Tyson, P. D.,1992: The modulation of sea surface temperature and rainfall association over southern Africa with solar activity and quasi-biennial oscillation, J. Geophys. Res. , **97**, 5847-5856

Mason. S. J., 1995: Sea-surface temperature - South African rainfall associations. 1910-1989. Int. J. Climatology, **15**, 119-135.

Meehl, G. A., 1988: Tropical mid-latitude interactions in the Indian and Pacific sectors of the Southern Hemisphere. Mon. Wea. Rev. **116**, 472-484.

Meehl, G. A., 1993: A coupled air-sea biennial mechanism in the tropical Indian and Pacific regions: role of the oceans. J. Climate, **6**, 31-41.

Meyers, S. D. and J. J. O'Brien, 1994: Spatial and temporal 26-day SST variations in the tropical Indian Ocean using wavelet analysis, Geo. Res. Let., **21**, 9, 777-780

Meyers S. D., Keley B. G. and J.J. O'Brien 1993:. An Introduction to wavelet analysis in oceanography and meteorology: with application to the dispersion of Yanai waves. Mon. Wea. Rev., **121**, pp. 2858-2866

Mirion, O. and Lindesay, J. A., 1983: A note on changes in airflow patterns between wet and dry spells over South Africa, 1963 to 1979, South African Geographical Journal, **65**, 141-147

Morlet J. 1983: Sampling theory and wave propagation.. NATO ASI Series, FI, Springer, pp. 233-261.

Mpeta, E. J. 1997: Intraseasonal convection dynamics over southwestern and northeastern Tanzania: An observational study, MSc. Thesis, University of Cape Town, 180pp

Mulenga, H. M., 1998: Southern African Climatic anomalies, summer rainfall and the Angola low. Ph. D. Thesis, Oceanogr. Dept. Univ. Cape Town, 261 pp

Nakamura, K., 1968: Equatorial Westerlies over East Africa and their climatological significance, Tokyo Metropolitan University Reports, **3**, 43-61.

Naujokat, B., 1986: An update of the observed quasi-biennial oscillation of the stratospheric winds over the tropics. J. Atmos. Sci., **43**, 1873-1877.

Nicholson, S.E.,1989: Rainfall variability in southern and its relationship to ENSO and the Atlantic and Indian Oceans, *Preprints of the Third International Conference on Southern Hemisphere Meteorology and Oceanography*, Amer. Met. Soc., 366-367.

Nicholson, S.E.,1986: Rainfall variability in southern and equatorial Africa: its relation to Atlantic sea surface temperatures and the Southern Oscillation, *Preprints of the second International Conference on Southern Hemisphere Meteorology*, Amer. Met. Soc., 472-475.

Nicholson, S. E. And Entekhabi, 1987: Rainfall variability in equatorial and southern Africa: relationships with seas surface temperature along the southwestern coast of Africa. J. Climate and Appl. Meteorology., **26**, 561-578

Numerical Algorithms Group Ltd, 1996: NAG Foundation Toolbox, MATLAB version.

Nyenzi, B.S., Kavishe, M.M., Tibaijuka, P.F.,Kululetera, V., Nassib, I., Tillya, F.F. 1997:A study on Long range weather forecasting in Tanzania, Res. Report no.**1/97**, 79pp

Nyenzi, B. S., 1988: Mechanism of East African rainfall variability. Ph.D. Thesis, Florida State University, 184pp.

Ogallo, L.A., 1994: Validity of ENSO-related Impact in Eastern and Southern Africa in Usable Science: Food Security, Early warning, El Nino, pp 179-184. UNEP (Nairobi) and NCAR (Boulder CO).

Ogallo, L. J.,1988: Relationship between seasonal rainfall in east Africa and the Southern Oscillation. J. Clim. **8**, 34-43.

Ogallo, L. J., 1989: The Spatial and temporal patterns of the East African seasonal rainfall derived from principal component analysis, Royal Meteorological Society, 145-167.

Palmer T. N, 1986: Influence of the Atlantic, Pacific and Indian oceans on Sahel rainfall, Nature, **322**, 251-2653

Preston-White, R.A., and Tyson, P.D. 1988: The atmospheric and weather of Southern Africa, Oxford Univ. Press, Cape Town 374pp

Reason C. J. C. and Mulenga, H. 1999: Relationship between South African rainfall and SST anomalies in the southwest Indian ocean. Int. J. of Climatol., **19**, 1651-1973.

Reason, C.J.C and Mulenga, H.M., 1999: Relationships between South African rainfall and SST anomalies in the SW Indian Ocean. Int. J. Climatol., **19**, 1651-1673.

Rocha, A., 1992: The influence of global SSTs on the southern African summer climate, PhD Thesis, University of Melbourne, Australia, 249pp

Rogers, J. C. 1984: The association between the North Atlantic Oscillation and the southern Oscillation in the northern hemisphere, Mon. Wea. Rev., **112**, 1999-21015

Ropelewski C. F., and M. S. Halpert, 1987: Global and regional scale precipitation patterns associated with the El Nino- Southern Oscillation (ENSO). Mon. wea. Rev. **115**, 1606-1626.

Sciremammano,F., 1979: Comments on "Correlations between Rainfall and Sea Surface Temperatures during GATE"J. Phys. Oceano. Vol. **9**, 1298.

Thacker, W.C., and R. Lewandowicz, 1996: Climatic indices, Principal Components and Gauss-Markov theorem, J. Clim., **9**,1942-1958

Thapliyal, V. and S. M. Kulshrestha, 1992: Recent models for long range forecasting of southwest monsoon rainfall in India. Mausam, **43**, 3, 239-248.

Thapliyal, V., 1982: Stochastic Dynamic Model for long range prediction of Monsoon rainfall in Penuinsular India. Mausam, **33**, pp. 399-404

Thapliyal, V., 1987: Prediction of Indian Monsoon Variability; Evolution and prospects including development of new model, Climate of China and global climate, (Eds) D. Ye, Fu., J. Chao & Yoshino M., China Ocean Press, Beijin. Pp. 397-416.

Thapliyal, V., 1991: Issue of tropical long range forecast: Status and development of new forecast models, World Meteorological Organization, Geneva, WMO, **395**, pp267-272.

Thapliyal, V.,1990: Long range prediction of summer monsoon rainfall over India: Evolution and development of new models, Mausam, **41**, pp. 339-346

Thapliyal, V., 1991: Issue of tropical long range forecast : Status and development of new forecast models. World Met. Org. Geneva, WMO/TD, **395**, pp. 267-272

Thapliyal, V., 1986: Longe range forecasting of monsoon rainfall in India. World Met. Org., Geneva, WMO/TD, **87**, pp. 723-732

Thapliyal, V., 1987: Prediction of Indian Monsoon Variability; Evolution and prospects including development of new model, Climate of China and global climate, (Eds) D. Ye, Fu., J. Chao & Yoshino M., China Ocean Press, Beijing. Pp. 397-416.

Torrence C. and G. P. Compo,1997: A practical guide to wavelet Analysis, Bull. Amer. Meteor. Soc., **79**, (1),61-79

Toure, Y. M. and W. B. White, 1995: ENSO signals in global upper-ocean temperature. J. Phys. Oceanogr., **25**, 1317-1332.

Tyson, P. D., 1984: The atmospheric modulation of extended wet and dry spells over South Africa, 1958-1978, J. Climatol., **4**, 621-635

Tyson, P. D., 1980: Temporal and spatial variation of rainfall anomalies in South Africa south of 22°S during the period of meteorological records, Climatic Change, **2**, 363-371.

Wahba,G., 1979: How to smooth curves and surfaces with splines and cross-validation. 24th Conference on the design of experiments, U. S. Army Res. Office, 167-192

Walker, N. D., 1989: Sea surface temperature-rainfall relationships and associated ocean-atmosphere coupling mechanisms in the southern African region, Unpublished PhD. Thesis, University of Cape Town, 171pp.

Walker, N. D., 1990: Links between South African summer rainfall and temperature variability of Agulhas and Benguela current systems, J. Geophys. Res., **95**, (C3), 3297-3319

Walker, G. T., 1910: Correlation in seasonal variation of weather II. Mem. India Met. Dep., XXI, XXII

Walker, G. T., 1923: Correlation in seasonal variation of weather VII : A preliminary study of world wether. Mem. India Met. Dep. **24**, pp. 75-131

Walker, G. T., 1924: Correlation in seasonal variation of weather IX : A further study of world weather, Mem. India Met. Dep., **24**, pp 275-332

Wang, B. and Wang, Y., 1996: temporal structure of the southern Oscillation by wave form and wavelet analysis, J. Climatol., **9**, 1586-1598

Ward, N.M. 1998: Diagnosis and short lead to\ime prediction of summer rainfall in tropical North Africa at inter-annual and multi-decadal time scales, J. Climate

Weare, B. C., 1977: Empirical orthogonal analysis of Atlantic Ocean surface temperatures. Quart. J. Royal Meteor. Soc., **103**, 467-478.

Webster, P. J; Moore, A.M.; Loschning, J. P.; and Leben, R. R., 1999: Coupled ocean-atmosphere dynamics in the Indian Ocean during 1997-98, Nature, Vol. **401**, 356-360

Weng, H., and K.-M. Lau, 1994: Wavelets, period doubling, and time-frequency localization with application to organization of convection over the tropical western Pacific. J.Atmos. Sci., **51**, 2523-2541

Yin, Z -Y., 1994: Moisture condition in the south-eastern USA and teleconnetion patterns, Int. J.Climatol., **14**, 947-967.

Appendix Chapter 4

Figures for chapter four. Figure numbers are given in alphanumeric

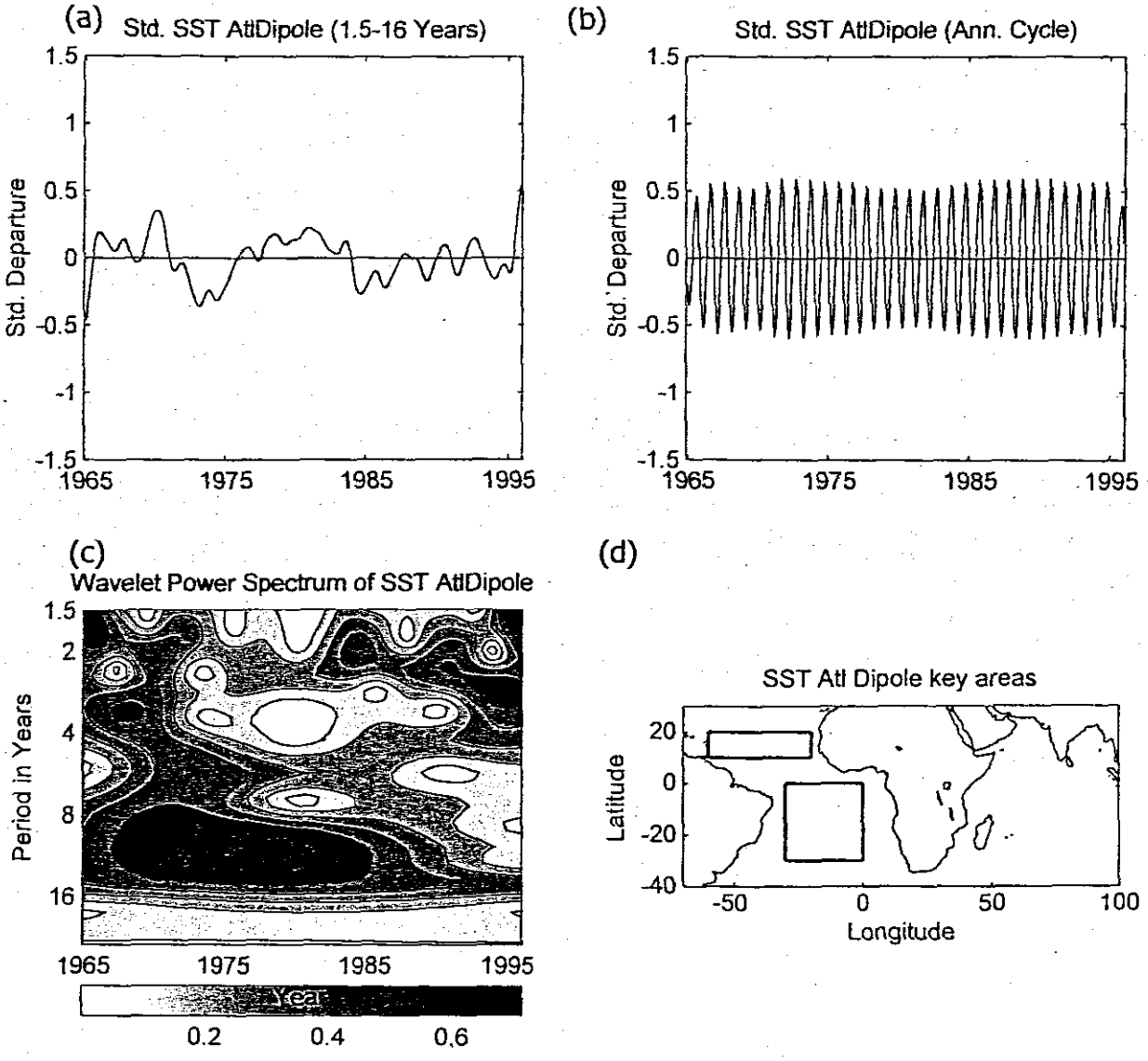

Fig. App4a: Plots of: (a) Inter-annual SST AtlDipole time series index (top left), **(b)** annual variabilty of SST AtlDipole (top right), **(c)** modulus of the wavelet transform coefficient for inter-annual variability of SST AtlDipole (bottom left), **(d)** box for SST AtlDipole key area (bottom right).

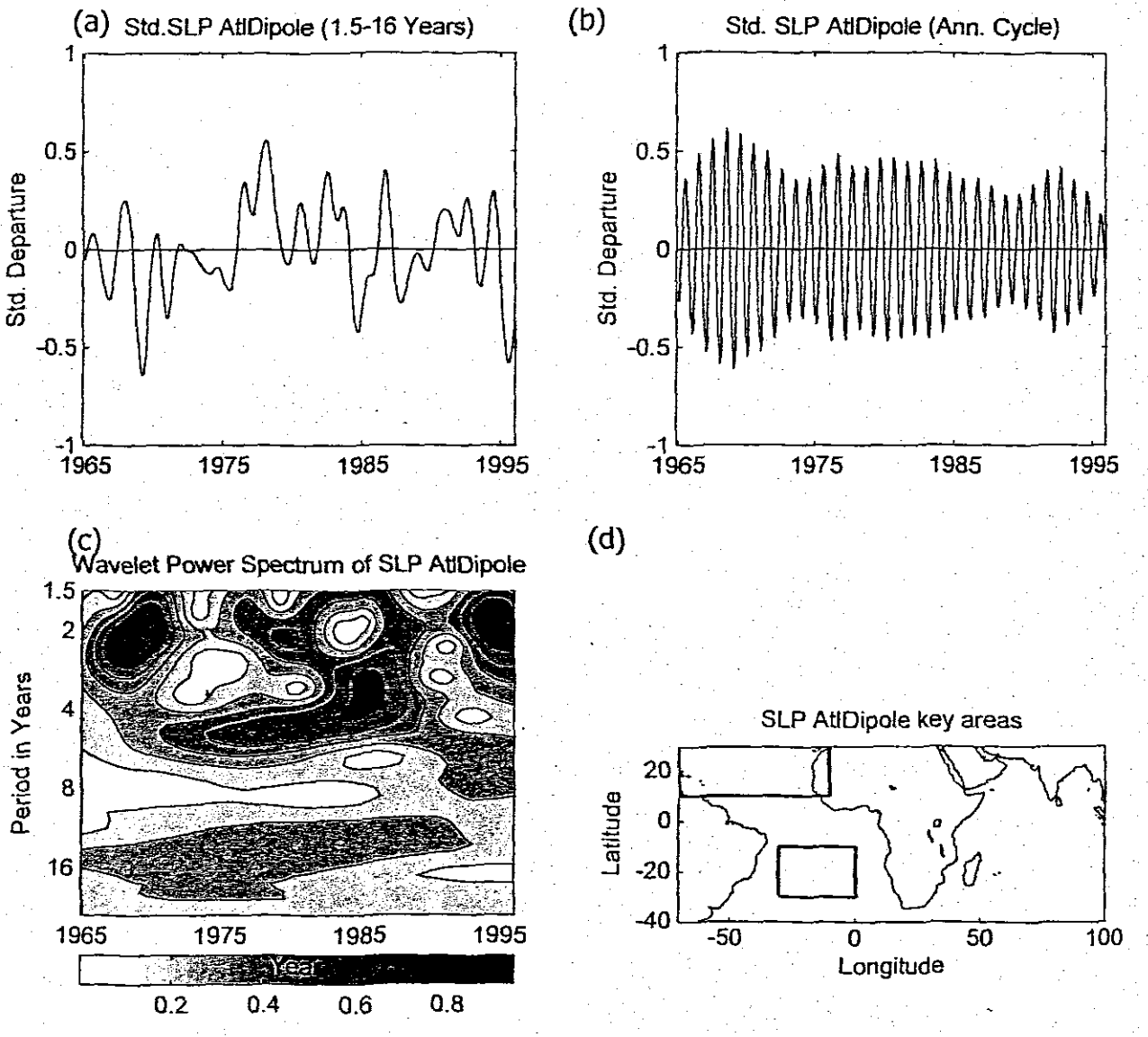

Fig. App4b: Plots of: (a) Inter-annual SLP AtlDipole time series index (top left), **(b)** annual variability of SLP AtlDipole (top right), **(c)** modulus of the wavelet transform coefficient for inter-annual variability of SLP AtlDipole (bottom left), **(d)** box for SLP AtlDipole key area (bottom right).

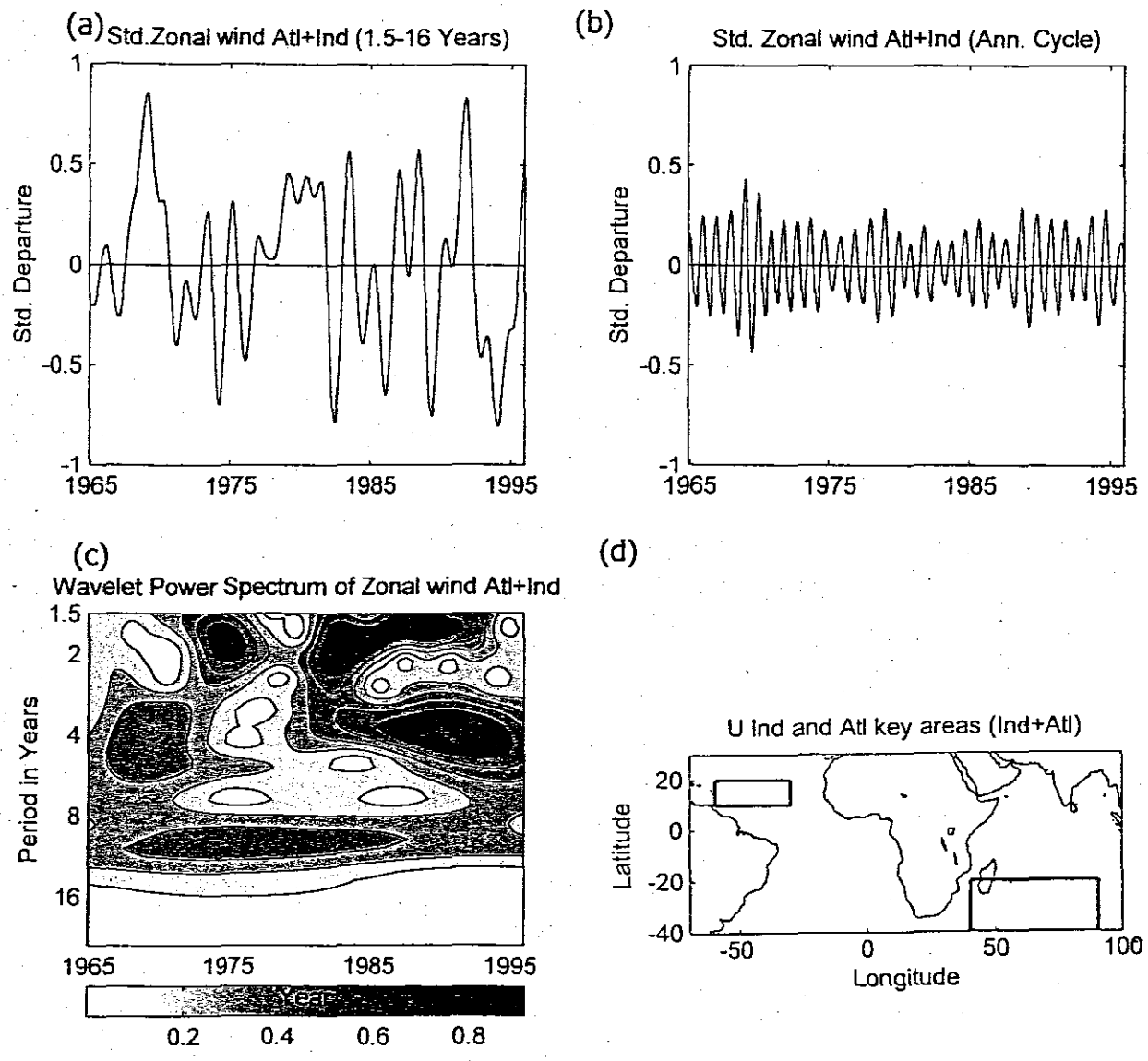

Fig. App4c: Plots of: (a) Inter-annual Zonal wind Atl+Ind time series index (top left), **(b)** annual variability of Zonal wind At+Ind (top right), **(c)** modulus of the wavelet transform coefficient for inter-annual variability of Zonal wind Atl+Ind (bottom left), **(d)** box for Zonal wind Atl+Ind key area (bottom right).

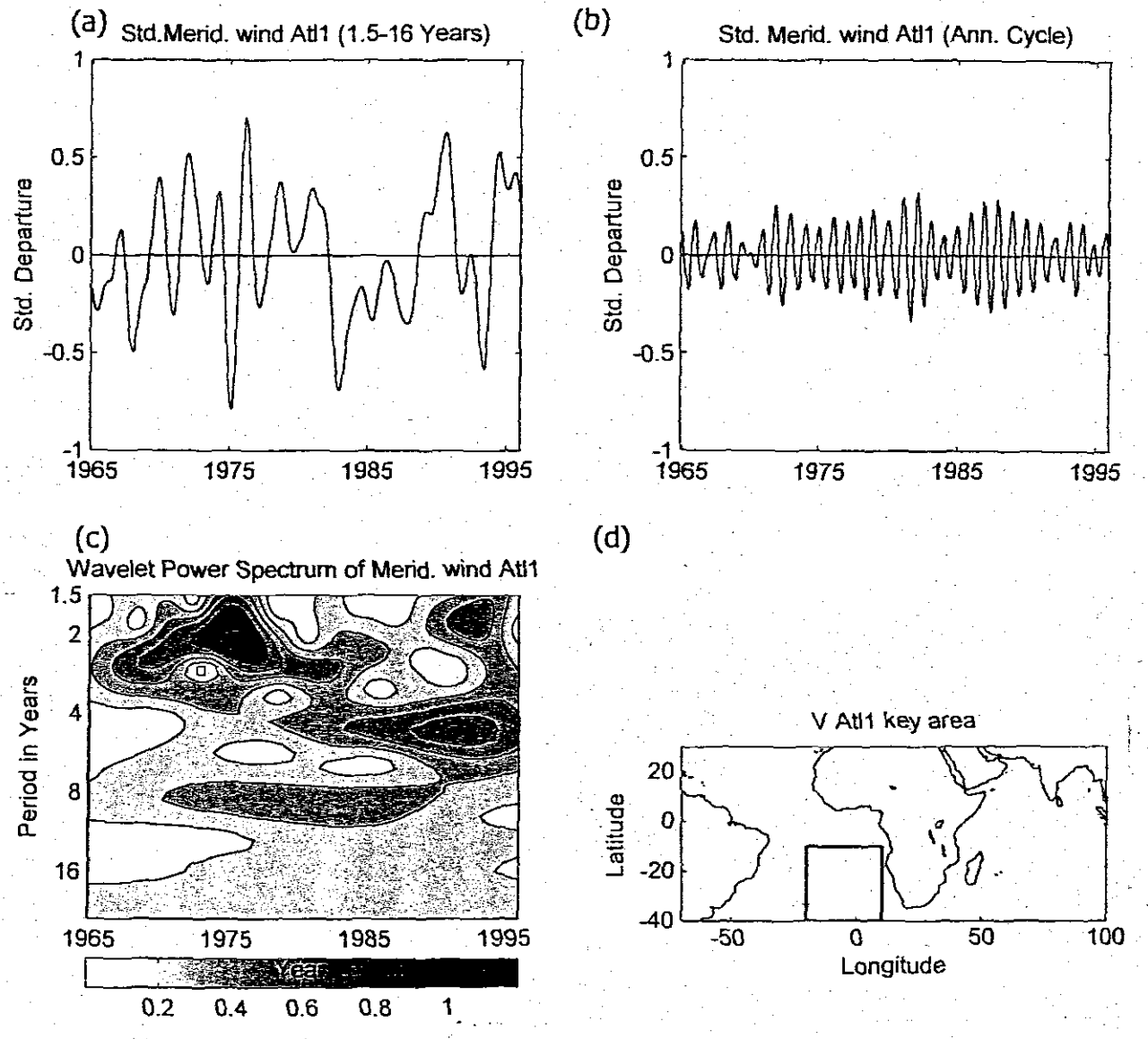

Fig. App4d: Plots of: (a) Inter-annual Meridional wind Atl1 time series index (top left), **(b)** annual variability of Meridional wind Atl1 (top right), **(c)** modulus of the wavelet transform coefficient for inter-annual variability of Meridional wind Atl1 (bottom left), **(d)** box for Meridional wind Atl1 key area (bottom right).

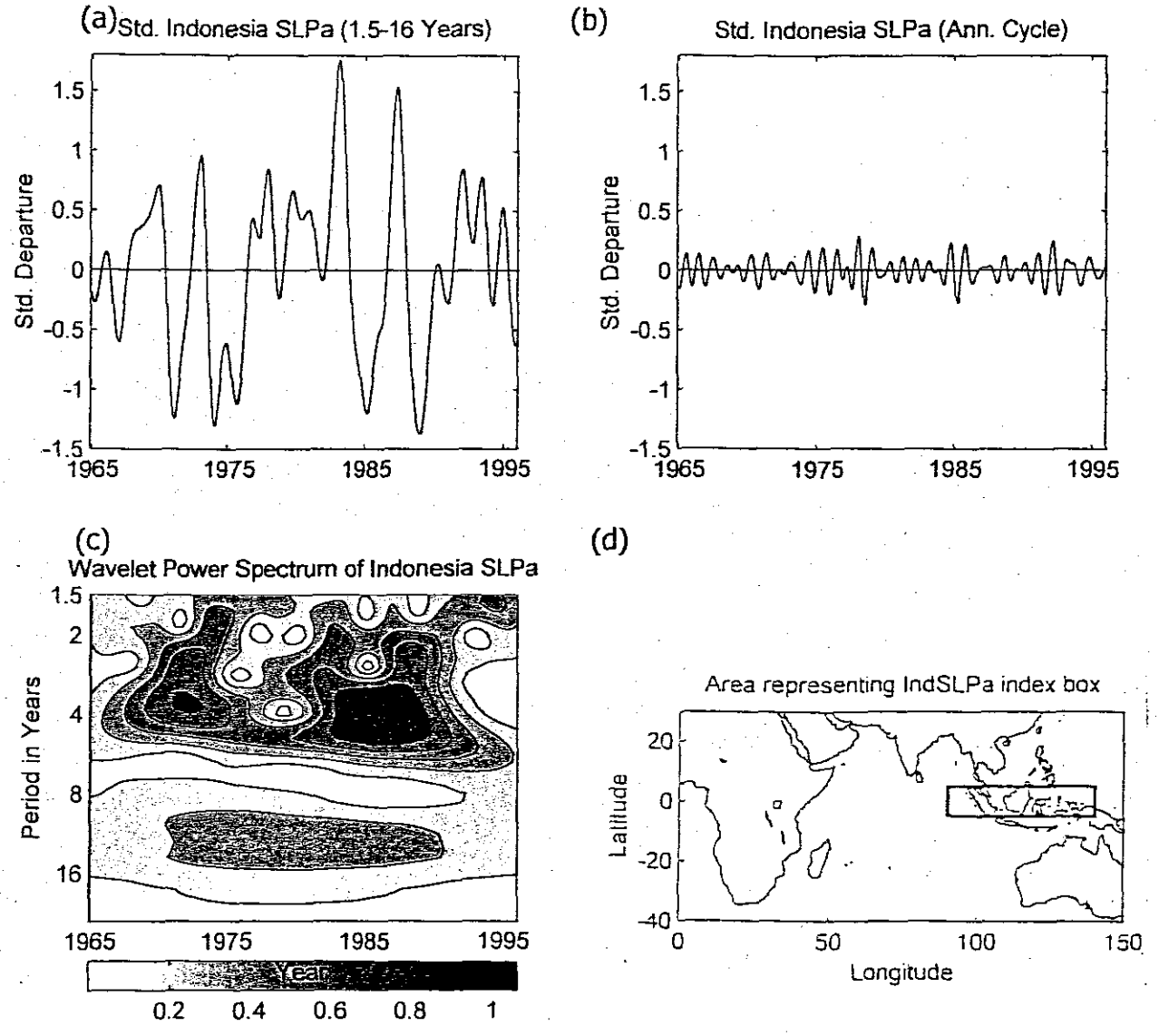

Fig. app4e: Plots of: (a) Inter-annual Indonesia SLPa time series index (top left), **(b)** annual variability of Indonesia SLPa index (top right), **(c)** modulus of the wavelet transform coefficient for inter-annual variability of Indonesia SLPa index (bottom left);**(d)** box for Indonesia SLPa index key area (bottom right)

Appendix Chapter 5

Figures for chapter five. Figure numbers are given in alphanumeric

(a)

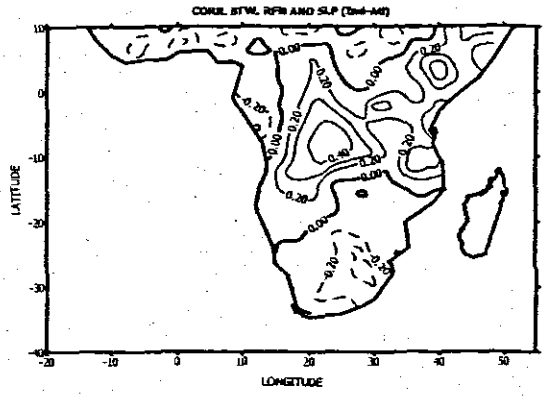

(b)

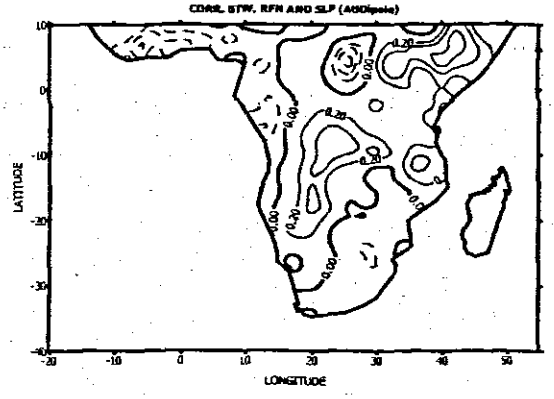

(c)

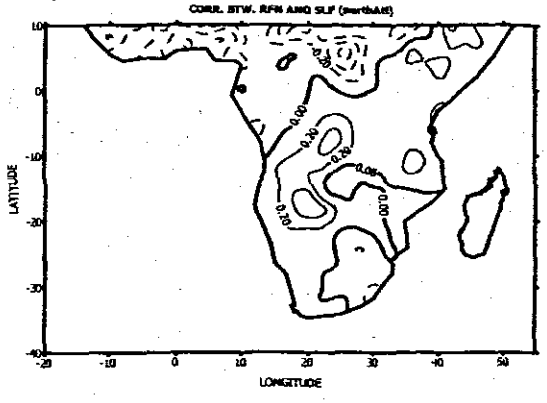

Fig. app5a: Correlation between continental Africa gridded rainfall and environmental indices. Dashed (continuous) lines represent negative (positive) Correlation coefficients. (a) Correlation btw rainfall and SLP Ind-Atl, (b) Correlation btw rainfall and SLP Atldipole (c) Correlation btw rainfall and SLP northAtl

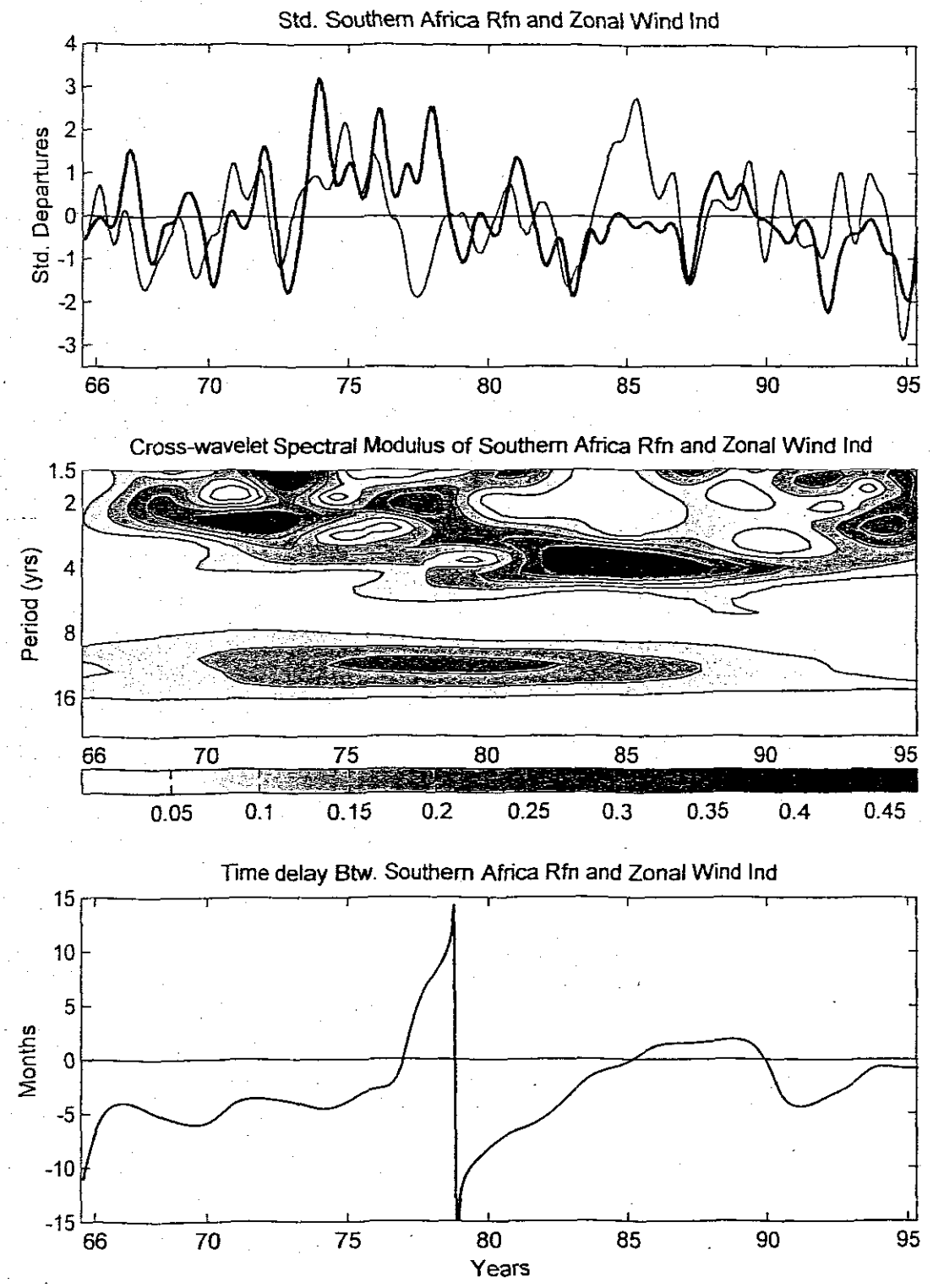

Fig. app5b: Low frequency variability of southern Africa rainfall (Filtered using an 18-month Gaussian filter) (bold) and U Ind (thin) for the period August 1965-May 1995. Modulus cross-wavelet spectrum coefficients of southern Africa rainfall and U Ind; comparing cycles in the two time series (middle). Time delay between southern Africa rainfall and U Ind (bottom), where U Ind leading is -ve

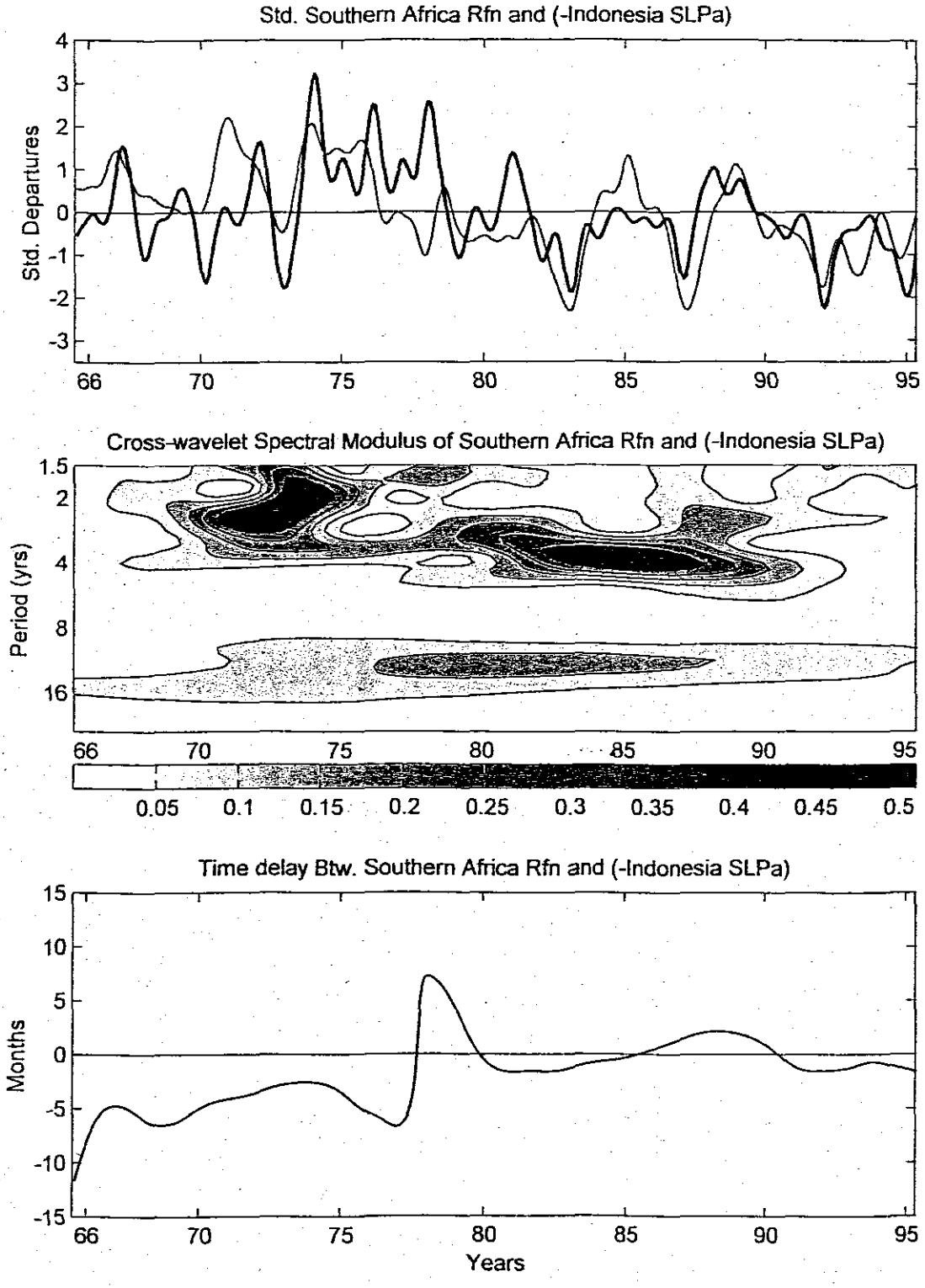

Fig. app5c: Low frequency variability of southern Africa rainfall (Filtered using an 18-month Gaussian filter) (bold) and –(Indonesia SLPa) (thin) for the period August 1965-May 1995. Modulus cross-wavelet spectrum coefficients of southern Africa rainfall and –(Indonesia SLPa); comparing cycles in the two time series (middle). Time delay between southern Africa rainfall and –(Indonesia SLPa) (bottom), where –(Indonesia SLPa) leading is -ve

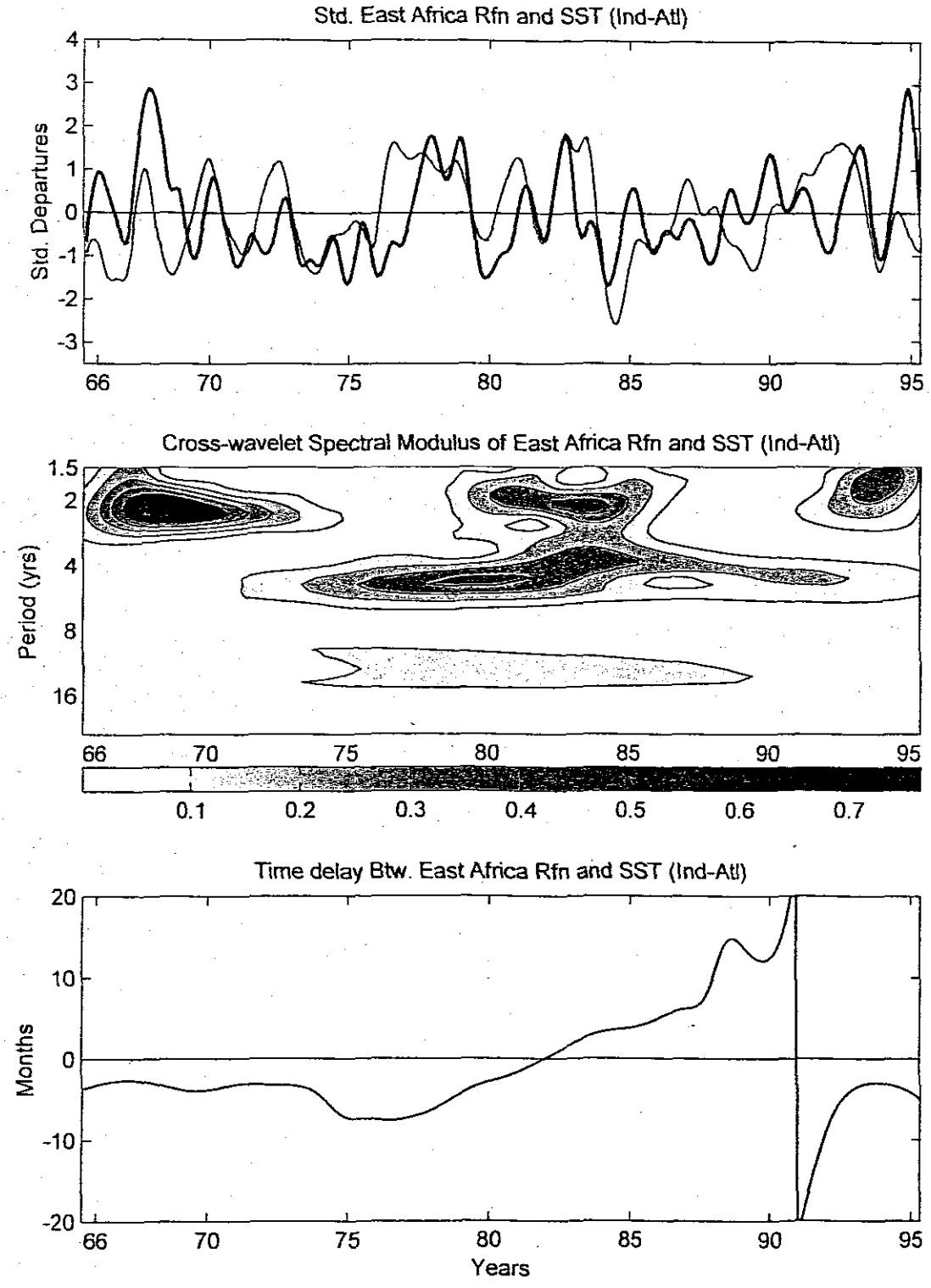

Fig. app5d: Low frequency variability of east Africa (Filtered using an 18-month Gaussian filter) (bold) and SST Ind-Atl (thin) for the period August 1965-May 1995. Modulus cross-wavelet spectrum coefficients of east Africa rainfall and SST Ind-Atl; comparing cycles in the two time series (middle). Time delay between east Africa rainfall and SST Ind-Atl (bottom), where SST Ind-Atl leading is -ve

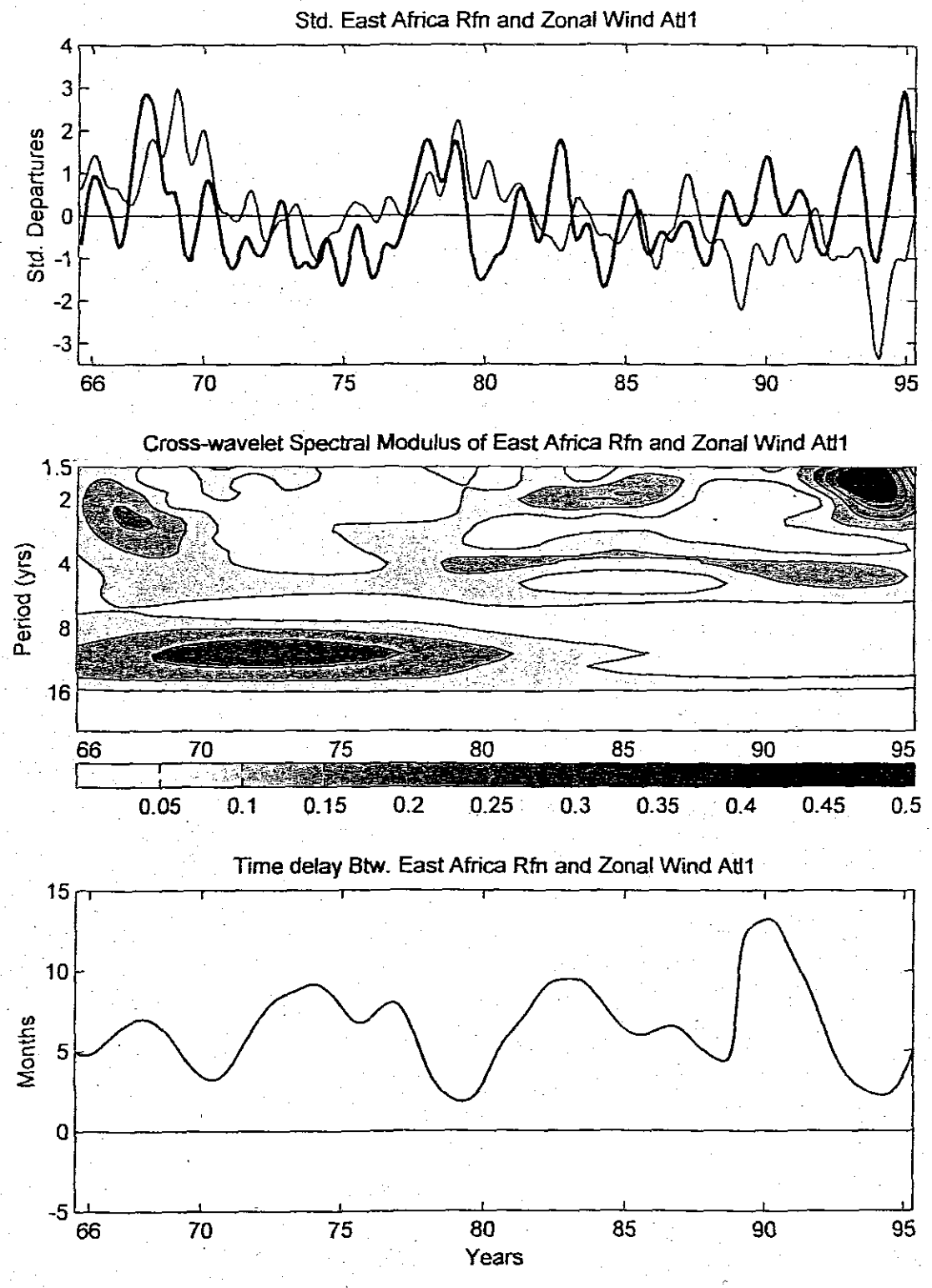

Fig. app5e: Low frequency variability of east Africa (Filtered using an 18-month Gaussian filter) (bold) and U Atl1 (thin) for the period August 1965-May 1995. Modulus cross-wavelet spectrum coefficients of east Africa rainfall and U Atl1; comparing cycles in the two time series (middle). Time delay between east Africa rainfall and U Atl1 (bottom), where U Atl1 leading is -ve

Appendix

Chapter 6

Figures for chapter six. Figure numbers are given in alphanumeric

(a)

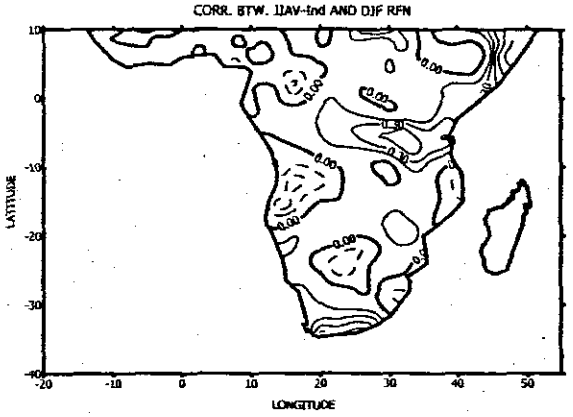

(b)

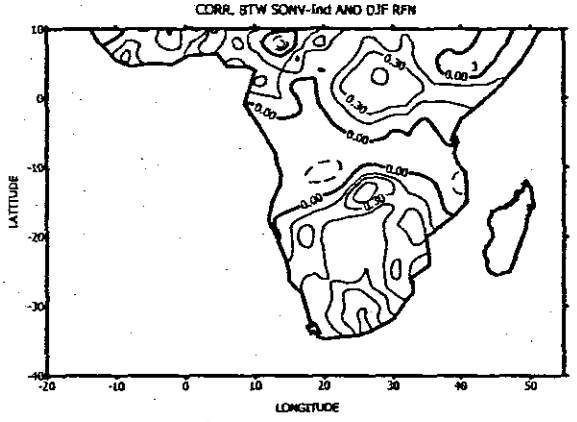

(c)

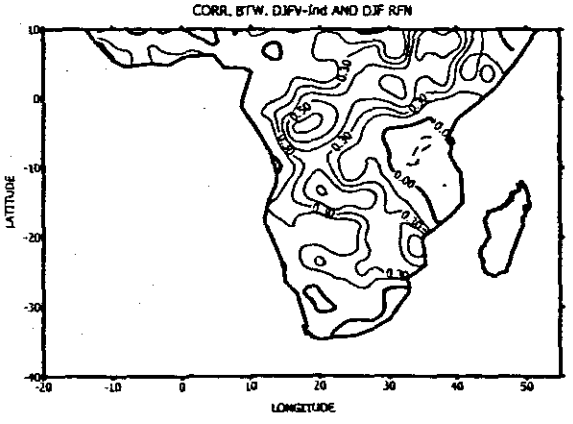

Fig. app6a: Correlation between continental Africa gridded DJF rainfall and environmental parameter indices. Dashed (continuous) lines represent negative (positive) correlation coefficients. (a) Correlation btw rainfall and JJA V wind component over Ind; (b) Correlation btw rainfall and SON V wind component ver Ind; (c) Correlatrion btw rainfall and DJF V wind component over Ind

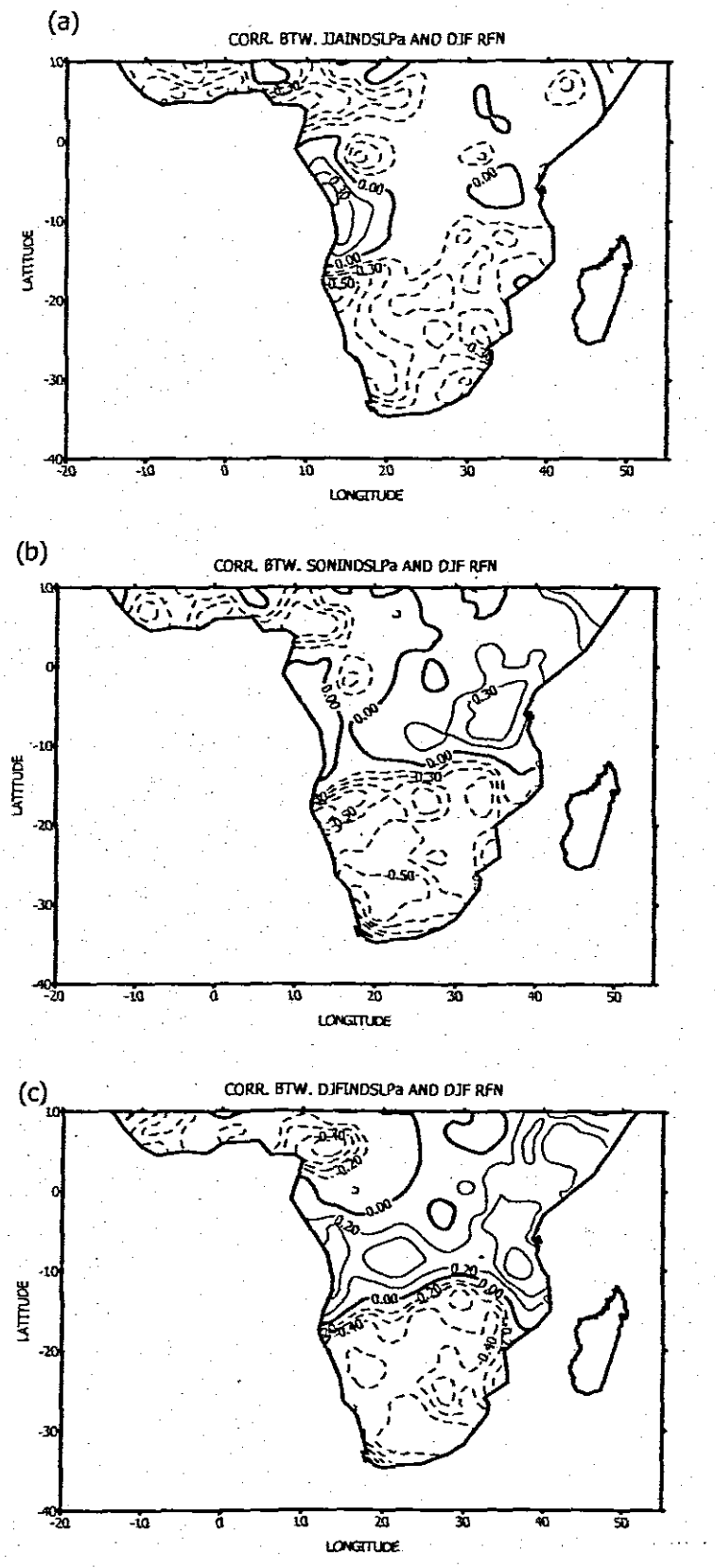

Fig. app6b: Correlation between continental Africa gridded DJF rainfall and environmental parameter indices. Dashed (continuous) lines represent negative (positive) correlation coefficients. (a) Correlation btw rainfall anf JJA IndSLPa; (b) Correlation btw rainfall and SON IndSLPa; (c) Correlation btw rainfall anfd DJF IndSLPa

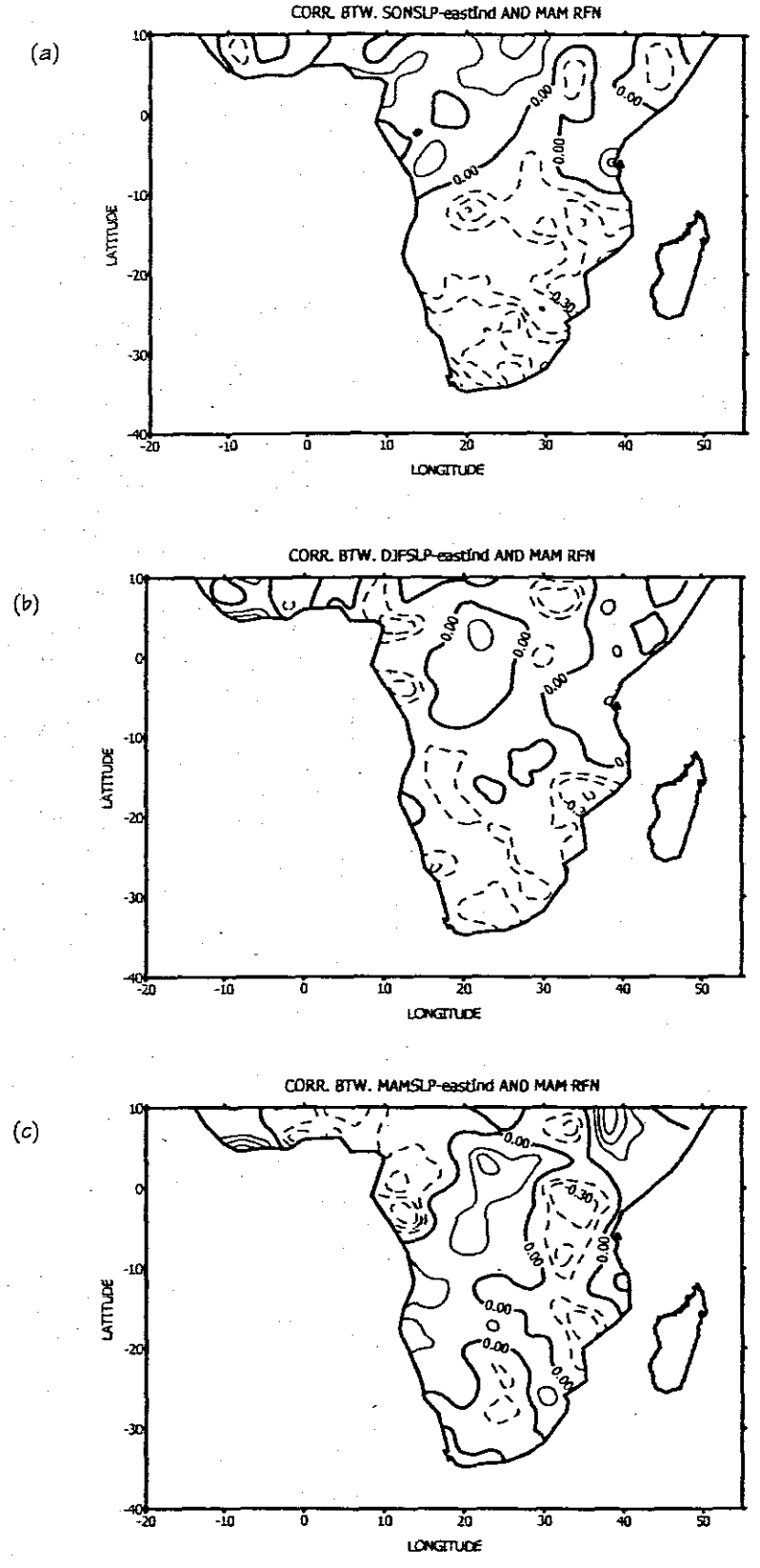

Fig. app6c: Correlation between continental Africa gridded MAM rainfall and environmental paramter indices. Dashed (continuous) lines represent negative (positive) correlation coefficients. (a) Correlation btw rainfall and SON SLP over eastInd; (b) Correlation btw rainfall and DJF SLP over eastInd; (c) Correlation btw rainfall and MAM SLP over eastInd

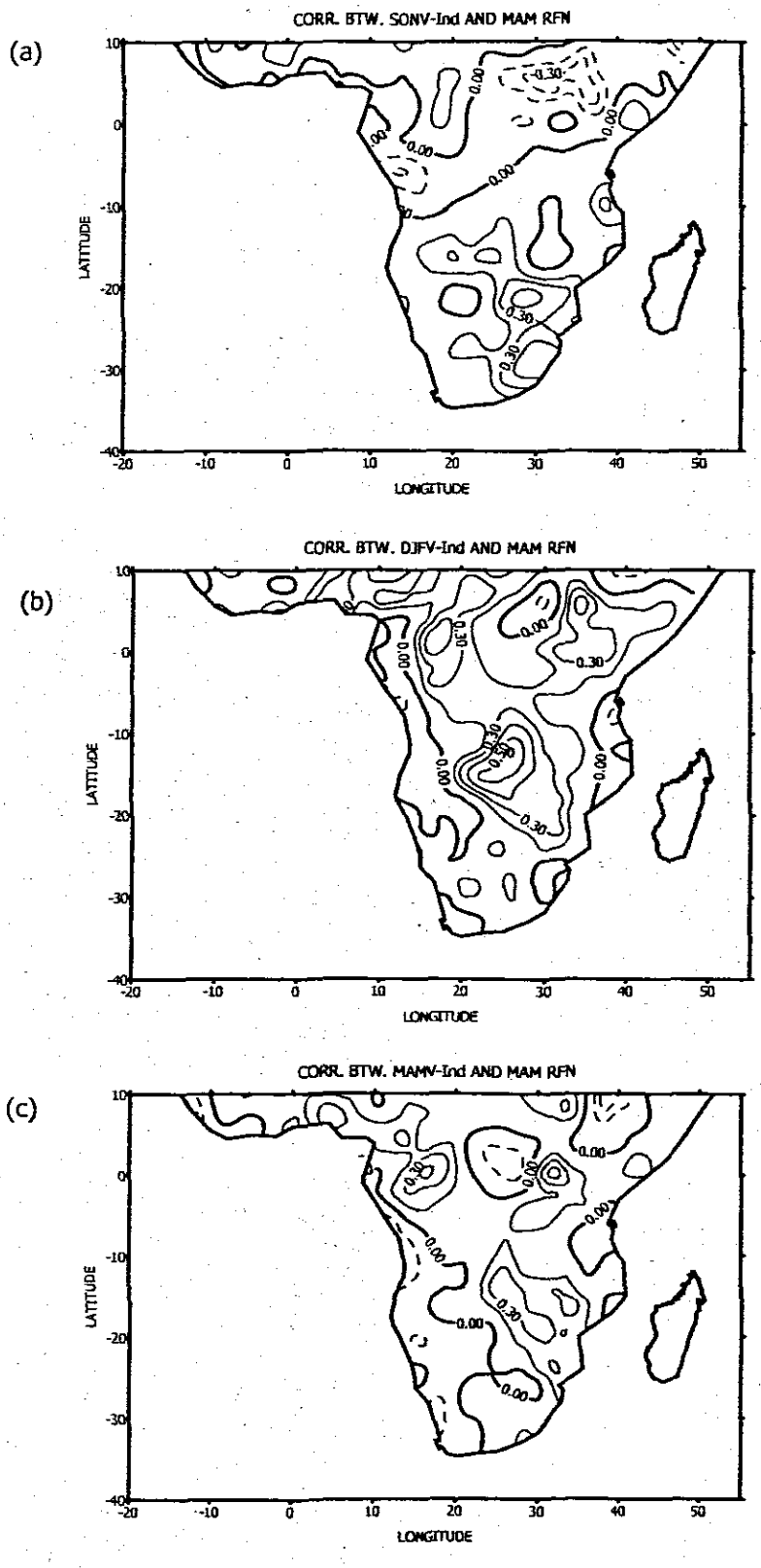

Fig.app6d: Correlation between continental Africa gridded MAM rainfall and environmental indices. Dashed (continuous) lines represent negative (positive) correlation coefficients. (a) Correlation btw rainfall and SON V wind component over Ind; (b) Correlation btw rainfall and DJF V wind component over Ind; (c) Correlation btw rainfall and MAM V wind component over Ind

(a)

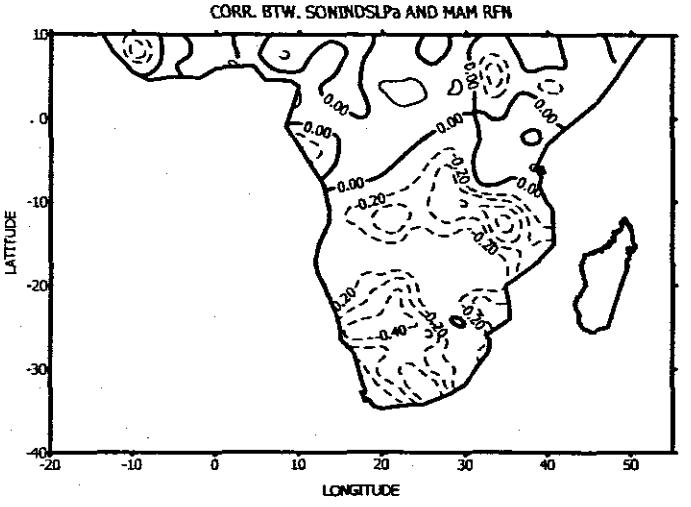

(b)

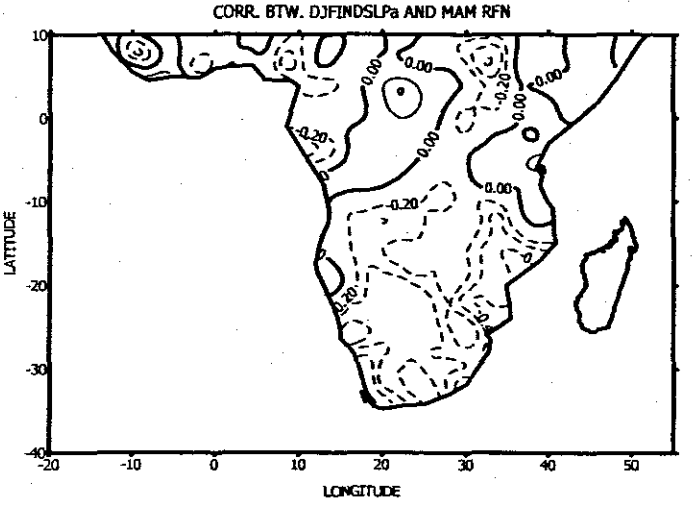

(c)

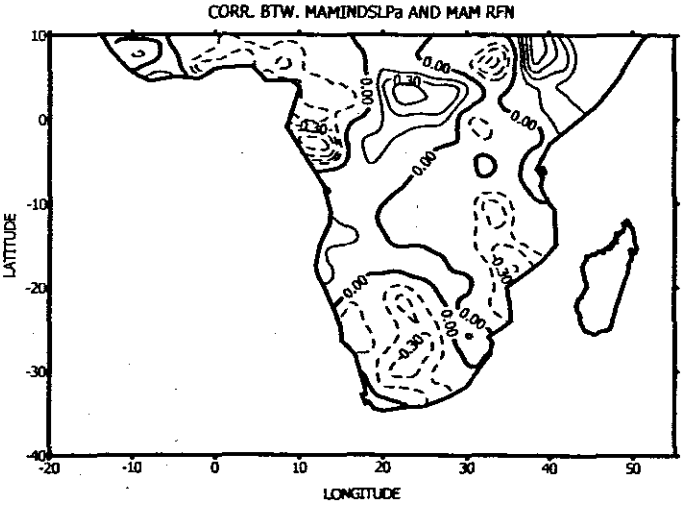

Fig. app6e: Correlation between continental Africa gridded MAM rainfall and environmental parameter indices. Dashed (continuous) lines represent negative (positive) correlation coefficients positive correlation coefficients. (a) Correlation btw rainfall anf SON IndSLPa; (b) Correlation btw rainfall and DJF IndSLPa; (c) Correlation btw rainfall anfd MAM IndSLPa